THE UNIVERSITY OF MICHIGAN

INDUSTRY PROGRAM OF THE COLLEGE OF ENGINEERING

DIGITAL COMPUTER SIMULATION OF OSCILLATORY FLOW IN CARBURETOR FUEL METERING CHANNELS

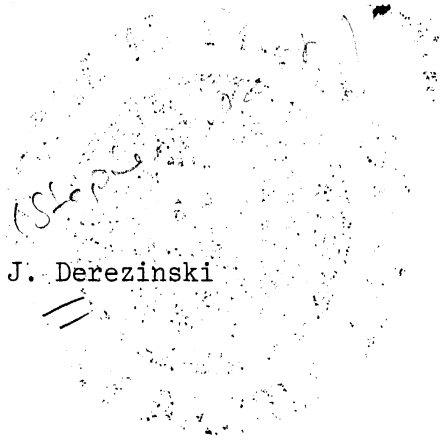

Stephen J. Derezinski

A dissertation submitted in partial fulfillment
of the requirements for the degree of
Doctor of Philosophy in the
University of Michigan
Department of Mechanical Engineering
1972

April 1972

IP-843

en fr

UMR0571

ACKNOWLEDGMENTS

I wish to thank all of the members of the Doctoral Committee for their council during this project. I am particularly grateful to Professor Jay A. Bolt, whose mature guidance was a determining factor in the completion of this project. Also, I would like to especially thank Professor Victor L. Streeter for aiding me through many of the difficulties of the simulation. The assistance of Doctor David L. Harrington, especially during the early phases of this program, is greatly appreciated. I also wish to thank the other members of the committee, who are Professor Robert B. Keller, Professor Franklin H. Westervelt, and Mr. Paul Braun.

The financial aid of the United States Public Health Service is gratefully acknowledged. It would not have been practical to conduct this research at the University of Michigan without this support.

I am grateful for the assistance of Mr. William Zoller, whose many talents greatly simplified the building of workable test equipment and gathering data.

The assistance of Miss Ruth Howard in preparing the original manuscript is gratefully acknowledged.

TABLE OF CONTENTS

TABLE OF CONTENTS (CONT'D)

LIST OF TABLES

LIST OF ILLUSTRATIONS

LIST OF ILLUSTRATIONS (CONT'D)

LIST OF ILLUSTRATIONS (CONT'D)

LIST OF ILLUSTRATIONS (CONT'D)

LIST OF ILLUSTRATIONS (CONT'D)

LIST OF ILLUSTRATIONS (CONT'D)

LIST OF ILLUSTRATIONS (CONT'D)

NOMENCLATURE

A	Area
C_D	Coefficient of Discharge
C_{DA}	Alternating Coefficient of Discharge
C_{DAID}	Ideal Alternating Coefficient of Discharge
C_{DMID}	Ideal Mean Coefficient of Discharge
C_{DP}	Coefficient of Discharge for Pulsating Pressure
C_{DS}	Coefficient of Discharge for Steady Pressure
CS	Direction Cosine
CSG	Direction Cosine of Gravity
D	Diameter
DP_j	Pressure Difference Between Reference Junction and Junction "j"
DPZ	Pressure Difference Due to Elevation
DZ	Elevation Difference
EL	Element
F	Force, Friction Factor
f	Frequency
FA	Friction Factor Due to an Area Change
FB	Friction Factor Due to a Bend
FT	Sum of All Friction Factors
G	Gravity Modulas
g	Gravity Modulas
H	Head
H_A	Alternating Component of Head
H_M	Mean Component of Head
H_{MAX}	Maximum Value of Head

H_{MIN}	Minimum Value of Head
H_R	Ratio of Two Heads
i	One End of an Element
J,j	Junction, End of an Element
JO	Origin Junction
JT	Junction Type
L	Length
LT	Element Type
$\dot{m}$	Mass Flow Per Unit Time
n	Normal
NELS	Total Number of Elements
NFLU	Fluid Number
NL	Number of Elements Attached to a Junction or Between Reference Junction and Boundary Junction
P	Pressure
P_A	Alternating Pressure Amplitude
P_{EL}	Pressure of an Element
P_i	Pressure at Point i
P_j	Pressure at Point j
P_M	Mean Component of Pressure
P_R	Ratio of Two Pressures
PT	Total Pressure
PG	Pressure Gradeline
PZ	Pressure Due to Elevation
Q	Volume Flow
Q_A	Alternating Component of Volume Flow

Q_j	Volume Flow Out of a Junction
Q_M	Mean Component of Flow
RE	Reynolds Number, $V*D/\nu$
R_{EL}	Conveyance of Flow of an Element
RHO	Density
RJ	Mass Ratio of Air at a Junction
ST	Strouhal Number, $\omega L/V$
ST_A	Alternating Strouhal Number, $\omega L/V_A$
ST_M	Mean Strouhal Number, $\omega L/V_M$
ST_{MH}	Mean Strouhal Number Based on Head, $\omega L/\sqrt{2g\ \Delta H_M}$
t	Time
T	Temperature
V	Velocity
∀	Volume
V_A	Alternating Component of Velocity
V_M	Mean Component of Velocity
V_q	Quality on a Volume Basis
X	Square root of Pressure Difference
x	Integer Array, Distance or Unknown
Δ	Used as a Prefix to Denote Finite Difference
θ	Angle
ρ	Density
ρ_a	Density of Air
ρ_f	Density of Fuel

ρ_s	Rate of Change of Density Along Length of Element
ω	Angular Frequency

CHAPTER I

DIGITAL COMPUTER SIMULATION OF OSCILLATORY FLOW IN CARBURETOR FUEL METERING NETWORKS

It is known that carburetors meter fuel at a different rate when they are tested on an engine than when they are tested on a flow-stand. Since the manifold pressure of an engine is known to pulsate, and the simulated manifold pressure during a flow-stand test is relatively free of pulsation, the difference in flow is thought to be, in part, due to oscillations which are induced into the flow by the pressure pulsations. Therefore, the overall objective of this thesis is to develop a technique utilizing the digital computer to analyse and simulate oscillating flow in carburetor metering channels.

The modern day, air-bleed type of carburetor can be described as a complicated network of interconnecting tubes and orifices. Liquid fuel flows in some of these elements, air flows in others and a mixture of air and fuel flows in still others. The liquid fuel is introduced into the network from a reservoir, which is commonly called a float bowl, and ambient air is introduced into the network at various points, which are called air bleeds. The fuel and bleed air mix in the network, and the mixture then flows out of the metering network via several ports. Some of these ports are located in the venturi walls of the carburetor, and the pulsating pressure force at these ports causes the flow in the metering network to oscillate.

In order to analyse transient flow phenomena in such a complicated device, the computer is indispensable. Recently, digital computer analysis of carburation and induction systems have been performed by several investigators, the most comprehensive of which is the carburetor

simulation of Harrington[20]. Other investigators, such as Streeter[38], have used the computer extensively to study transient flow in pipelines and piping networks. Therefore, the goal of this thesis is to extend the technology of analyzing carburetor fuel-flow with the computer to include the influence of oscillating flow. Existing techniques of analyzing transient flow with the computer will be used wherever possible, and new methods will be developed when necessary.

In order to make an accurate analysis of carburetor flow, precise knowledge of the flow characteristics of the metering orifices is necessary. Orifices are used extensively in the fuel metering network to control both the fuel flow from the float bowl and the flow of bleed air at several points. Since the flow through the orifices oscillates, and since flow oscillation is known to influence the coefficient of discharge, it is necessary to gain quantitative information on this effect. Therefore, another major objective of this thesis is to experimentally determine the coefficient of discharge of small orifices for oscillating flow of an incompressible fluid, and to find the dimensionless parameters which are needed to describe the results.

There are many variations of carburetor designs, and, without a comprehensive simulation, it is almost impossible for the carburetor engineer to evaluate the effect that design variations have on carburetor flow characteristics without building and testing a prototype. For this reason, the simulation is to be as general as practical. This will be accomplished by making the flow network of the carburetor a variable in the simulation program. That is, the lengths and diameters of all the flow elements, as well as the pattern in which they are connected to form the flow network, will be changed without the need for

altering the computer program. This information be designated as input data and must be specified each time it is used. This feature allows the flow-path of the gasoline and air in the carburetor to easily be changed, as well as the lengths and diameters of the elements which constitute the flow-path. Other parameters, such as the force due to gravity or other accelerations, or the fluid properties of the fuel, will be also specified as input data. Thus, the influence of many factors on the fuel metering by carburetors will be evaluated, and the performance of different carburetor designs can be studied without the need of building and testing them. It is, therefore, hoped that the carburetor engineer will use the methods developed in this thesis to ease his burden in designing carburetors which will have desirable performance under all operating conditions.

CHAPTER II

PRESSURE PULSATIONS IN THE CARBURETOR: ENGINE TESTING

2.1 Reasons for Engine Test

Since carburetors meter fuel differently on an engine than they do on a flow bench with steady air flow, it is beneficial to investigate the amount of this difference for a typical carburetor. At the same time, measurement of the pressure pulsations, which exist at several points in the carburetor which is on an engine, would be useful in explaining the difference in fuel flow. Therefore, one of the goals of this test program is to measure the fuel-to-air ratios provided by a carburetor which is in operation on an engine, and to compare the results to fuel-to-air ratios for flow-bench operation. Simultaneously, highly responsive pressure-transducers will be used to measure the amplitude and frequency of the pressure pulsations, which will be related to fuel-to-air ratio differences that exist between the engine test and the bench test.

Another reason for testing an engine-carburetor combination is to obtain detailed data on the carburetor pressures, as a function of time, with which to compare the computer simulation. The venturi pressures are used as input variables for the simulation. The simulation program then calculates the main-metering channel pressure as a function of time, which should then be the same as the measured main-channel pressure. When agreement is accomplished, it is assumed that the computer simulation is accurately predicting the oscillating flow in the carburetor.

A third reason is to provide some quantitative knowledge of the extent of pressure pulsations in the carburetor venturis for the use of future investigators. Even though this data is only for one particular carburetor, venturi configurations tend to be similar enough to allow this data to be applied to other carburetors in lieu of no data.

This is particularly true of the influence of the throttle plate on the pressure pulsations, since the butterfly design of throttle is most universally used.

2.2 Previous Studies

Experimental studies on the effect of pressure pulsations on fuel metering by carburetors have been performed by a few investigators. Prien (28) did an experimental study of the influence of pressure pulsation on the fuel-to-air ratio for a simple carburetor, which lacked air bleeds, on a single-cylinder engine. He tested his carburetor with steady air flow, with air flow for the engine motoring, and with air flow for the engine firing. For his simplified carburetor he obtained fuel-to-air ratios for firing and motoring conditions which were as much as three times greater than for steady air-flow conditions.

Hosho (21) also tested a simplified carburetor, which was very similar to that used in the work of Prien. However, his carburetor had an air bleed and he used a stroboscopic light and a high-speed camera to study the flow oscillations at the fuel discharge port. He varied the air bleed diameter and the venturi suction and noted the effect on the amplitude of pulsations and the fuel-to-air ratio. He found that flow oscillations which occurred when no bleed air was introduced were largest for low venturi vacuum. He also found that the introduction of air caused the flow oscillations to be greatly increased. The greatest amount of oscillation was found to be for small venturi vacuum at the minimum mixture ratio, and that the flow mode for the fuel and bleed air was slug flow for maximum oscillations. He also tested three typical commercial carburetors and found similar results.

In a later work, Hosho (22) continued his photographic study of flow oscillation of the fuel as it leaves the main discharge nozzle. He studied a Stromberg type down-draft carburetor, with a high-speed movie camera, in operation on an engine and on a flow stand. He concluded that, "Pulsations will occur regardless of whether the carburetor is operated in an engine with a pulsating air flow or in a Cox carburetor test stand with constant flow". He found that the pulsations are minimized by the elimination of bleed air. He further states that, "the pulsations during fuel jet of the main fuel system are caused by the air introduced through the air bleed, not by a pulsating air flow". However, his photographic testing technique is qualitative in nature and it will be shown by more accurate testing methods that the pulsating back-pressure at the venturi is the only source of pressure pulsations at low engine speeds and large throttle-openings.

Oyama, Tejima and Hosho (27) continued this study of the transient flow phenomena caused by the bleed air by creating a one-dimensional flow model of the two-phase flow in the carburetor emulsion-tube. For this model they divided the flow elements into small increments along the direction of flow, and assumed an average fluid density which was based on the relative volume of fuel (liquid) and air (gas) to enter each incremental section. They then solved the equations of motion and continuity, for increments in time and space, with the computer, and were able to accurately compute fuel-discharge lag-time for the Stromberg carburetor for sudden acceleration. Their experimental results compared very well with their calculated values, but they did not extend their analysis to the flow oscillations which they found to occur under steady engine-load conditions in the previous work of Hosho.

Many investigators have measured and analyzed the pressure pulsations in the manifold of an engine, and much discussion is available on the topic. Taylor, Livengood and Tsai (30) experimented with a single-cylinder engine in order to study the pulsing phenomena with regards to the "ram effect" on the intake air and improvement of volumetric efficiency. They measured the inlet port pressure and cylinder pressure as a function of time for different lengths of inlet pipe. Their work contains considerable discussion of the physics of the pulsating pressure in the intake manifold.

Later work on the "ram effect" was done by Huber and Brown (23) in which they simulated the engine cycle with the digital computer in order to study the influence of dimensional changes of valves and manifolds on the induction process and volumetric efficiency. Their work included the effects of heat, finite time of combustion and variable gas-specific heat, but it was done for single-cylinder engine only and does not include the influence of a throttle or other restrictions in the intake and exhaust systems.

More recent studies of intake and exhaust systems of single-cylinder engines were performed by Goyal, Scharpf and Borman (19). Their work includes experimental study of the wave damping within the manifold during the time the intake valve is closed. In the same work they perform a digital-computer solution of the pressure in the intake and exhaust manifolds for which they assume one-dimensional compressible-flow in a straight pipe of constant area with friction and heat. However, the work does not include the influence of a throttle valve, and it is only for a single-cylinder engine.

A study of the formation of the combustible mixture in the intake manifold, which includes the influence of flow oscillations, was performed by Brandstetter (17). The study was performed on an idealized intake manifold, which consisted of a straight pipe with each end connected to a plenum chamber. A vacuum was created in one chamber which induced flow through the pipe. The flow was caused to oscillate by a rotary type of sleeve valve, which was located in the pipe, and the influence of liquid and vapor fuel, which was introduced into the flow, was investigated. The transient flow was analyzed with the digital computer by the method of characteristics, and the calculated values of air flow, fuel flow, and air-to-fuel ratio compared well with the experimental results.

The same investigator continued his work (18) by modeling single-cylinder engine flow with intake and exhaust pipes. In this later effort he included the influence of the throttle plate and intake and exhaust valves. The work is only theoretical, and contains no supportive experimental results.

It was found that much study has been performed on the intake manifold of a four-stroke engine. However, in all cases only a single-cylinder engine was studied, and the pulsating pressure phenomena in a multi-cylinder manifold was not found to be discussed in the literature. Therefore, the analysis of the transient flow in a multi-cylinder manifold is a topic which should be investigated. It was also found that few investigators have studied the pressure pulsations which are caused in the carburetor fuel-metering network by the pulsating back pressure at the venturi, and how these pulsations can, under steady load conditions, influence the flow of fuel in the metering network.

This is the problem which has been chosen for further study in this thesis.

2.3 Testing Procedure

A Ford C8AF-L 2-barrel carburetor was specially modified to accept highly responsive electronic pressure transducers to measure boost venturi pressure, main-venturi pressure above and below the throttle, and main-metering-channel pressure. Tubes of 1/8 inch diameter were inserted through the carburetor walls to provide pressure taps at the desired points. The transducers were then attached to the ends of the tubes on the outside of the carburetor. The tubing length was made as short as possible to minimize frictional damping of the signal, and the diameter of the tubing was small to minimize capacity for absorbing pressure signal. Figure 1 shows the location of the four pressure taps to which the transducers were connected. Appendix A gives more details on the test equipment and procedure for the engine-carburetor test.

2.4 Results of Engine Tests

The results, as shown by Figures 2 through 5, illustrate that pressure fluctuations do occur throughout the carburetor and in the intake manifold. The pressure pulsations occur at all times in the manifold, as shown by Figure 2, but they only occur at throttle angles greater than about 30 degrees (90 degrees is wide open throttle) in the main venturi and boost venturi, as shown in Figures 3 and 4. This is expected since the flow at small throttle openings is choked which prevents changes in manifold pressure from being transmitted upstream of the throttle. Figure 5 shows the pressure pulsations in the main metering channel to be present also for throttle angles greater than 30 degrees.

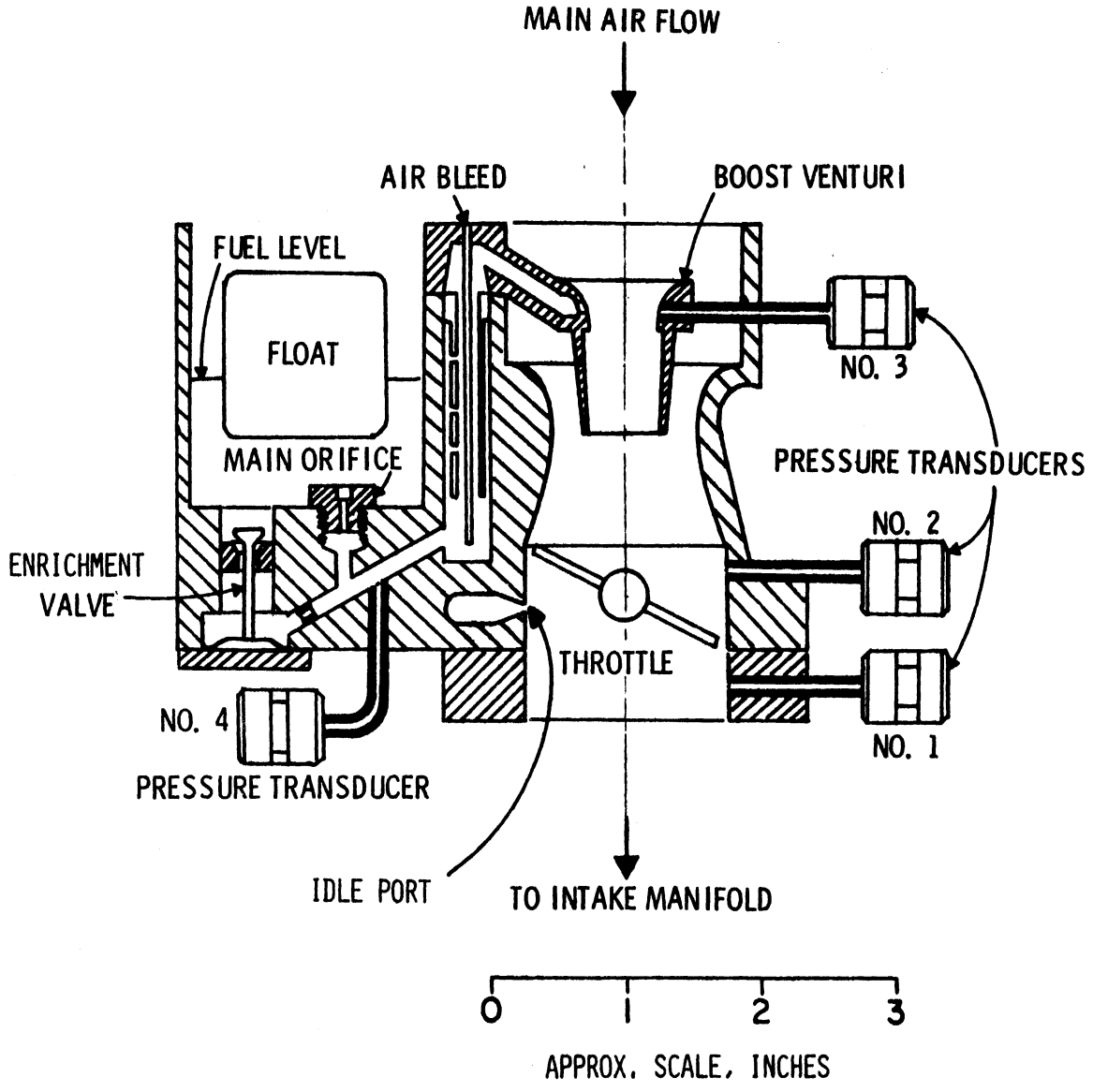

Figure 1. Cut-away Drawing of the Test Carburetor.

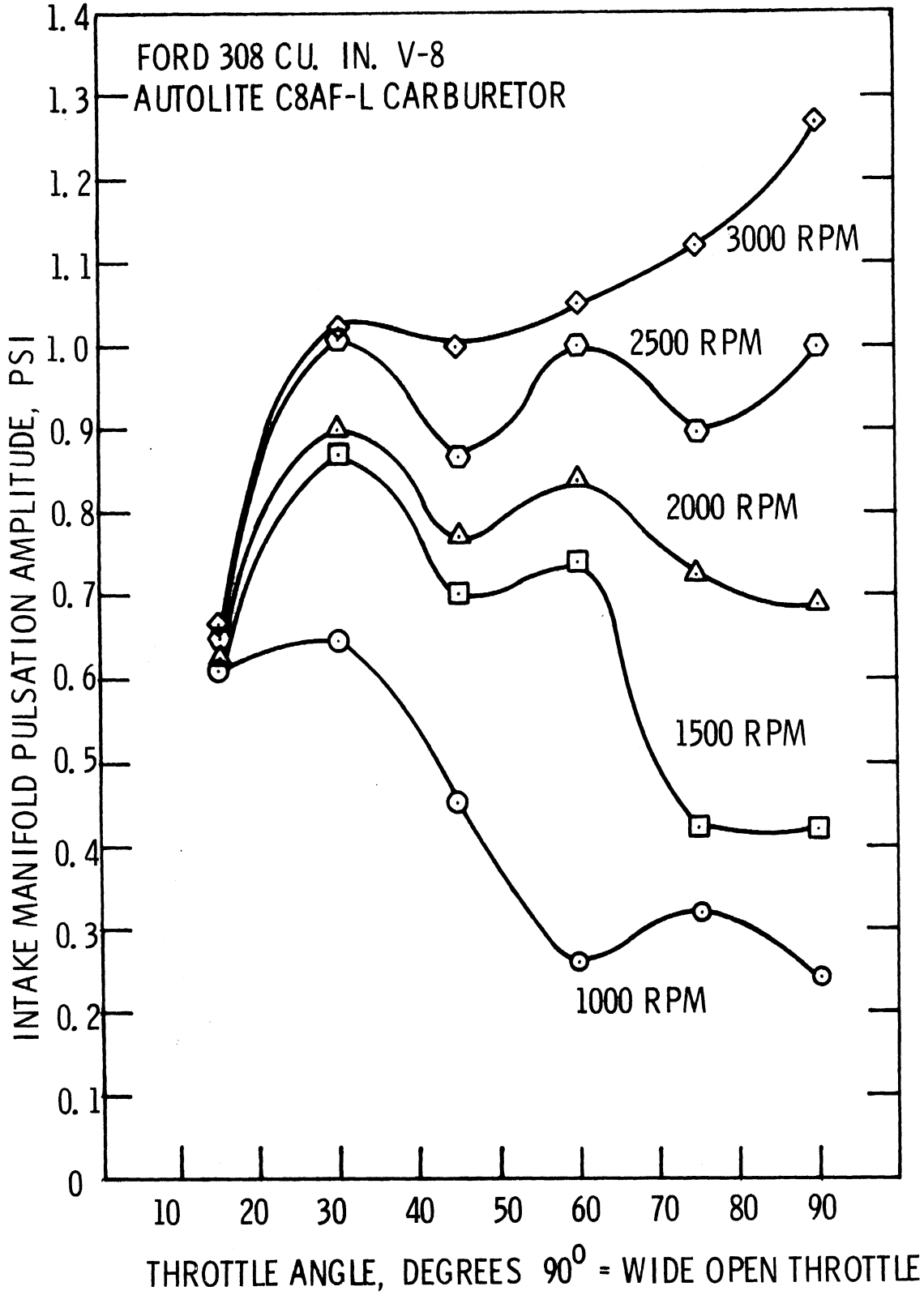

Figure 2. Intake Manifold Pressure Pulsation.

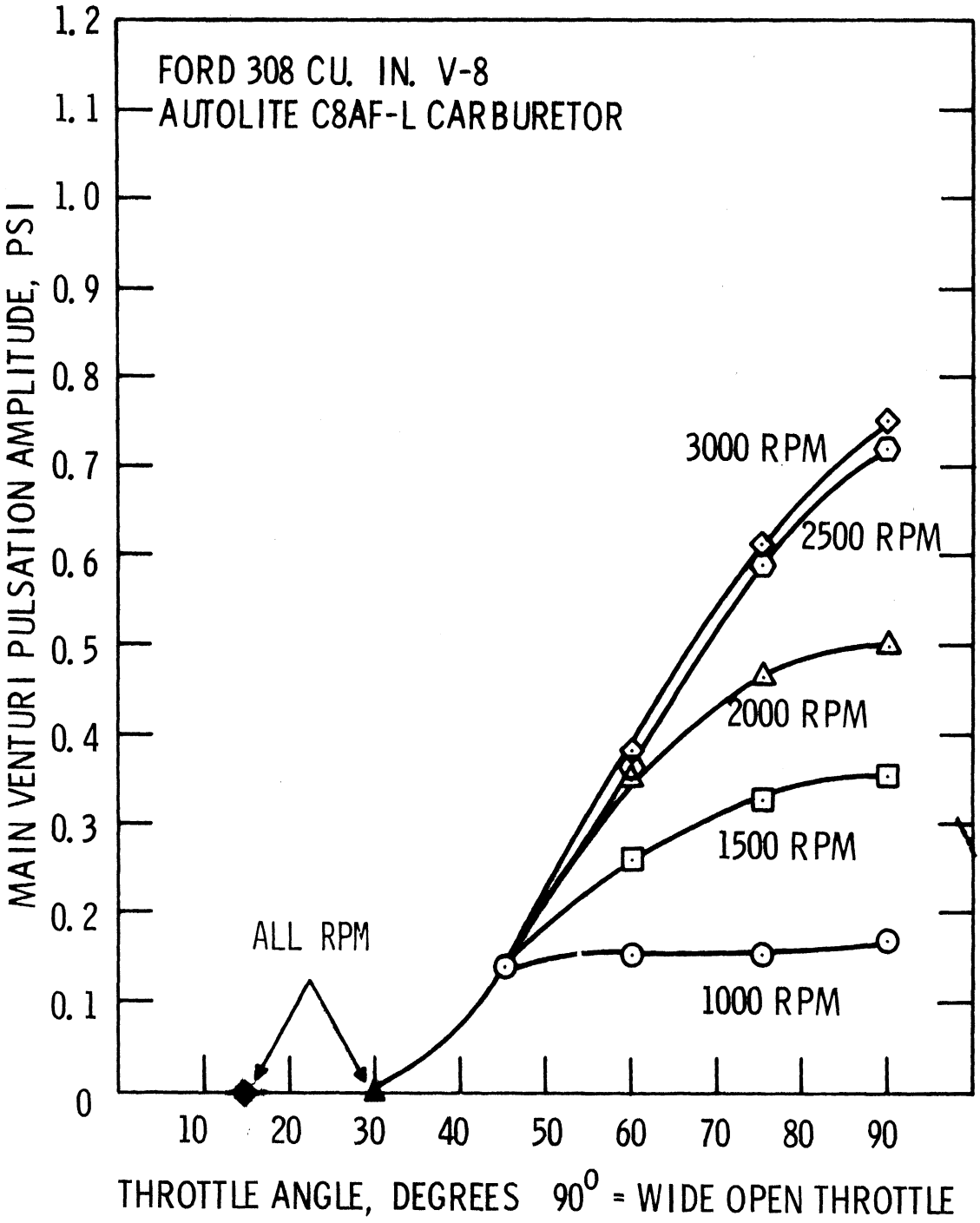

Figure 3. Main Venturi Pressure Pulsation.

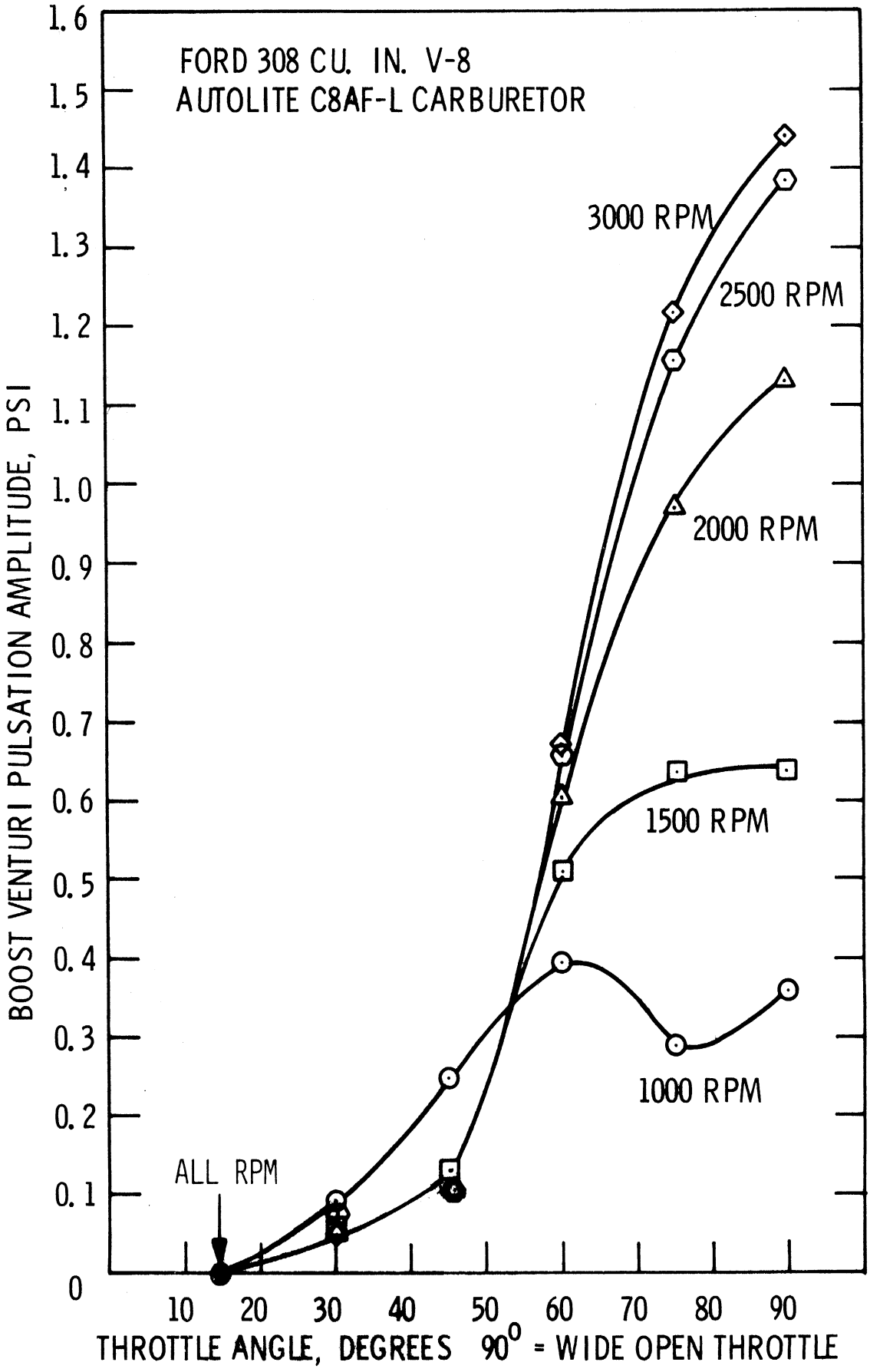

Figure 4. Boost Venturi Pressure Pulsation.

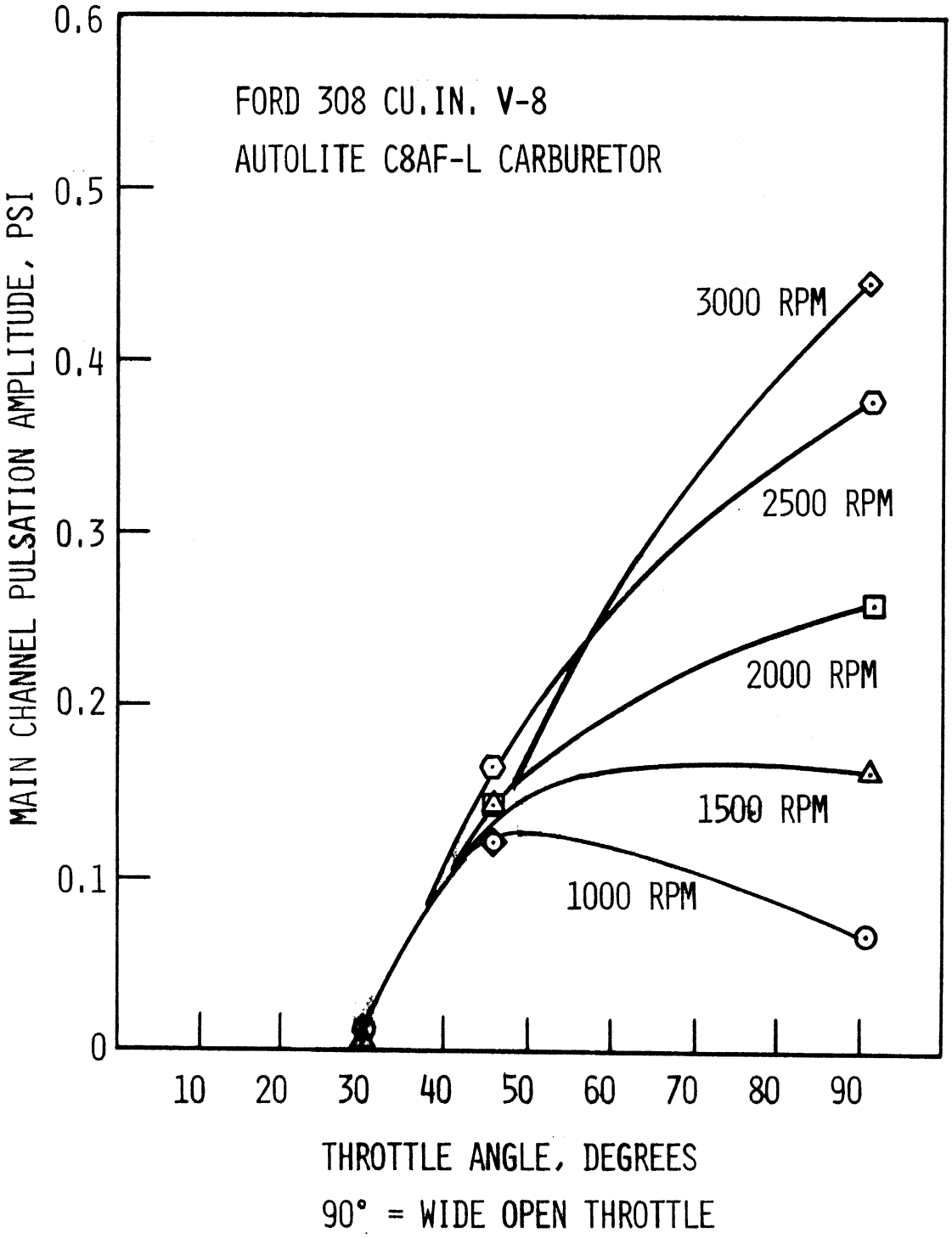

Figure 5. Main Channel Pressure Pulsation.

The frequency of all of the pulsations is equal to twice that of the engine revolutions. For the dual level manifold, each venturi of the carburetor services four cylinders, and each cylinder performs an intake stroke every 720 degrees of crankshaft rotation. Since the four-intake strokes are nearly evenly spaced in time, they occur at 180 degree intervals of crankshaft rotation and create a pressure pulse at the same interval. Therefore, two intake strokes occur for each complete rotation of the crankshaft so that the pressure pulsations have a frequency which is twice the engine speed, or equal to rpm/30cps. This frequency corresponds to the number of intake strokes per second for the 8-cylinder engine.

2.5 Manifold Pressure Pulsations

Figure 2 shows that large pressure pulsations exist in the intake manifold, for all combinations of engine speed and throttle angle. The greatest amplitude of pulsation is seen to occur at the highest engine speed, and the influence of the throttle opening is seen to depend upon engine speed. Larger throttle opening makes the fluctuations smaller at low speed (1000 and 1500 rpm), and larger at high speeds (3000 rpm). At intermediate speeds, the throttle angle has a small influence upon the pressure pulsations in the intake manifold. This phenomena has been well researched for single-cylinder engines, as previously mentioned, but little has been published on analyzing pulsating pressure in multi-cylinder engine intake manifolds.

2.6 Venturi Pressure Pulsations

The pressure pulsations, which have been shown to exist in the manifold at all engine speeds and throttle settings, influence the pressure above the throttle plate in the carburetor main and boost venturis as shown in Figures 3 and 4. The boost venturi pressure tap is in the

same position as the ports for the main-system fuel flow as shown in Figure 1, which means that the fuel-metering network will be exposed to these fluctuations. The figures clearly indicate the large effect the throttle has on the pressure pulsations, because no pulsations are present at throttle angles less than 30 degrees (90 degrees is wide open throttle). This phenomenon is explained by the fact that the air flow reaches sonic velocity at the throttle for small throttle opening, and, therefore, no pressure disturbance can be transmitted from the manifold, upstream from this point. At throttle openings between 30 and 50 degrees, the amplitude of the pressure pulses in the carburetor are measurable, but the throttle still substantially restricts the amount of pulsation which is transmitted from the intake manifold. However, at throttle angles greater than 50 degrees, the throttle does little to dampen the pressure amplitude. The pressure amplitudes are substantial in size, and for the boost venturi, are even greater than those in the intake manifold.

The analysis of the oscillatory flow which occurs in the manifold and in the venturis, as shown in Figures 2-4, is very complicated and presents a formidable problem. As mentioned earlier, many investigators have tested and analyzed simplified versions of the air intake system, but none were found who attempted to analyze the oscillatory flow in the multi-cylinder engine intake system. Harrington (21) studied the problem for steady flow, and included the influence of compressibility, fuel droplet size, fuel atomization, and the throttle plate, where sonic flow occurs. The problem is also complicated by the influence of flow-path curvature, two-phase flow with part of the liquid phase clinging to the walls, area changes, and evaporation. Analyzing

this complicated system, which has oscillatory flow, is a challenging problem for future investigators.

2.7 Main Fuel Channel Pressure Pulsations

Figure 5 shows the amplitude of the pressure in the main fuel channel which is immediately downstream of the main metering orifice (see Figure 1). The frequency of these pulsations is the same as the frequency of the pressure in the manifold and the venturis (rpm/30 cps), which indicates that the venturi pressure fluctuations are causing the pressure in the main fuel-metering channel to pulsate. Further evidence of this is that the metering-channel pressure-pulsations at these frequencies do not exist at throttle angles less than 30°, because pressure pulsations do not exist in the venturis for the same throttle angles. This indicates that only the main-metering system transmits pressure pulsations to the main fuel channel, and that the idle system has a large damping effect on the pressure pulses which are transmitted to the metering network via the idle port. The pressure pulsations at the idle port are similar to those of the manifold, hence, they are always present. The damping effect of the idle system was substantiated by testing the engine for two identical points of speed and throttle angle with the idle screw open in one instance and closed for the other. No difference could be noted between the amplitudes of the pressure wave in the main channel of these two cases.

2.8 Waveshape of Pressure Traces

Most of the pressure-time traces taken from the carburetor could be approximated very well with a single harmonic of fundamental frequency. However, some exceptions do exist, and these should be noted now. Manifold pressure for throttle angles greater than 60 degrees

deviated noticeably from a purely sinusoidal wave shape. However, it appeared to be very close to a sinusoid for all speeds at throttle angles which are equal to or less than 60 degrees. Just above the throttle, at the point in the main venturi, the pressure wave shape always contained noticeable amounts of higher harmonics, but the magnitude of the fundamental harmonic was still predominant. Similar results were noted for the pressure wave of the boost venturi, which appeared to contain a substantial second harmonic because the wave was well rounded at high pressure, and pointed during the other half of the cycle at low pressure. The fundamental frequency of the pressures in the venturis and the manifold was always equal to twice the engine speed.

The pressure pulsations in the main channel also had a frequency of twice the engine speed. However, another pulsation also occurred which had a frequency between 15 and 25 cps, regardless of engine speed. Therefore, the waveshape of the pressure in the main channel was a combination of a 15-25 cps wave and a wave with a frequency equal to twice the engine speed. The 15-25 cps portion of the wave did not exist at or below 1000 rpm, but became evident at 1500 rpm. At speeds greater than 1500 rpm, the amplitude of the 15-25 cps pulsations became proportionally larger, and the amplitude of the pulsations with a frequency of rpm/30 also increased. All of the data for the pressure amplitude in the main channel, which is shown in Figure 5, is for the harmonic of frequency which is equal to twice the engine speed. This means that the pressure amplitude shown in Figure 5 is only caused by the pulsating pressure at the boost venturi. The total pressure amplitude is actually greater, because it includes a 15-25 cps component.

Some phenomena, other than the pulsating back pressure at the boost venturi, must be causing the pressure disturbance of 15-25 cps the main channel. This phenomena has been noted by Hosho (22), who did high-speed photographic studies of carburetor fuel-flow. Unfortunately, he did not measure the pressures, so that the results of his studies are only qualitative. He was only able to determine the frequency of the flow oscillations, and had no way of measuring their magnitude. The oscillations had a frequency of 10-20 cps for his carburetor, and these were independent of engine speed. Also, the same phenomenon occurred when the carburetor was operated on a flow bench with constant venturi pressures. He was able to minimize these oscillations by making the air-bleed flow zero, and he concluded that the flow oscillations in the carburetor are due to the two-phase flow and are not due to fluctuating back pressure in the engine manifold or carburetor venturis. However, the data of Figure 5 does show that, for this particular carburetor, pressure fluctuations do occur at the main metering orifice which are due to the pulsations of the back pressure in the venturis. At engine speeds below 1500 rpm, these are the only pulsations which are present in the main fuel channel, and the influence of the bleed on pulsation is negligible. At greater engine rpm, the pressure fluctuations due to the bleed air are comparable to the fluctuations due to the pulsating back-pressure in the venturis.

2.9 Comparison of Engine Tests with Flow Stand Tests

The venturi pressures and the manifold pressure have both been shown to pulsate (Figures 2-4), and these pulsations are now known to be transmitted into the main fuel metering channel (Figure 5). Since these pulsations only occur for engine operation, it is now of interest to

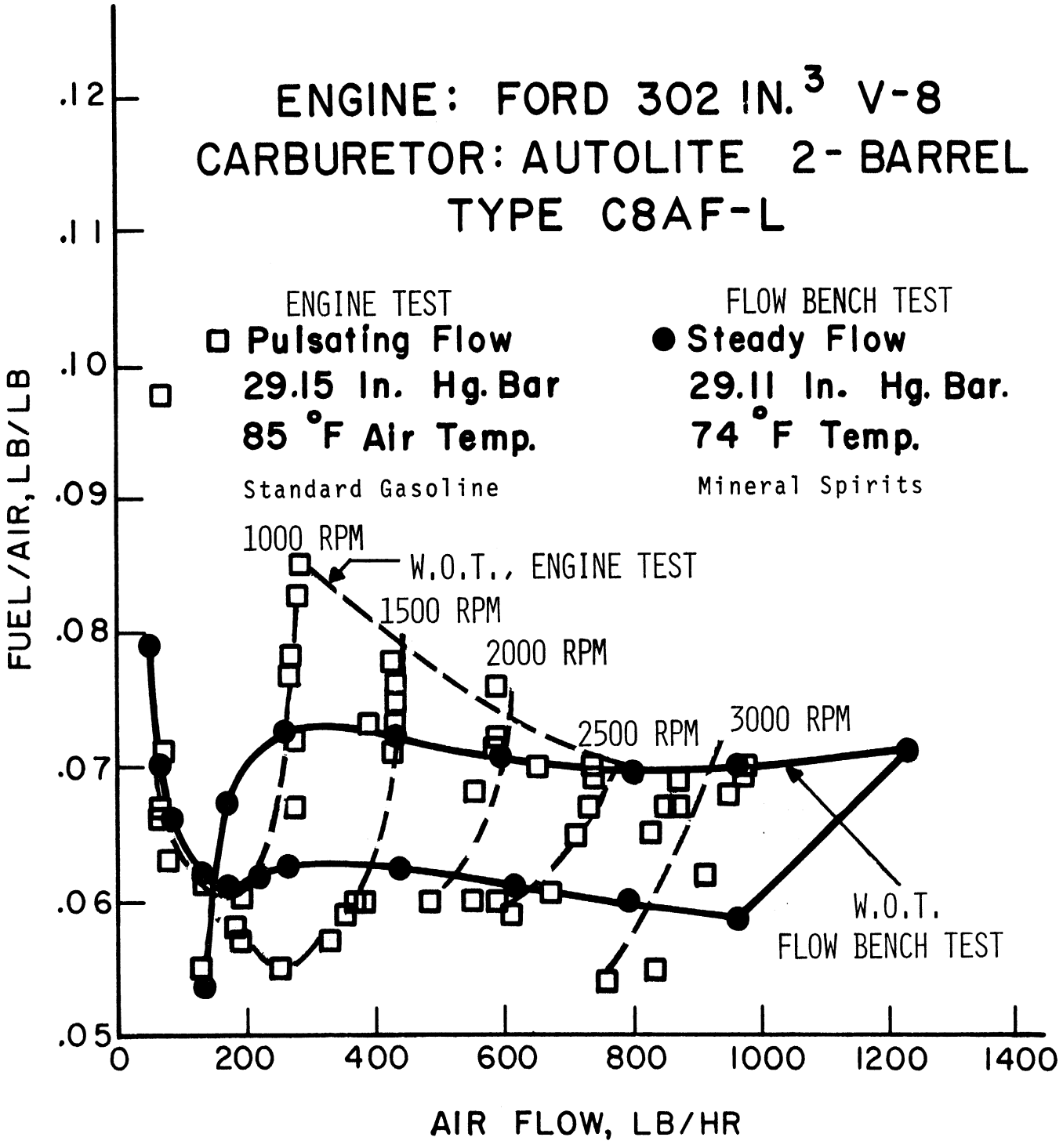

Figure 6. Comparison of Laboratory Airbox (Steady Flow) Fuel/Air with Engine Fuel/Air (Pulsating Flow).

investigate the effect they may have on the average fuel-to-air ratio provided by the carburetor. A comparison of engine fuel-to-air ratios with flow-bench fuel-to-air ratios is shown in Figure 6, which is a plot of fuel-to-air ratio versus air flow, and shows many data points for different throttle angles and engine speeds. The data indicate that the carburetor performed on the engine almost exactly as it did on the flow bench at air flows greater than 600 pounds per hour. This is particularly true of the upper curve, or full power line. However, at air flow rates less than 600 pounds per hour, the engine fuel-to-air ratios are shown to be greater (at full power), than the flow-bench fuel-to-air ratios. These points coincide with the points of low engine rpm and large throttle opening, which is when nearly all pressure pulsations in the main fuel-metering channel are caused by the fluctuating back pressure in the boost venturi. These fluctuations in the boost venturi only occur when the carburetor is operated with an engine, and are, therefore, thought to be the cause of the difference between the test bench and engine fuel-to-air ratios.

The difference between the engine test points and the flow-bench test-points is also noted for the lower curve in Figure 6, or the off-idle and cruise ranges of operation. This difference cannot be attributed to boost venturi pressure pulsation, because it has been shown that small throttle angles (large pressure ratios or choked flow) greatly dampen the pressure amplitude at the boost venturi. This difference in fuel-to-air ratio between engine operation and flow-bench operation can be attributed to fuel property variations. The flow test was performed with a special testing fluid, and the engine tests were performed with gasoline. As stated by Bolt, Derezinski, and Harrington[17], fuel

property variations can cause substantial differences in fuel metering by carburetors, and their engine test data, for the same type of carburetor and engine, shows that this is particularly true in the idle, off-idle, and low power ranges of operation. Pressure pulsations are thought to be the cause of the fuel-to-air ratio difference between flow bench tests and engine tests at wide open throttle and low air flow (low engine speed), and it is postulated that it is the influence of these pulsations on the metering characteristics of the main-metering orifice which cause this difference. This leads to an important phase of this thesis, which is the influence of pressure pulsations on the time-average flow through small orifices.

2.10 Conclusions from Engine Tests

1. Pressure pulsations were found to exist in the induction and fuel metering system of a Ford V-8 engine with a C8AF-L two-barrel carburetor. The frequency of the pulsations was always rpm/30 cps, with exception of the metering channel. The waveshape of the pulsations was primarily of one harmonic, but noticeable amounts of second harmonics and some higher harmonics were also apparent.

2. The throttle angle was found to greatly influence the amplitude of the pulsations at the main venturi and boost venturi. The amplitude was maximum at wide open throttle (90 degrees). The throttle angle had a minor influence on the pressure amplitude in the intake manifold.

3. Greater engine speed resulted in increased pressure fluctuation amplitude in the intake manifold, main venturi, and boost venturi.

4. The pressure wave in the main channel was generally composed of two components, one at a frequency in the range of 15-25 cps

and one at a frequency dependent upon engine speed or rpm/30. The amplitude of the former did not appear to be related to engine speed or throttle angle, and the amplitude of the latter followed a relationship to engine speed and throttle angle which is very similar to that of the boost venturi pressure fluctuation. The constant-frequency component has been shown by Hosho (22) to be caused by fuel pulsations due to the introduction of bleed air.

5. Different fuel/air ratios between the engine test data and the flow-bench data for the same carburetor was found to exist at low air flows (low engine speed). At wide-open-throttle, this difference at small throttle angles can not be attributed to the same cause. At high air flows and wide-open-throttle, no difference between the fuel/air for bench test and engine test is noted.

CHAPTER III

INCOMPRESSIBLE OSCILLATING FLOW THROUGH ORIFICES

3.1 Introduction

A carburetor contains many small orifices which serve to control the flow of fuel and bleed air. These orifices are on the order of 0.05 inches in diameter and range in length from 0.05 to 0.2 inches. Most of them are of a "square-edged" design; that is, their geometry is congruent to a drilled hole. However, the main-metering orifice, which controls the main fuel-flow from the float bowl, has a unique geometry. It has sections of different areas, camfers, and a screw-driver slot. It is easily removed with a screwdriver since it is threaded into place, whereas the rest of the orifices are permanently pressed into place. The main orifice is made to be removable because it is a major flow-controlling element of the carburetor, and the metering characteristics of the carburetor can be easily adjusted by changing it. The importance of the main metering orifice, and the other orifices, makes the knowledge of the flow characteristics of these elements vital to the accuracy of any carburetor analysis. Fluid flow through the orifices must be known in terms of any independent variables which could change during carburetor operation. The variables which influence flow through orifices for steady flow have been thoroughly studied by Harrington (20), and the results applied in his digital computer simulation of the carburetor. It has previously been shown here that the pressure at the main orifice is pulsating. Therefore, the task is now to determine how pressure pulsations and the corresponding flow-oscillations influence the rate of fuel flow through orifices.

The study of periodic flow of an incompressible fluid involves several variables which are; the frequency of the pulsation, the amplitude and mean values of the pressure differential, and the amplitude and mean values of flow. Figure 7 illustrates the meaning of the variables for a sinusoidal flow, which is typical of carburetor flow. However, waveshape is an important variable, and the results contained here can only be applied to flow which resembles a sinusoidal form. The variables can be combined into three dimensionless groups as follows:

$$\frac{\omega L}{V_M} = \text{Strouhal number, } ST_M$$

$$\frac{Q_A}{Q_M} = \text{flow ratio, } Q_R, \text{ and}$$

$$\frac{\Delta P_A}{\Delta P_M} = \text{pressure ratio, } \Delta P_R.$$

As the literature indicates, all three of these dimensionless numbers are pertinent to oscillating flow through orifices.

3.2 Previous Work

The influence of flow oscillations on metering by orifices has wide-spread practical application because many fluid systems inherently contain oscillations due to the use of a piston pump or a flow instability. The metering characteristics of any orifice are influenced by the flow oscillations, and their effect must not be overlooked when precise metering is desired. Hence, considerable study has been performed about the influence of flow oscillation on fluid metering by orifices. However, little analytical study of oscillating flow through orifices was found in the literature. Most of the work is experimental and deals with the measurement and correlation of coefficients of discharge and other types of correction factors.

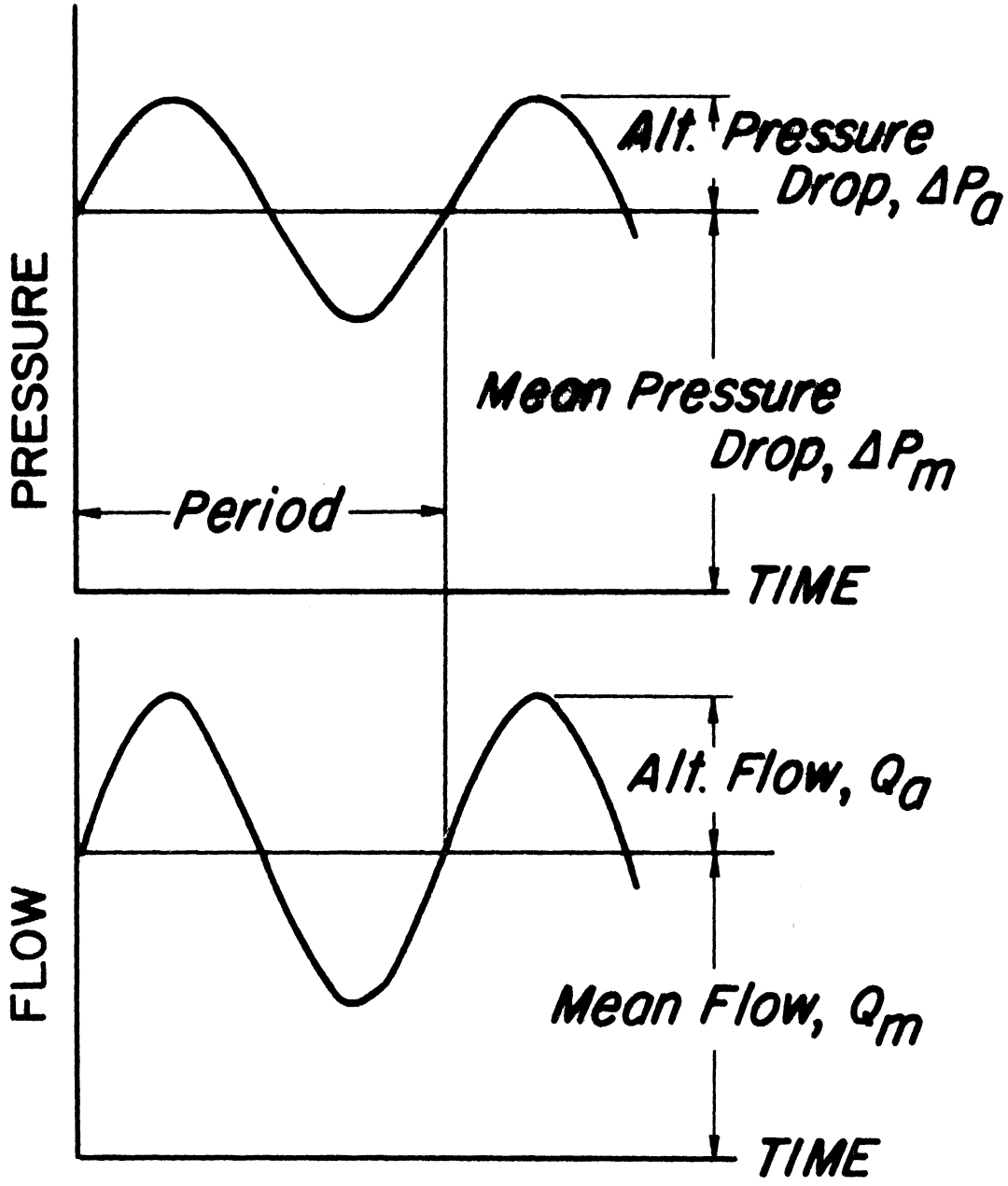

Figure 7. Mean and Alternating Components of Pressure and Flow.

Even though a complete theoretical analysis of oscillating flow through orifices has not been performed, the solution to the closely related problem of transient flow in an infinite tube has been published. Daneshyar (5) solved this problem for a pressure gradient which is an arbitrary function of time. However, the results of his studies can only be used in a qualitative way in reference to the orifice problem because entrance and exit effects and flow turbulence, which are not included in his studies, are most important.

Benson and Shafie (4) performed a theoretical and experimental study of the use of sharp-edged orifices to measure instantaneous air flow. They modeled the orifice as if it were composed of two sections: 1) sudden contraction and 2) sudden expansion. They then solved the one-dimensional, non-steady equations of continuity, energy and momentum for the two sections, and equate the solutions at their common plane, which is the exit plane of the orifice. Their experiments show that their analysis is limited to large orifice-to-pipe area-ratios and small pressure differences. They conclude that their analysis can be used to determine instantaneous mass flow rates if the aforementioned limitations are maintained.

The literature primarily contains experimental solutions to the orifice problem, and includes studies of both incompressible and compressible oscillating flow. For this work, incompressible flow is of interest, but the results of previous experiments with compressible fluid are also useful since many similarities do exist. Most of the previous testing has been done with compressible fluid, and, in some cases, the results have been applied to both compressible and incompressible flow.

A very comprehensive study of experimental work on pulsating-flow measurement by Oppenheim and Chilton (11) summarized the techniques of measuring oscillating flow. They presented a discussion of the fundamental aspects which must be considered when measuring oscillating flow, and then discussed the merits of several different methods of measuring it. This work also contains a large bibliography which makes it very useful to any further study of the subject.

Earles and Zarek (7) studied the flow of air through orifices of diameters 0.75 to 1.75 inches for oscillations up to 16 cycles/second. They measured a correction factor which is needed to adjust the steady-state coefficient of discharge to account for the influence of pressure pulsations. They correlated their correction factor with the dimensionless numbers of pressure intensity and Strouhal number, but they did not consider dependence of the correction factor upon Reynolds number, which varied from about 30,000 to 60,000, or upon Mach number, which varied approximately from .03 to .09. They did investigate the dependence of flow upon geometry and found that the position of the orifice along the pipe-length had a small measurable influence in most instances. Since their results are for a compressible fluid, it is not possible to quantitatively compare them to the results which are presented in this study. However, they do state that pressure intensity and Strouhal number are both important parameters in determining the influence of pressure pulsations on fluid flow.

Jeffery (9), under the supervision of Zarek, continued the study of the influence of pulsations on air metering by orifices. He extended the range of frequency to 33 cycles/second, and found that the time-average flow for pulsating pressure is dependent upon frequency,

pressure intensity, orifice-to-pipe area-ratio and mean flow. His data contains information on the influence of waveform of the pulsations upon the time-averaged flow.

In a later work, Zarek (14) summarized the efforts on measuring oscillating flow. He applied recent findings to the problem and made recommendations as to how inaccuracies, encountered in flow measurement with orifices, due to flow oscillation can be minimized. His data, plus that of Earles and Jeffery, showed that the true flow can be greater or less than that predicted by the average square-root of the pressure differential.

Sparks (12) measured the instantaneous flows of air through orifices in order to study the influence of pressure pulsations on time-averaged flow. He accomplished this with a hot-wire anemometer and attempted to plot his data as a function of flow ratio, but his plots show no consistent pattern. He further admits that he needed to consider the additional effects of Reynolds number, Eulers number, Mach number, pressure ratio and Strouhal number. He did observe the time-averaged flow to be different for pulsating pressure compared to the steady pressure, and his data show that flow oscillations can cause time-averaged flow to be greater or less than that for steady flow. He stated that he needed an order of magnitude of additional data in order to fully investigate the influence of all of the dimensionless variables.

Moseley(10) studied the influence of pulsation on water flow. He measured the periodic flow with a magnetic flow-meter up to frequencies of 9 cps and flow intensities (ratio of flow amplitude to mean flow) of 6.5 for orifices of about 2 inches diameter. His

Reynolds numbers ranged from 65,000 to 400,000. He presented a quasi-steady theory for accounting for the pulsations, and shows that the neglected effect of temporal acceleration is a good approximation for his low-frequency data. He plots his data in the form of an error parameter as a function of flow ratio. The error parameter is defined by coefficients of discharge for steady and pulsating flow as follows:

$$\text{error} = \frac{C_{DS}}{C_{DP}} - 1$$

His data show that pipe diameter-to-orifice diameter ratio has a small influence on the error parameter, and that the error can be negative at low flow ratio, which means the average flow under pulsating conditions can be greater than for steady conditions with the same average pressure differential.

Almost all of the recent literature on measuring oscillating flow mentions the square-root error. This is based upon the mathematical fact that in general:

$$\frac{1}{t} \int_0^t \Delta P^{1/2} \, dt \neq \frac{1}{t} \left[\int_0^t \Delta P \, dt \right]^{1/2},$$

or the square root of the integral does not equal the integral of the square root. Flow is known to be approximately proportional to the square root of pressure differential, but a manometer measures the average pressure-differential. Hence, the square-root error arises when the average flow is taken as proportional to the square root of the average pressure-differential, as measured by the manometer, and not proportional to the average of the square root of the pressure differential.

To summarize, no theory was found to accurately predict the time-averaged flow through an orifice when the flow is oscillating. However, the important dimensionless quantities have been defined, but

no experimenter was found to have taken sufficient data to correlate the flow with all of the necessary dimensionless numbers. All of the data found shows scatter of at least ±10%, and any correlation of flow or coefficient of discharge with any dimensionless variable has been for limited ranges of the other important dimensionless variables. Most important, as to the work performed here, no data was found for the influence of flow oscillations on small orifices. Also, few investigators attempted to measure instantaneous flow, but rather only measured the instantaneous pressure differential, and most data is for relatively low frequency (less than 50 cps).

3.3 Objectives of Orifice Tests

The main objective of the orifice test program was to determine the influence of flow oscillation, and, consequently, pressure pulsation of a sinusoidal wave form, on the time-average flow through an orifice. This was to be done for one incompressible fluid (mineral spirits) and several geometrically different, small orifices (about .050 inch in diameter). Instantaneous pressure and flow were to be measured for steady-oscillatory flow conditions at frequencies up to 100 cps. The fluid viscosity and density were to be accurately determined for use in analyzing the data.

The objectives were also to include the correlation of the data in terms of the important independent variables. Several independent dimensionless variables, which have been suggested in the literature, were to be investigated as to their influence on the flow through small orifices. A systematic method of organizaing the data for the small orifices was sought, which would include a simplified analysis to indicate the relative importance of the many independent variables.

3.4 Description of Orifice Testing Rig

Figure 8 is a schematic diagram of the testing facility, which is used to determine the influence of flow oscillations. Its most unique feature is the use of pistons to force the fluid through the orifice, and, thereby, provide the desired volume-flow. As shown, two pistons are used: one piston is moved at a steady rate to provide steady flow, and the second piston is moved at an oscillating rate to provide an oscillating component of flow. A strain-gage pressure transducer is used to measure the instantaneous pressure differential. The entire facility can also be pressurized to minimize the possibility of cavitation, which would destroy the continuity relationship needed to calculate the flow from the motion of the pistons.

The detail of the orifice test-block can be more closely examined in Figure 9, which is a cutaway scale drawing of it. As the figure indicates, all of the seals are of the O-ring type, including the sliding seal for the oscillating piston. The figure also indicates the location of the pressure transducer with respect to the orifice and the alternating piston. The fluid reservoir and valve which connect it to the orifice block are also shown as well as the fluid-flow-path through the orifice block.

Figure 10 shows the entire orifice testing rig, including the instrumentation, which is shown on the rack at the left. The Visicorder, which is used to record the time traces of pressure and flow, is on the top shelf of the rack, two Carrier Bridge amplifiers, which power the strain gage circuits and amplify their signal, are on the middle two shelves, and a galvonometer amplifier is on the bottom shelf. The testing rig is shown on the bench to the right.

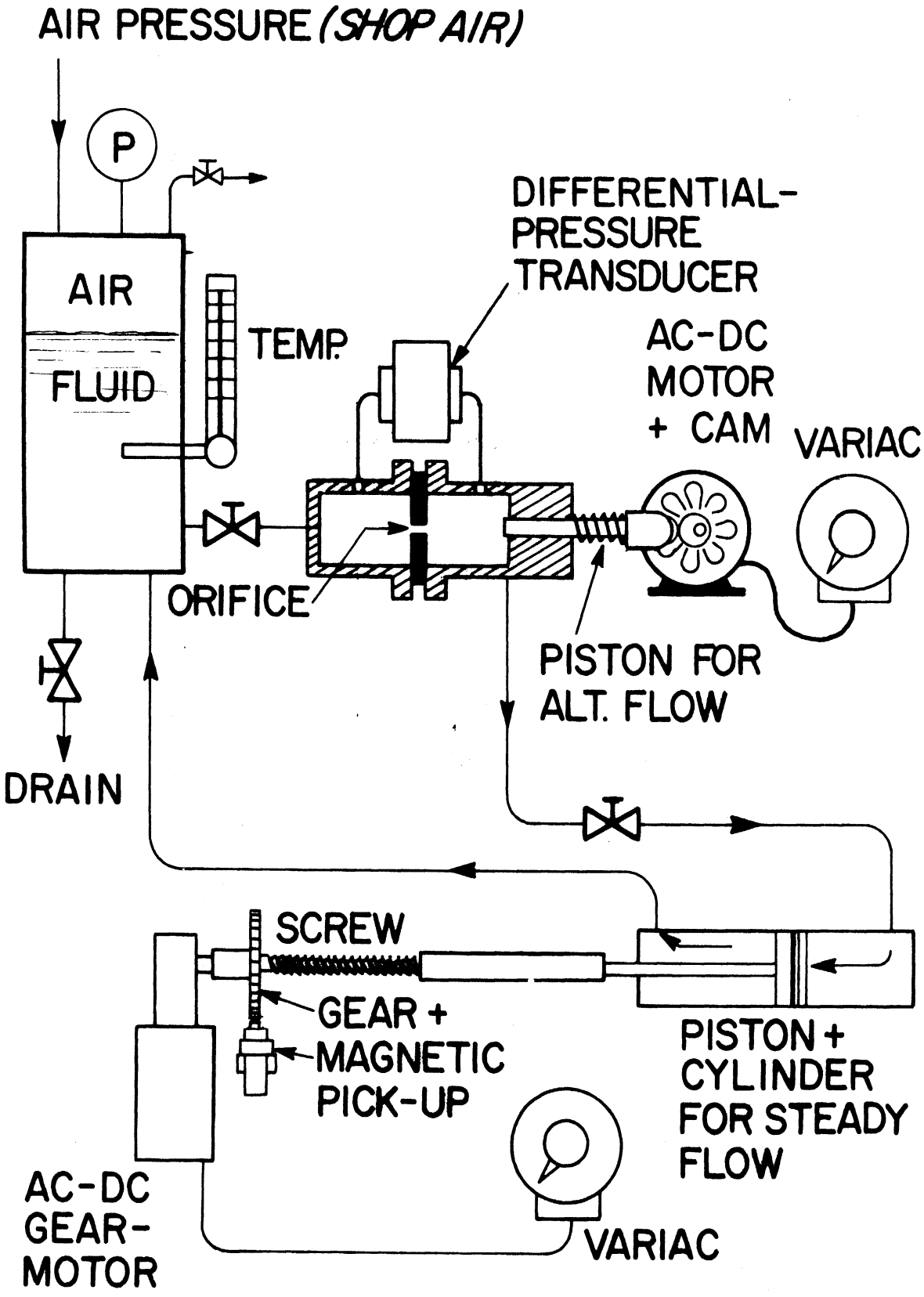

Figure 8. Schematic of Orifice Testing Rig.

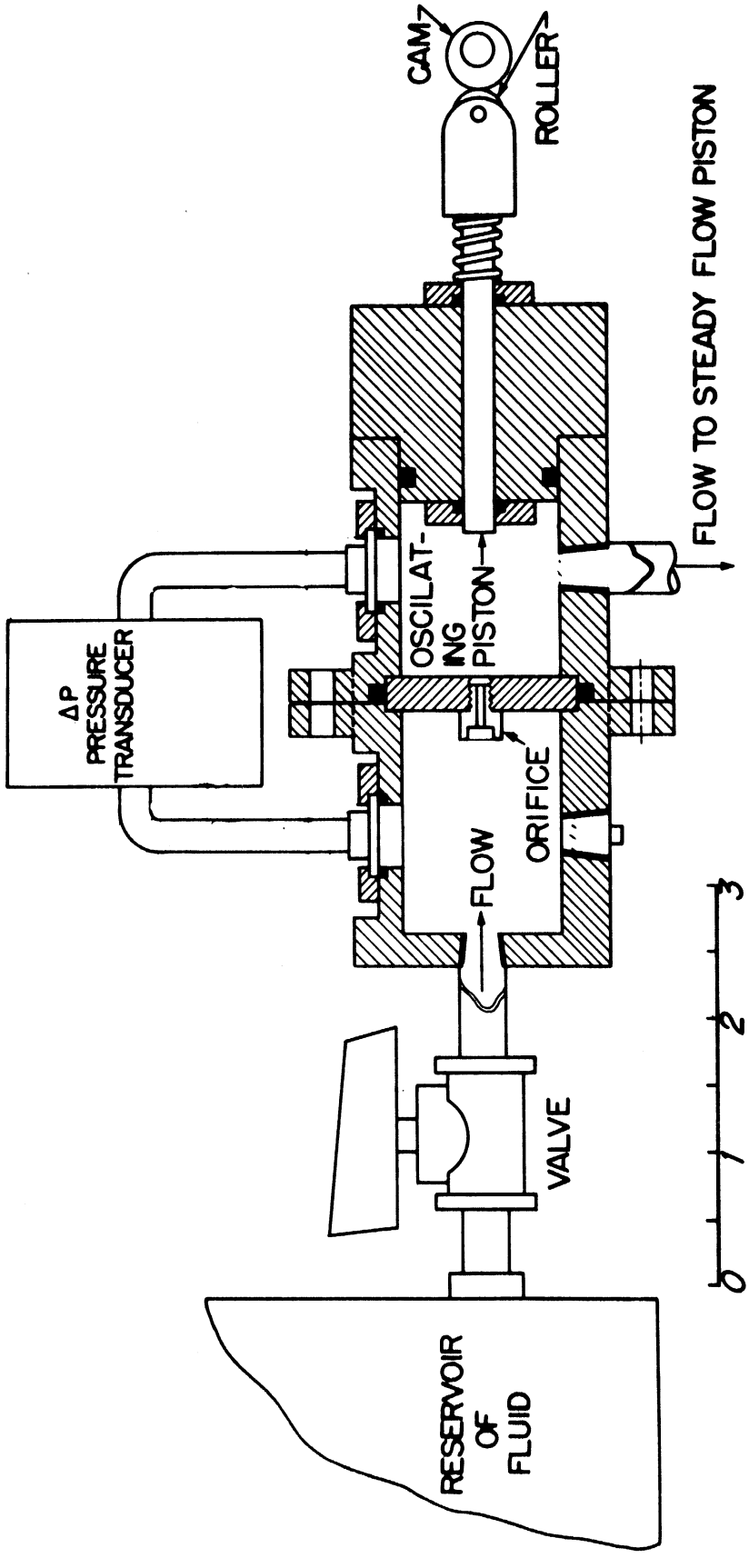

Figure 9. Cut-away of Orifice Test Block.

Figure 11 shows an overall view of the testing rig. The large cylinder with the temperature and pressure gages is the fluid reservoir. The orifice block is connected to the fluid reservoir on the right by a valve. The cam and motor drive mechanism for the oscillating piston are shown to the right of the orifice block. The mean-flow cylinder is hidden immediately below the orifice test block, but its gear-motor and screw drive mechanism are visible to the left. Two Variacs are visible in the foreground which are used to control the speed of the motors. The switches in the box at the left are used to turn on the gear-motor and reverse its direction.

3.5 Instrumentation

Basically, five quantities must be measured which are: 1) mean pressure differential, 2) alternating pressure differential, 3) mean flow, 4) alternating flow, and 5) frequency. A standard commercial pressure transducer is used to obtain mean and alternating pressure differentials. Mean flow is obtained from the period of the signal from the magnetic pick-up. Alternating flow is determined from a strain gage displacement transducer mounted to the oscillating piston, and frequency is found with the use of a timing mark provided by the Visicorder. Table I lists the commercial instruments which were used in the testing as well as the other commercially made apparatus.

Pressure Transducer

The pressure transducer, which is connected to each side of the orifice block as shown in Figure 12 was initially calibrated with a water manometer. A pressure (or vacuum) was applied to one side of the transducer and it was measured with the manometer. The pressure was set at increments of about 10 inches of water over the range of ± 45in.H_2O.

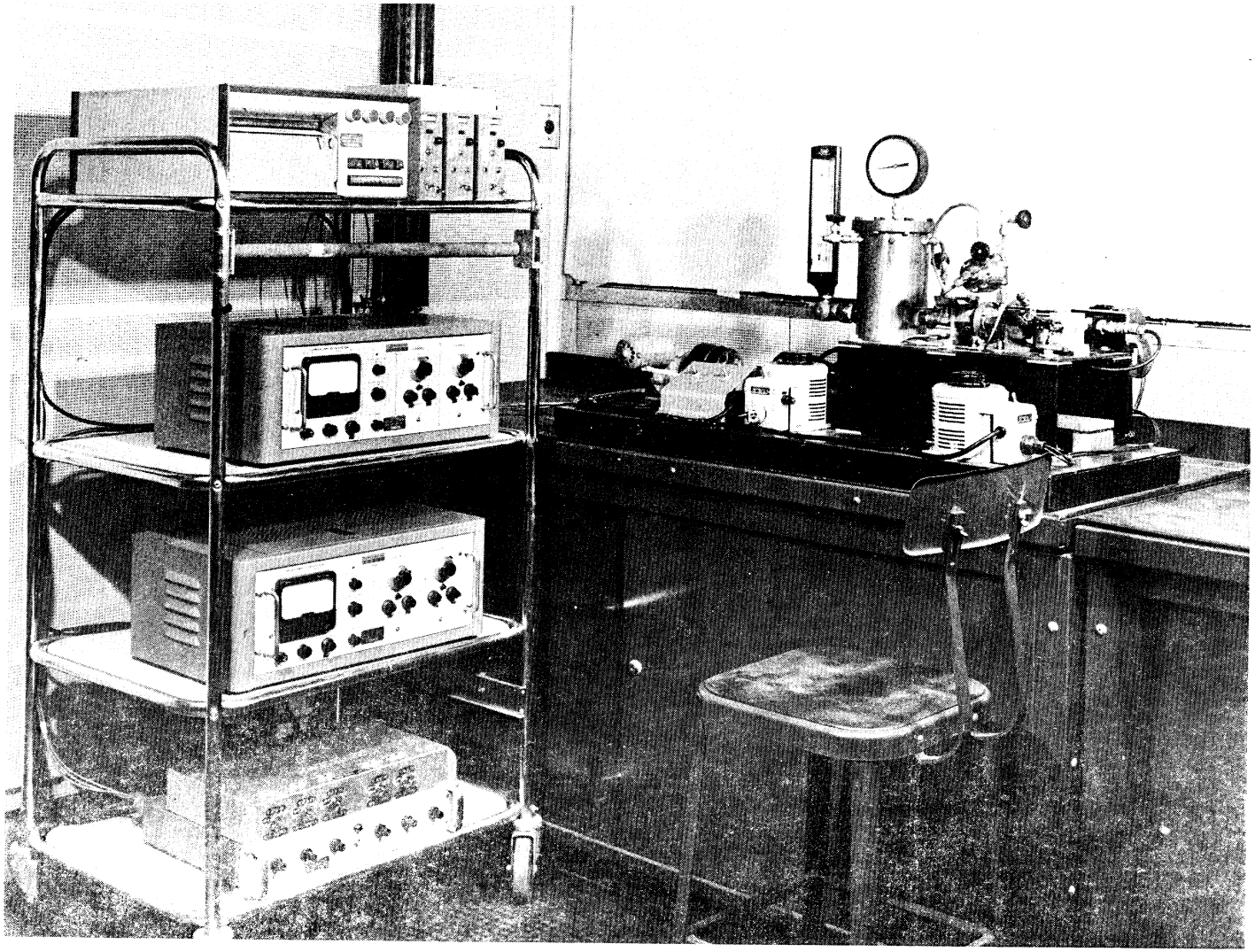

Figure 10. Orifice Testing Equipment and Instrumentation.

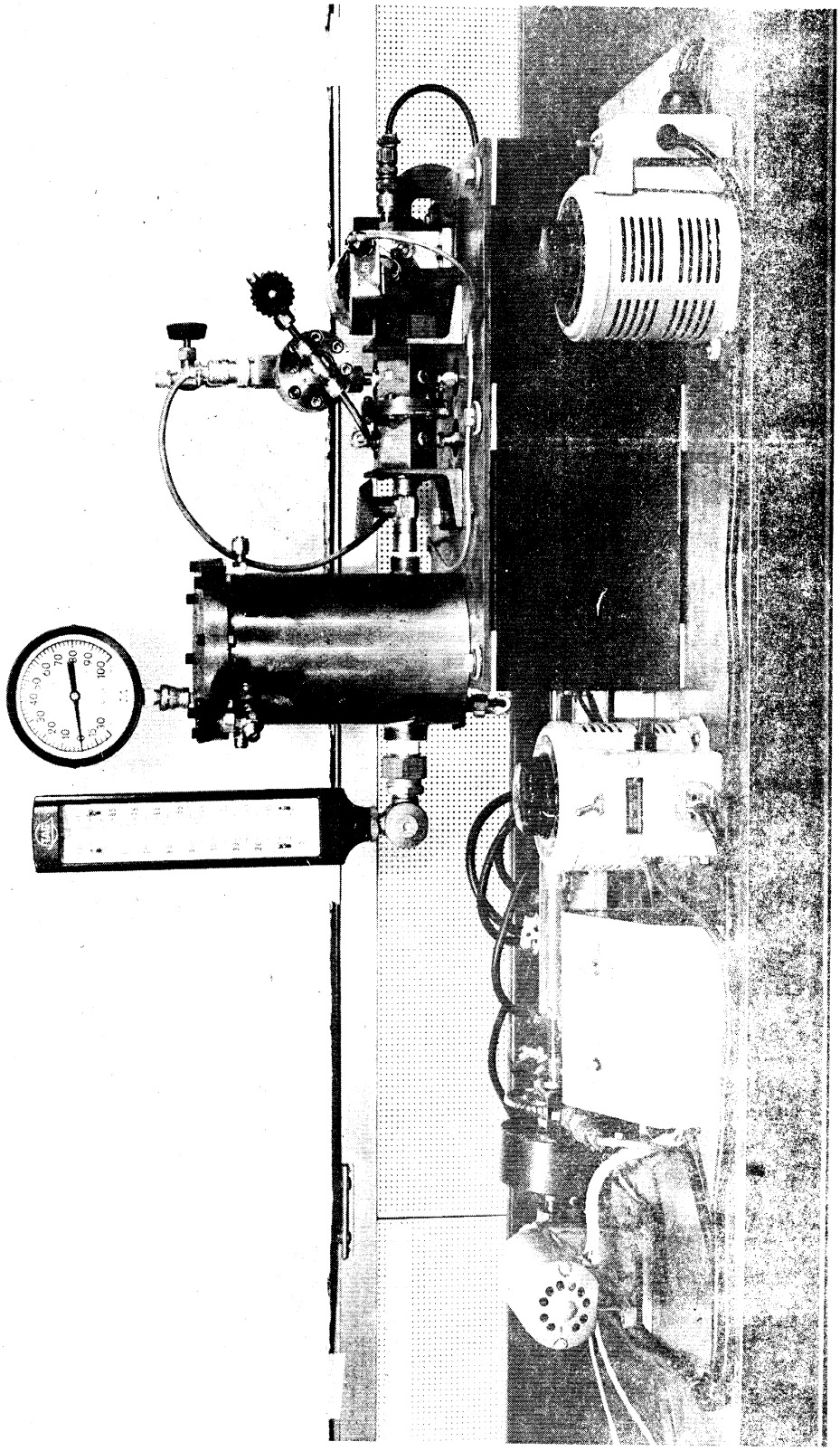

Figure 11. Orifice Testing Equipment.

TABLE I

EQUIPMENT LIST FOR ORIFICE TESTING RIG

Item	Brand	Model Number	Serial Number	Range
Magnetic pick-up	Electro-Mation	3010-AN		
Thermometer	Tagliable			0-100°F
Pressure gage	Marshalltown			30 in Hg. vac 100 psi.
Variac	Superior	116-B		1.4 kva, 0-140 volts out
Gearmotor AC-DC	Dayton	4K872		0-306 N/L rpm 0-100 F/L rpm
Motor AC-DC	Dayton	2M139		1/5 HP at 10,000 rpm.
Differential Pressure Transducer	Viatran	PTB 209	142469	±10 psid

The deflection of the Visicorder trace was recorded for each pressure point. Then a plot was made of inches of water pressure versus inches of recorder deflection. Figure 13 shows the calibration curve for the pressure transducer.

The calibration curve also shows values of deflection (in tabular form) for calibration resistors. These are special resistors which are contained in the amplifier and can be switched in parallel with one of the strain gages of the 4-gage bridge circuit of the pressure transducer. When this is done, an electrical unbalance in the transducer bridge circuit is created which simulates the same unbalance created by pressure on the transducer. These calibration resistors can then be used to later set the gain of the amplifiers to different values without the need of recalibration. That is, if the deflection for a given calibration resistor is twice what it is for the calibration curve, then the gain of the amplifier must be double what it was for the calibration curve. Therefore, values of pressure taken from the calibration curve are twice the actual pressure, or the actual pressure is only half the indicated value on the calibration curve.

Steady Flow

As previously mentioned, the steady flow is measured with a gear and magnetic pick-up arrangement. The gear is connected to the drive screw of the steady-flow cylinder, as shown in Figure 14. The drive screw has a pitch of 0.1 inch and the gear has 54 teeth, so that the period of the signal from the magnetic pick-up corresponds to 1/540 inch of piston travel. The diameter of the piston is one inch; therefore, the period of the signal corresponds to .00144 cu. in. of

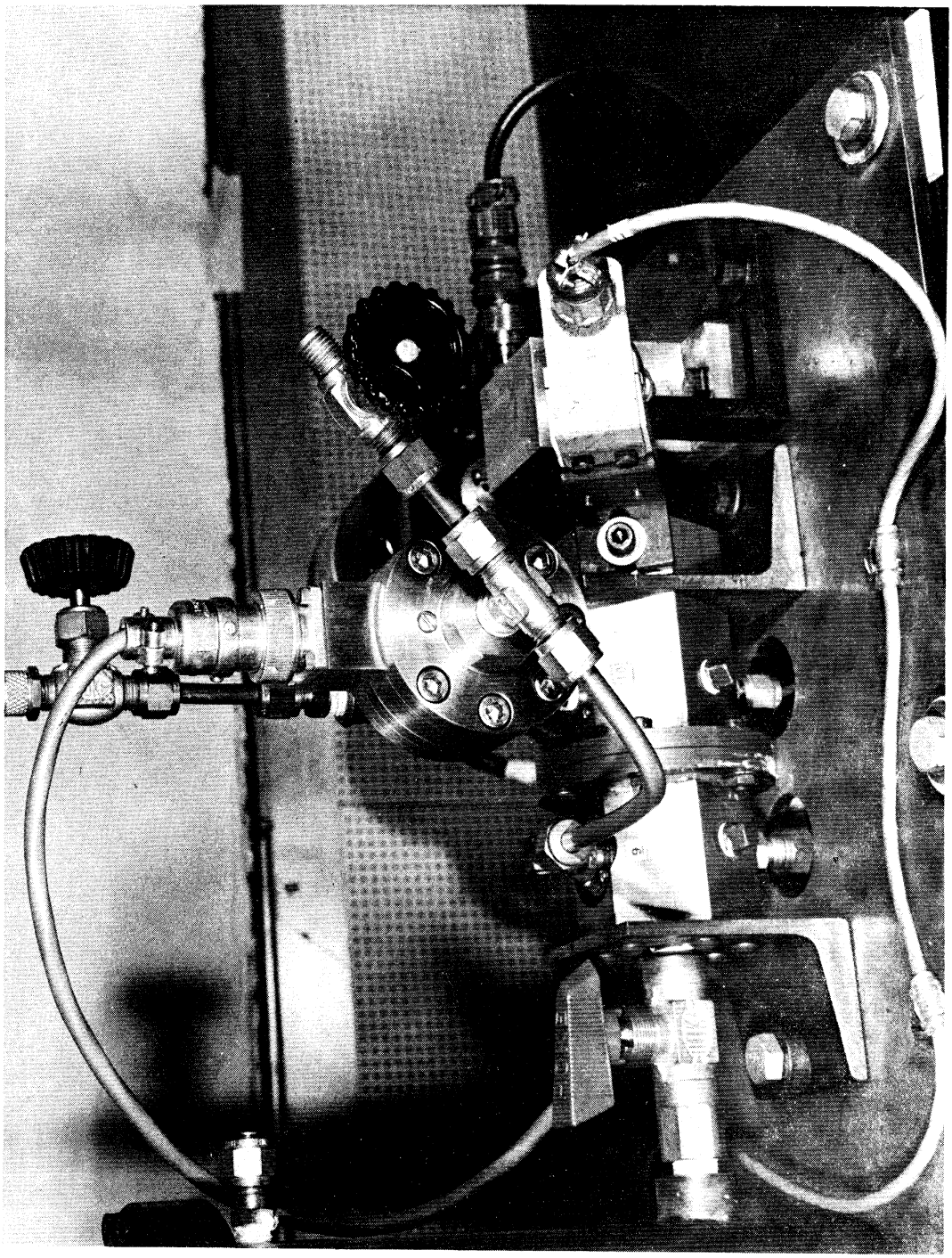

Figure 12. Orifice Test Block and Pressure Transducer.

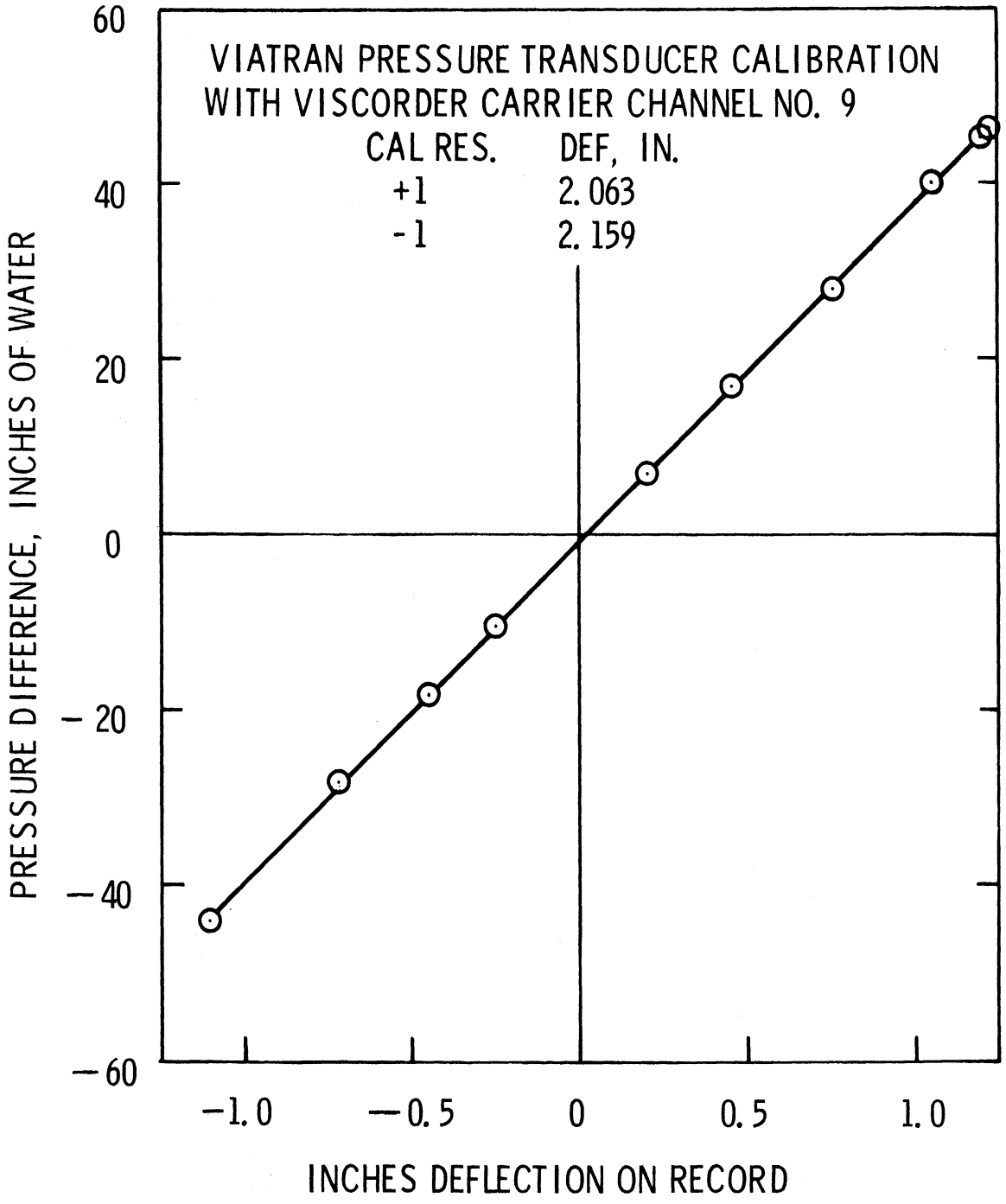

Figure 13. Pressure Transducer Calibration Curve.

piston displacement. Maximum no-load speed of the gear motor is 306 rpm, which gives a maximum flow capacity of 6.25 gph.

Alternating Flow

Figure 15 shows the transducer used to measure the displacement of the alternating piston. It is constructed of a piece of flat spring steel (.020 x 0.500 inch in cross-section; 2-1/2 in. long) which is firmly attached to the orifice block at one end and to the alternating piston at the other end. Four strain gages are mounted to the flat part of the spring to measure the strain in the spring, hence indicate the motion of the end of the spring which is attached to the piston. The four strain gages are wired in a Wheatstone bridge circuit and are powered by a Carrier Amplifier, the same as for the pressure transducer. The trace recorded by the Visicorder indicates the displacement of the alternating piston. A dial-gage indicator is used to calibrate this displacement transducer to thousandths of an inch of accuracy. Also, the frequency of the displacement is used to determine the frequency of the flow.

3.6 Fluid Compression: Blank Orifice Test

The means of measuring the alternating flow from the motion of the oscillating piston requires that the flow be incompressible, and the testing rig be infinitely stiff. This, of course, is not true, and some fluid compression and testing rig strain will occur when the fluid pressure within the orifice test block is changed. The fluid compression and testing rig strain represent a volume change; hence, part of the alternating-piston motion. This leads to an error in flow measurement if the flow through the orifice is assumed equal to the swept volume of the piston. Therefore, a blank test was performed to measure the amount of

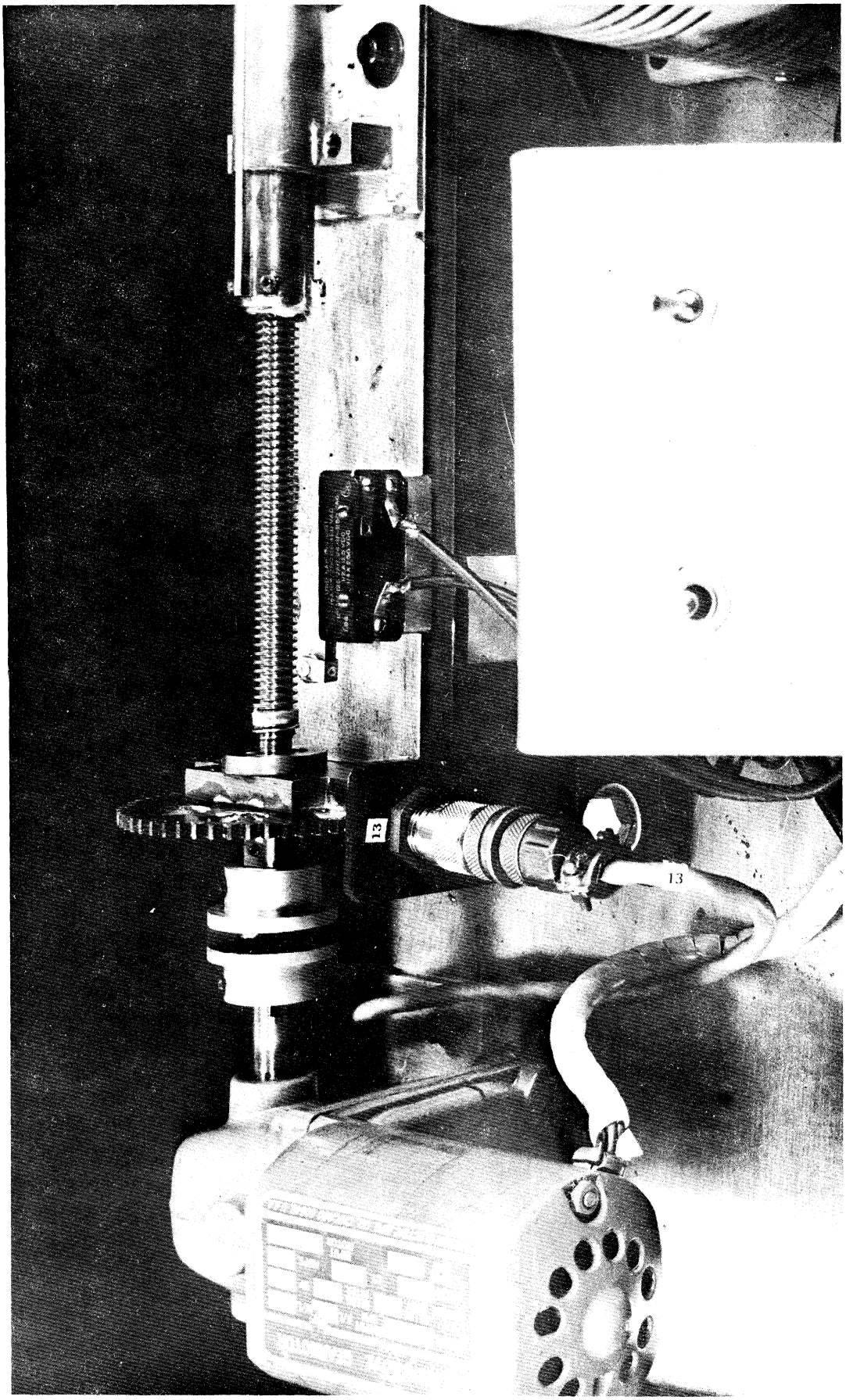

Figure 14. Drive Mechanism for Steady-Flow Piston.

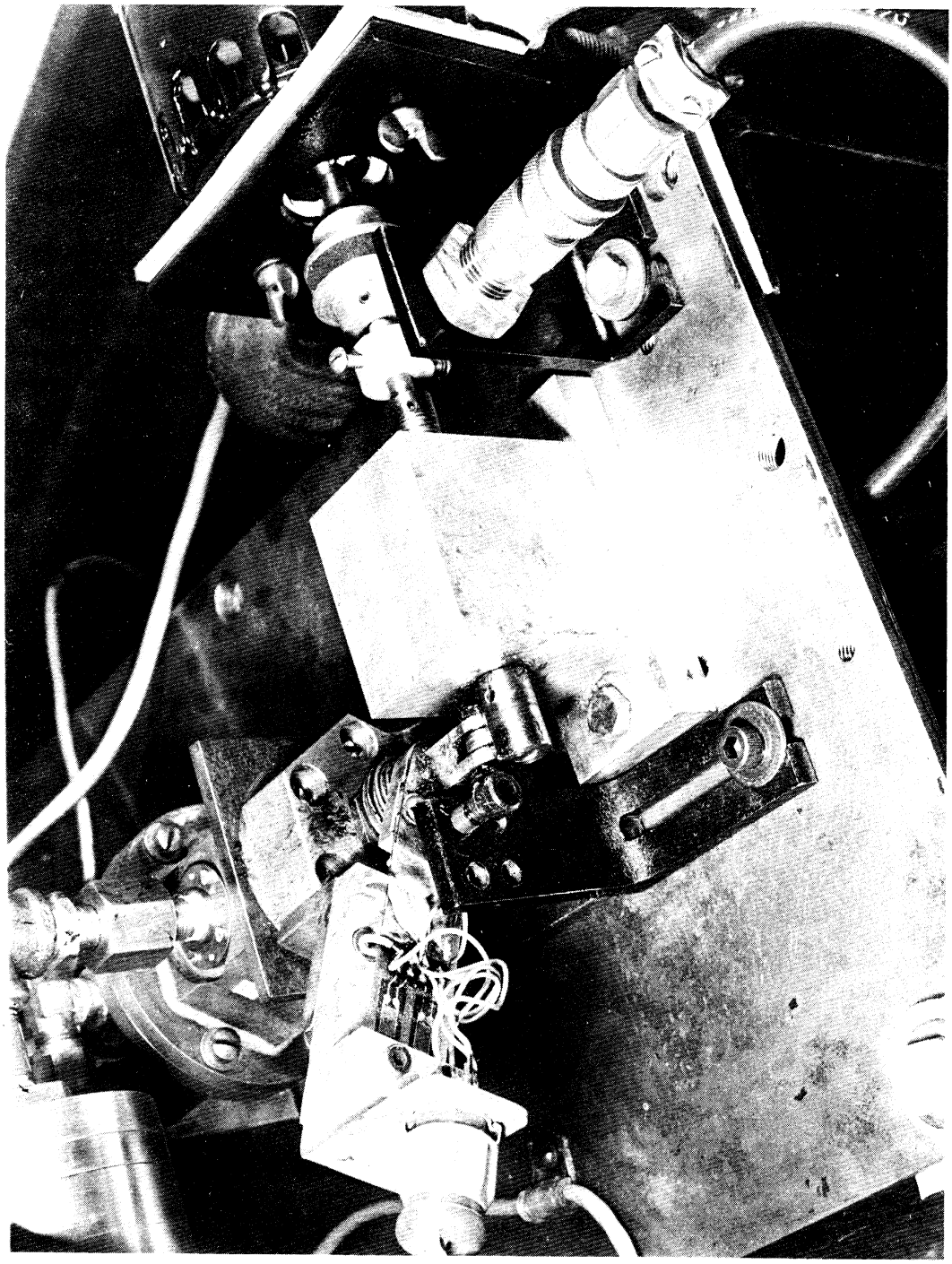

Figure 15. Cam Mechanism for Alternating-Flow Piston.

piston motion which serves to strain the orifice testing-rig and to compress the fluid.

A blank was installed in place of an orifice, as shown in Figure 16, which made the orifice test block, mean flow cylinder, and pressure transducer into a sealed cavity full of mineral spirits. Any piston motion, therefore, represented fluid compression and system strain. The alternating piston was then oscillated at a very small amplitude and the corresponding increase in pressure measured with the pressure transducer. This was done for several frequencies, and the results of pressure amplitude versus frequency are shown in Figure 17.

The results show that the pressure amplitude is relatively constant up to a frequency of 80 cps, and the pressure of the system is in phase with the piston motion. In other words, quasi-steady conditions prevail, and any change in volume created by the piston motion is offset by compression of the fluid and strain of the orifice testing block.

On the other hand, at frequencies greater than 100 cps, the pressure amplitude is much greater than the constant value at lower frequencies. A phase shift is also noted between pressure and displacement, which means that the system remained in a state of strain while the piston partially returned to its starting position. In other words, the response of the strain is limited to 100 cps, and considerable error will be encountered if data for frequencies greater than 100 cps are taken.

Any air, that is trapped in the system, will also negate the assumption of incompressibility which is needed to calculate the flow from the motion of the pistons. Notice the glass tube and shut-off valve above the pressure transducer in Figure 11. This tube was

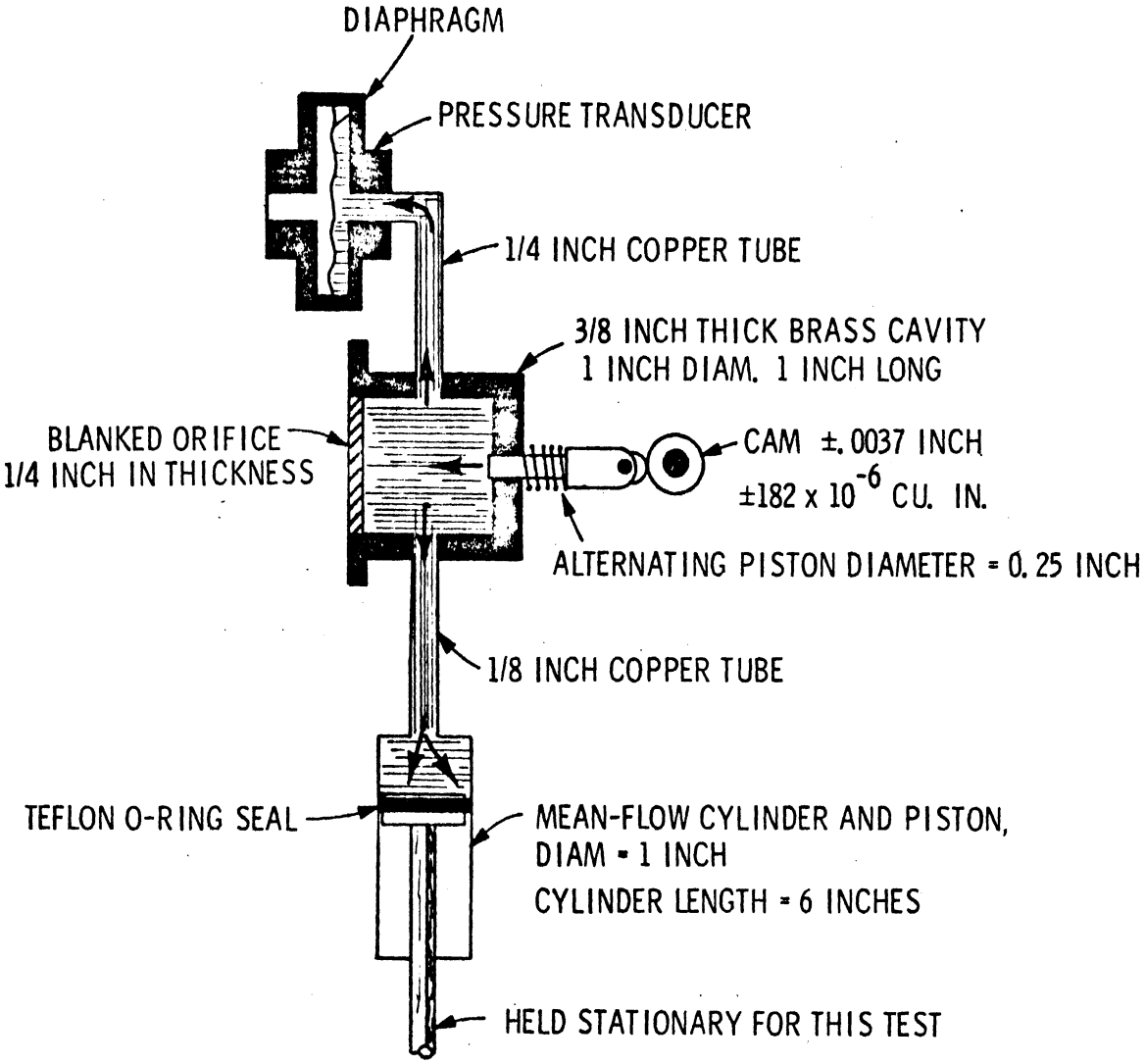

Figure 16. Schematic for Blanked Orifice Test.

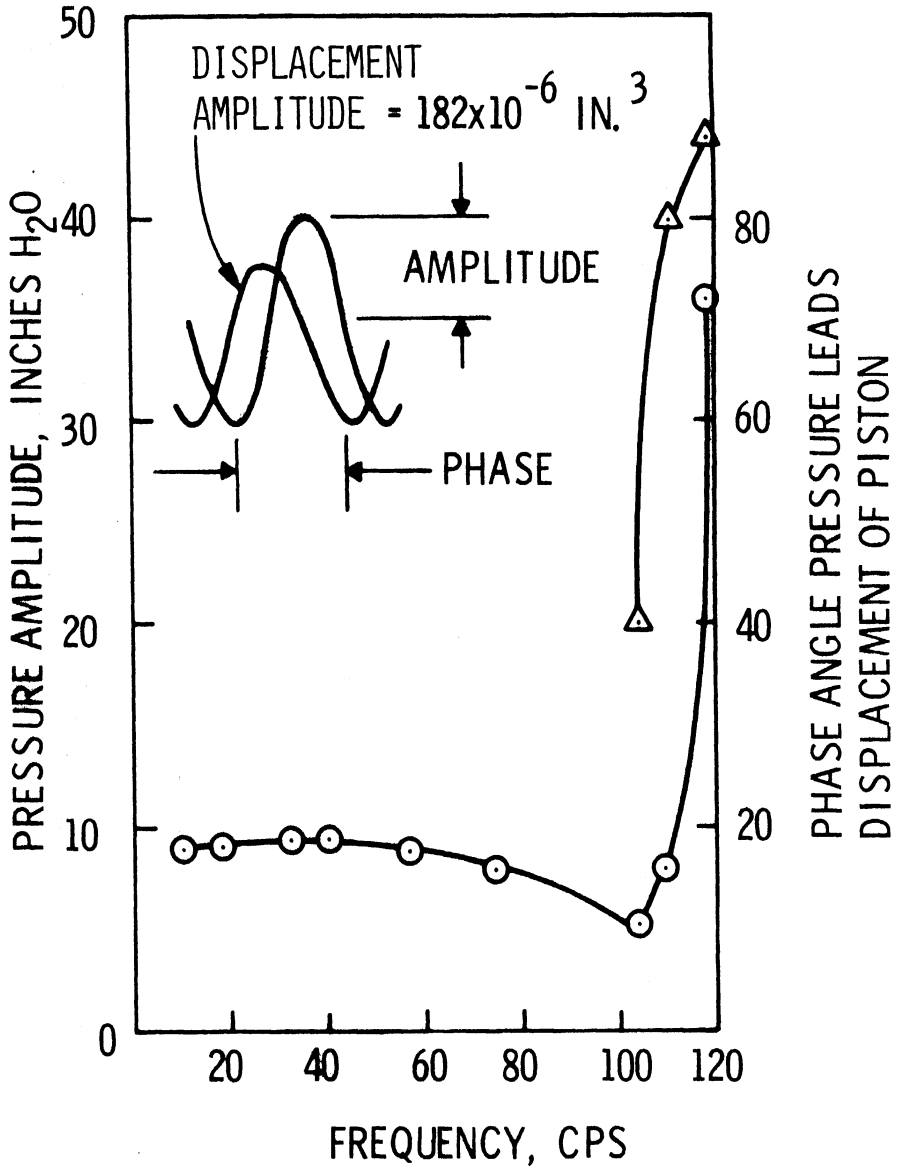

Figure 17. Results of Blanked Orifice Test.

partially filled with fluid to form a miniscus, the shut-off valve was opened, and the valve to the reservoir was closed. Pressure was applied (about 1.0 psi) to the open end of the tube, and any motion of the miniscus was noted. When the test cavity was completely full of liquid with no entrapped air, only a slight motion (about .030 inch) of the miniscus was caused by a pressure of 1.0 psi. This represents little compression since the tube is only .125 inch i.d. Any slight bubble of air, which was trapped in the system, caused a large increase in miniscus motion (greater than 0.5 inch). The miniscus motion was so sensitive to entrapped air that the mean flow cylinder had to be completely assembled while immersed in test fluid. This insured that no air was trapped in the tiny cavities between o-rings and o-ring groves, and was the only method found successful in eliminating entrapped air.

3.7 Test Procedure

The procedure for taking data is started by setting the speed of the alternating piston motor to correspond to some desired frequency. The variac for the mean-flow piston motor is then set to a value to give some desired mean flow-rate. The mean flow is then started by switching on the gear motor. About 100 cycles is recorded on the Visicorder paper for the data of one setting of flow and frequency. The setting of the mean flow is then changed and the procedure is repeated.

When the frequency of the alternating flow is to be changed, the cam which drives the alternating piston must also be changed in order to maintain the same magnitude of alternating flow-rate, because the alternating flow is proportional to the product of the piston displacement and the frequency. Therefore, if the frequency is to be doubled, the cam displacement must be halved. The cams are fixed by

TABLE II

ORIFICE SPECIFICATIONS

Test No.	Orifice Type	Diam., inches	Length, inches	Length, diam.
2470	F-50**	0.0497	0.1837	3.70
7770	S.E.*	0.0518	0.0375	7.24
78701	S.E.*	0.0518	0.1880	3.63
78702	S.E.*	0.0518	0.0319	0.62

* S.E.: Square Edge Orifice

** F-50: Standard Ford Main-Metering Orifice

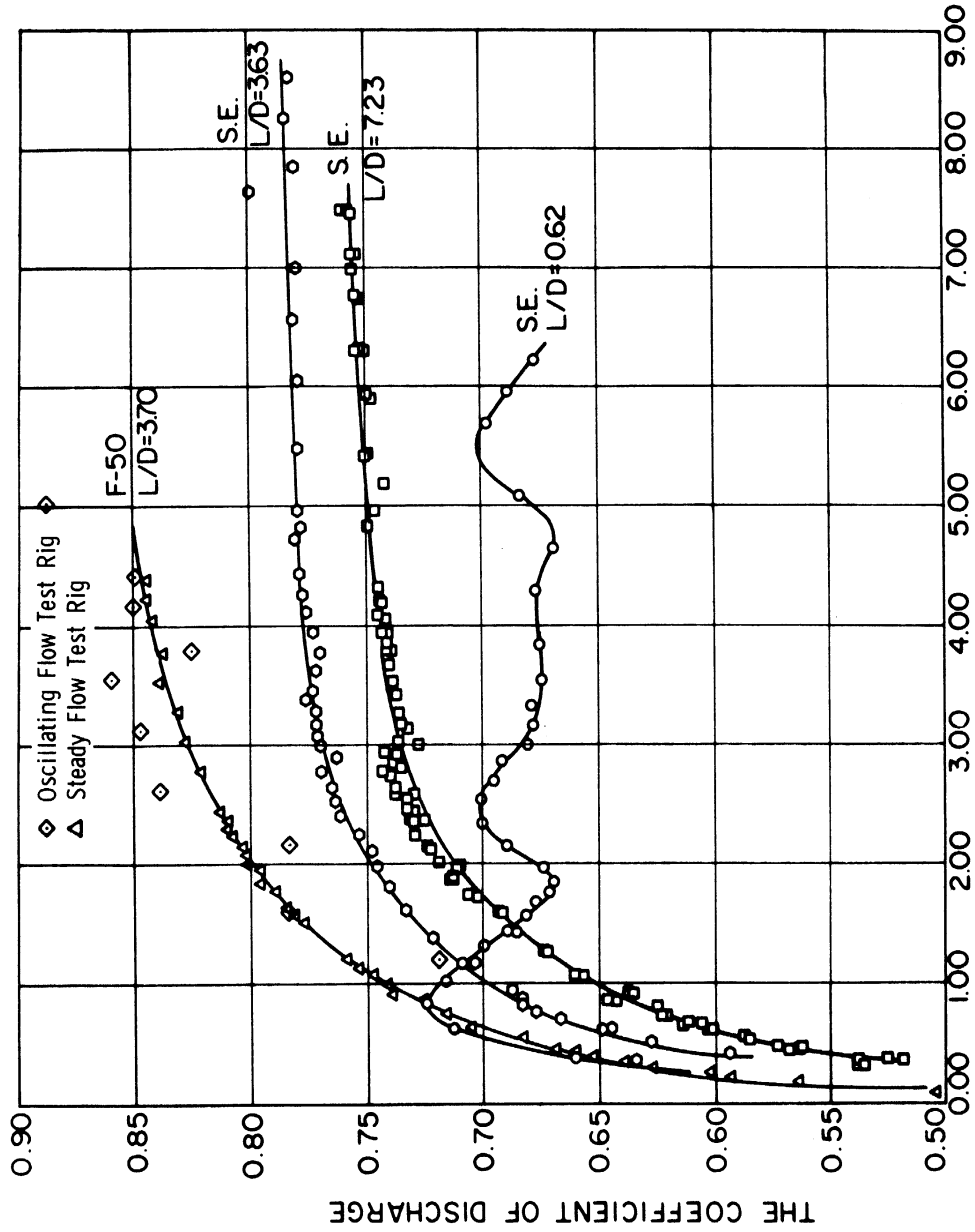

Figure 18. Steady-State Flow Coefficients of Discharge.

TABLE III

ORIFICE TEST VARIABLES

Test No.	Fluid Temp °F	Max. Freq. cps	Max. Flows			Max. Pressure Diff.		
			Mean cu.ft/hr.	Alt. cu.ft/hr.	Alt / Mean	Mean	Alt. psi.	Alt. / Mean
2470	77.8-84.2	99.7	0.85	0.49	2.54	2.45	2.44	7.80
7770	88.8-89.2	91.7	0.85	0.52	2.04	2.42	3.90	8.30
78701	75.1-78.9	88.0	0.80	0.50	1.65	1.95	3.18	3.80
78702	75.2-75.7	90.9	0.79	0.51	1.60	3.01	2.58	1.59

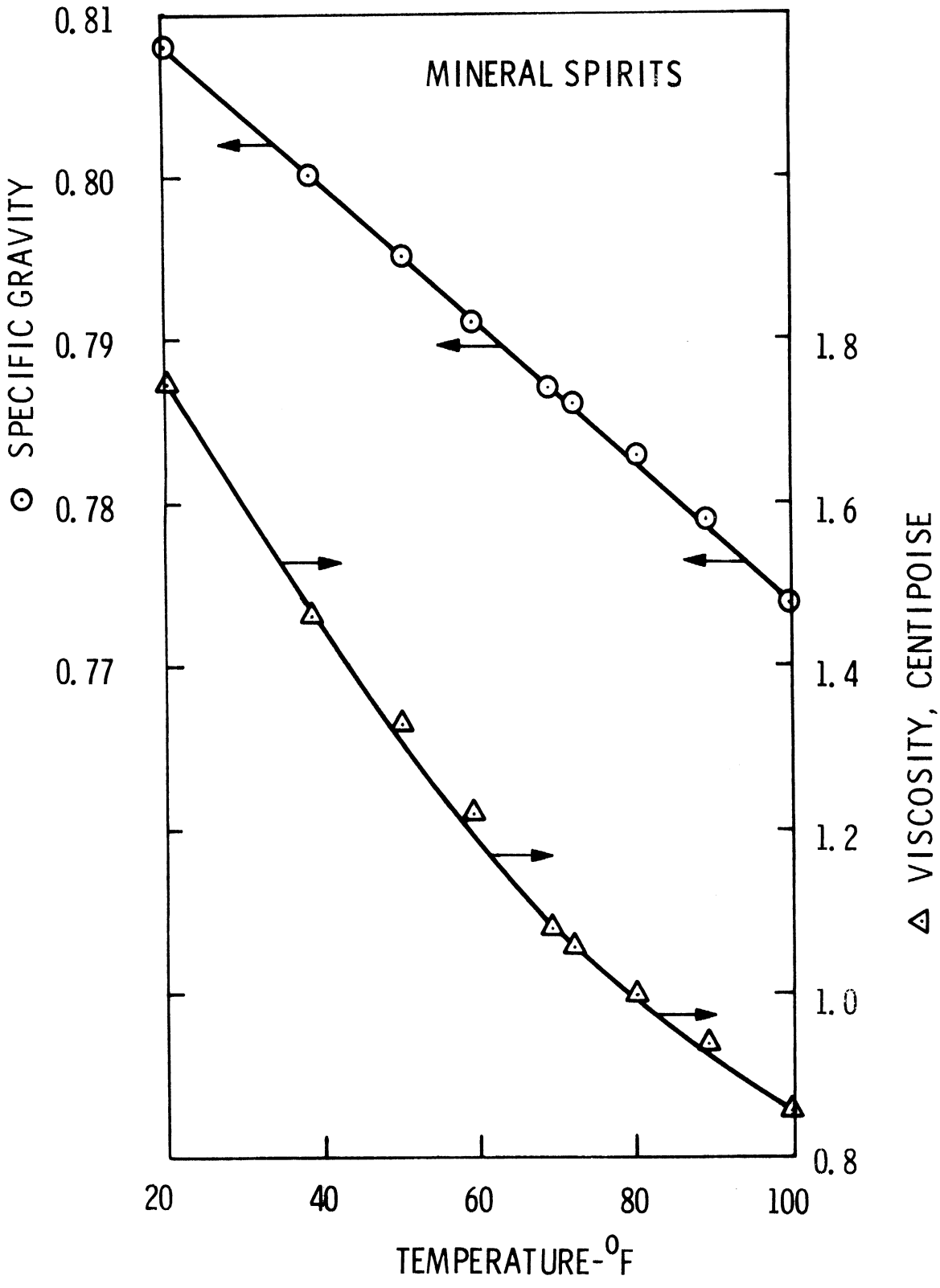

Figure 19. Test Fluid Properties.

an allen-head set screw, which can be seen in Figure 15, and are easily changed.

The test orifices are similar to those found in carburetors (about .050 inches in diameter) and are of different lengths as shown in Table II. The square-edged orifices (S.E.) are made of brass, while the F-50 orifice is of steel. Steady flow data for the orifices is shown in Figure 18, and it was obtained by a means independent of the tests performed here. The data is, however, for the very same orifices, but the method for measuring only the steady-flow performance was much more accurate than the method used here. This is the data used by Harrington (21) in his digital computer simulation of carburetor metering, and his work discusses the details of the steady-state flow measurements. As indicated in the figure, steady-state coefficients for the F-50 orifice were also taken with the oscillating-flow test rig for comparison to the data of Harrington. The amount of scatter indicates that the accuracy with which the average flow can be measured with the oscillating-flow test rig is about $\pm 5\%$.

A total of four tests were run, and the variables of the tests are listed in Table III. About 200 data points were taken for each orifice for various combinations of frequency, average flow, and alternating flow. The fluid used for the tests was mineral spirits, a fluid similar to gasoline, and its properties are shown in Figure 19.

3.8 Ideal Oscillating Flow Through an Orifice

In order to gain some insight into the flow of an oscillating fluid through an orifice, a very simple model of the flow was devised. The information obtained from the model leads to the development of some dimensionless variables which are needed to describe the results of the

experiments. More important, however, is that the model also gives an idealized function which relates the dimensionless variables. Therefore, not only are the axes determined on which to plot the data, but also an approximation of the function which the data should follow.

Ideal flow through an orifice is described by the equation of motion for the orifice flow. Frictionless flow and a uniform velocity profile are assumed. Also, all of the fluid which oscillates is assumed to be contained within the orifice length. These assumptions make the solution ideal because frictional losses are not considered, nor are the inertial forces which are caused by the oscillation of the fluid outside the orifice length.

Consider the orifice and control volume shown in Figure 20. The equation of motion for this control volume is written as:

$$A(P_1-P_2) = \frac{d}{dt} \rho V d\forall = \rho AL \frac{dV}{dt} \tag{3.1}$$

$$P_1-P_2 = \rho L \frac{dV}{dt} \tag{3.2}$$

The pressure tap at the upstream point, P_1, will record the total pressure which is given by the Bernoulli equation as:

$$P_{T1} = P_1 + \frac{\rho V^2}{2} \tag{3.3}$$

whereas the downstream pressure tap will record the static pressure of the jet of the fluid issuing from the orifice. Therefore, the equation of motion can again be written as:

$$P_{T1} - \frac{\rho V^2}{2} - P_2 = \rho L \frac{dV}{dt} \tag{3.1a}$$

or

$$\Delta P - \frac{\rho V^2}{2} = \rho L \frac{dV}{dt} \tag{3.1b}$$

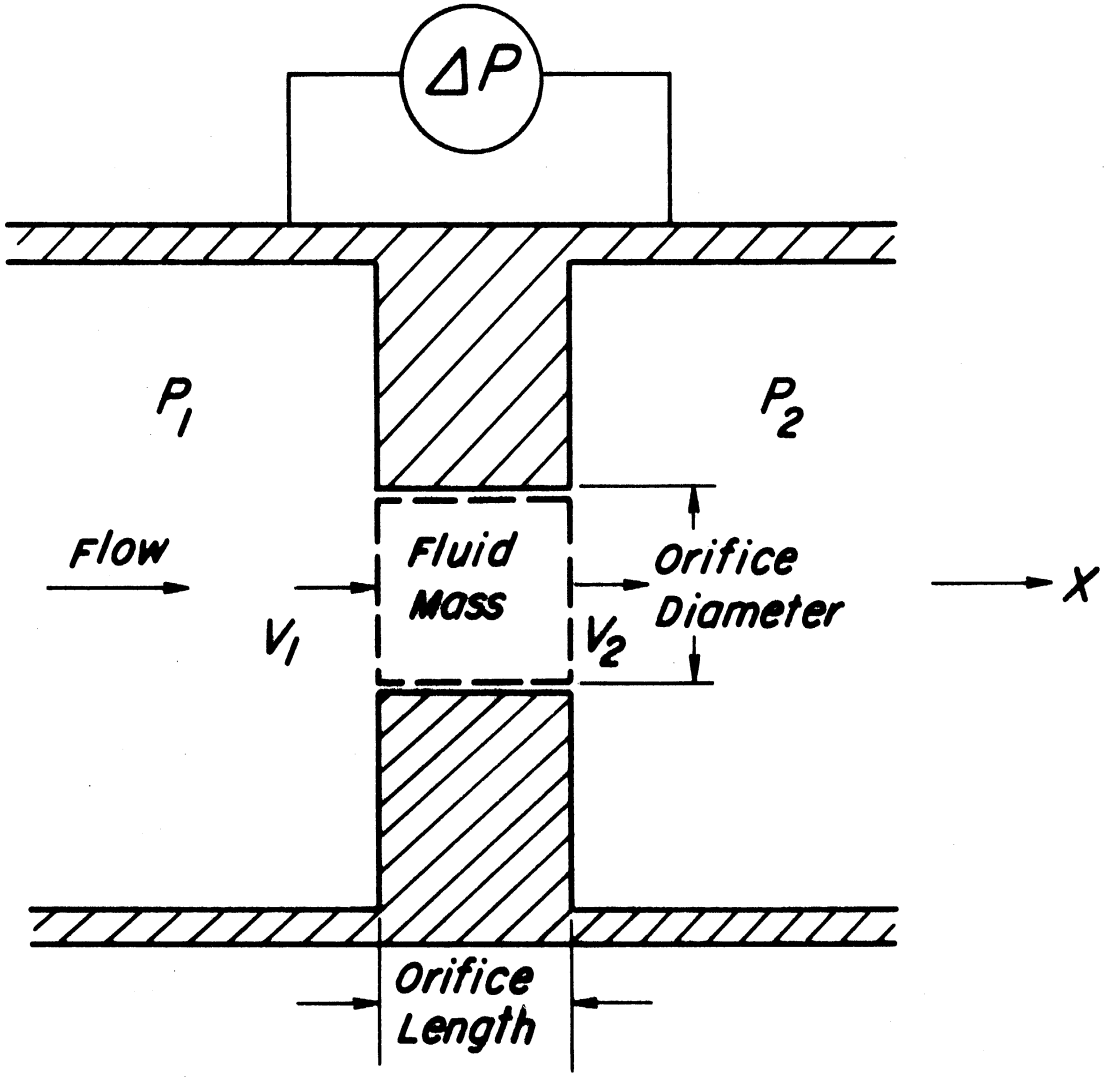

$$\Delta Q = \Delta Q_m + \Delta Q_a \sin(wt)$$

Figure 20. Control Volume for Orifice Analysis.

where ΔP is the pressure difference which would be recorded by the meter with taps immediately upstream and downstream of the orifice, as shown in Figure 20.

It must be noted, however, that when the flow reverses, the pressure at tap #1 would be static pressure, and at tap #2 would be total pressure. Equation 3.1b then becomes:

$$\Delta P + \frac{\rho V^2}{2} = \rho L \frac{dV}{dt} \tag{3.1c}$$

or, in general, for both cases of flow direction:

$$\Delta P - \frac{\rho V|V|}{2} = \rho L \frac{dV}{dt} \tag{3.1d}$$

The flow through the orifice is oscillatory and has a mean component and a sinusoidally varying alternating component so that it can be expressed mathematically as follows:

$$Q(t) = Q_M + Q_A \text{ SIN } (\omega t) \tag{3.4}$$

$$V = Q/A \tag{3.5}$$

$$V(t) = V_M + V_A \text{ SIN } (\omega t) \tag{3.6}$$

$$\frac{dV}{dt} = \omega V_A \text{ COS } (\omega t) \tag{3.7}$$

By substituting the above relationships, Equation 3.1d becomes:

$$\Delta P(t) = \omega V_A \rho L \text{ COS}(\omega t) + \frac{\rho}{2} (V_M + V_A \text{ SIN}(\omega t))|V_M + V_A \text{ SIN } (\omega t)| \tag{3.1e}$$

Since;

$$H(t) = \Delta P(t)/\rho g \tag{3.8}$$

Equation can be finally written as;

$$H(t) = \frac{\omega V_A L}{g} \text{ COS}(\omega t) + \frac{1}{2g} (V_M + V_A \text{ SIN}(\omega t))|V_M + V_A \text{ SIN}(\omega t)| \tag{3.1f}$$

The above equation gives the instantaneous head differential across the orifice in terms of the mean and alternating components of sinusoidally varying flow or velocity. The equation becomes that for steady ideal flow (Bernoulli equation) when the alternating term of the velocity is made zero. The equation is made dimensionless by dividing it by "$V_M^2/2g$" to form;

$$\frac{2g\ H(t)}{V_M^2} = \frac{2L\omega}{V_M}\frac{V_A}{V_M}\,COS(\omega t) + \left(1 + \frac{V_A}{V_M}\,SIN(\omega t)\right)\left|1 + \frac{V_A}{V_M}\,SIN(\omega t)\right| \qquad (3.1g)$$

Four dimensionless terms are formed which are:

1. $2gH(t)/V^2_M$, dimensionless instantaneous head differential
2. $V_A/V_M = V_R$, velocity ratio
3. $L\omega/V_M = ST_M$, mean Strouhal Number
4. ωt, angle in radians

Therefore, the instantaneous ideal head differential is a function of three dimensionless groups; velocity ratio, mean Strouhal Number, and angle, or mathematically;

$$2gH(t)/V_M^2 = f(V_R,\ ST_M,\ \omega t)$$

The function is represented by Equation 3.1g and contains two terms, temporal acceleration and convective acceleration. Figure 21 shows the form of these terms for a Strouhal Number of 1.0 and a velocity ratio of 1.5. The function is also shown as the total of the two terms and indicates the instantaneous ideal dimensionless head differential for an orifice. Of course, the actual dimensionless head is not the same as the ideal dimensionless head. Figure 22 shows the ideal dimensionless head function for a Strouhal Number of .213 and a velocity ratio of .108. The dimensionless head is also plotted for data

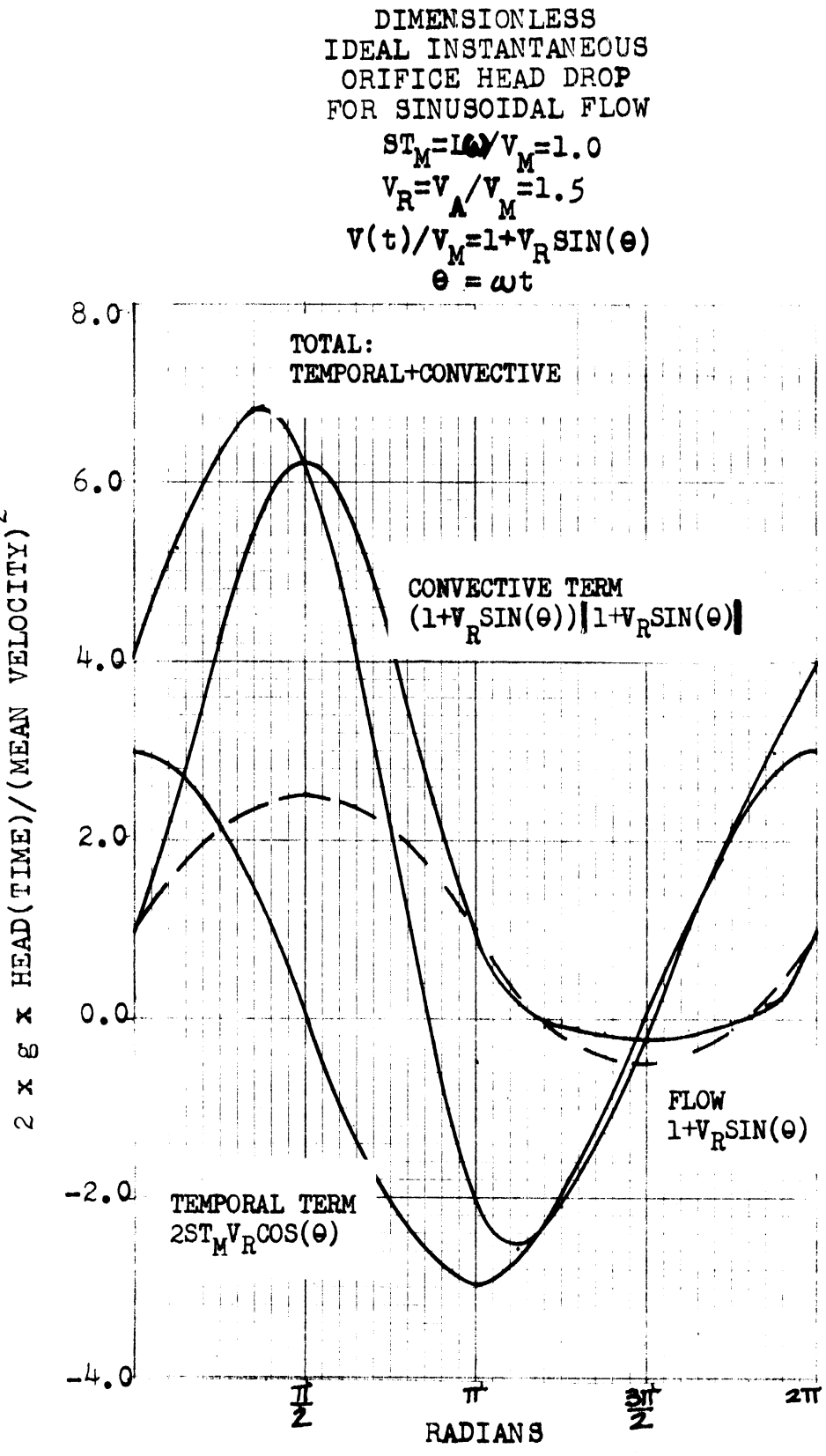

Figure 21. Example of Dimensionless Ideal Head Function.

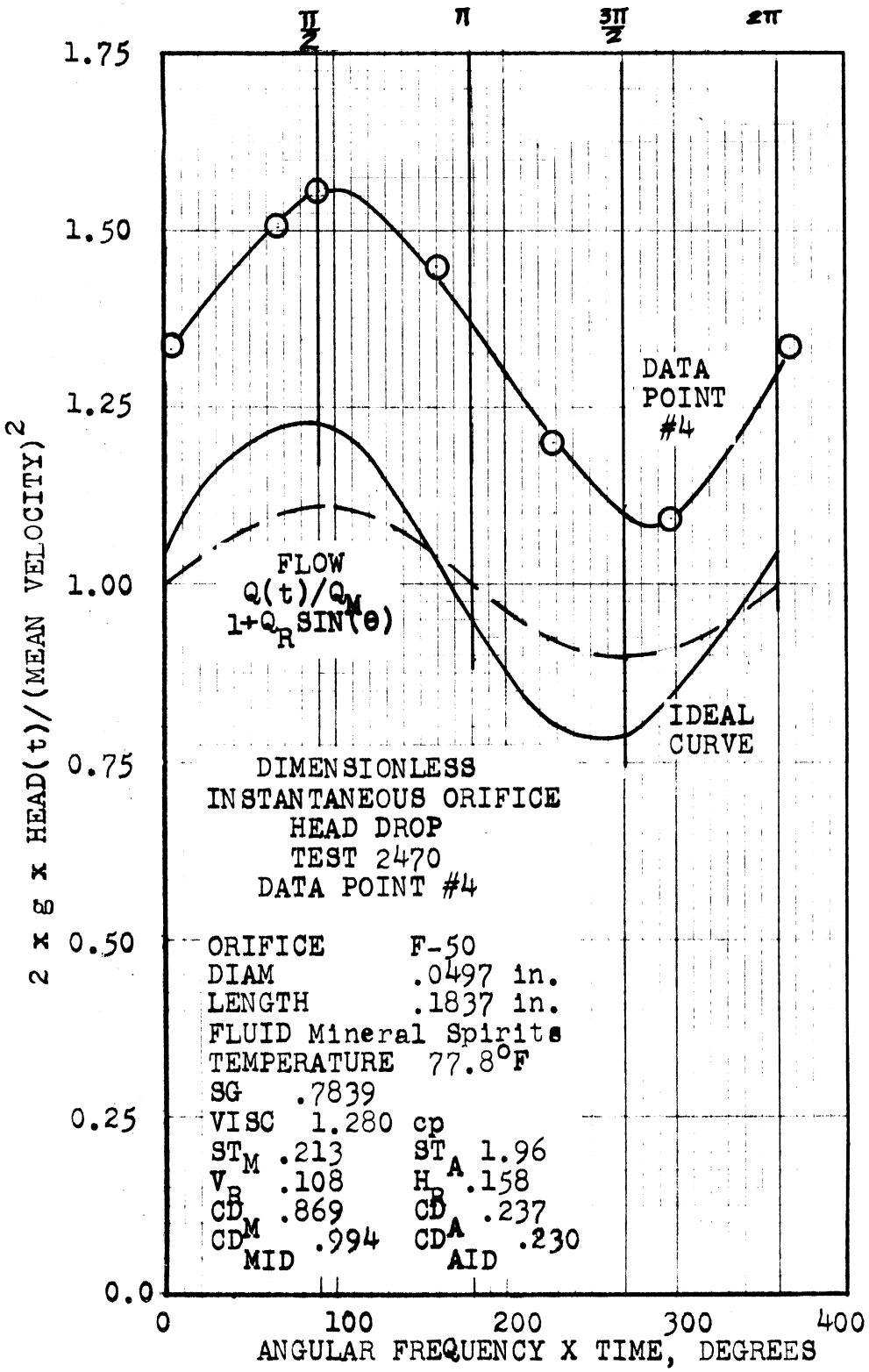

Figure 22. Comparison of Ideal Head and Actual Head Functions.

point #4 of test 2470, which has the same value of Strouhal Number and velocity ratio. It is readily apparent from the figure that the real head is greater than the ideal head at any instant during the cycle. The greater instantaneous head of the real flow indicates that the ideal analysis has not fully accounted for the forces which exist in the actual flow. Therefore, experimental work is necessary in order to accurately determine the flow through an orifice which has oscillating flow. The ideal flow analysis does provide a useful guide as to what general form the experimental results should be, and that two important parameters for plotting the results are velocity ratio and Strouhal Number.

3.9 Ideal Coefficient of Discharge

In order to study the influence of flow oscillations on average flow, it is desirable to define the average value of the dimensionless head function as follows:

$$2gH_M/V^2_M = 2g(H_{max} + H_{min}) \times .5/V^2_M \qquad (3.9)$$

Making the average head as one-half the sum of the maximum and minimum values instead of an integrated average is preferred because it is much simpler. This is particularly true when the same averaging process is to be done on the data for flow and pressure, for which no mathematical function is available. However, both must be nearly sinusoidal to be applicable to this analysis.

The average value of dimensionless head is now seen to be a form of a mean ideal coefficient of discharge:

$$2gH_M/V^2_M = 1/C^2_{DMID} \qquad (3.10)$$

The averaging process has eliminated time, so that the mean ideal coefficient of discharge is only a function of the mean Strouhal Number and the velocity ratio as given by:

IDEAL ORIFICE COEFFICIENTS
OF DISCHARGE
FOR OSCILLATORY FLOW

$$C_{DMID}=V_M/\sqrt{2g\Delta H_M}$$

$$C_{DAID}=V_A/\sqrt{2g\Delta H_A}$$

$$V(t)=V_M+V_A\,SIN(\omega t)$$

$$2gH(t)=2L\omega V_A COS(\omega t)+(V_M+V_A SIN(\omega t))\,|V_M+V_A SIN(\omega t)|$$

$$H_M=(H_{MAX}+H_{MIN})x.5$$

$$H_A=(H_{MAX}-H_{MIN})x.5$$

$$ST_M=L\omega/V_M$$

$$V_R=V_A/V_M$$

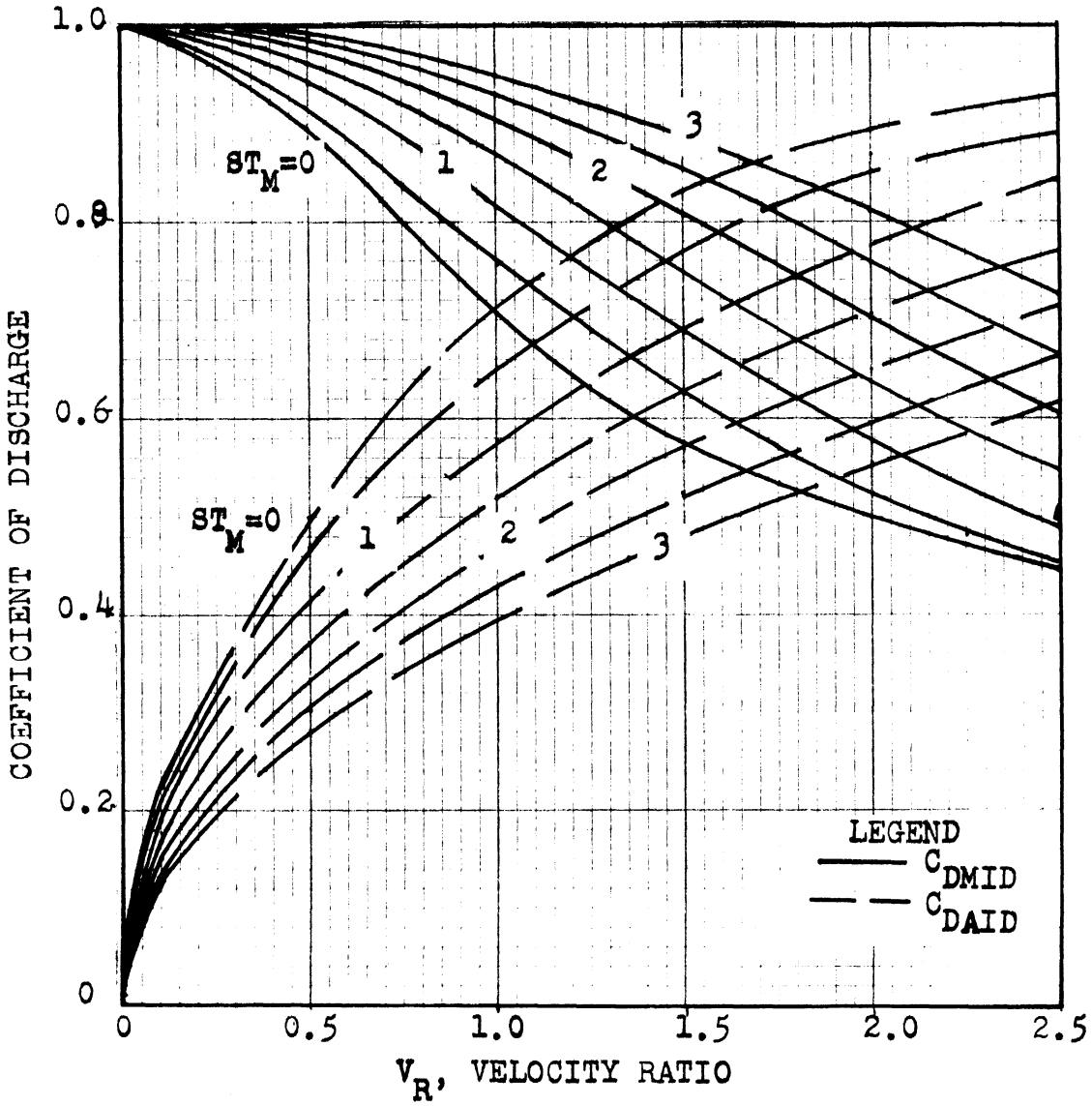

Figure 23. Ideal Coefficients of Discharge versus Velocity Ratio.

$$C_{DMID} = f_1(ST_M, V_R). \tag{3.11}$$

The maximum and minimum values of the ideal instantaneous head were found from Equation 3.1g for many combinations of flow ratio and Strouhal Number, and the results were used to calculate the ideal coefficient of discharge from Equation 3.9. Figure 23 shows the resulting ideal coefficients.

Another useful number which can be derived from the dimensionless head function is the alternating value of dimensionless head. This is calculated by;

$$2gH_A/V^2_M = 2g(H_{max} - H_{min}) \times .5/V^2_M \tag{3.12}$$

This value is also a function of velocity ratio and mean Strouhal Number. Furthermore, it can be divided by the square of the velocity ratio to yield a new value which is still only a function of velocity ratio and mean Strouhal Number. The quotient is given by:

$$(2gH_A/V^2_M)/(V_A/V_R)^2 = 2gH_A/V^2_A. \tag{3.13}$$

The alternating form of dimensionless head is now used to define the ideal alternating coefficient of discharge;

$$2gH_A/V_A^2 = 1/C^2_{DAID} \tag{3.14}$$

The ideal alternating coefficient of discharge, as defined above, is a function of the velocity ratio and the mean Strouhal Number, as given by;

$$C_{DAID} = f_2(ST_M, V_R) \tag{3.15}$$

It is also represented graphically as a function of the two independent variables in Figure 23.

Both of the independent variables used for determining the ideal mean and alternating coefficients of discharge require knowledge of the orifice flow versus time. However, in practice orifice flow

will probably not be known, but head difference will be known. Therefore it is desirable to represent the ideal coefficients of discharge in terms of independent variables which contain values of head, rather than flow. Some different dimensionless numbers, which do not contain flow, are now defined, and used as independent variables. The first new number, head ratio, is defined as:

$$H_R = (C_{DMID}/C_{DAID})^2 \times (V_R)^2 = H_A/H_M \qquad (3.16)$$

Another useful number is the mean Strouhal Number which is based on mean head and it is defined as;

$$ST_{MH} = ST_M \times C_{DMID} = L\omega/\sqrt{2gH_M} \qquad (3.17)$$

It must be emphasized that nothing new has really been added to the analysis, since the previous dimensionless variables have been combined only to make the functions more convenient to use. Therefore, the ideal values of the coefficients of discharge can be also written as functions of the new variables which are defined above;

$$C_{DMID} = f_3(ST_{MH}, H_R) \qquad (3.18)$$

$$C_{DAID} = f_4(ST_{MH}, H_R) \qquad (3.19)$$

where the independent variables in f_3 and f_4 do not contain flow terms. These two functions are shown in Figure 24.

Finally, the last number, which proves useful in examining the alternating coefficient data, is the alternating Strouhal Number, as defined by:

$$ST_A = L\,\omega/V_A = ST_M/V_R \qquad (3.20)$$

It is particularly useful for studying the data of these tests because it is constant for each cam used to oscillate the flow. This is true

IDEAL ORIFICE COEFFICIENTS
OF DISCHARGE
FOR OSCILLATORY FLOW

$$C_{DMID}=V_M/\sqrt{2g\Delta H_M}$$

$$C_{DAID}=V_A/\sqrt{2g\Delta H_A}$$

$$V(t)=V_M+V_A\,SIN(\omega t)$$

$$2gH(t)=2L\omega V_A COS(\omega t)+(V_M+V_A SIN(\omega t))\,|V_M+V_A SIN(\omega t)|$$

$$H_M=(H_{MAX}+H_{MIN})x\tfrac{1}{2}$$

$$H_A=(H_{MAX}-H_{MIN})\ x\ \tfrac{1}{2}$$

$$ST_{MH}=L\omega/\sqrt{2gH_M}$$

$$H_R=\Delta H_A/\Delta H_M$$

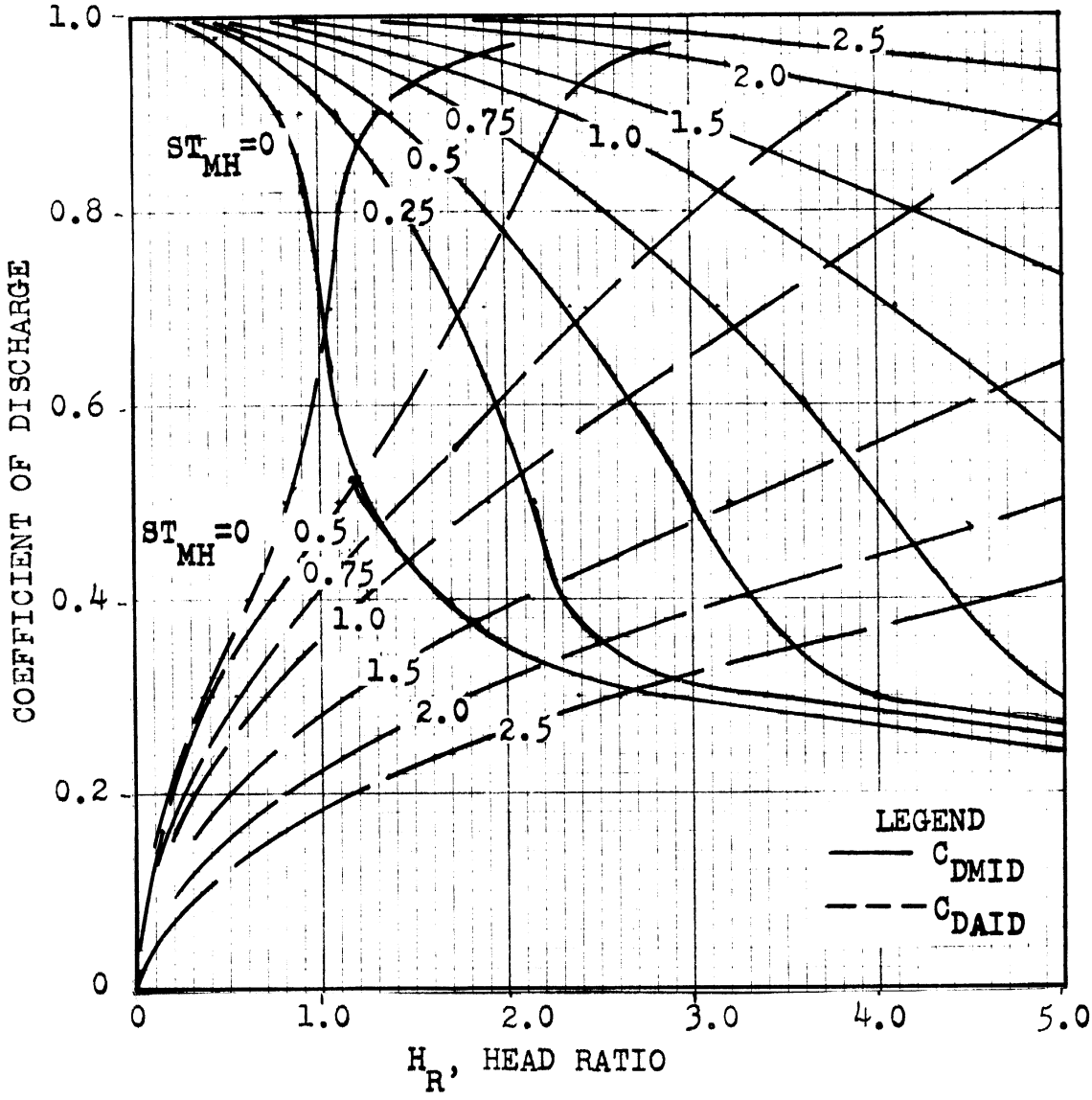

Figure 24. Ideal Coefficients of Discharge versus Head Ratio.

because oscillating flow is a product of cam displacement and frequency, therefore:

$$ST_A = L\,\omega/DISP\omega = L/DISP \tag{3.21}$$

since

$$C_{DA} = f(ST_A, V_R), \text{ and } ST_A = ST_M/V_R,$$

then

$$C_{DA} = f(ST_A, V_R)$$

and for constant "ST_A";

$$C_{DA} = f(V_R) \tag{3.22}$$

The data for alternating coefficient of each cam then follows one curve when plotted as a function of velocity ratio. Figures 89 through 105 of Appendix B illustrate this point.

3.10 Results of Orifice Tests

The ideal orifice equations show that the coefficient of discharge is a function of two variables; Strouhal Number and velocity ratio. However, actual orifice flow also depends on frictional forces, and requires the consideration of fluid viscosity and orifice geometry. Dimensional analysis shows that the Reynolds number can be used to account for viscous effects. Geometry is also an important influence on the flow; hence, it must be considered by including the dimensionless geometrical variables. The number of these variables depends upon the complexity of the geometry, and for the tests performed here only one, L/D, was used. Therefore, the functions, which are used to represent the experimental results are as follows:

$$C_{DM} = f_1\,(V_R, ST_M, Re, L/D) \tag{3.23}$$

$$C_{DM} = f_2(H_R, ST_M, Re, L/D) \tag{3.24}$$

$$C_{DA} = f_3 (V_R, ST_A) \tag{3.25}$$

$$C_{DA} = f_4 (H_R, ST_A) \tag{3.26}$$

Figures 25 through 32 show the mean coefficient of discharge data as represented by the first two functions for four different orifices: the F-50 main orifice, and three square-edged orifices.

Figures 25 and 26 show the results of pulsation on the coefficient of discharge for a typical main metering orifice. It is immediately apparent that the influence of the pulsation is to increase the flow if the flow ratio is small (0-.3). This phenomenon has also been noted by Mosely (10) and Zarek (14), and is illustrated by both figures. However, the ideal flow analysis does not predict this phenomenon. Compared to steady flow, slight pulsations diminish the viscous losses, which are not included for the ideal flow, and cause a slightly larger coefficient of discharge. However, as the flow ratio is increased, the influence of the inertia of the oscillating flow becomes evident, which is predicted by the ideal equation. At flow ratios greater than .3, the curves are similar to the idealized curves for which friction is neglected. It is also interesting to note that the coefficient of discharge is substantially influenced by the Reynolds Number. The Strouhal Number lies within a small range (0-.6) so that its affect is minimal for this data.

Figures 27 and 28 show similar data which is plotted for a very short, square-edged orifice. In contrast to the data for the main orifice, the Reynolds Number has little influence on the

MEAN COEFFICIENT OF DISCHARGE
VERSUS
FLOW RATIO
TEST 2470

STROUHAL NUMBERS= 0-0.6

ORIFICE	F-50
DIAM	.0497 in.
LENGTH	.1837 in.
FLUID	Mineral Spirits
TEMP	77.8-84.2 °F
SG	.7839-.7809
VISC	1.219-1.280 cp

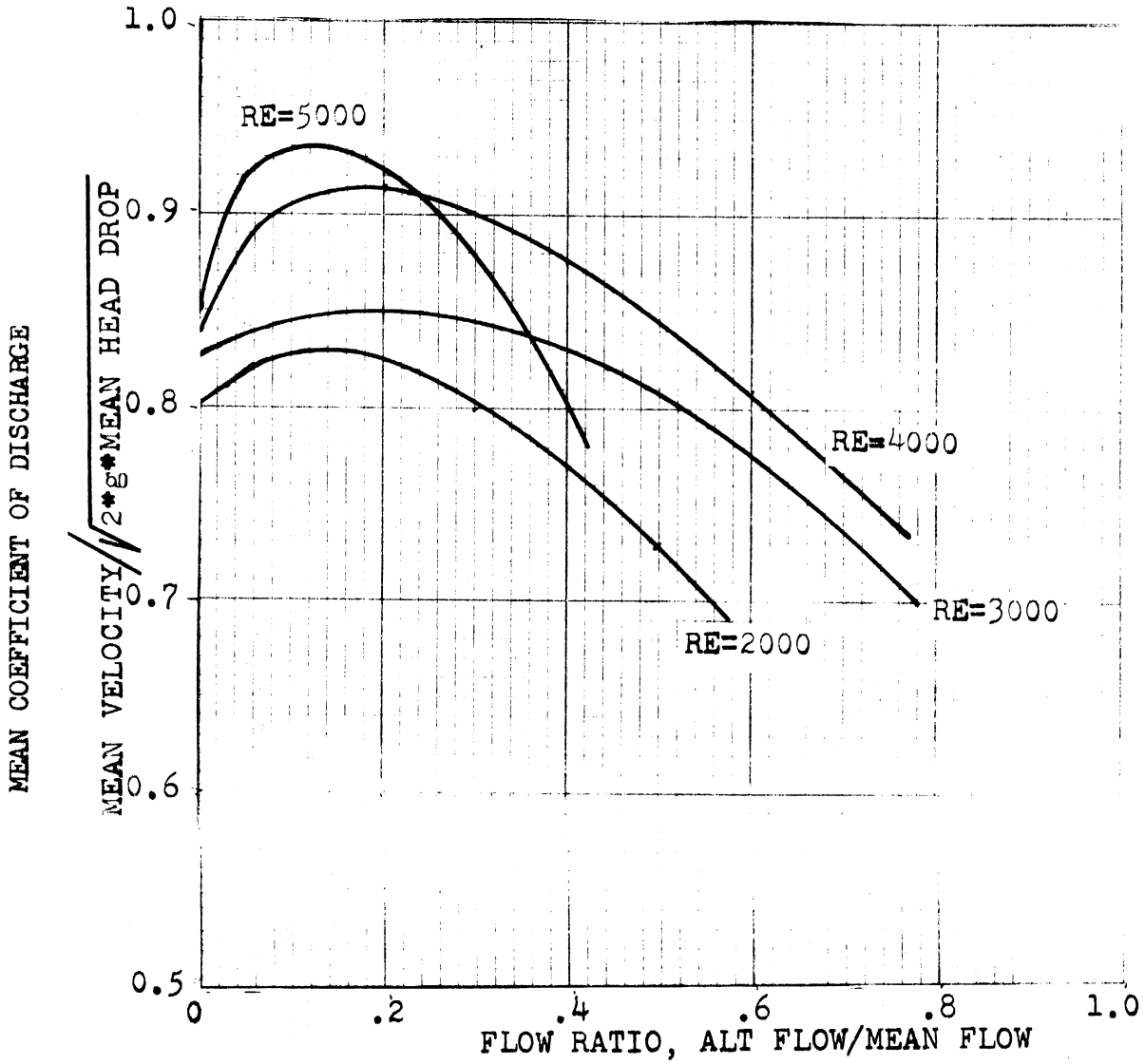

Figure 25. Coefficient of Discharge versus Flow Ratio, F-50 Orifice.

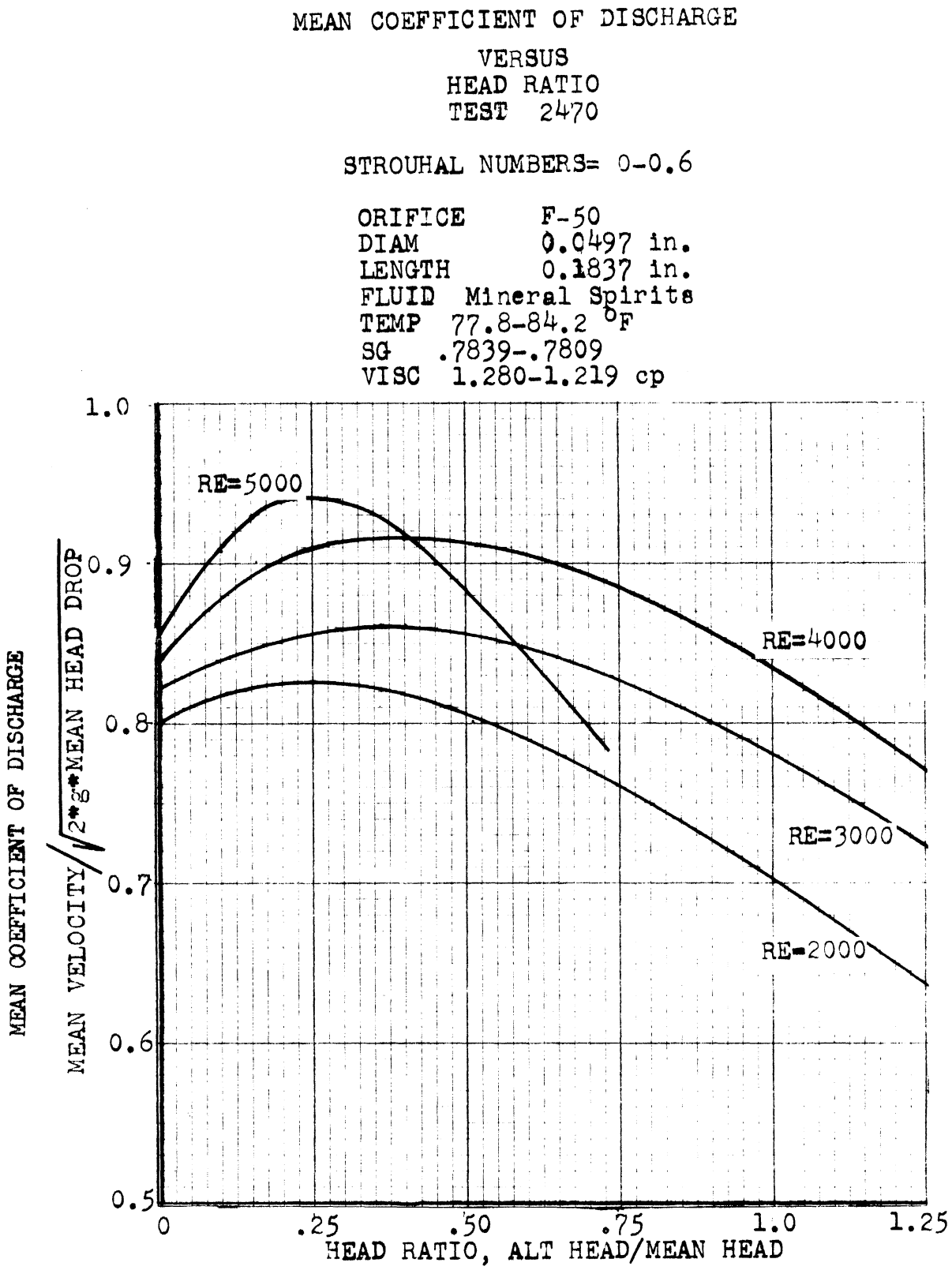

Figure 26. Coefficient of Discharge versus Head Ratio, F-50 Orifice.

MEAN COEFFICIENT OF DISCHARGE
VERSUS
FLOW RATIO

TEST NUMBER 78702
ORIFICE: SQUARE EDGED
DIAMETER: 0.0518 inch
LENGTH: 0.0319 inch
L/D: 0.6158
FLUID: MINERAL SPIRITS
TEMPERATURE: 75.2-75.7 °F
SPECIFIC GRAVITY: .7852-.7850
VISCOSITY: 1.306-1.301 cp

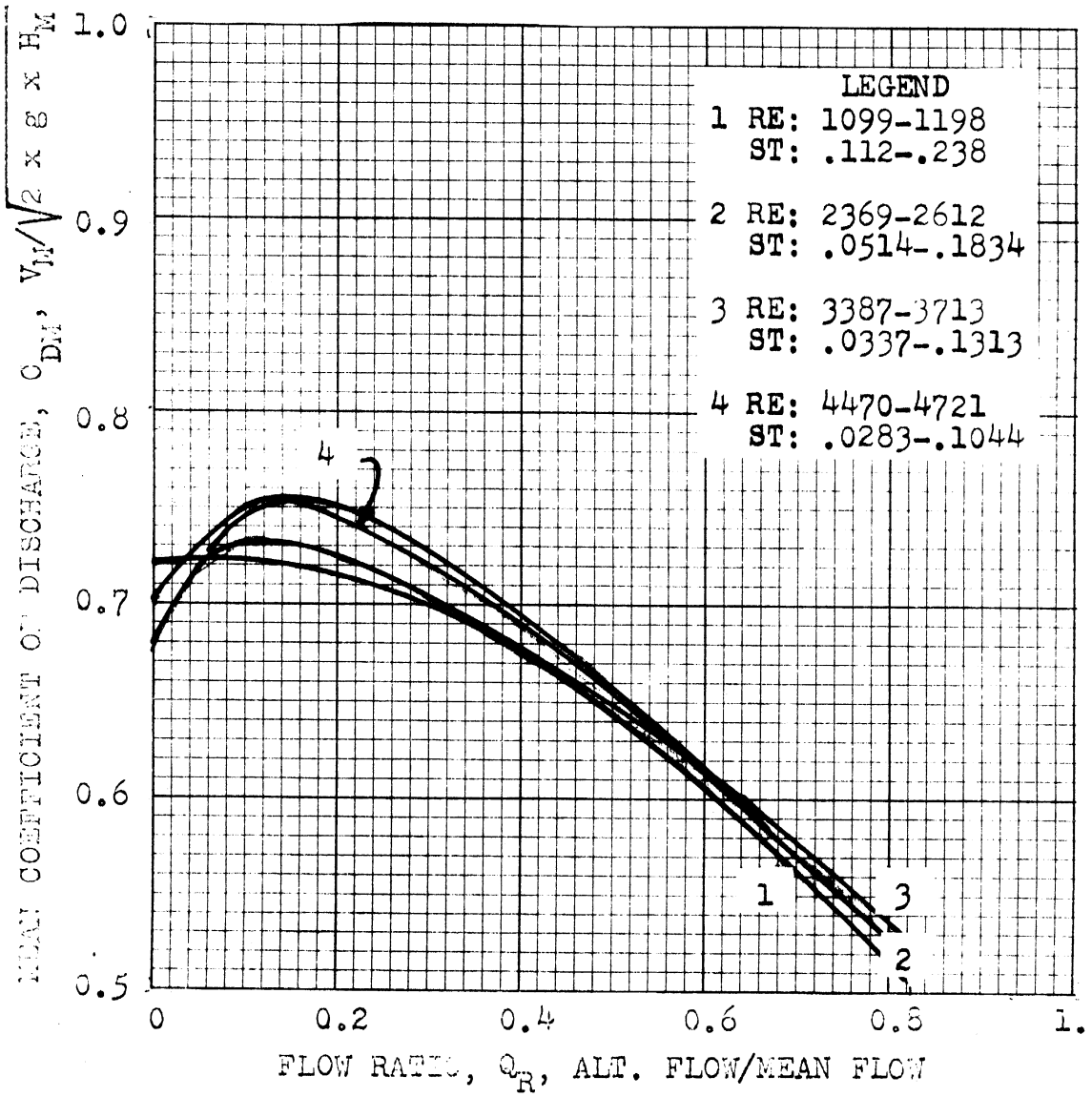

Figure 27. Coefficient of Discharge versus Flow Ratio, L/D=0.62.

MEAN COEFFICIENT OF DISCHARGE VERSUS HEAD RATIO

TEST NUMBER 78702
ORIFICE: SQUARE EDGED
DIAMETER: 0.0518 inch
LENGTH: 0.0319 inch
L/D: 0.6158
FLUID: MINERAL SPIRITS
TEMPERATURE: 75.2-75.7°F
SPECIFIC GRAVITY: .7852-.7850
VISCOSITY: 1.306-1.301 cp

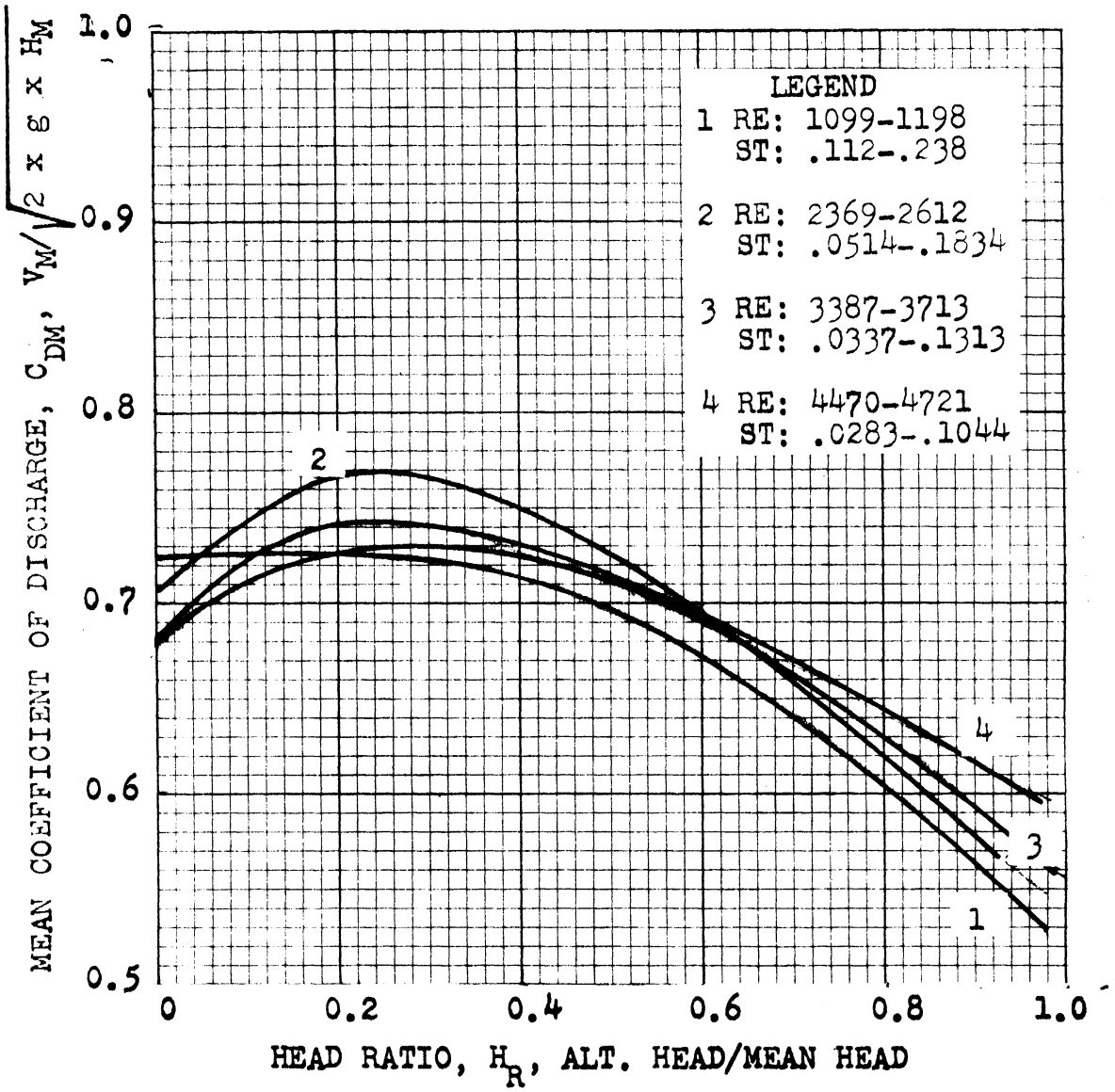

Figure 28. Coefficient of Discharge versus Head Ratio, L/D=0.62.

MEAN COEFFICIENT OF DISCHARGE
VERSUS
FLOW RATIO

TEST NUMBER 78701
ORIFICE: SQUARE EDGED
DIAMETER: 0.0518 inch
LENGTH: 0.1880 inch
L/D: 3.693
FLUID: MINERAL SPIRITS
TEMPERATURE: 75.1-78.9°F
VISCOSITY: 1.307-1.269 cp
SPECIFIC GRAVITY: .7853-.7834

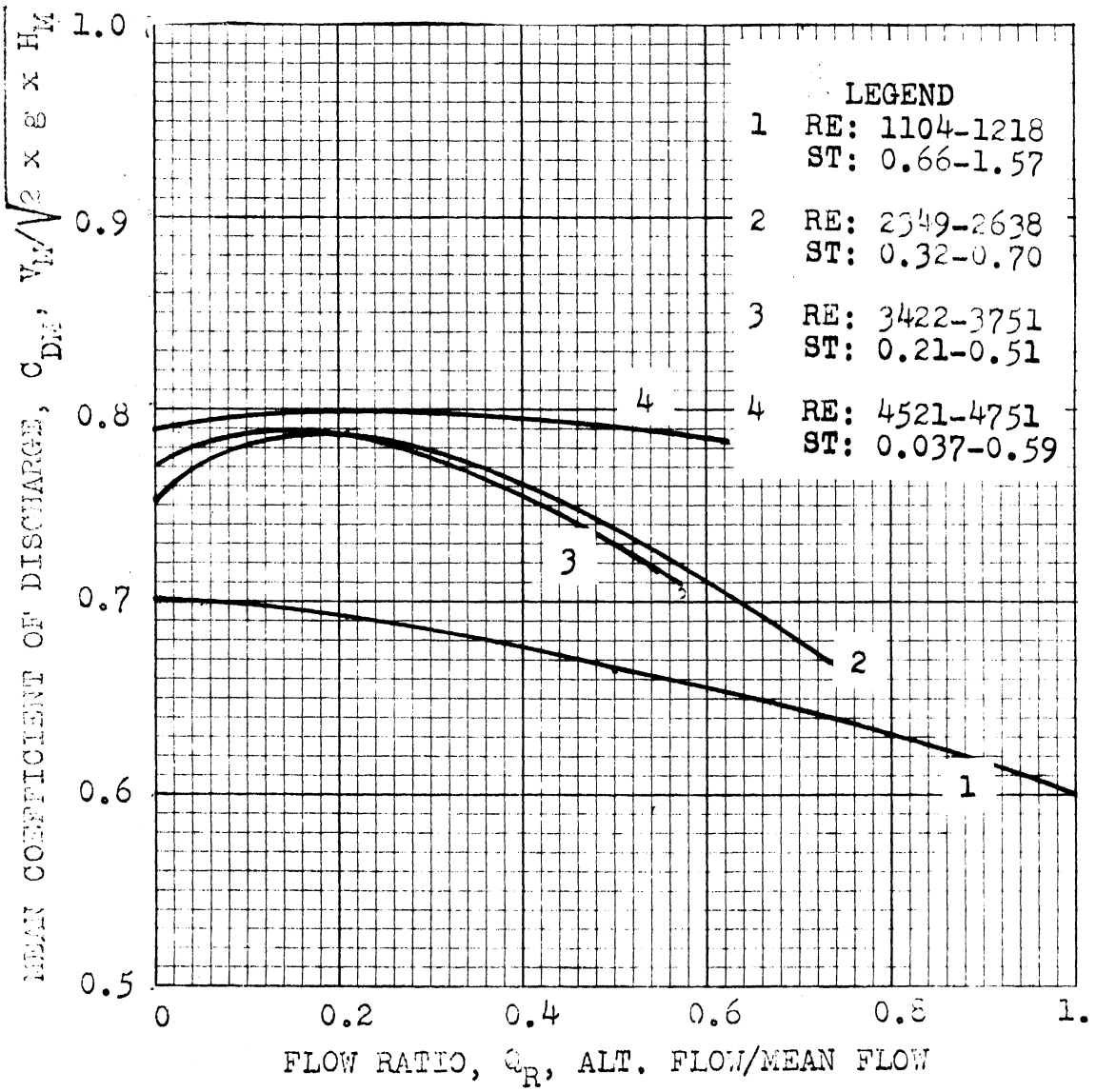

Figure 29. Coefficient of Discharge versus Flow Ratio, L/D=3.63.

MEAN COEFFICIENT
OF DISCHARGE
VERSUS
HEAD RATIO

TEST NUMBER 78701
ORIFICE: SQUARE EDGED
DIAMETER: 0.0518 inch
LENGTH: 0.1880 inch
L/D: 3.6293
FLUID: MINERAL SPIRITS
TEMPERATURE: 75.1-78.9 °F
VISCOSITY: 1.307-1.269 cp
SPECIFIC GRAVITY: .7853-.7834

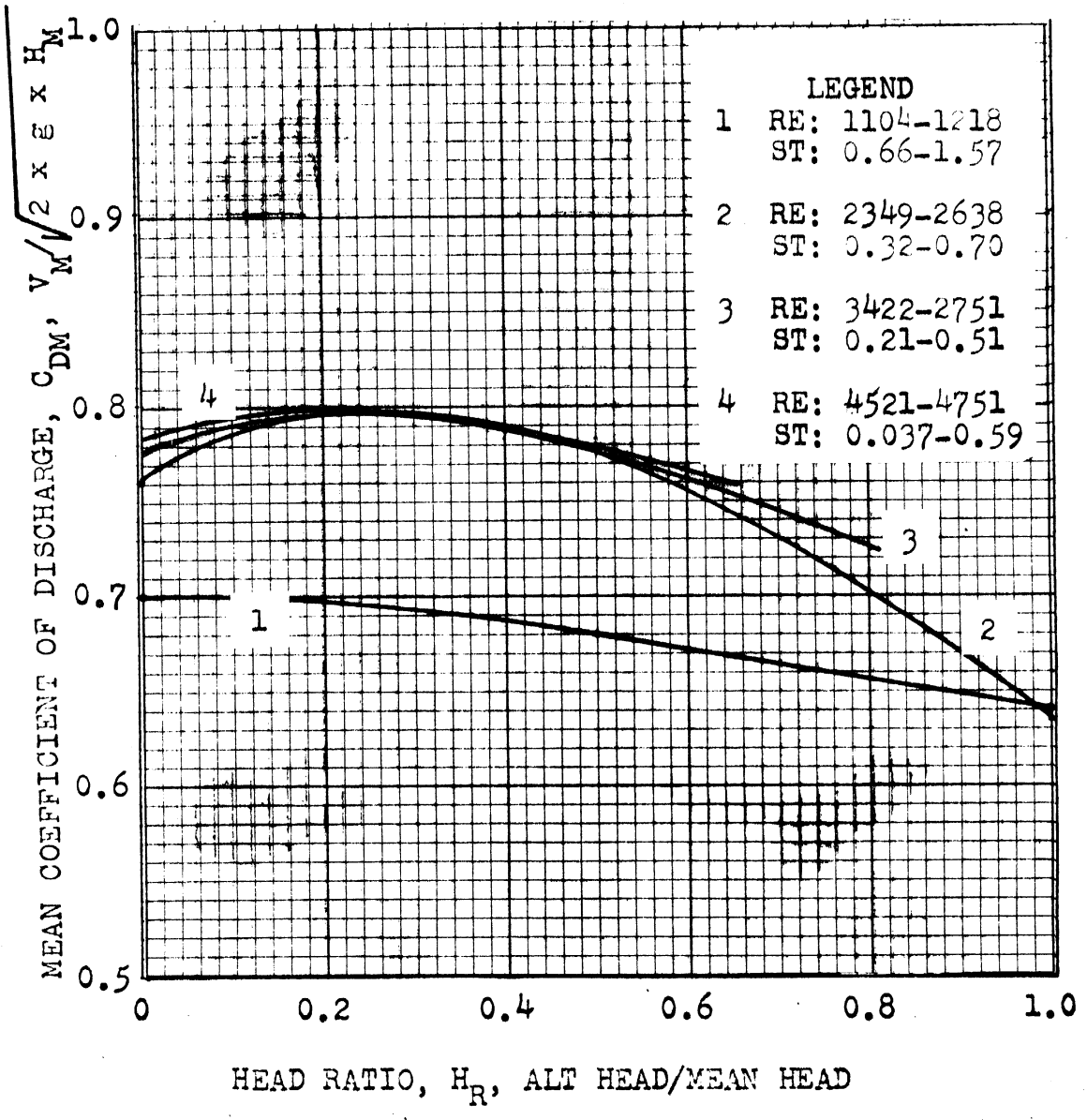

Figure 30. Coefficient of Discharge versus Head Ratio, L/D=3.63.

MEAN COEFFICIENT OF DISCHARGE
VERSUS
FLOW RATIO

TEST NUMBER 7770
ORIFICE: SQUARE EDGED
DIAMETER: 0.0518 in.
LENGTH: 0.3750 in.
L/D: 7.2394
FLUID: MINERAL SPIRITS
TEMP. RANGE: 88.8-89.2°F
VISCOSITY RANGE: 1.179-1.176 cp
SPECIFIC GRAVITY: .7786-.7788

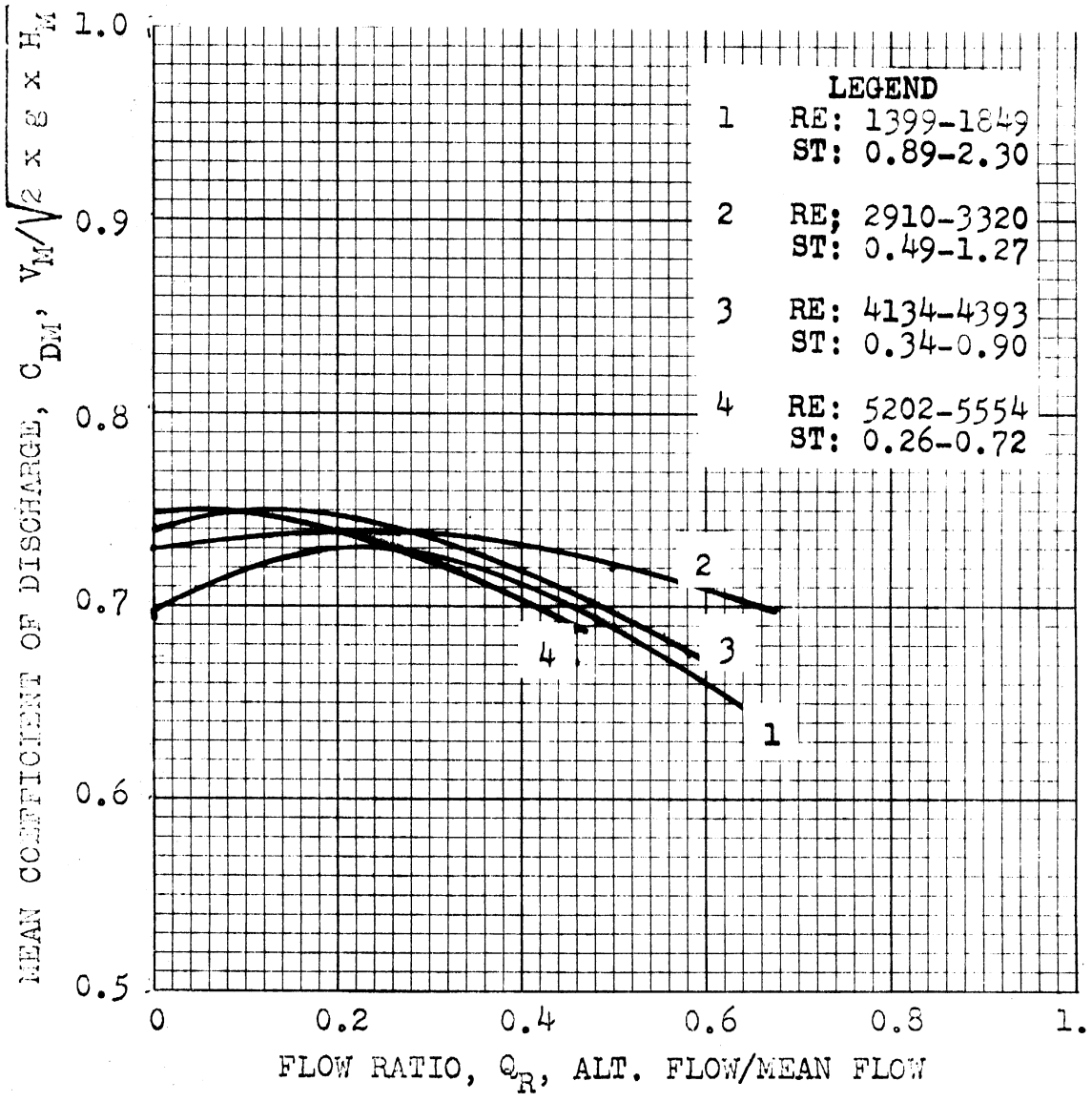

Figure 31. Coefficient of Discharge versus Flow Ratio, L/D=7.24.

MEAN COEFFICIENT OF DISCHARGE VERSUS HEAD RATIO

TEST NUMBER 7770
ORIFICE: SQUARE EDGED
DIAMETER: 0.0518 in.
LENGTH: 0.3750 in.
L/D: 7.2394
FLUID: MINERAL SPIRITS
TEMP. RANGE: 88.8-89.2°F
VISCOSITY RANGE: 1.179-1.176 cp
SPECIFIC GRAVITY: .7786-.7788

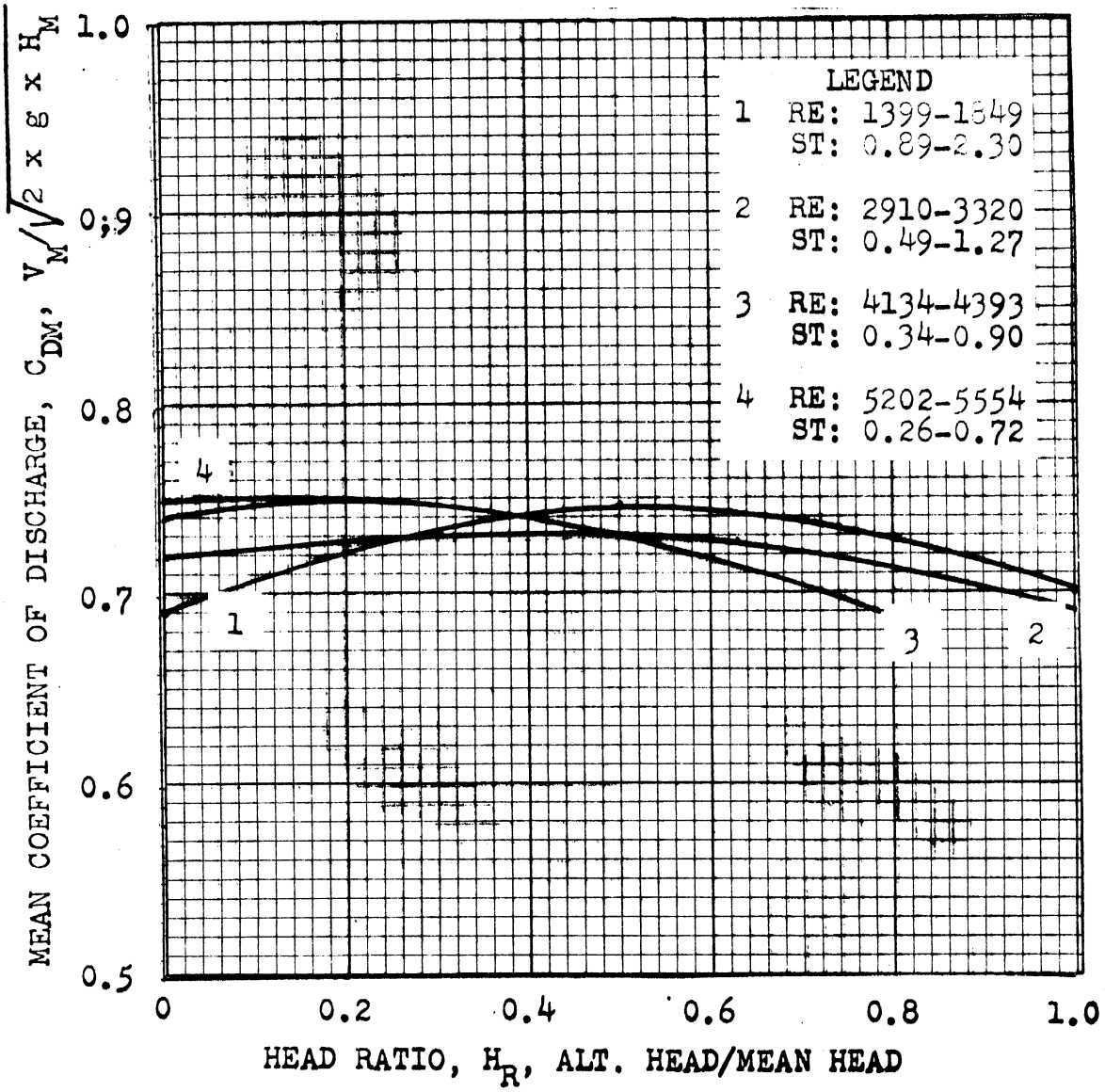

Figure 32. Coefficient of Discharge versus Head Ratio, L/D=7.24.

coefficient for the very short orifice. This is similar to coefficient data for short orifices under steady flow in that little change in the coefficient is measured for Reynolds numbers greater than 2000. However again, an increase in the coefficient is seen to occur at small velocity ratios. The Strouhal Number for this orifice is also within a small range (0-.238) which minimizes its influence.

Figures 29 and 30 show data for a square orifice which has an L/D nearly equal to that of the main metering orifice (data of Figures 25 and 26). The influence of the Reynolds number is not as pronounced as it is for the main orifice, but it is greater than that of the very short orifice (data of Figures 27 and 28). The greatest affect of Reynolds number is seen to occur at a value of about 1000, and Reynolds numbers greater than 2000 show little influence on the coefficient. Again, the Strouhal number is small, which minimizes its affect.

Figures 31 and 32 show the data for a long orifice (L/D = 7.24). For the range of independent variables shown, the coefficient of discharge varies very little. The flow oscillation (Figure 31) and the head pulsation (Figure 32) show almost no affect. Also, the data indicates that the influence of the Reynolds number is also almost constant. It is also interesting to note that the Strouhal number range is considerably larger (0-2.3) for this data than for the data of the shorter orifices owing to its dependence upon length. This may partially be the reason for the relative flatness of the curves since the ideal analysis showed that large Strouhal numbers decrease the influence of pulsations on average flow.

The increase in coefficient of discharge can now be related to the test data of Chapter II, which shows that the fuel air ratio is

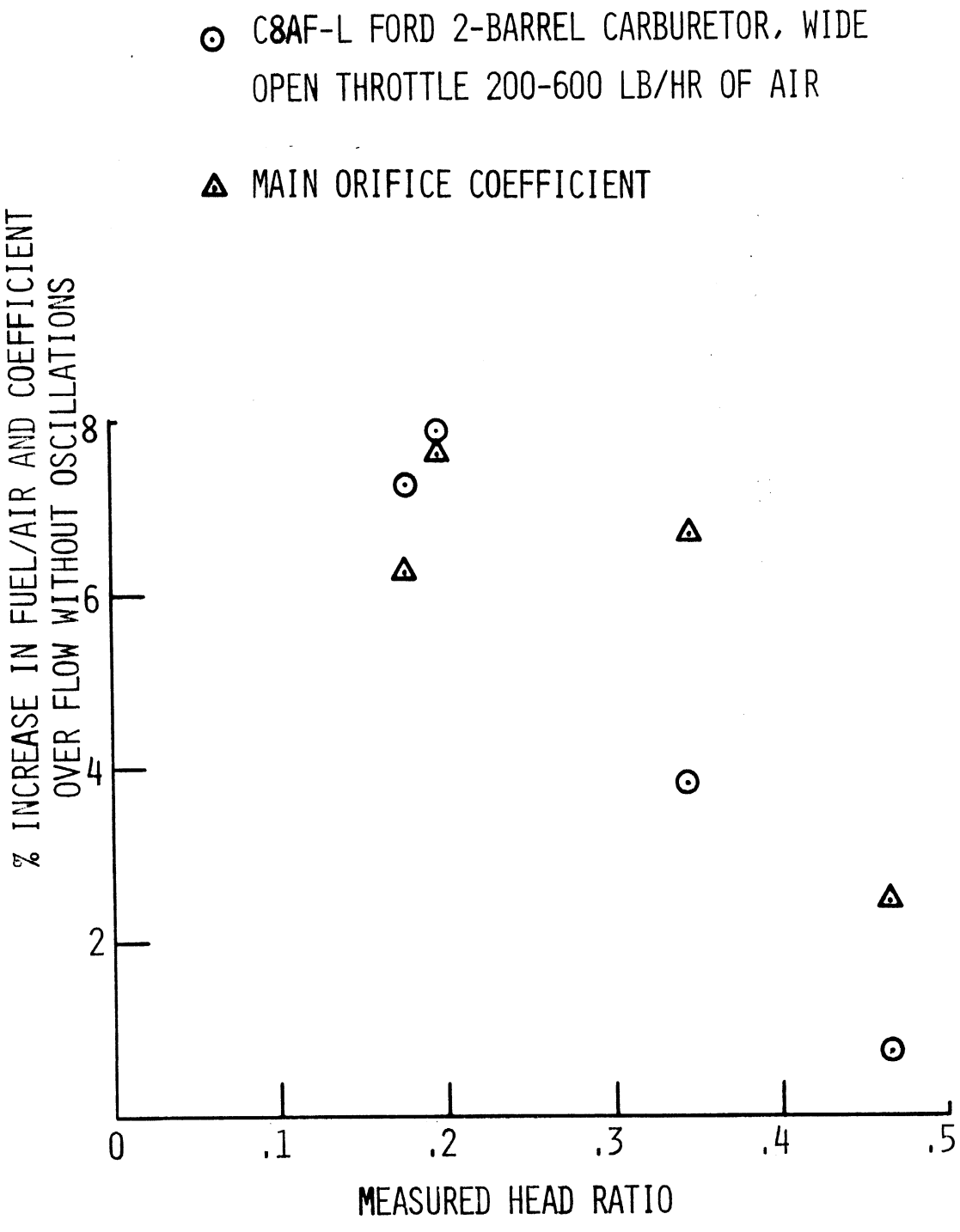

Figure 33. Percent Change in Fuel/Air and Coefficient of Discharge versus Head Ratio.

greater when the carburetor is functioning on an engine with pulsations than when it is operated under steady flow conditions. Figure 33 shows the percent increase of fuel/air ratio for the engine test of Chapter II as compared to the steady bench test of the same carburetor. It is plotted as a function of head ratio which was measured across the main metering orifice during the engine tests. Similar data from the orifice tests is also plotted as a percent increase in the coefficient of discharge for oscillating flow over steady flow as determined experimentally. As can be seen, the influence of the pressure pulsations on the orifice metering characteristics accounts for the difference between fuel/air ratio for the carburetor on an engine and on a test bench. This is due to the increase in the average flow through the main metering orifice which is caused by slight flow oscillations.

Experimental results for the alternating coefficient of discharge, as defined by Equation 3.14, are shown in Figures 34 through 39. It must be emphasized that this data is for the same test runs as the time-average flow results in the preceding section. However, now the relationship of oscillating flow to oscillating pressure difference is being investigated rather than the relationship of the average values of flow and pressure. This relationship has been defined as the alternating coefficient of discharge, and is given as:

$$C_{DA} = V_A / \sqrt{2g\Delta H_A}$$

The alternating coefficient of discharge is shown as a function of flow ratio and alternating Strouhal number or head ratio and alternating Strouhal number. The curves for the main orifice (Figures 34 and 35) and the curves for the very short square-edged orifice (Figures

36 and 37) are unique. That is, they cannot be plotted together as was the data for the medium and long square-edged orifices, as shown by Figures 38 and 39. The alternating Strouhal Number accounted very well for the influence of orifice length on the fluctuating flow for medium and long orifices. However, the data for the main orifice and short square-edged orifice could not be plotted in Figures 38 and 39 and give results consistent with the orifices of medium lengths.

The experimental data for the alternating coefficient of discharge shows that it is always less than or equal to the ideal value of alternating coefficient. At low velocity ratios, the ideal alternating coefficient is very nearly equal to the experimental value for all four orifices. At velocity ratios greater than 0.1 the experimental values are less than the ideal values. The amount of this difference is dependent upon the orifice, the velocity ratio, and the Strouhal Number.

It must be noted that the variation in Reynolds number was obtained for these tests only by varying the average flow, and that the viscosity of the fluid never appreciably changed. Therefore, the results should only be applied to orifices with fluids of similar viscosity to mineral spirits. Also, the diameters of all four orifices were nearly nearly equal (.050 inch) so that orifices which are much larger, or much much smaller, may not give the same results, even though they may be geometrically similar (same L/D). The waveform of the flow oscillation and the pressure pulsation was always nearly sinusoidal. No attempt was made to investigate the influence of different wave shape on the time-average flow. Study of these limitations is a worthwhile topic for further investigation.

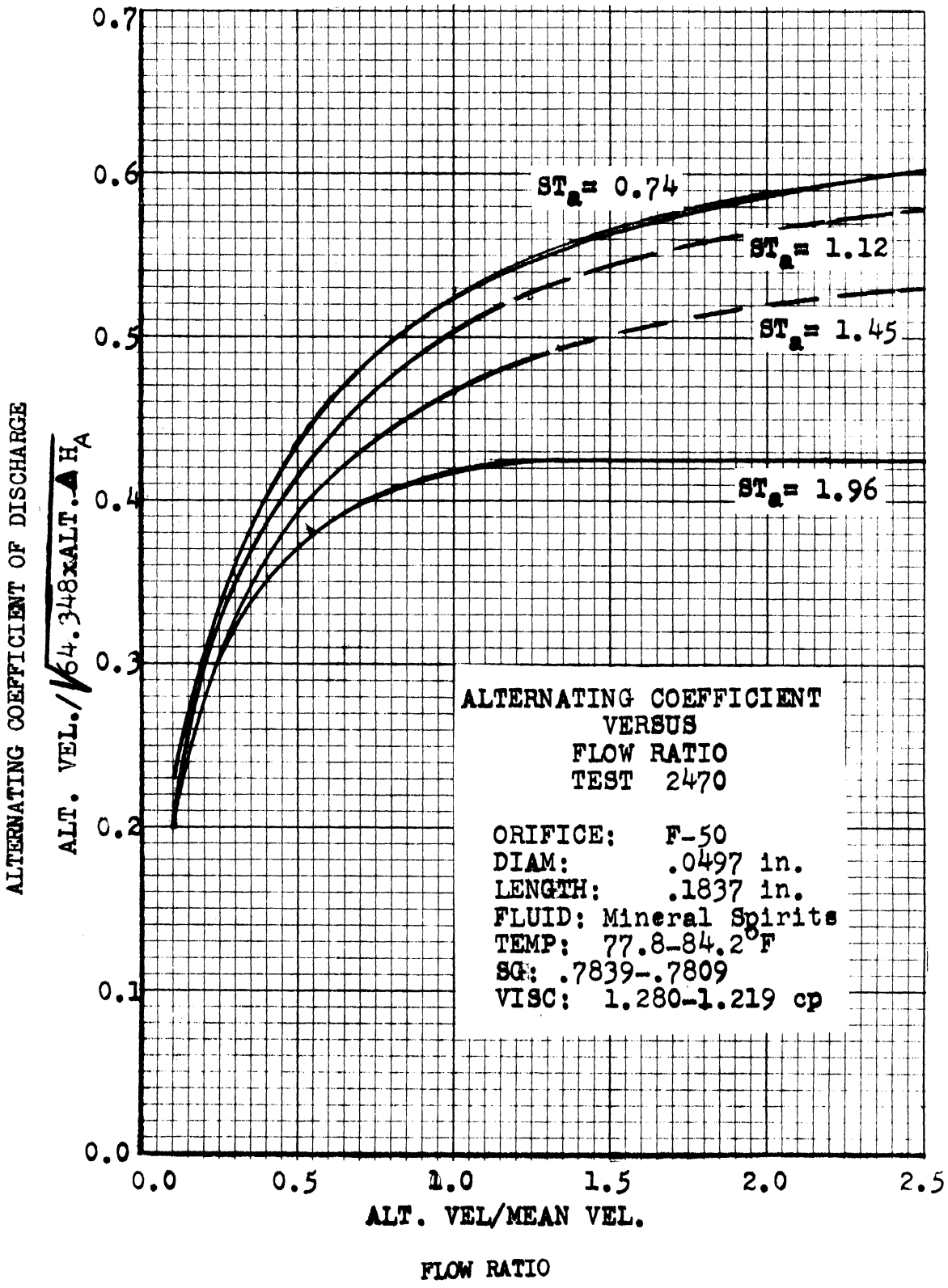

Figure 34. Alternating Coefficient of Discharge versus Flow Ratio, F-50 Orifice.

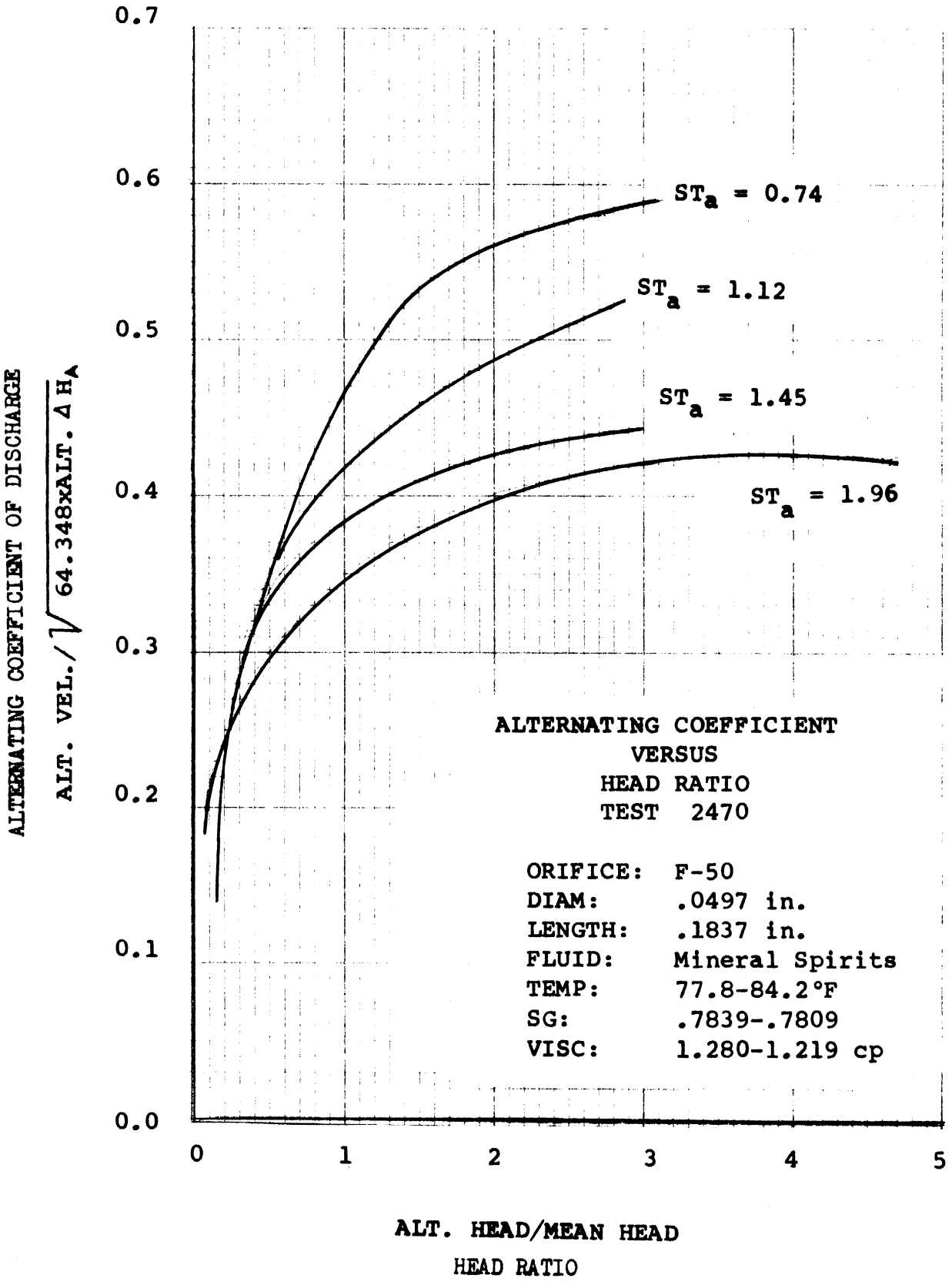

Figure 35. Alternating Coefficient of Discharge versus Head Ratio, F-50 Orifice.

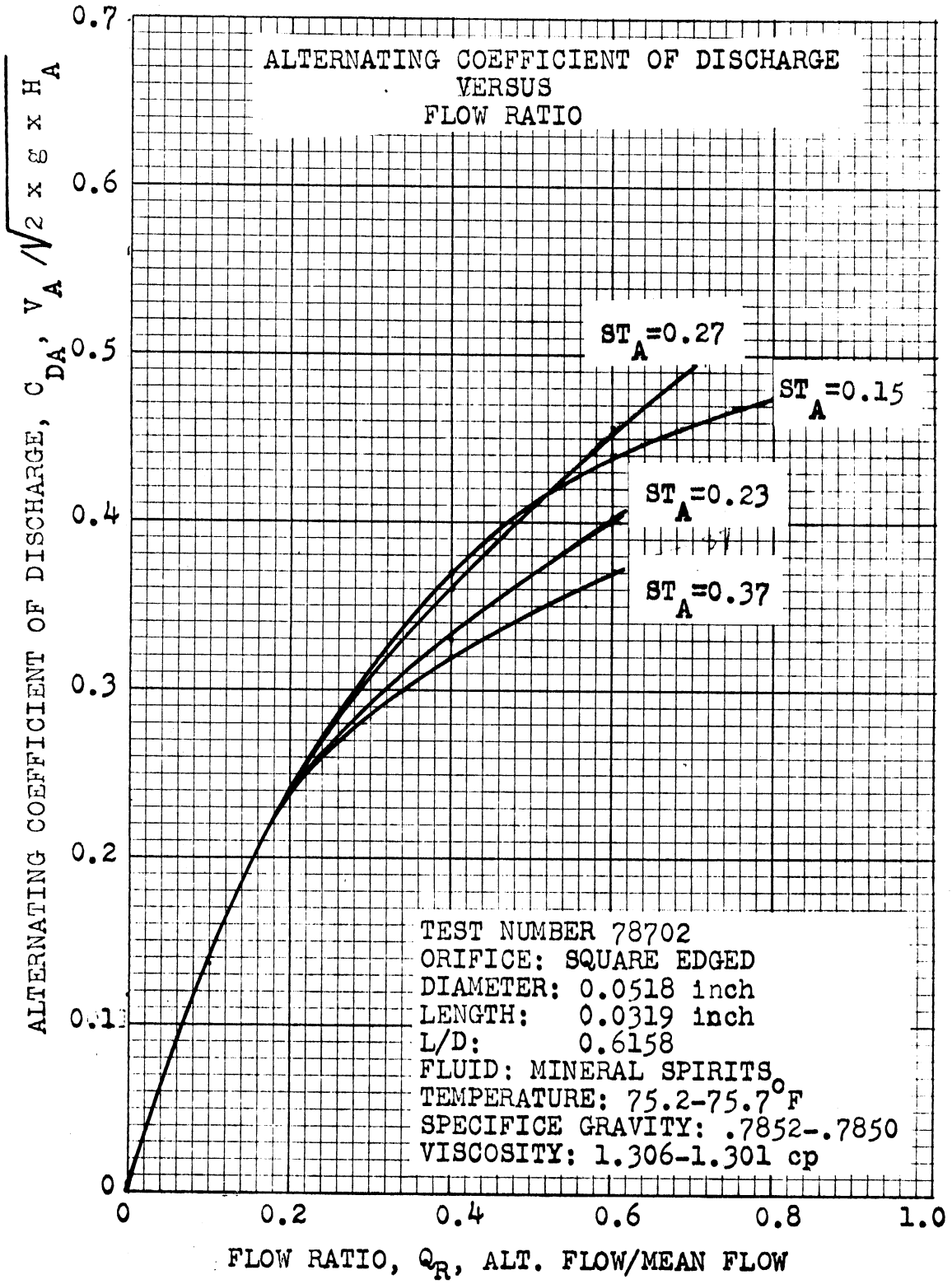

Figure 36. Alternating Coefficient of Discharge versus Flow Ratio, L/D=0.62.

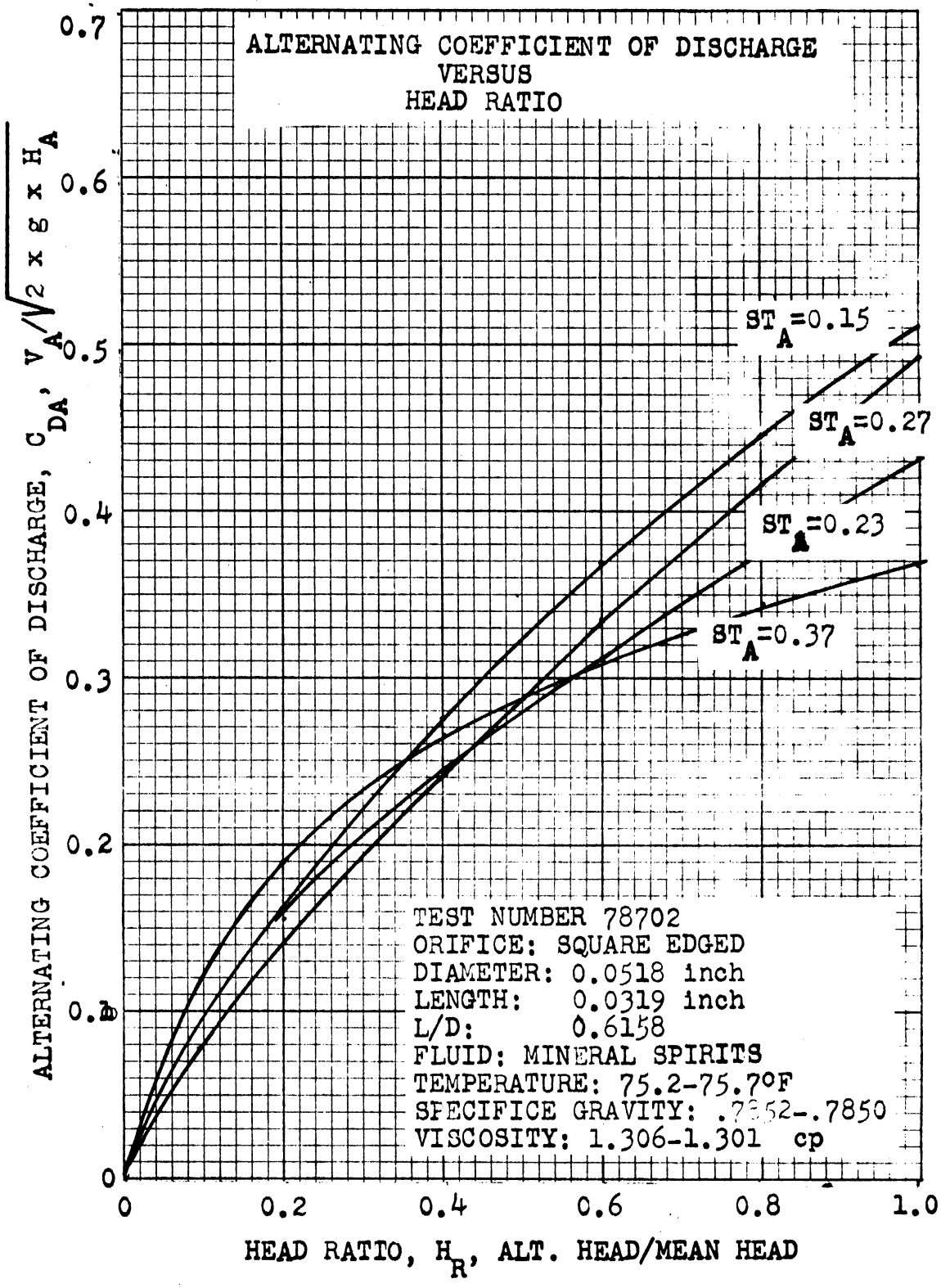

Figure 37. Alternating Coefficient of Discharge versus Head Ratio, L/D=0.62.

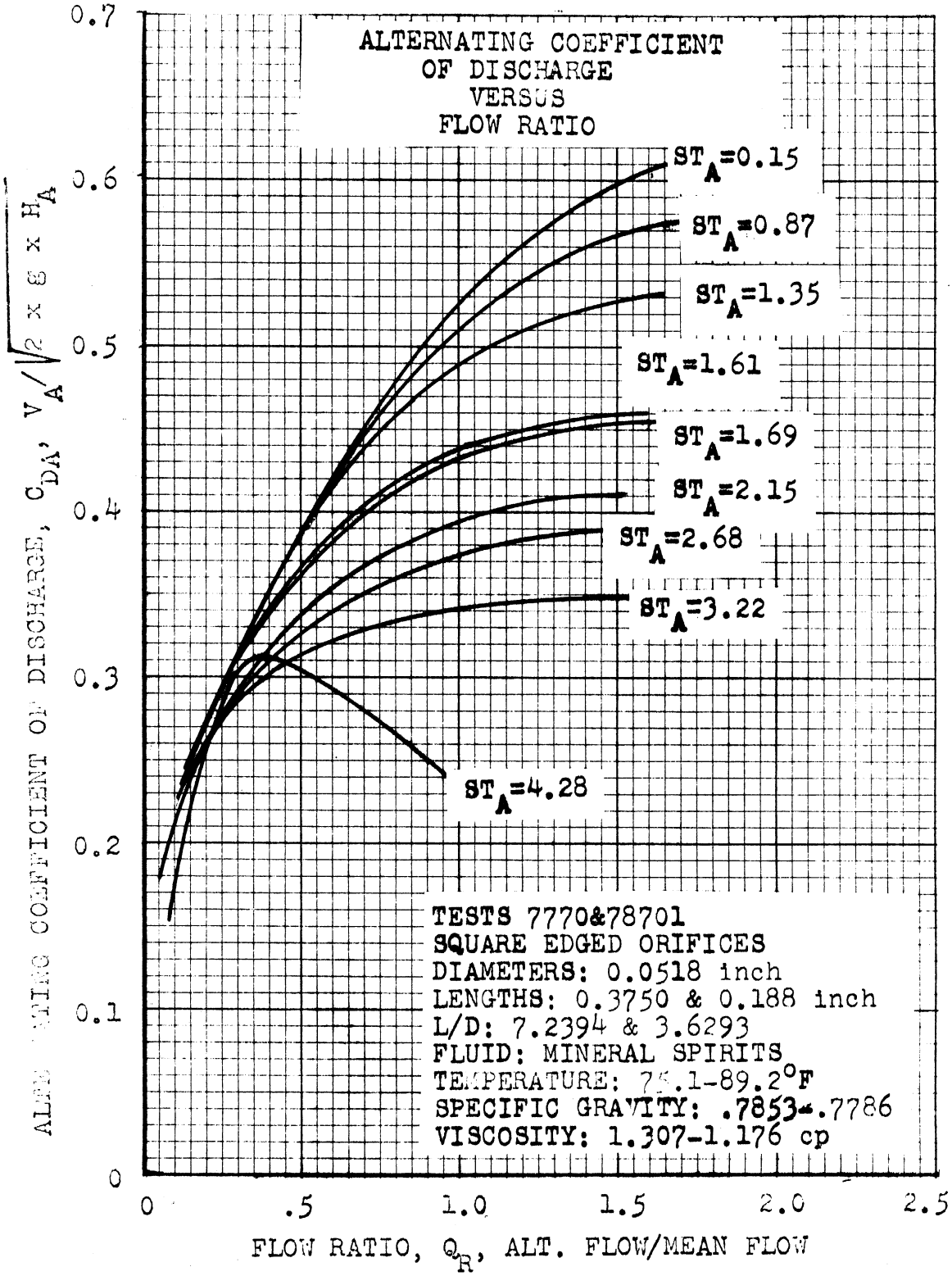

Figure 38. Alternating Coefficient of Discharge versus Flow Ratio, L/D=3.63 and L/D=7.24.

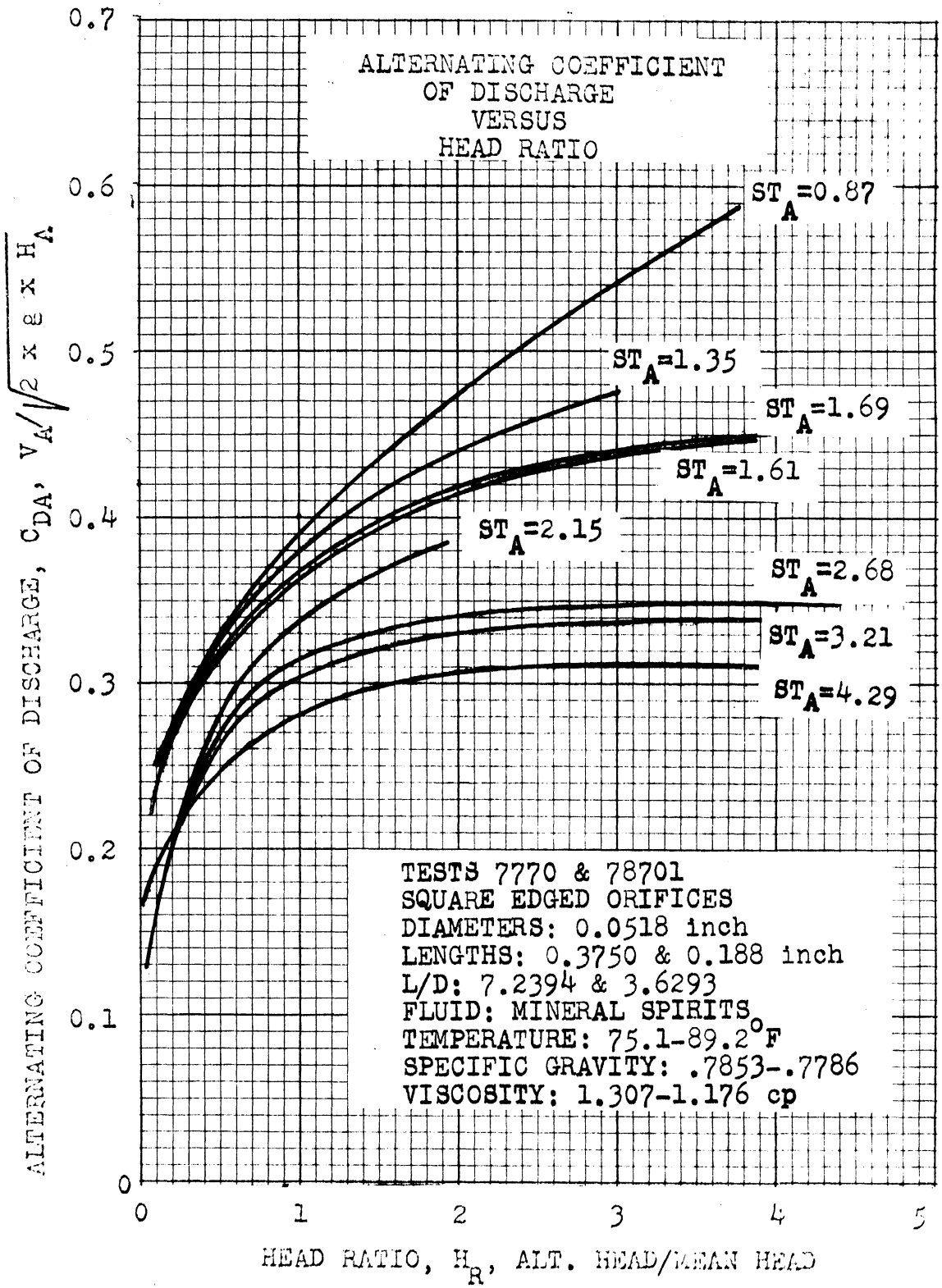

Figure 39. Alternating Coefficient of Discharge versus Head Ratio, L/D=3.63 and L/D=7.24.

Any further experimental study of orifice flow with oscillations should be done with control over the dimensionless numbers. For the experiments done here, no attempt was made to maintain any independent dimensionless variable at a constant value. That is, in the test procedure, when the mean flow was changed, three dimensionless numbers, Re, S_T, and V_R, also changed. It would, therefore, be advisable for future tests to be able to vary only one dimensionless number in order to generate the test curves. Much of the scatter in the present data could have been eliminated if this had been done.

The data for the mean coefficient and the alternating coefficient provides a method for calculating the instantaneous flow from pressure measurements in the following way.

From Equation 3.4

$$Q(t) = Q_M + Q_A \text{ SIN } (\omega t) \tag{3.4}$$

From the definition of the mean coefficient;

$$Q_M = C_{DM} A \sqrt{2g\Delta H_M} \tag{3.27}$$

and from the definition of the alternating coefficient

$$Q_A = C_{DA} A \sqrt{2g\Delta H_A} \tag{3.28}$$

Therefore, the instantaneous flow is given as:

$$Q(t) = A \left(C_{DM} \sqrt{2g\Delta H_M} + C_{DA} \sqrt{2g\Delta H_A}\right) \tag{3.29}$$

The two coefficients can be found in the experimental data of Figures 25 through 39. Equation 3.29 gives the instantaneous flow from values of mean and alternating head difference, both of which can be easily measured.

3.11 Conclusions to Orifice Tests

1. The time-average flow of incompressible fluid through a small orifice can be related to the time-average head difference by a mean coefficient of discharge as given by:

$$C_{DM} = \frac{V_M}{\sqrt{2g\Delta H_M}}$$

2. The coefficient of discharge for time-average flow through a small orifice is a function of three dimensionless variables: 1) Velocity ratio, 2) Strouhal number, and 3) Reynolds number.

3. The influence of the velocity ratio can either cause the coefficient to be greater or less than that for steady-state flow. Small velocity ratios cause a greater coefficient with a maximum occurring at velocity ratios of 0.12 to 0.16. At velocity ratios below this range, the coefficient tends toward the steady-state value. At velocity ratios greater than this range, the coefficient decreases as velocity ratio is increased.

4. The influence of the Strouhal number on the coefficient of discharge depends greatly upon the velocity ratio. At velocity ratios less than 0.5, its influence is negligible but it becomes noticeable at velocity ratios which are greater than 0.5. An increase in the Strouhal number increases the time-average flow.

5. The influence of the Reynolds number on the average flow is very similar to its influence upon steady flow without oscillations. In general, an increase in the Reynolds number increases the mean coefficient of discharge. The Reynolds number has its greatest influence upon the flow of the main metering orifice and the square orifice of

L/D equal to 3.63. The influence of it upon the coefficient of the long and short square edged orifices is negligible.

6. The coefficient of discharge for time-average flow is also a function of head ratio, Strouhal number based upon head, and Reynolds number. The influences of each of these new variables is similar to those of velocity ratio and Strouhal number. The maximum value of coefficient occurs at a head ratio of 0.2 to 0.25.

7. The coefficient of discharge for the long orifice (L/D = 7.24) is not substantially influenced by pressure pulsation and flow oscillation. The greatest influence of flow oscillation on average flow occurs for the short orifice (L/D = 0.6) and for the main metering orifice (L/D = 3.63).

8. The alternating flow of an incompressible fluid through a small orifice can be related to the alternating head difference by an alternating coefficient of discharge as given by:

$$C_{DA} = \frac{V_A}{\sqrt{2g\Delta H_A}}$$

9. The coefficient of discharge for the alternating component of flow through a small orifice is a function of two dimensionless numbers:

1. alternating Strouhal number and
2. velocity ratio.

10. An increase in the velocity ratio causes an increase in the alternating coefficient of discharge for alternating Strouhal numbers less than 3.5. Above 3.5, the curve of alternating coefficient versus velocity ratio is maximum at a velocity ratio of about 0.4.

11. An increase in the alternating Strouhal number decreases the alternating coefficient of discharge.

12. The alternating coefficient of discharge is also a function of head ratio, and the curves are very similar to those plotted as a function of velocity ratio. However, no maximums occur in the curves of alternating coefficient as a function of head ratio.

13. The alternating Strouhal number accounts for the influence of length and frequency very well for square orifices which have L/D between 3.5 and 7.24. An increase in the alternating Strouhal number, which is caused by an increase in length or an increase in frequency of oscillation, will cause the same change in alternating coefficient. However, this is not true for very short orifices, or orifices of complex shape.

CHAPTER IV

SIMULATION OF FUEL METERING NETWORKS

4.1 Reasons for Simulation

Carburetors have been in use on automobiles for many years, so a logical question is: "Why make a detailed study of something that has been working satisfactorily for over half a century?" The answer lies in the fact that today's problems of air pollution and dwindling resources require further understanding of how best to use our resources. Specifically, in the case of carburetion, this means developing better techniques for understanding the metering process so that the internal combustion engine can be made more efficient. Until now, practically all carburetor study has been done by cut-and-try experimentation methods. Now, the digital computer allows a much more detailed theoretical study of the metering process than ever before possible. All that is required is that the proper techniques for using the computer to calculate fuel flow be developed.

Even though this study is directed specifically toward carburetors and the fuel metering process, the possibility of so-called "spin-off" benefits also exists. Many fluid flow problems involve flow through networks of pipes. For example, the water distribution system and sewage disposal system of a city is a very complex network of pipes. Also, many chemical processes require the accurate metering and mixing of different fluid components in order to produce a desirable product. Even the human circulatory system can be described as a fluid network with oscillating flow. Therefore, the possibility exists that some of the technology developed herein can have wide spread applications.

4.2 The Typical Air-Bleed Carburetor

The fuel metering system of a carburetor is a very complex network of interconnecting tubes and orifices. Fuel enters the network at atmospheric pressure from a float bowl, or reservoir as shown in Figure 40, and flows towards the venturis where it enters the low-pressure stream of engine intake-air. Each carburetor, depending on manufacturer, has its own flow scheme, which will include several points where the fuel enters the intake air. The typical metering network also includes several points where ambient air can enter the fuel flow, which creates a two-phase mixture of air and fuel. The points at which air enters are called air bleeds, and the amount of air which is in the metering network is called bleed air, which distinguishes it from intake-air. Figure 40 illustrates the flow scheme of fuel and air in the metering network of a simplified version of a carburetor.

An actual carburetor contains many more elements (about 50) in its metering scheme than the simple carburetor of Figure 40. Therefore, analysis of the fuel flow in the various elements is nearly an impossible task if it is to be done by hand calculations. This is especially true if the effects of flow oscillations, viscosity, and the mixing of air and fuel are to be considered. Therefore, any detailed analysis of carburetor metering requires the use of a computer. This will require the translation of the metering network into an algorithm which can be manipulated by the computer. The technique of making such a transformation and its results comprises the subject of this chapter.

4.3 Previous Work

In the past, the carburetor has been greatly studied. Most of the work on carburetor research has been of a purely experimental nature,

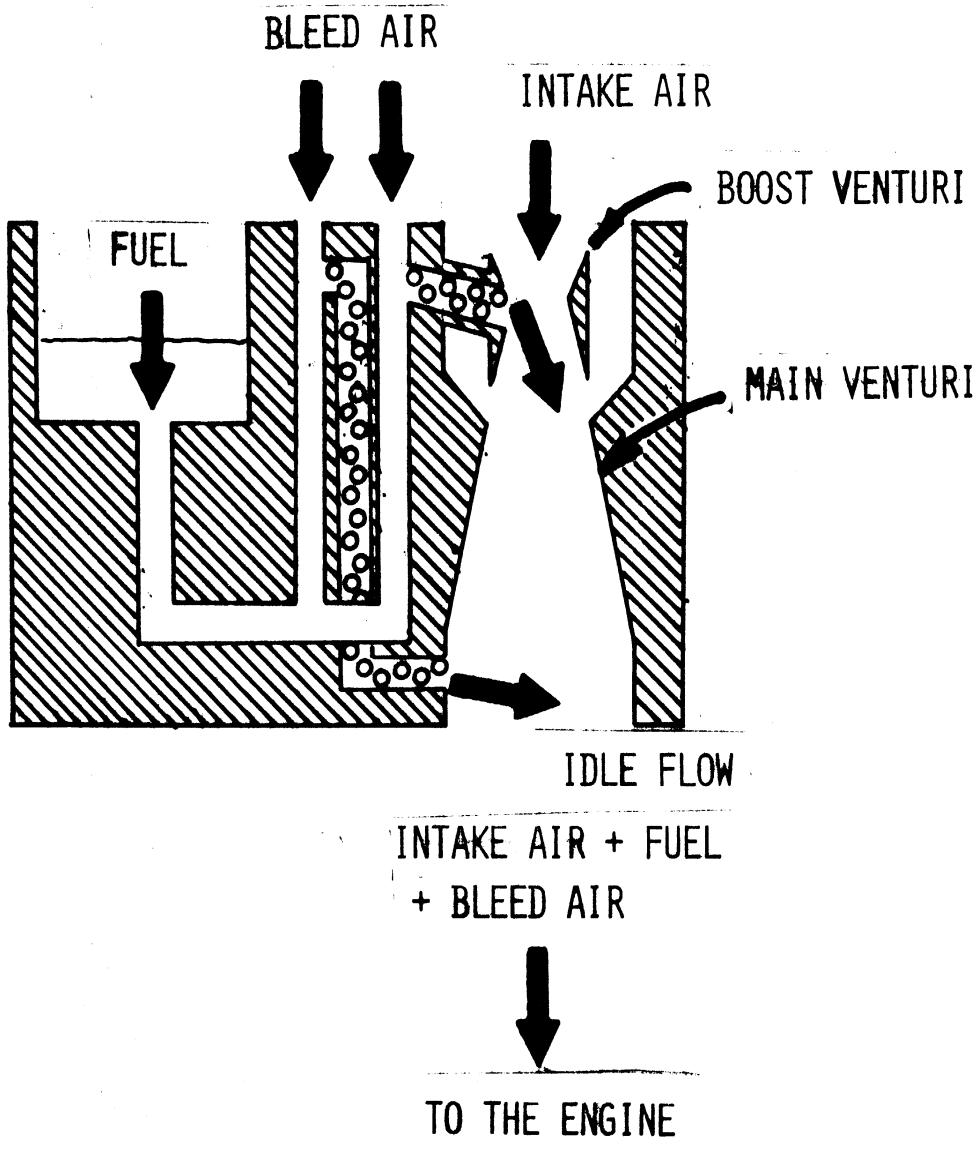

Figure 40. Simplified Version of a Typical Air-Bleed Carburetor.

and any theoretical analysis has contained so many simplifing assumptions as to make the results very questionable. Such simplification was necessary in order to limit the mathematics enough to allow a solution by hand calculations. However, the great speed and large storage capacity of the digital computer now allows the analysis of the carburetor in much greater detail.

Recently, Harrington (20) used the computer to do a comprehensive analysis of carburetor operation. His analysis included the interacting influences of the carburetor, engine, and vehicle at a certain steady condition of engine speed and load. In order to accomplish this, he had to simulate the carburetor metering network, the carburetor venturi system and throttle plate, the intake manifold, the engine, and the vehicle. However, for his metering network analysis, he assumed steady flow, and the analysis was restricted to one metering network. Therefore, a logical extension of his effort is to include the effects of flow oscillation as caused by pressure pulsations which exist in the venturis, and to make the simulation general enough to allow analysis of any metering network. This is the task which has been undertaken here.

The feasibility of modeling transient flow in carburetors was demonstrated by Oyama, Tejima, and Hosho (27) in their investigation of the influence of bleed air on fuel-discharge lag-time. They showed that the transient flow of a mixture of air and gasoline in the emulsion tube can be accurately approximated by single-phase flow which has the same volume-weighted density. Their flow schematic does not contain the idle system and the air is considered to be incompressible, but the results compare very well with experimental results. However, they do

not apply their technique to solving steady oscillatory flow, nor is their method general enough to be applicable to any carburetor flow-network.

Although very few have applied computer solution techniques to carburetors, many have studied methods for solving transient flow in pipe lines and in piping networks. The most common method is the method of characteristics as discussed by Streeter (37), (38), (39), or Benson (31), (32), and many others. This methods involves knowledge of the wavespeed of the pressure pulse, which makes its use in carburetor problems difficult because the wavespeed is not accurately known, especially in the channels which contain a mixture of gasoline and air.

Another method of solving steady oscillatory flow in a pipe is the impedance method, as shown by Streeter (38). It is a very economical method, since the steady oscillatory solution is provided immediately, and no computer time is needed in calculating an initial transient in order to reach the steady oscillatory solution. This method requires the linearization of the governing equations, which limits the solution to small amplitudes of flow oscillation with large average flow. In other words, flow reversal cannot take place. Unfortunately, flow reversal does take place in the carburetor metering network, which makes the impedance method unsuitable for studying carburetors. However, in a most recent work by Yow (43), an impedance method has been developed which can have flow reversal. In future study of steady oscillatory flow in carburetors, this method must be considered.

The method ultimately used here to calculate the unsteady flow in the fuel channels is a finite difference solution based upon a spacially lumped formulation. The formulation is modified to account for compression of any gas phase (bleed air) which may be contained in each of the metering channels. The method requires the assumption of linear density distribution in space, but it does not require knowledge of the pressure-pulse wavespeed. The details of this linear-density method will be discussed later in this chapter.

4.4 Objectives of Simulation

In general, the major objective of the simulation is to provide detailed flow analysis of the metering network. The pressure must be supplied at each point of the network where fuel or air enters or leaves, and the results will contain the flow at each of these points. This will be done for both steady pressures, and pressures as a function of time. Consequently, the results will contain both steady flow values and transient flow values.

Since bleed-air and fuel enter and mix in the fluid network, the flow which leaves the network is a mixture of bleed-air and fuel. This complicates the mass-flow balance in that two species of flow must be balanced, as well as the entire flow. The simulation therefore, must also account for the fraction of air in the total flow on a mass basis (termed quality) and on a volume basis (termed volume quality).

Even though many manufacturers use an air-bleed type of carburetor, many different fuel metering schemes do exist. Also, designers are anxious to try to improve the metering characteristics of their carburetor by modifying its metering network. Such modifications might include merely changing the dimensions of some of the elements

(i.e. perhaps an extra off-idle port). The effect of such modifications on the metering characteristics has usually been determined by building a prototype, and testing it. This becomes a very time consuming process, especially if many different alternatives are to be investigated. Therefore, another goal of this study is to provide a technique which can be used to analyze any fuel metering scheme. This means the fuel metering scheme must be represented in the input data required by the simulation program, and not built into the simulation program.

To summarize the objectives, given the network configuration and the pressure forces at its boundaries, the simulation program will provide the time-steady mass flow, the transient mass flow, and the fraction of air contained by the flow.

4.5 Overall Solution Plan

The problem of completing the objectives requires that the task be logically separated into smaller tasks, and that a method of solution for each smaller task be found separately. Each of the separate solutions can then be combined to achieve the simulation of the metering network.

In order to ultimately achieve a transient solution to pipe flow, a good steady-state solution is required. The steady state solution will establish the initial conditions of pressure and flow for the transient solution, the friction factors for the transient solution, and quality, or fraction of air, in the flow. Therefore, the first major step of the overall solution plan is to solve the steady flows and pressures of the metering network.

Once a steady-state solution has been obtained, the transient solution can be performed. It will provide the pressures as a function

of time at each interior junction as well as the transient flow in the metering elements and at the boundary points. It will provide the dimensionless head ratios for each orifice so that the influence of the flow oscillations on the friction factors of the various orifices can be evaluated from the data of Chapter III. The steady state solution, with the new friction factors, can then again be used to find the time-average flow under the influence of pressure pulsation.

4.6 Describing the Fuel Metering Network

In order to apply the laws of continuity and motion to a fluid metering network, it must be systematically divided into subsections, or flow elements about which detailed general knowledge of the flow characteristics are known. These flow elements in the carburetor, for example, would include the metering orifices and inter-connecting tubes. The flow elements, then comprise the fluid network by being joined to one another at junction points, or junctions.

A mathematical model of the carburetor is then created by first describing the flow in the individual fluid elements with the equations of motion and continuity. The elemental equations are then related to one another by continuity at each junction, and the system of simultaneous equations which results is used to simulate the entire metering network. The accuracy of the simulation then depends upon the accuracy of the information about the flow characteristics of the elements

Three types of elements were used to describe the network: 1) pipe, 2) square edged orifices, and 3) main metering orifices. Each element is assumed to have constant area; therefore, its dimensions can be described by one length and one diameter.

The orientation in space of each element is specified in terms of direction cosines. This requires that one end of the element be designated as the origin point or origin junction for that element in order to determine the positive direction of the orientation. This assumed positive direction is used in the flow equations to maintain the proper sign of the flow.

The points at which the elements are connected to form the metering network are called junctions. Three types of junctions are needed to specify the network which are: 1) interior junctions, 2) boundary junctions exposed to fuel, and 3) boundary junctions exposed to air. In the computer program, continuity is satisfied at each interior junction, and boundary conditions of pressure are required as input data at each boundary junction. The number of elements which join together at each junction are required for each interior junction in order use the continuity relationship. Also, the number of elements which connect the boundary junction to the reference junction are needed in order to use use the boundary conditions in the steady-state solution. The reference junction is one boundary junction which is taken at zero head. For this simulation the float bowl, where the fuel enters the main channel, is always taken as the reference junction.

In order to specify the fluid network to the computer, the elements and junctions must be given consecutive numbers. This is done by starting with "1" at the float bowl, and consecutively numbering the junctions. The elements are then also numbered consecutively by starting with one. The integer numbers given to each junction and element are then used to form a sequence of integers which describes the entire flow network to the simulation program.

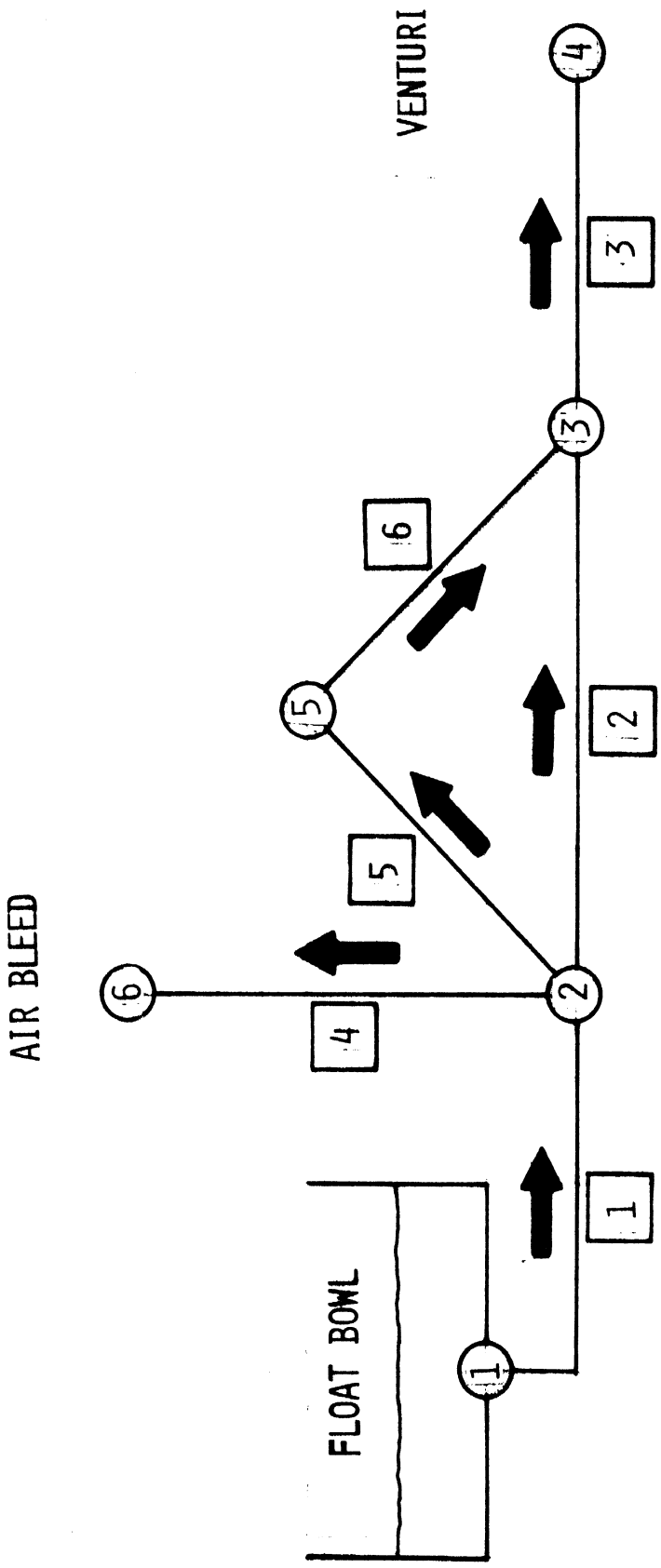

Figure 41. Schematic of a Simple Network.

At this point, an example of a simple network will help clarify the method of describing the fluid network. Figure 41 shows a simple fluid network of 6 elements and 6 junctions. The reference junction is junction #1, the boundary junctions are 1, 4, and 6, and the interior junctions are 2, 3, and 5. The scheme of specifying the sequence which represents the fuel network is developed by considering each junction. For each junction, a portion of the sequence is written, and the rule used to create its portion depends upon the type of junction. For an interior junction type, such as junction #2, the sequence rule is as follows:

Junction number [(element, junction at other end of the element)] repeated for each element attached to junction.

or for junction #2

2, 1, 1, 4, 6, 5, 5, 2, 3

For a boundary junction, such as junction number 6, the sequence rule is as follows:

Junction number, (element, junction) along path from Ref. junction

or for junction number 6:

6, 1, 2, 4, 6

However, some boundary junctions have more than one path which connects them to the reference junction, such as junction number 4. In this case, a sequence must be written for each path as follows:

4, 1, 2, 2, 3, 3, 4,

7, 1, 2, 5, 5, 6, 3, 3, 4

Notice that the second sequence does not start with a junction number (there are only six junctions). The numbers which begin these portions

of the sequence to represent the second and succeeding paths for boundary junctions start at the number of junctions plus 1, in this case 6 + 1. Finally, the entire sequence which represents the simple network is as follows:

X = 1, 1, 2,
2, 1, 1, 4, 6, 5, 5, 2, 3,
3, 2, 2, 6, 5, 3, 4,
4, 1, 2, 2, 3, 3, 4,
5, 5, 2, 6, 3,
6, 1, 2, 4, 6,
7, 1, 2, 5, 5, 6, 3, 3, 4

Notice that junction #1, the reference junction, does not follow the sequence rules, because it has no path to itself, since it is the reference junction. Lines 2 through 7 contain the information which is necessary to describe the network to the simulation program.

Of course, information about the dimensions of the elements, length and diameter or L and D, are also required by the simulation. The total number of elements, NELS, is also required, which is 6 for the case of the simple network. The direction cosines, CS, for each element are given by picking a fixed set of reference coordinates, picking a positive element direction, and then by giving the cosines in the positive direction in reference to the fixed coordinate frame. The positive element direction is defined by specifying one end of the element as the origin junction. The positive direction is then away from this end. Figure 42 illustrates the direction cosines for one element, and the origin junctions and direction cosines for the simple network are:

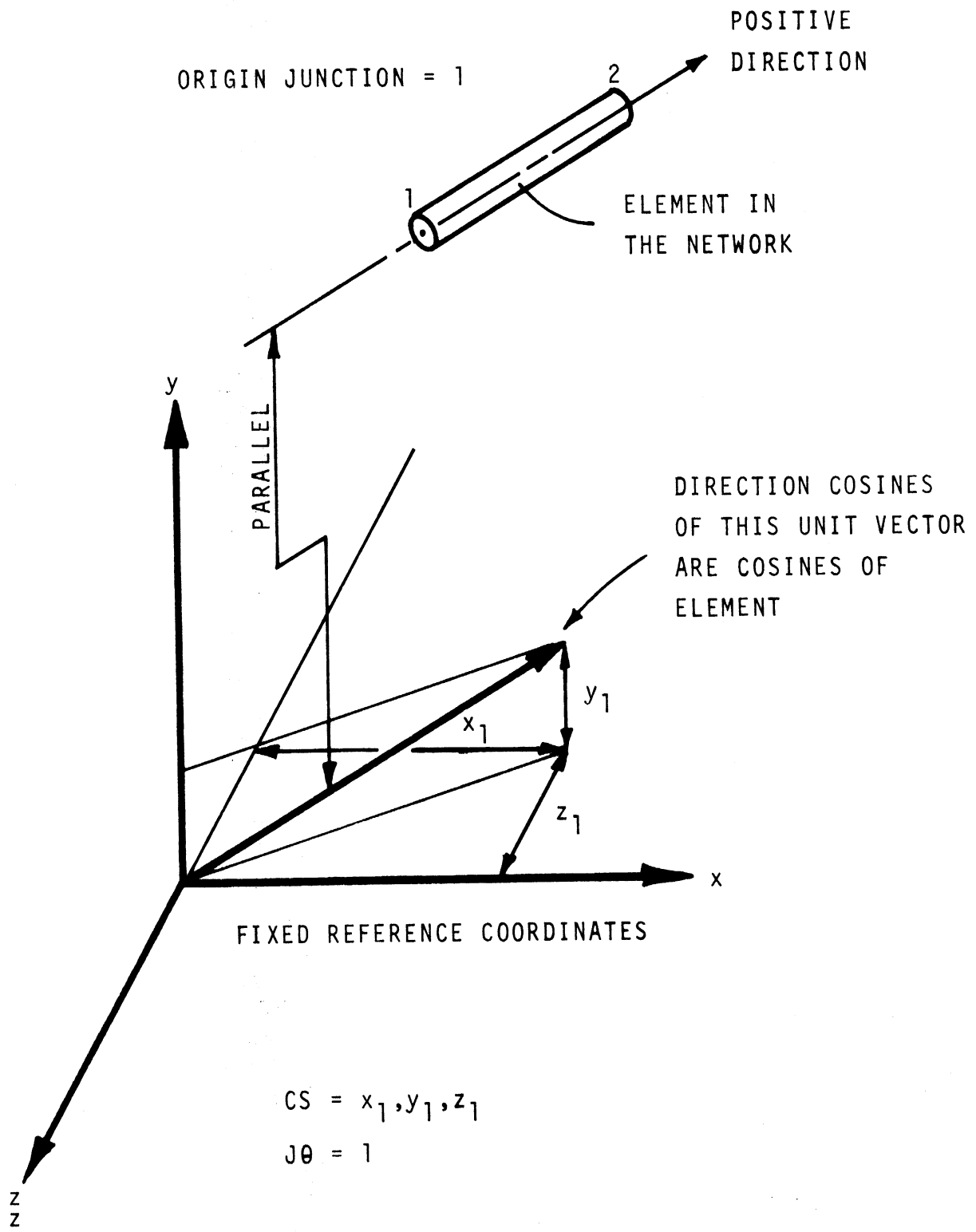

Figure 42. Direction Cosines of an Element.

JO = 1, 2, 3, 2, 2, 5

CS = 0,1,0, 0,1,0, 0,1,0, 0,1,0, 0,1,0, 0,1,0,

The number of elements of each junction (NL) is also needed, as well as the element type (LT). For the simple network of Figure 41, the number of elements is given as:

NL = 1, 4, 3, 3, 2, 2, 4, and

the element types are given as:

LT = 6 * 0

The integer code used to describe the element types is as follows:

LT = 0: pipe

LT = 1: main orifice

LT = 2: square edged orifice.

The element type is used for the friction factor, and a larger number of element types could be used as soon as detailed information about their pressure versus flow characteristics are known.

The junction type (JT) is also needed so that the simulation can treat each junction as a boundary point exposed to air or fuel, or an interior junction. The following sequence supplies the information about the six junctions of the simple network:

JT = 1,0,0,2,2,0,2,

where

JT = 0: interior junction

JT = 1: boundary junction exposed to fuel

JT = 2: boundary junction exposed to air

Parameters needed for a Solution:

The steady-state solution technique requires that an initial guess be made for the quality (RJ) at each junction, for the friction

factor of each element (FT) and for the pressure at each junction. Of course, the values used at the boundary junctions are not guesses, but known values. The following values are used for one solution of steady flow in the simple network:

RJ = 0.,2*.05,1.,1.,.05,

FT = 6*.5

PT = 15.,14.,13.,12.,15.,13.5

Some additional flow parameters are also needed, which are the direction of gravity (CSG, in terms of three direction cosines) the magnitude of gravity (G), the fluid temperature (T), and the fluid (NFLU). For the simple network, the following values are given:

CSG = 0.,-1.,0., G = 32.2

T = 75., NFLU = 1

The parameters NFLU and T are used to atain the fluid properties of viscosity and specific gravity. The fluid number, NFLU, corresponds to a certain fuel for which the properties, as a function of temperature, are known. See the listing in Appendix C of SUBROUTINE FPROP for all of the fluids which are available for this simulation.

The entire data set, which is used for a steady-state solution of the simple network of Figure 41 is now given as

X = 1,1,2

2,1,1,4,6,5,5,2,3,

3,2,2,6,5,3,4,

4,1,2,2,3,3,4,

5,5,2,6,3,

6,1,2,4,6,

7,1,2,5,5,6,3,3,4,

```
D = 6*.1,
L = 6*1.,
NELS = 6,
CS = 0.,1.,0.,0.,1.,0.,0.,1.,0.,
     0.,1.,0.,0.,1.,0.,0.,1.,0.,
JT = 1,0,0,2,2,0,2,
NL = 1,4,3,3,2,2,4,
LT = 6*0,
JO = 1,2,3,2,2,6,
RJ = 0.,2*.05,1.,1.,.05,
FT = 6*.5,
PT = 15.,14.,13.,12.,15.,13.5,
CSG = 0.,-1.,0., G = 32.2, T = 75., NFLU = 1
G = 32.2,
T = 75.,
NFLU = 1
```

4.7 Basic Assumptions

Each element of the carburetor, which may contain air, fuel, or a mixture of the two, is assumed to have constant dimensions. Its length and diameter are fixed. Hence, its cross-sectional area is also constant. The proportion of air and fuel, which flows through it, is also constant, and the density of the fluid varies linearly along the element length. The proportion of the flow which is air, is assumed to have a density which is isothermally dependent upon pressure, and no fuel vaporization or condensation is allowed.

The elements are assumed to be connected by volume less junctions or points. Therefore, these points cannot contain any mass or accumulate any mass, nor can they cause any frictional force. Perfect mixing of bleed air and fuel is also assumed to occur at each interior junction. This means that the fraction of air is equal in all the elements connected to one junction for which the flow is away from the junction. This is best illustrated by the following simple example:

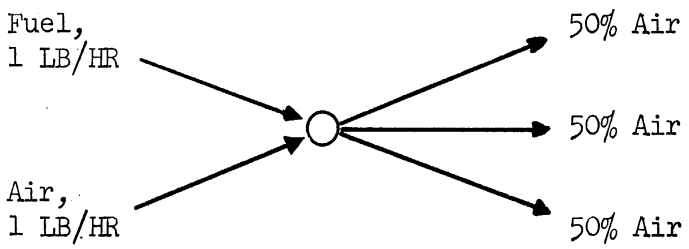

The fraction of air is assumed to remain constant for the transient solution.

4.8 Steady State Flow

Harrington (20) showed that the assumption that flow is proportional to the square root of the pressure drop is appropriate for steady flow in carburetor channels. A flow conveyance factor, R, can be introduced to create the following equation for each element:

$$\dot{m} = R_{EL}\sqrt{\Delta P_{EL}} \tag{4.1}$$

where:

$$R_{EL} = A\sqrt{\rho}\ /FT$$

Continuity is written for each interior junction as follows:

$$\sum_{1}^{NL} \dot{m} = 0 = \sum_{EL=1}^{NL} R_{EL}\ \sqrt{\Delta P_{EL}} \tag{4.2}$$

The pressure drop between junction #1 and each boundary junction is written as follows for each path between 1 and j:

$$P_j - P_1 = \sum_{EL=1}^{NL} \sqrt{\Delta P_{EL}}\,\sqrt{\Delta P_{EL}} \qquad (4.3)$$

A set of equations is, therefore, obtained which describes the pressure drops of the network.

Since the equations are non-linear, an iterative solution is used to solve the system of equations. The equations are rewritten as follows:

$$0 = \sum_{EL=1}^{NL} R_{EL} x_{EL} \quad ; \qquad \text{Interior Junction Equation (4.2a)}$$

$$DP_j = \sum_{EL=1}^{NL} X_{EL}\, x_{EL} \qquad \text{Boundary Junction Equation (4.2b)}$$

where

$$x_{EL} = \sqrt{\Delta P_{EL}}\,, \quad \text{independent variable} \qquad (4.4)$$

$$X_{EL} = \sqrt{\Delta P_{EL}}\,, \quad \text{from previous solution, specified initially to get solution started.} \qquad (4.4a)$$

$$DP_j = P_j - P_1 \qquad (4.5)$$

For the simple network, the system of equations which results by using the information of the X vector to determine which elements connect to which junctions is as follows:

$0=R_1\sqrt{\Delta P_1}$	$-R_2\sqrt{\Delta P_2}$	$+0$	$-R_4\sqrt{\Delta P_4}$	$-R_5\sqrt{\Delta P_5}$	$+0$
$0=0$	$+R_2\sqrt{\Delta P_2}$	$-R_3\sqrt{\Delta P_3}$	$+0$	$+0$	$+R_6\sqrt{\Delta P_6}$
$P_4-P_1=\Delta P_1$	$+\Delta P_2$	$+\Delta P_3$	$+0$	$+0$	$+0$
$0=0$	$+0$	$+0$	$+0$	$+R_5\sqrt{\Delta P_5}$	$-R_6\sqrt{\Delta P_6}$
$P_6-P_1=\Delta P_1$	$+0$	$+0$	$+\Delta P_4$	$+0$	$+0$
$P_4-P_1=\Delta P_1$	$+0$	$+\Delta P_3$	$+0$	$+\Delta P_5$	$+\Delta P_6$

The solution of this system of equations will then give the pressure difference for each element.

Solution Technique, Steady State

Initially, a guess is made for each element pressure drop, and the square root of the guess is used as a coefficient in the boundary junction equations. The coefficient of the terms in the interior junction equations are the conductances which relate flow to the square root of pressure drop for each of the adjoining elements.

The values of "x_{EL}" are found by solving the system of equations with subroutine DGELG in the scientific subroutine package (*SSP). The values are compared to the previous values, and the iterative process is terminated if the difference is small (less than TOLP). Otherwise the process continues by selecting new values of X_{EL} according to:

$$(X_{EL})_{NEW} = (X_{EL}\ x_{EL})^{1/2} \tag{4.6}$$

and solving the system of equations again for the values of x_{EL}.

Next, from Equation 4.1, the flow through each of the elements is calculated according to:

$$\dot{m} = (R_{EL})\ (x_{EL}). \tag{4.1a}$$

The flow out of each boundary junction is equal to the flow of the element which leads to the junction, since each boundary is joined by only one element.

The pressure gradeline at each junction is then calculated from the pressure drops. This is accomplished by adding the pressure drop for each element in the sequence specified for the boundary junction equations. This is illustrated as follows:

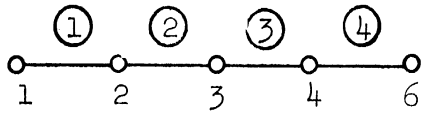

$P_2 = P_1 + \Delta P_1$ P_1 is known

$P_3 = P_2 + \Delta P_2$ ΔP's were previously calculated

$P_4 = P_3 + \Delta P_3$

$P_5 = P_4 + \Delta P_4$

The pressure loss due to changes in elevation is calculated from the density of each element and the change in elevation for each element. The change in elevation is found by the formula:

$$DZ = L * COS\ \theta * G. \qquad (4.7)$$

where

L = element length

θ = angle between element and acceleration, G

G = magnitude of acceleration, normally 32.2 ft/sec.^{2}

Therefore, the pressure difference due to changes in elevation for an element is:

$$DPZ = RH\theta * DZ \qquad (4.8)$$

The pressure due to elevation for each junction is then calculated the same as the pressure gradeline

$$PZ_2 = PZ_1 + DPZ_1$$

$PZ_3 = PZ_2 + DPZ_2$, or, in general

$$PZ_j = \sum_{i=1}^{j-1} PZ_i \tag{4.9}$$

PZ_1 is known reference, usually 0.

The total pressure at each junction is then easily obtained as follows:

$$PT = PG - PZ \tag{4.10}$$

4.9 Fraction of Air: Quality

As mentioned previously, some of the elements contain bleed air, some contain fuel, and some contain a mixture of the two. Since the fluid properties are based on a weighted value according to the percentage of air in the total flow, or quality, this quantity for each element and each junction must be known for the steady-state solution. Initially, the values are guessed, but calculations of steady flow are used to calculate the values of quality for successive iterations for the steady-state solution.

The quality of a junction, Q_j, is defined as the mass flow of air into the junction divided by the total mass flow into the junction:

$$Q_j = \frac{\dot{m}_a}{\dot{m}_T} \quad \frac{\text{LB/HR air}}{\text{LB/HR total flow}} \tag{4.11}$$

Perfect mixing is assumed, which means:

$$Q_j \sum_{IN} \dot{m} = \sum_{IN} Q_i \dot{m} \tag{4.12}$$

where Q_i is the quality of the junctions at the other ends of the elements which have flow towards junction J. A system of linear equations results by writing the above equation for each interior junction as follows:

$$Q_j \sum_{IN} \dot{m} - \left[\sum_{IN} Q_i \dot{m} \right]_{\substack{\text{Int.} \\ \text{Junction}}} = \left[\sum_{IN} Q_i \dot{m} \right]_{\substack{\text{Boundary} \\ \text{Points}}} \qquad 4.12a$$

The right-hand side may be zero if all junctions from which fluid is flowing toward J are interior junctions. A simple example will clarify the method of solution as shown below.

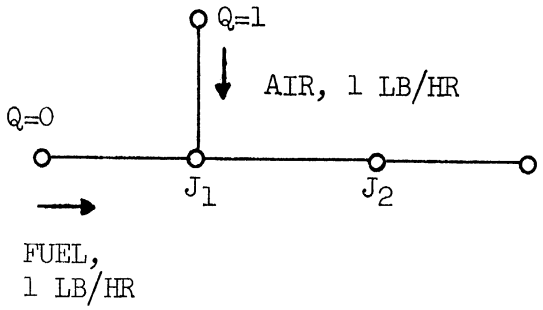

$$Q_{J_1}(1 + 1) - 0 = 0(1) + (1)(1)$$

$$Q_{J_2}(2) - Q\ (2) = 0$$

So:

$$Q_{J_1} = 0.5$$

$$Q_{J_2} = 0.5$$

The flow at J_1 and J_2 is 50% air by mass. Subroutine QUAL contains the programming for the solution of quality.

4.10 Friction Factors

Harrington (20) gives a very complete discussion of friction factors for steady flow. For the simulation performed here, the forces which are due to friction were assumed to be one of three types:

1. Wall friction factor, F,
   a. pipe flow (LT = 0)
   b. main orifice flow (LT = 1)
   c. Square orifice flow (LT = 2)
2. area change factor, F_A,
3. bend loss factor, F_B.

As shown, the wall friction is divided into three catagories. If the element type is an orifice, the area change loss factor is already included in the coefficient of discharge. Also, area change factors are not included when more than two elements join at a junction. Bend loss factors are not included if the element is an orifice.

The total friction factor, F_T is taken as:

FT = FA + FB+F,

and this is the factor which is used in the steady and transient flow equations to give the frictional force when multiplied by the square of the velocity. Subroutine FRIC is the part of the simulation which provides the friction factors.

Pipe Friction Factor: Elements which are too long to be considered as orifices are modeled by using the Moody friction factors for smooth pipe, as shown by Streeter (36). The Reynolds number is required to obtain the friction factor, and it is easily calculated from the flow, element dimensions and fluid properties. In the case of two-phase-flow, the pipe friction factor was multiplied by 4.5,

as suggested by Harrington (20). The factor of 4.5 is based on empirical data for the Ford carburetor used in this study; consequently, it may be different for other flow configurations. Frictional forces for two-phase-flow are not well studied and more work on this topic should be performed.

Orifice Friction Factor: As previously mentioned, the main metering orifice and other square orifices are the flow controlling elements in the fuel metering network. Consequently, orifice friction factors, or conversely, coefficients of discharge must be accurately known. This was the motivation for the study in Chapter III, the study of the influence of flow oscillation on the flow through small metering orifices. Harrington (20) used empirical data for the coefficients as follows:

$$C_d = f\ (Re,\ L/D)$$

However, the study of Chapter III showed that the effect of flow oscillation on the flow coefficient can be accounted for by head ratio, HR, as follows:

$$C_d = f\ (Re,\ L/D,\ HR)$$

Empirical values of the coefficients of discharge are stored in SUBROUTINES CDMEAN and CDSQ. CDMEAN contains the data for the F-50 main orifice and CDSQ contains the data for the square-edged orifices. This empirical data of Appendix B is curve-fitted for Reynolds Number, and then parabolically interpolated for its dependence upon L/D and head ratio.

Area Change Factors: When only two elements join at a junction, usually they are of different diameters. The resulting area

change adds to the frictional losses of the network, and are accounted for in the following way:

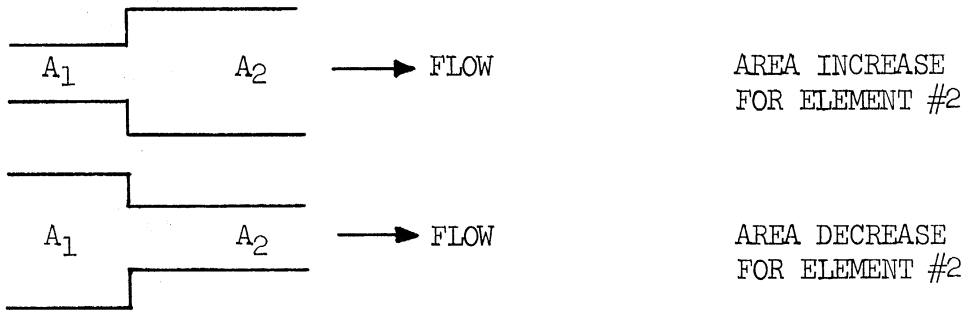

Harrington (21) gives the formulas used in this simulation to account for area changes.

Bend Loss Factors: A bend loss factor occurs when two elements are not aligned on a common axis, or when three elements form a tee section. Empirical data is used for these factors and the equations are well documented by Harrington (20). The loss which occurs for two elements is given as a function of the angle between them. This was easily calculated in the simulation from the direction cosines of the adjoining elements as follows:

$$\cos\theta = \cos\alpha \ \cos\alpha_2 + \cos\beta \ \cos\beta_2 + \cos\gamma \ \cos\gamma_2$$

where θ is the angle between the directed elements. The loss for tee sections was given only for 90° tee sections, and was neglected in the simulation for tee sections other than 90°.

4.11 Results of Steady-State Flow Simulation of a Simple Network

Table IV shows the steady-flow results which were obtained from the simple network example of the preceding discussion. Notice that data is represented for two major catagories, junctions and elements. The pressures of the junctions are given as well as the flows. The sign of the flow is minus for flow into the network, and, of course, the flow for each interior junction is zero. For the elements, the

TABLE IV
STEADY-FLOW RESULTS FOR A SIMPLE NETWORK
JUNCTIONS

J	PRESSURE, LB/SQ-IN TOTAL	GRADE	HEAD	FLOW, LB/HR TOTAL	AIR	FUEL	AIR/TOT
1	15.000	15.000	0.0	-23.19621	0.0	-23.19621	0.0
2	14.942	14.968	0.02627	0.0	0.0	0.0	0.052036
3	14.093	14.121	0.02783	0.0	0.0	0.0	0.052036
4	12.000	12.029	0.02861	24.46951	1.27329	23.19621	0.052036
5	15.000	15.026	0.02631	-1.27329	-1.27329	0.0	1.000000
6	14.518	14.545	0.02705	0.0	0.0	0.0	0.052036
7	-0.000	-0.000	0.0	0.0	0.0	0.0	1.000000

ELEMENTS

EL	DIMENSIONS DIAM, INCH	LENGTH INCH	PRESS DROP PSI	FLOWS, LB/HR TOTAL	AIR	FUEL	AIR/TOT	RE NUM	FRIC	DENSITY LB/CU-FT	VOLUME RATIO
1	.100	1.000	0.03153	23.1962	0.0	23.196	0.0	3659.	0.907	45.3575	0.0
2	.100	1.000	0.84818	14.6278	0.7455	13.882	0.0510	3042.	1.917	1.3497	0.972
3	.100	1.000	2.09246	24.4695	1.2471	23.222	0.0510	5101.	1.685	1.3497	0.972
4	.100	1.000	-.05784	-1.2733	-1.2733	0.0	1.0000	4826.	0.880	0.0708	1.000
5	.100	1.000	0.42370	9.8417	0.5016	9.340	0.0510	2059.	2.114	1.3497	0.972
6	0.100	1.000	0.42370	9.8417	0.5016	9.340	0.0510	2059.	2.114	1.3497	0.972

dimensions are given in inches as well as the pressure loss and the flows of air and fuel. The sign of the flow for each element depends upon the chosen positive direction for each element. Plus flow is away for the chosen origin junction, JO. The sign of the pressure drop follows the same rule. Some unbalance of continuity can be noted due to the iterative nature of the solution.

4.12 Solution of Transient Flow: Linear Density Method

Harrington (20) and Hosho (22) have both observed, with high speed movies, the transient nature of the fluid flow out of the carburetor for an engine at a steady load and speed condition. The cause of this transient behavior can be divided into two main phenomena: that which occurs due to the pulsating nature of the pressure at the venturi and that which occurs due to the "slugging" of fuel in the fuel-air mixture which exists in the metering channels. Hosho claims that the later phenomenon is the only cause of transient fuel flow. However, the experimental studies of Chapter II showed that at wide open throttle and low engine speed, the former phenomenon is predominant. For this study, the mixture of air and fuel is assumed to be homogeneous, and the fluid properties are based on a weighted average of the two constituents. Therefore, the work that follows only considers the influence of the pressure pulsation at the venturis on the oscillations of the flow, and not the influence pulsations caused by slugging of two-phase-flow.

The procedure developed is very similar to that for steady flow: that is, each individual element is described by the equations of motion and continuity, and then the equations are related by continuity at the interior junctions to form a system of simultaneous

equations. The X vector is used to specify how the equations are to be related and the solution of the system of equations at successive points in time generates the transient solution under the action of the prescribed boundary conditions (venturi, air bleed and float bowl pressures).

Transient Flow in an Element: Linear Density

Figure 43 shows the control volume used to analyze a flow element. Continuity is written for the control volume, which utilizes the assumption that the density varies linearly along the element length.

$$\frac{\partial}{\partial x}(\rho V) = -\frac{\partial}{\partial t}\rho \tag{4.13}$$

$$\rho = \rho_1 + \rho_s x \tag{4.14}$$

$$\frac{\partial}{\partial t} = \frac{d\rho_1}{dt} + \frac{d\rho_s}{dt}x = \dot{\rho}_1 + \dot{\rho}_s x \tag{4.15}$$

$$\int_0^x \partial(\rho v) = -\int_0^x (\dot{\rho}_1 + \dot{\rho}_s x)\, dx \tag{4.16}$$

$$(\rho v)_x - (\rho v)_1 = -\dot{\rho}_1 x - \dot{\rho}_s \frac{x^2}{2} \tag{4.16a}$$

or

$$(\rho v)_x = (\rho v)_1 - \dot{\rho}_1 x - \dot{\rho}_s \frac{x^2}{2} \tag{4.16b}$$

The linear density relationship can also be expressed in terms of the density at the downstream end, point #2.

$$\rho = \rho_2 - \rho_s (L-x) \tag{4.17}$$

$$\frac{\partial \rho}{\partial t} = \dot{\rho}_2 - \dot{\rho}_s (L-x) \tag{4.18}$$

$$\int_x^L \partial(\rho v) = -\int_x^L \left[\, \dot{\rho}_2 - \dot{\rho}_s (L-x) \,\right] dx \tag{4.19}$$

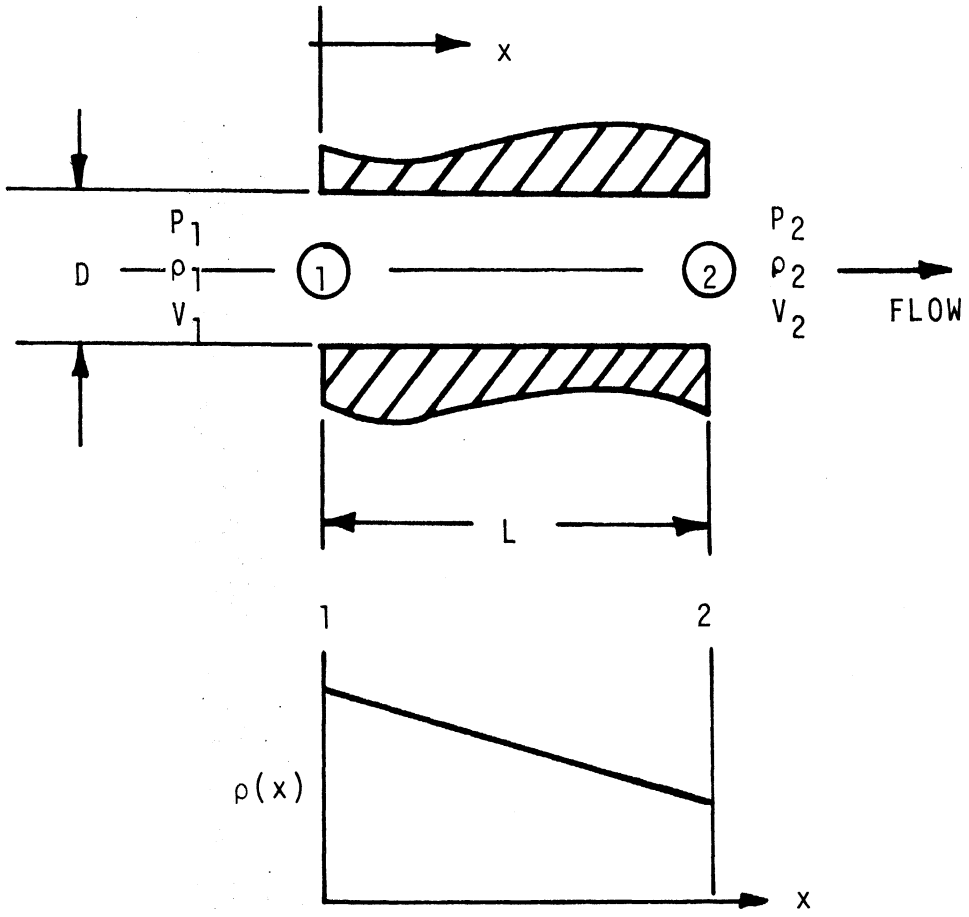

Figure 43. Control Volume for Transient Flow in an Element.

$$(\rho v)_2 - (\rho v)_x = -\dot{\rho}_2 (L-x) + \dot{\rho}_s \frac{(L-x)^2}{2} \tag{4.20}$$

$$(\rho v)_x = (\rho v)_2 + \dot{\rho}_2 (L-x) - \dot{\rho}_s \frac{(L-x)^2}{2} \tag{4.20a}$$

Now the equation of motion can be used to describe the flow at each end of the element.

$$\sum F = \frac{d}{dt} \int_{\Psi} \rho V d\Psi + \int_A \rho V (V.n)\, dA \tag{4.21}$$

The surface forces are the pressure force at each end of the element, and the viscous shear forces on the peripheral walls, as represented by friction force per cross-sectional area.

$$\sum F = (P_1 - P_2 - F_r)A \tag{4.22}$$

The temporal inertial force is found by substituting the mass flux relationship found from continuity, Equation 4.16b:

$$\frac{d}{dt}\int_{\Psi} \rho V d\Psi = \frac{d}{dt} \int_0^L \left[(\rho V)_1 - \dot{\rho}_1 x - \dot{\rho}_s \frac{x^2}{2} \right] A\, dx$$

$$= A \frac{d}{dt} \left[(\rho V)_1 L - \dot{\rho}_1 \frac{L^2}{2} - \frac{\dot{\rho}_s L^3}{6} \right]$$

$$= A \left[L \frac{d}{dt} (\rho V)_1 - \ddot{\rho}_1 \frac{L^2}{2} - \ddot{\rho}_s \frac{L^3}{6} \right] \tag{4.23}$$

The convective inertial force is evaluated as:

$$\int_A \rho V (V \cdot n)\, dA = (\rho_2 V_2^2 - \rho_1 V_1^2) A \tag{4.24}$$

When the three terms are combined by equation 4.21, the constant area term is cancelled and the equation of motion is then given by:

$$P_1 - P_2 - F_R = L \frac{d(\rho V)_1}{dt} - \ddot{\rho}_1 \frac{L^2}{2} - \ddot{\rho}_s \frac{L^3}{6} + \rho_2 V_2^2 - \rho_1 V_1^2 \tag{4.25}$$

Instead of using $(\rho V)_x$ as given by equation 4.16b, $(\rho V)_x$ as given by equation 4.20a is now used in the temporal term of the equation of motion, equation 4.23, to give:

$$\frac{d}{dt}\int_{\forall} \rho V d\forall = A\frac{d}{dt}\int_{o}^{L}\left[(\rho V)_2 + \dot{\rho}_1 (L-x) - \dot{\rho}_s \frac{(L-x)^2}{2} \right] dX$$

$$= A\frac{d}{dt}\left[(\rho V)_2 L + \dot{\rho}_2\frac{L^2}{2} - \dot{\rho}_s\frac{L^3}{6} \right]$$

$$= A\left[L\frac{d}{dt}(\rho V)_2 + \ddot{\rho}_2\frac{L^2}{2} - \ddot{\rho}_2\frac{L^3}{6}\right] \qquad (4.26)$$

The equation of motion is then re-written as:

$$P_1-P_2-F_R = L\frac{d}{dt}(\rho V)_2 + \ddot{\rho}_2\frac{L^2}{2} - \dddot{\rho}_s\frac{L^3}{6} + \rho_2 V_2^2 - \rho_1 V_1^2 \qquad (4.27)$$

Equations 4.25 and 4.27 can now be used to solve for the rate of change of mass flux at either end of the element in terms of properties at the ends of the elements, as follows:

$$d(\rho V)_1 = \frac{dt}{L}\left\{ P_1-P_2-F_R+ \ddot{\rho}_1\frac{L^2}{2} + \dddot{\rho}_s\frac{L^3}{6} + \rho_1 V_1^2 - \rho_2 V_2^2 \right\} \qquad (4.25a)$$

$$d(\rho V)_2 = \frac{dt}{L}\left\{ P_1-P_2-F_R- \ddot{\rho}_2\frac{L^2}{2} + \dddot{\rho}_s\frac{L^3}{6} + \rho_1 V_1^2 - \rho_2 V_2^2 \right\} \qquad (4.27a)$$

Density

A volume-fraction weighted-density is used to approximate the density of the mixture of fuel and air which flows in the elements. It is given as:

$$\rho = \rho_f (1-V_q) + \rho_a V_q \qquad (4.28)$$

The fuel density, ρ_f, and the volume quality of air, V_q, are constants for each element. Therefore,

$$\ddot{\rho} = V_q \ddot{\rho}_a \qquad (4.29)$$

An isothermal relationship is assumed to relate the density of the air to that of the pressure, and it is given as:

$$\rho_a = \frac{P}{RT} \qquad T = \text{CONSTANT} \tag{4.30}$$

Therefore, equations 4.28 and 4.29 can now be written in terms of pressure as:

$$\rho = \rho_f (1-V_q) + \frac{P}{RT} V_q \tag{4.28a}$$

$$\ddot{\rho} = \frac{\ddot{P} V_q}{RT} \tag{4.29a}$$

Also, the slope of the linear density equation can be evaluated in terms of the densities at the ends of the element as follows:

$$\rho_s = \frac{\rho_2-\rho_1}{L} \tag{4.31}$$

and by substituting and differentiating pressure into equation 4.31:

$$\ddot{\rho}_s = \frac{1}{L} (\ddot{\rho}_2-\ddot{\rho}_1) = \frac{V_q}{LRT} (\ddot{P}_2-\ddot{P}_1) \tag{4.32}$$

By substituting the density-pressure relationships into the equations of motion for the element and combining terms, the following equations result:

$$d(\rho V)_1 = \frac{dt}{L} \left\{ P_1-P_2-F_R + \frac{V_q L^2}{3RT} \left[\ddot{P}_1 + .5\, \ddot{P}_2 \right] + \left[\rho_f (1-V_q) + \frac{P_1 V_q}{RT} \right] V_1^2 - \left[\rho_f (1-V_R) + \frac{P_2 V_q}{RT} \right] V_2^2 \right\} \tag{4.25b}$$

$$d(\rho V)_2 = \frac{dt}{L} \left\{ P_1-P_2-F_R - \frac{V_q L^2}{3RT} \left[\ddot{P}_2 + .5\, \ddot{P}_1 \right] + \left[\rho_f (1-V_q) + \frac{P_1 V_q}{RT} \right] V_1^2 - \left[\rho_f (1-V_q) + \frac{P_2 V_q}{RT} \right] V_2^2 \right\} \tag{4.27b}$$

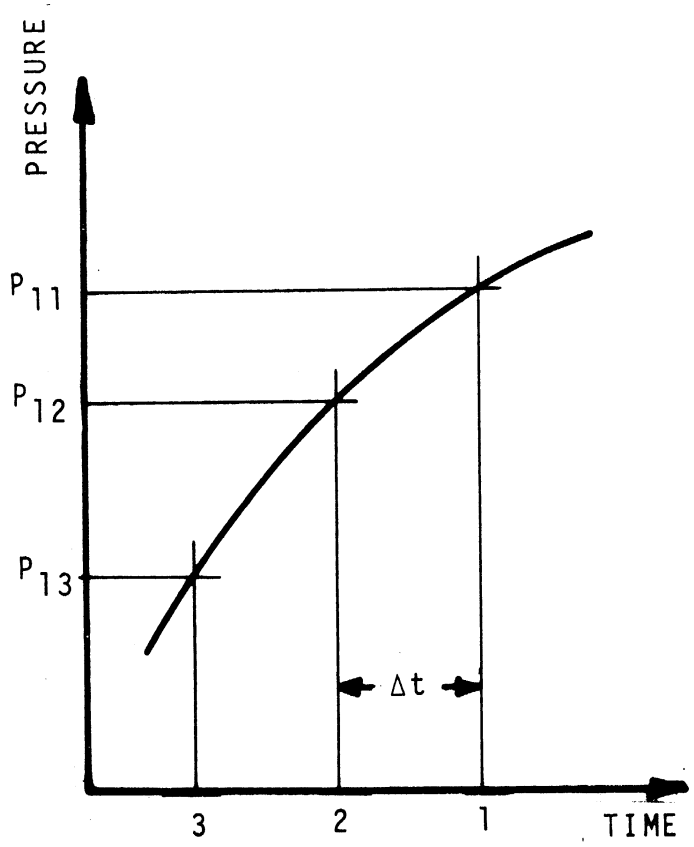

$$\frac{d^2P}{dt^2} \approx \frac{P_{11} - 2P_{12} + P_{13}}{\Delta t^2}$$

Figure 44. Finite Difference Form of the Second Derivative.

The double subscript for pressure is now used to indicate position and time, as follows:

$$P_{(\text{position})(\text{time})}$$

where a position of "1" is the upstream end, and of "2" is the downstream end. Time is indicated as first, second or third interval, with the first as current time, as shown in Figure 44.

The second derivatives of pressure in equations 4.25b and 4.27b are now written in finite difference form as:

$$\ddot{P}_1 + .5\,\ddot{P}_2 = \frac{P_{11}-2P_{12}+P_{13}+.5\,(P_{21}-2P_{22}+P_{23})}{\Delta t^2} \tag{4.33}$$

$$\ddot{P}_2 + .5\,\ddot{P}_1 = \frac{P_{21}-2P_{22}+P_{23}+.5\,(P_{11}-2P_{12}+P_{13})}{\Delta t^2} \tag{4.34}$$

The equation of motion for the element can now be written in a form which is suitable for finite difference solution as follows:

$$\Delta(\rho V)_1 = \frac{\Delta t}{L}\left\{ P_{11}-P_{21}-F_R + \frac{V_q L^2}{3RT}\left[\frac{P_{11}-2P_{12}+P_{13}+.5P_{21}-P_{22}+.5P_{23}}{\Delta t^2} \right] \right.$$

$$\left. + \left[\rho_f(1-V_q) + \frac{P_{11}V_q}{RT} \right] V_1^2 - \left[\left(\rho_f(1-V_q) + \frac{P_{21}V_q}{RT}\right] V_2^2 \right\} \tag{4.25c}$$

$$\Delta(\rho V)_2 = \frac{\Delta t}{L}\left\{ P_{11}-P_{21}-F_R - \frac{V_q L^2}{3RT}\left[\frac{P_{21}-2P_{22}+P_{23}+.5P_{11}-P_{12}+.5P_{13}}{\Delta t^2} \right] \right.$$

$$\left. + \left[\rho_f(1-V_q) + \frac{P_{11}V_q}{RT} \right] V_1^2 - \left[\left(\rho_f(1-V_q) + \frac{P_{21}V_q}{RT}\right] V_2^2 \right\} \tag{4.27c}$$

The above equations are now simplified by combining like terms of pressure to obtain the following two equations

$$\Delta(\rho V)_1 = \frac{\Delta t}{L}\left\{\left(1+\frac{V_q L^2}{3RT\,\Delta t^2}+\frac{V_q V_1^2}{RT}\right)P_{11}\right.$$

$$-\left(1+\frac{V_q L^2}{6RT\,\Delta t^2}+\frac{V_q V_2^2}{RT}\right)P_{21}-F_R$$

$$\left.+\frac{V_q L^2}{3RT\,\Delta t^2}(-2P_{12}+P_{13}-P_{22}+.5P_{23})+\rho_f(1-V_q)(V_1^2-V_2^2)\right\} \qquad (4.25d)$$

$$\Delta(\rho V)_2 = \frac{\Delta t}{L}\left\{\left(1-\frac{V_q L^2}{6RT\,\Delta t^2}+\frac{V_q V_1^2}{RT}\right)P_{11}\right.$$

$$-\left(1+\frac{V_q L^2}{3RT\,\Delta t^2}+\frac{V_q V_2^2}{RT}\right)P_{21}-F_R$$

$$-\frac{V_q L^2}{3RT\,\Delta t^2}(-2P_{22}+P_{23}-P_{12}+.5P_{13})$$

$$\left.+\rho_f\,(1-V_q)(V_1^2-V_2^2)\right\} \qquad (4.27d)$$

This concludes the analysis of a single element. Now the above equations for each element must be related by continuity at the junctions where they connect in the network. The system of simultaneous equations which results will then describe the network in terms of the conservation of mass and of momentum.

Continuity at a Junction

Since a junction, by definition, has no volume, it cannot accumulate mass. Continuity is, therefore, simply written as:

$$\sum \dot{m} = 0 \qquad (4.35)$$

Also,

$$\dot{m}_{new} = \dot{m}_{old} + d\dot{m} \qquad (4.36)$$

Therefore,

$$\sum \dot{m}_{new} = \sum \dot{m}_{old} + \sum d\dot{m} = 0 \qquad (4.35a)$$

Since,

$$\sum \dot{m} = 0; \tag{4.35}$$

then

$$\sum d\dot{m} = 0 \tag{4.37}$$

or for constant area and in finite difference form:

$$\sum A\,\Delta(\rho V) = 0 \qquad \text{at a junction} \tag{4.38}$$

Now, equations 4.25d or 4.27d can be substituted into the above equation for each junction of the network. This will result in a number of simultaneous equations equal to the number of junctions, or the number of unknown pressures. The equation which is used for the substitution depends upon the junction for which equation 4.38 is being written. If, in the summation, the junction is the upstream junction of the element, equation 4.25d is substituted, and if the junction is the downstream junction, equation 4.27d is substituted. The two equations can be expressed as a single equation by using a double subscript with a comma notation as follows:

$$\pm P_{x,y}$$

which means $+ P_x$ or $- P_y$

The following equation for continuity at a junction results when using the above notation:

$$\sum_{1}^{NL} \frac{A}{L} \left\{ \pm \left(1 + \frac{V_q}{3RT}\frac{L^2}{\Delta t^2} + \frac{V_q}{RT} V_{1,2}{}^2\right) P_{11,21} \right.$$

$$\left. \mp \left(1 \pm \frac{V_q}{6RT}\frac{L^2}{\Delta t^2} + \frac{V_q}{RT} V_{2,1}{}^2\right) P_{21,11} \right\}$$

$$= \sum_{1}^{NL} \frac{A}{L} \left\{ \pm \frac{V_q}{3RT} \frac{L^2}{\Delta t^2} (-2P_{12,22}+P_{13,23}-P_{22,12}+.5P_{23,13}) \right.$$

$$\left. + \rho_f(1-V_q)(V_1^2-V_2^2) + F_R \right\} \qquad (4.39)$$

This equation is programmed in the simulation for each interior junction. The set of simultaneous equations which result are solved for the unknown pressures, P_{11} and P_{21}.

Friction Force, F_r

The frictional force is based upon the square of the velocity through the element. The loss due to viscous friction is assumed to be equal to

$$F_R = \frac{\rho F(V_1^2+V_2^2)}{4} \frac{L}{D} \qquad (4.40)$$

since the velocity is varying along the length of the element. The variation is small, therefore Equation 4.40 is a good approximation to the usual friction term for pipe flow as given by

$$F_R = \frac{\rho F V^2}{2} \frac{L}{D}$$

Subroutine FRIC calculates the frictional factors (FL/D) for both the steady solution and the transient solution, as described in 4.10.

4.13 Checking the Linear Density Solution

At this point, it is advisable to compare the solutions of a simple flow problem for the linear density method with the accepted method of characteristics. This was done for a 2-inch long tube with only air flowing. The wavespeed is well known for the pure air which means the results obtained from the method of characteristics must be reliable. The boundary conditions, as shown by Figure 45, are a steady pressure at one end and a sinusoidal pressure at the opposite

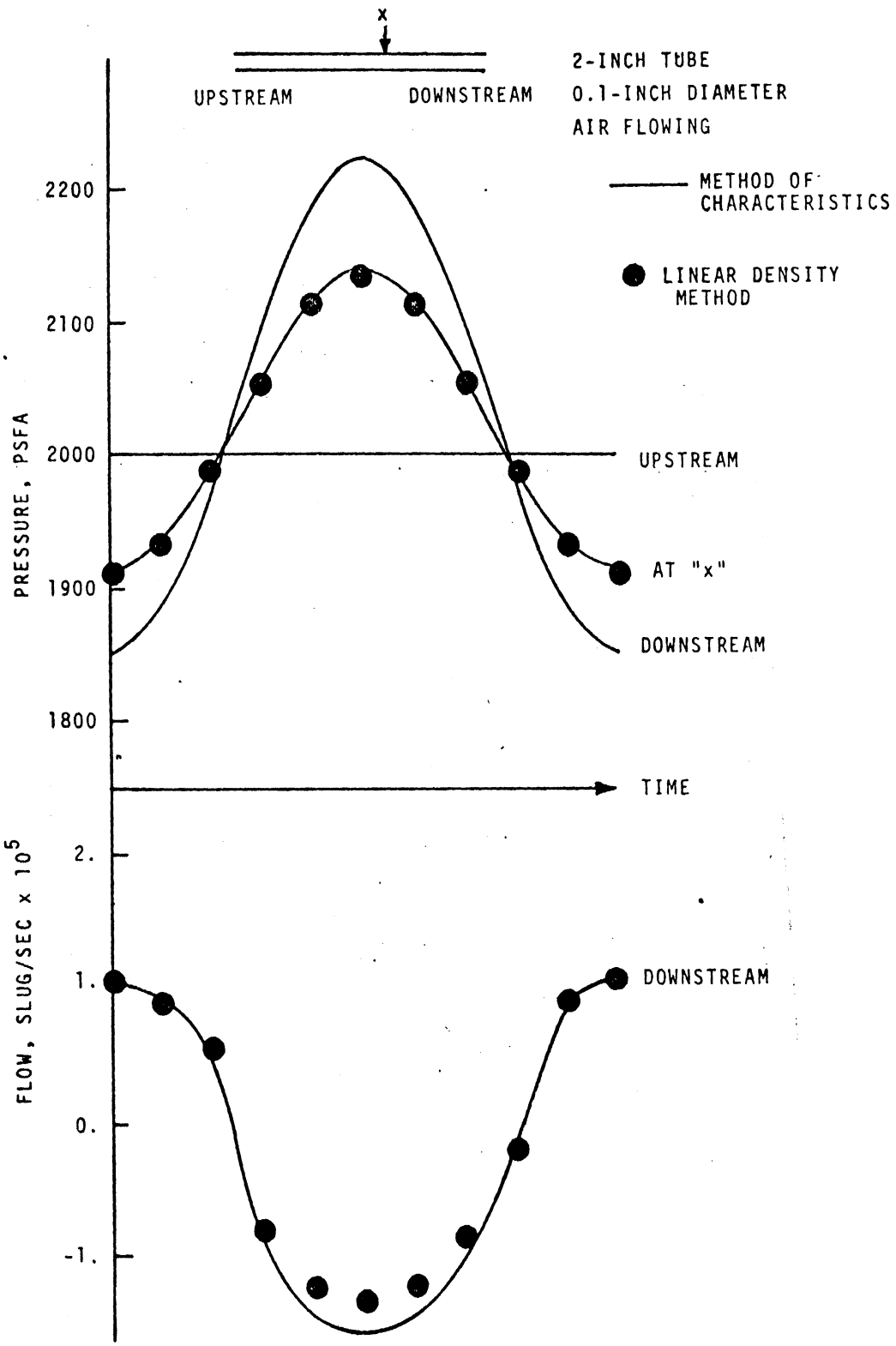

Figure 45. Comparison of Linear Density Method to Method of Characteristics.

end of the pipe. The results of calculated pressure at an interior point and for flow at the downstream end compare very well. A slight difference in flow is noted, which is due to a convective force term contained in the linear density solution. The results show that the linear density method does accurately simulate compressible transient flow in small, short pipes.

4.14 Simulation of a Ford Carburetor

The Ford C8AF-L two-barrel carburetor, as depicted in Figure 1 of Chapter II, was simulated by using the techniques just described for steady-flow and for oscillatory flow. Figure 46 shows the network which was needed to describe the flow path for the simulation. Notice that it contains four air bleeds, two main venturi ports, six boost venturi ports, and one connection to the float bowl. The enrichment system was blocked, since it contains the soft diaphragm of the enrichment valve. Softness of the channel walls is not included in the transient flow simulation, and it does greatly affect the transient behavior. The enrichment system was in use for the complete tests of Chapter II. Separate tests were run without the enrichment system to check the transient simulation. Figure 47 shows the input data which is needed to describe the network of Figure 46, and to simulate one operation point, 1500 rpm and wide open throttle.

The steady-state results for the 1500 rpm run are shown in Tables V and VI. The flows in each element as well as the pressure at each junction are given. The friction factor and Reynolds number are shown as well as the average densities. The fraction of air on a mass and on a volume basis is given as well as the separate flows of air and fuel. It is of interest to note that the flow in the idle system is shown to be reversed, which means that the idle port and

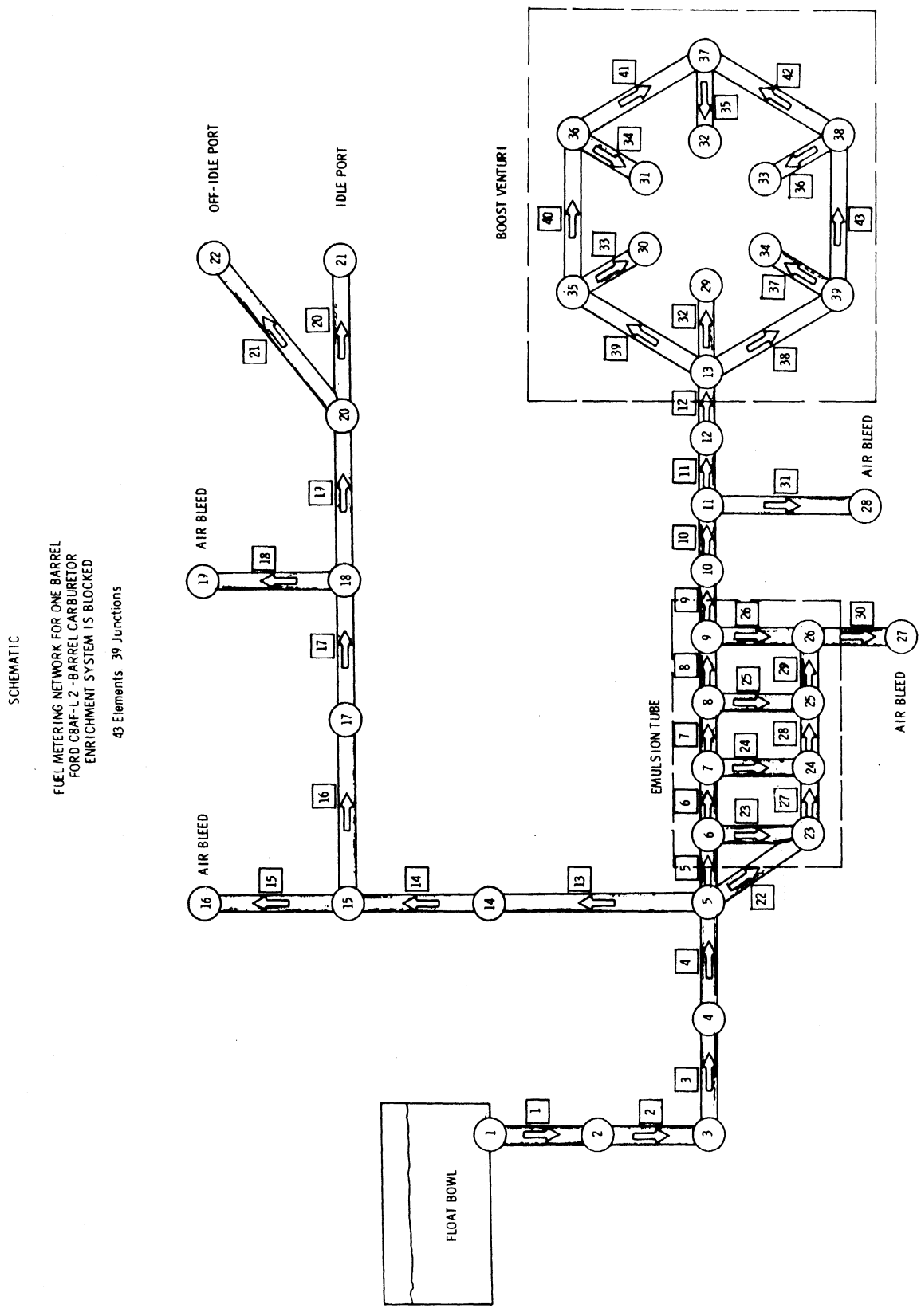

Figure 46. Schematic Network for C8AF-L Carburetor.

```
000218   09-27-71   000218   09-27-71   000218   09-27-71   000218   09-27-71   000218   09-27-71   000218

 $DIN X=1,1,2,
 2,1,1,2,3,
 3,2,2,3,4,
 4,3,3,4,5,
 5,4,4,22,23,   5,6,13,14,
 6,5,5,23,23,6,7,
 7,6,6,24,24,7,8,
 8,7,7,25,25,8,9,
 9,8,8,26,26,9,10,
 10,9,9,10,11,
 11,10,10,31,28,11,12,
 12,11,11,12,13,
 13,12,12,32,29,39,35,38,39,
 14,13,5,14,15,
 15,14,14,15,16,16,17,
 16,1,2,2,3,3,4,4,5,13,14,14,15,15,16,
 17,16,15,17,18,
 18,17,17,19,20,18,19,
 19,1,2,2,3,3,4,4,5,13,14,14,15,16,17,17,18,18,19,
 20,19,18,20,21,21,22,
 21,1,2,2,3,3,4,4,5,13,14,14,15,16,17,17,18,19,20,20,21,
 22,1,2,2,3,3,4,4,5,13,14,14,15,16,17,17,18,19,20,21,22,
 23,22,5,27,24,23,6,
 24,27,23,28,25,24,7,
 25,28,24,29,26,25,8,
 26,29,25,30,27,26,9,
 27,1,2,2,3,3,4,4,5,22,23,27,24,28,25,29,26,30,27,
 28,1,2,2,3,3,4,4,5,5,6,6,7,7,8,8,9,9,10,10,11,31,28,
 29,1,2,2,3,3,4,4,5,5,6,6,7,7,8,8,9,9,10,10,11,11,12,12,13,32,29,
 30,1,2,2,3,3,4,4,5,5,6,6,7,7,8,8,9,9,10,10,11,11,12,12,13,39,35,33,30,
 31,1,2,2,3,3,4,4,5,5,6,6,7,7,8,8,9,9,10,10,11,11,12,12,13,39,35,40,36,34,31,
 32,1,2,2,3,3,4,4,5,5,6,6,7,7,8,8,9,9,10,10,11,11,12,12,13,39,35,40,36,41,37,35,
 32,
 33,1,2,2,3,3,4,4,5,5,6,6,7,7,8,8,9,9,10,10,11,11,12,12,13,38,39,43,38,36,33,
 34,1,2,2,3,3,4,4,5,5,6,6,7,7,8,8,9,9,10,10,11,11,12,12,13,38,39,37,34,
 35,39,13,33,30,40,36,
 36,40,35,34,31,41,37,
 37,35,32,42,38,41,36,
 38,43,39,42,37,36,33,
 39,38,13,43,38,37,34,
 40,1,2,2,3,3,4,4,5,5,6,23,23,27,24,28,25,29,26,30,27,
 41,1,2,2,3,3,4,4,5,5,6,6,7,24,24,28,25,29,26,30,27,
 42,1,2,2,3,3,4,4,5,5,6,6,7,7,8,25,25,29,26,30,27,
 43,1,2,2,3,3,4,4,5,5,6,6,7,7,8,8,9,26,26,30,27,
 44,1,2,2,3,3,4,4,5,5,6,6,7,7,8,8,9,9,10,10,11,11,12,12,13,38,39,43,38,42,37,35,
 32,
 D=.0502,.1870,.1470,.2910,5*.158,.270,.160,.160,.061,.026,.039,.094,.042,
 .035,.094,.059,.055,.214,.0566,3*.0566,3*.214,.045,.0270,6*.092,6*.120,
 L=.183,.312,.9375,.250,.125,4*.250,.34,.406,.406,1.930,.093B,.125,.78,.106,
 .106,2.0,.106,.100,.125,.0283,3*.0283,3*.250,.125,.140,6*.055,6*.4,
 NELS=43,LFT=20,
 CS=0.,-1.,0., 0.,-1.,0., .898,.438,0., .898,.438,0., 0.,1.,0., 0.,1.,0.,
 0.,1.,0.,
 0.,1.,0., 0.,1.,0., 0.,1.,0., -.259,.970,0., -.259,.970,0., 0.,1.,0., 0.,1.,0.,
 0.,1.,0., 0.,-.966,.259, 0.,-.966,.259, 0.,1.,0., 0.,-1.,0., 1.,0.,0.,
 1.,0.,0., 0.,1.,0., 1.,0.,0., 1.,0.,0., 1.,0.,0., 1.,0.,0., 0.,1.,0.,
 0.,1.,0., 0.,1.,0., 0.,1.,0., 0.,1.,0., 1.,0.,0., .5,0.,.866, -.5,0.,.866,
 -1.,0.,0., -.5,0.,-.866, .5,0.,-.866,.5,0.,.866,.5,0.,-.866, 1.,0.,0.,
 .5,0.,.866, .5,0.,-.866,1.,0.,0.,
 JT=1,14*0,2,2*0,2,0,2,2,4*0,8*2,5*0,5*2,
 NL=1,2,2,2,4,4*3,2,3,2,4,2,3,7,2,3,9,3,10,10,4*3,9,11,13,14,15,16,15,14,
 5*3,4*10,16,
 LT=1,12*0,2,2,0,2,2,0,2,2,0,4*2,4*0,7*2,6*0,
 JO=1,2,3,4,5,6,7,8,9,10,11,12,5,14,15,15,17,18,18,20,20,5,6,7,8,9,23,24,25,26,
 11,13,35,36,37,38,39,13,13,35,36,38,39,
 LIM=10,  TOLP=1.    $END
 $DIN2 FREQ=50., PRAR=14.5,
 PR(1,16)=-.0755, -.0472,-.0189,-.0605,-.0870,-.0566,-.0756,.0265,-.0151,-.087,
 PR(1,19)=-.0755, -.0472,-.0189,-.0605,-.0870,-.0566,-.0756,.0265,-.0151,-.087,
 PR(1,21)=-.573,-.501,-.363,-.334,-.291,-.137,-.01815,.0726,-.0908,-.399,
 PR(1,22)=-.0755, -.0472,-.0189,-.0605,-.0870,-.0566,-.0756,.0265,-.0151,-.087,
 PR(1,27)=-.0755, -.0472,-.0189,-.0605,-.0870,-.0566,-.0756,.0265,-.0151,-.087,
 PR(1,28)=-.0755, -.0472,-.0189,-.0605,-.0870,-.0566,-.0756,.0265,-.0151,-.087,
 PR(1,29)=-.89,-1.42,-1.27,-1.20,-1.11,-.922,-.535, .0748,.0295,-.221,
 PR(1,30)=-.89,-1.42,-1.27,-1.20,-1.11,-.922,-.535, .0748,.0295,-.221,
 PR(1,31)=-.89,-1.42,-1.27,-1.20,-1.11,-.922,-.535, .0748,.0295,-.221,
 PR(1,32)=-.89,-1.42,-1.27,-1.20,-1.11,-.922,-.535, .0748,.0295,-.221,
 PR(1,33)=-.89,-1.42,-1.27,-1.20,-1.11,-.922,-.535, .0748,.0295,-.221,
 PR(1,34)=-.89,-1.42,-1.27,-1.20,-1.11,-.922,-.535, .0748,.0295,-.221,
 NPOINT=10,NDIV=500,NCYC=1,
 PI=14.5,14.4,14.39,14.38,14.37,14.36,14.35,14.34,14.33,14.32,14.31,14.30,14.29,
 14.36,14.35,14.44,14.34,14.33,14.44,14.32,14.24,14.24,14.37,14.38,14.39,14.40,
 14.46,14.46,6*13.75,14.2,14.15,14.1,14.14,14.21,
 CSG=0.,-1.,0.,G=32.2,T=73.5,NFLU=1,ISOL=1,NSPACE=50,ITP=10   $END
                                                    84  LINES PRINTED
```

Figure 47. Data for Simulation of C8AF-L Carburetor.

TABLE V
STEADY-FLOW RESULTS FOR THE C8AF-L CARBURETOR
AT THE JUNCTIONS

JUNCTIONS

	PRESSURE, LB/SQ-IN			FLOW, LB/HR			
I	TOTAL	GRADE	HEAD	TOTAL	AIR	FUEL	AIR/TOT
1	14.500	14.500	0.0	-16.57448	0.0	-16.57448	0.0
2	14.126	14.121	-0.00473	0.0	0.0	0.0	0.0
3	14.134	14.121	-0.01237	0.0	0.0	0.0	0.0
4	14.114	14.113	-0.00221	0.0	0.0	0.0	0.0
5	14.113	14.113	0.00066	0.0	0.0	0.0	0.017328
6	14.104	14.105	0.00095	0.0	0.0	0.0	0.021480
7	14.094	14.096	0.00142	0.0	0.0	0.0	0.029128
8	14.063	14.065	0.00176	0.0	0.0	0.0	0.033841
9	14.036	14.039	0.00202	0.0	0.0	0.0	0.050576
10	14.002	14.004	0.00221	0.0	0.0	0.0	0.050576
11	13.994	13.995	0.00248	0.0	0.0	0.0	0.057417
12	13.935	13.938	0.00275	0.0	0.0	0.0	0.057417
13	13.878	13.881	0.00302	0.0	0.0	0.0	0.057417
14	14.123	14.124	0.00074	0.0	0.0	0.0	1.000000
15	14.309	14.309	0.00074	0.0	0.0	0.0	1.000000
16	14.460	14.461	0.00075	-0.22296	-0.22296	0.0	1.000000
17	14.307	14.308	0.00071	0.0	0.0	0.0	1.000000
18	14.273	14.273	0.00071	0.0	0.0	0.0	1.000000
19	14.460	14.461	0.00071	-0.19766	-0.19766	0.0	1.000000
20	14.267	14.268	0.00063	0.0	0.0	0.0	1.000000
21	14.240	14.241	0.00062	0.16528	0.16528	0.00000	1.000000
22	14.240	14.241	0.00062	0.14597	0.14597	0.00000	1.000000
23	14.113	14.114	0.00025	0.0	0.0	0.0	1.000000
24	14.113	14.114	0.00142	0.0	0.0	0.0	1.000000
25	14.113	14.115	0.00176	0.0	0.0	0.0	1.000000

TABLE V (CONT'D)
STEADY-FLOW RESULTS FOR THE C8AF-L CARBURETOR
AT THE JUNCTIONS

JUNCTIONS

J	PRESSURE, LB/SQ-IN TOTAL	GRADE	HEAD	FLOW, LB/HR TOTAL	AIR	FUEL	AIR/TOT
26	14.117	14.115	0.00202	0.0	0.0	0.0	1.000000
27	14.460	14.462	0.00232	-0.77355	-0.77355	0.0	1.000000
28	14.460	14.462	0.00246	-0.12671	-0.12671	0.0	1.000000
29	13.750	13.753	0.00302	4.49064	0.25784	4.23280	0.057417
30	13.750	13.753	0.00302	2.94193	0.16891	2.77292	0.057417
31	13.750	13.753	0.00302	2.21671	0.12728	2.08943	0.057417
32	13.750	13.753	0.00302	2.77639	0.15941	2.61698	0.057417
33	13.750	13.753	0.00302	2.21671	0.12728	2.08943	0.057417
34	13.750	13.753	0.00302	2.94193	0.16891	2.77292	0.057417
35	13.839	13.842	0.00302	0.0	0.0	0.0	0.057417
36	13.807	13.810	0.00302	0.0	0.0	0.0	0.057417
37	13.793	13.796	0.00302	0.0	0.0	0.0	0.057417
38	13.807	13.810	0.00302	0.0	0.0	0.0	0.057417
39	13.839	13.842	0.00302	0.0	0.0	0.0	0.057417
40	-0.000	-0.000	0.0	0.0	0.0	0.0	1.000000
41	-0.000	-0.000	0.0	0.0	0.0	0.0	1.000000
42	-0.000	-0.000	0.0	0.0	0.0	0.0	1.000000
43	-0.000	-0.000	0.0	0.0	0.0	0.0	1.000000
44	-0.000	-0.000	0.0	0.0	0.0	0.0	1.000000

TABLE VI
STEADY-FLOW RESULTS FOR THE C8AF-L
IN THE ELEMENTS

EL	DIAM, INCH	LENGTH INCH	PRESS DROP PSI	FLOWS, LB/SEC TOTAL	AIR	FUEL AIR/FUEL		RE NUM	PRIC	DENSITY LB/CU-FT	VOLUME RATIO
1	0.250	0.133	0.37871	16.5745	0.0	16.574	0.0	4977.	1.418	45.2233	0.0
2	0.187	0.313	0.00012	16.5745	0.0	16.574	-0.0	1335.	0.087	45.2233	0.0
3	0.147	0.038	0.00767	16.5745	0.0	16.574	-0.0	1700.	2.111	45.2233	0.0
4	0.291	0.250	0.00009	16.5745	0.0	16.574	-0.0	850.	0.394	45.2233	0.0
5	0.153	0.125	0.00876	16.2667	0.2637	16.603	0.0156	851.	0.268	4.0963	0.911
6	0.153	0.250	0.01877	16.9383	0.3439	16.594	0.0203	1004.	0.454	3.2215	0.930
7	0.153	0.250	0.02122	17.0717	0.4835	16.588	0.0283	1286.	0.376	2.3569	0.949
8	0.153	0.250	0.02689	17.2443	0.6637	16.581	0.0385	1663.	0.353	1.7587	0.963
9	0.153	0.250	0.03352	17.4574	0.8829	16.574	0.0506	2134.	0.331	1.3510	0.972
10	0.221	0.340	0.00917	17.4574	0.8829	16.574	0.0506	1249.	0.774	1.3510	0.972
11	0.153	0.406	0.05703	17.5841	1.0104	16.574	0.0575	2391.	0.517	1.1934	0.975
12	0.153	0.406	0.05703	17.5841	1.0104	16.574	0.0575	2391.	0.517	1.1934	0.975
13	0.361	1.938	-.01078	-0.1094	-0.1094	-0.000	1.0000	645.	3.142	0.0703	1.000
14	0.226	0.094	-.18445	-0.1094	-0.1094	-0.000	1.0000	1512.	1.778	0.0703	1.000
15	0.039	0.125	-.15212	-0.2330	-0.2330	0.0	1.0000	2066.	1.781	0.0703	1.000
16	0.294	0.781	0.00001	0.1136	0.1136	0.000	1.0000	439.	1.392	0.0703	1.000
17	0.242	0.156	0.03427	0.1136	0.1136	0.000	1.0000	983.	2.064	0.0703	1.000
18	0.335	0.156	-.18726	-0.1377	-0.1377	0.0	1.0000	2044.	1.807	0.0703	1.000
19	0.294	2.000	0.00555	0.3113	0.3113	0.000	1.0000	1200.	1.144	0.0703	1.000
20	0.253	0.156	0.02718	0.1653	0.1653	0.000	1.0000	1016.	3.024	0.0703	1.000
21	0.255	0.100	0.02718	0.1460	0.1460	0.000	1.0000	962.	2.928	0.0703	1.000
22	0.214	0.125	-.00006	-0.1929	-0.1929	-0.000	1.0000	260.	0.144	0.0703	1.000
23	0.057	0.028	-.00906	-0.0716	-0.0716	-0.000	1.0000	511.	4.326	0.0703	1.000
24	0.057	0.028	-.02835	-0.1334	-0.1334	-0.000	1.0000	890.	3.942	0.0703	1.000
25	0.057	0.028	-.05090	-0.1725	-0.1725	-0.000	1.0000	1149.	4.207	0.0703	1.000

TABLE VI (CONT'D)
STEADY-FLOW RESULTS FOR THE C8AF-L
IN THE ELEMENTS

ELEMENTS

EL	DIMENSIONS DIAM. INCH	LENGTH INCH	PRESS DROP PSI	FLOWS, LB/HR TOTAL	AIR	FUEL	AIR/FUEL	RE NUM	FRIC	DENSITY LB/CU-FT	VOLUME RATIO
26	0.257	0.228	-.07725	-0.2131	-0.2131	-0.000	1.0000	1398.	4.299	0.0703	1.000
27	0.214	0.250	-.00011	-0.2545	-0.2545	-0.000	1.0000	395.	0.139	0.0703	1.000
28	0.214	0.250	-.00012	-0.3870	-0.3870	-0.000	1.0000	631.	0.119	0.0703	1.000
29	0.214	0.250	-.00012	-0.5404	-0.5404	-0.000	1.0000	934.	0.083	0.0703	1.000
30	0.245	0.125	-.34688	-0.7736	-0.7736	0.0	1.0000	6201.	0.599	0.0703	1.000
31	0.327	0.140	-.46728	-0.1267	-0.1267	0.0	1.0000	1702.	3.983	0.0703	1.000
32	0.092	0.255	0.12312	4.4906	0.2580	4.233	0.0575	1063.	1.942	1.1934	0.975
33	0.092	0.255	0.03831	2.9413	0.1690	2.773	0.0575	696.	3.140	1.1934	0.975
34	0.092	0.255	0.05463	2.2167	0.1274	2.089	0.0575	524.	3.515	1.1934	0.975
35	0.092	0.255	0.04356	2.7764	0.1595	2.617	0.0575	656.	1.723	1.1934	0.975
36	0.092	0.255	0.05663	2.2167	0.1274	2.089	0.0575	524.	3.518	1.1934	0.975
37	0.092	0.255	0.03831	2.9413	0.1690	2.773	0.0575	696.	3.140	1.1934	0.975
38	0.123	0.400	0.03921	6.5447	0.3762	6.171	0.0575	1186.	0.809	1.1934	0.975
39	0.123	0.400	0.03921	6.5447	0.3762	6.171	0.0575	1186.	0.809	1.1934	0.975
40	0.123	0.400	0.03228	3.6049	0.2071	3.398	0.0575	653.	2.202	1.1934	0.975
41	0.123	0.400	0.01328	1.3282	0.0708	1.308	0.0575	251.	6.016	1.1934	0.975
42	0.123	0.400	0.01328	1.3282	0.0708	1.308	0.0575	251.	6.016	1.1934	0.975
43	0.123	0.400	0.03228	3.6049	0.2071	3.398	0.0575	653.	2.202	1.1934	0.975

off-idle port are functioning as air bleeds. This phenomenon was noted by Harrington, but his simulation was restricted to one flow direction. If the flow were to be reversed from the assumed direction for his simulation, it was automatically made equal to zero.

Figure 48 summarizes the steady-state flow for four test runs at wide open throttle. Average flow is plotted as a function of boost venturi vacuum for 1500, 2000, 2500, and 3000 rpm. Two fuel temperatures are shown, and its slight influence is noted. It is seen that the computer prediction compares very well with the experimental data.

Figures 49 through 52 show the results for the transient pressure solution of the same four tests of Figure 48. Notice that these plots of pressure as a function of time contain curves for the air bleeds, main venturi and the boost venturi as well as the main fuel channel. These pressures were all measured with transducers, and the first three listed are used as input to the simulation (they are boundary conditions). The main channel pressure is calculated by the simulation, and then plotted together with the experimental data. Very close agreement is seen to exist for the four trial runs. The simulation is, therefore, assumed to be accurately predicting the transient flow in the carburetor.

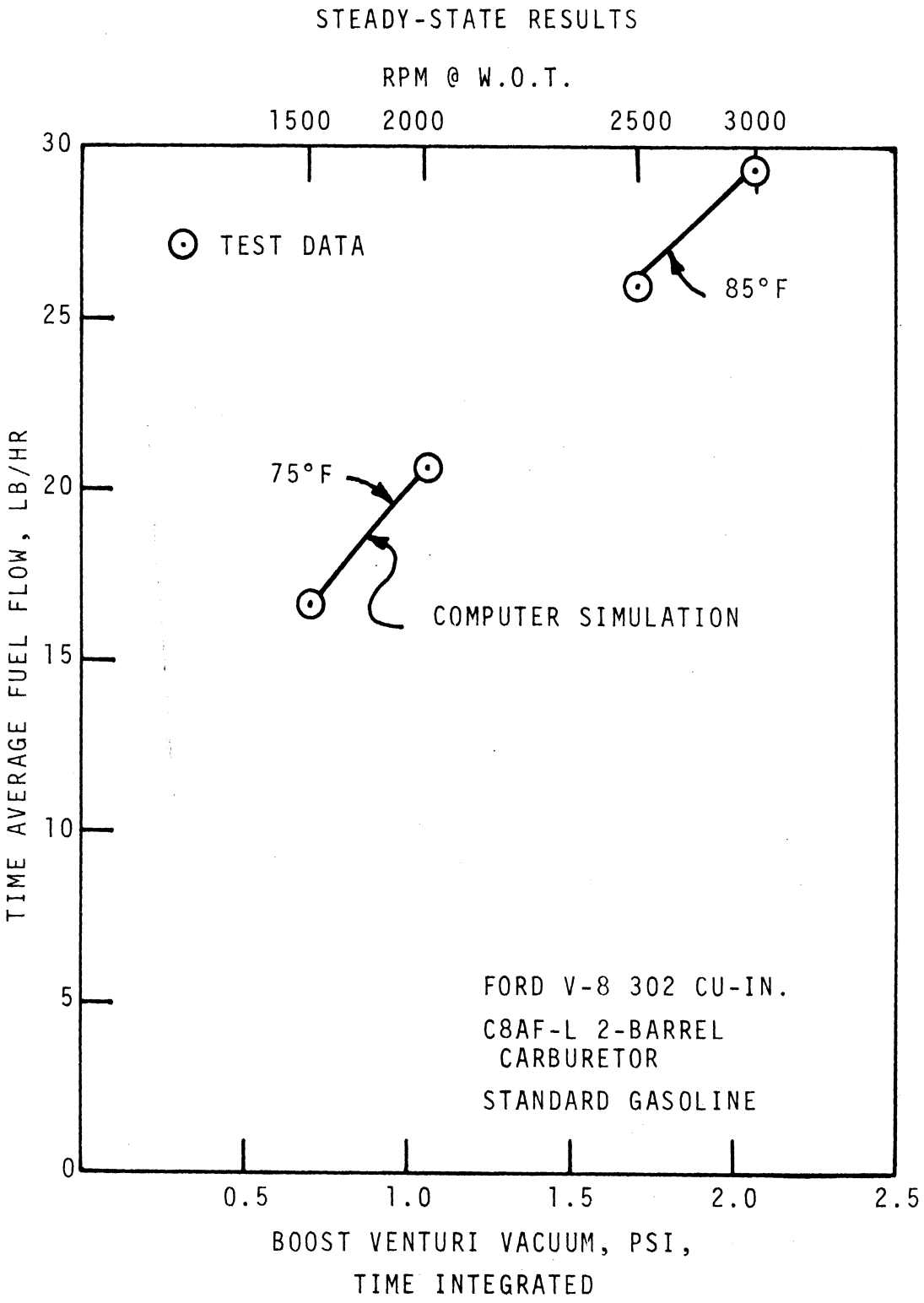

Figure 48. Simulated Steady-State Results for C8AF-L Carburetor.

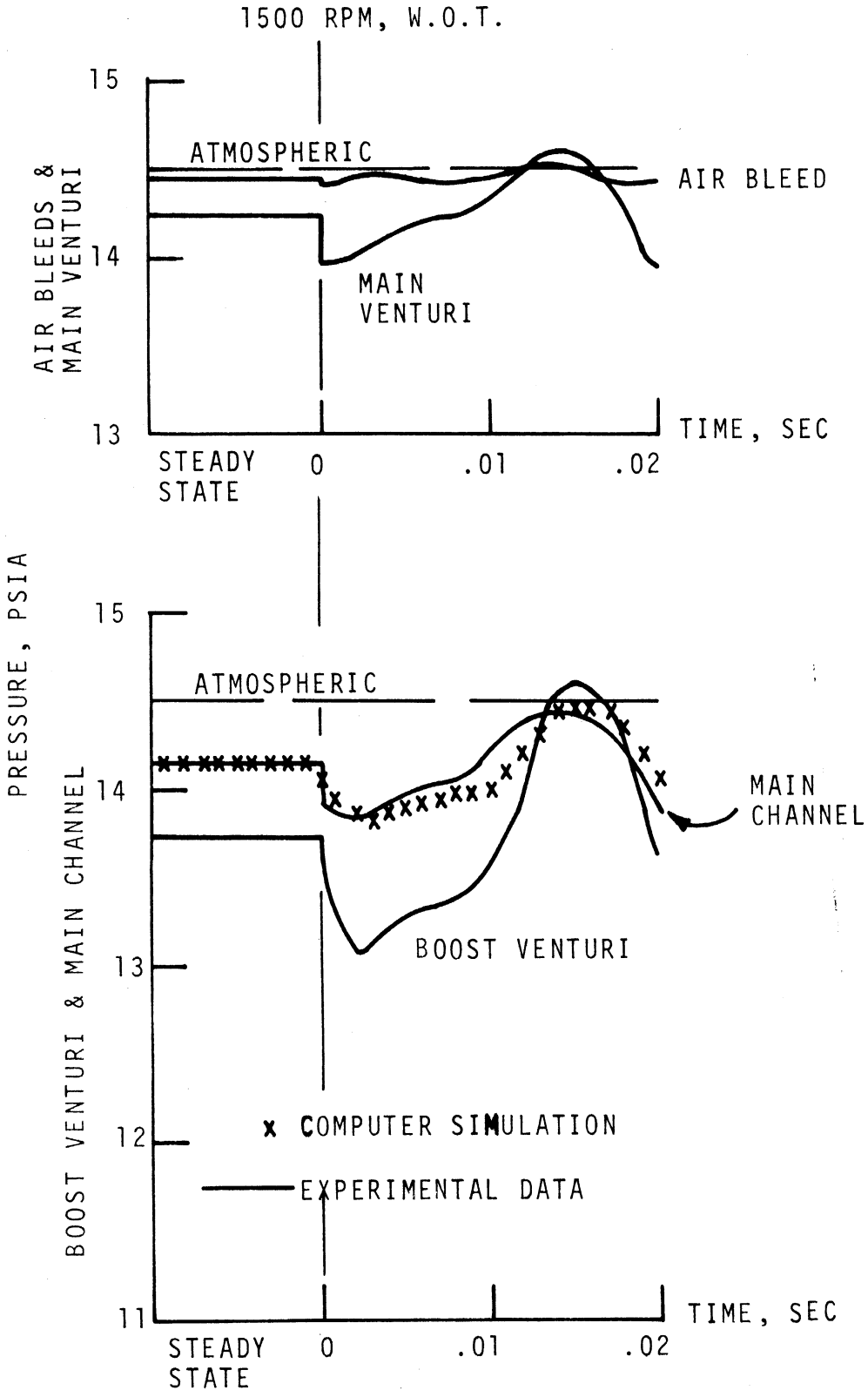

Figure 49. Simulated Transient Pressure for C8AF-L Carburetor, 1500 RPM.

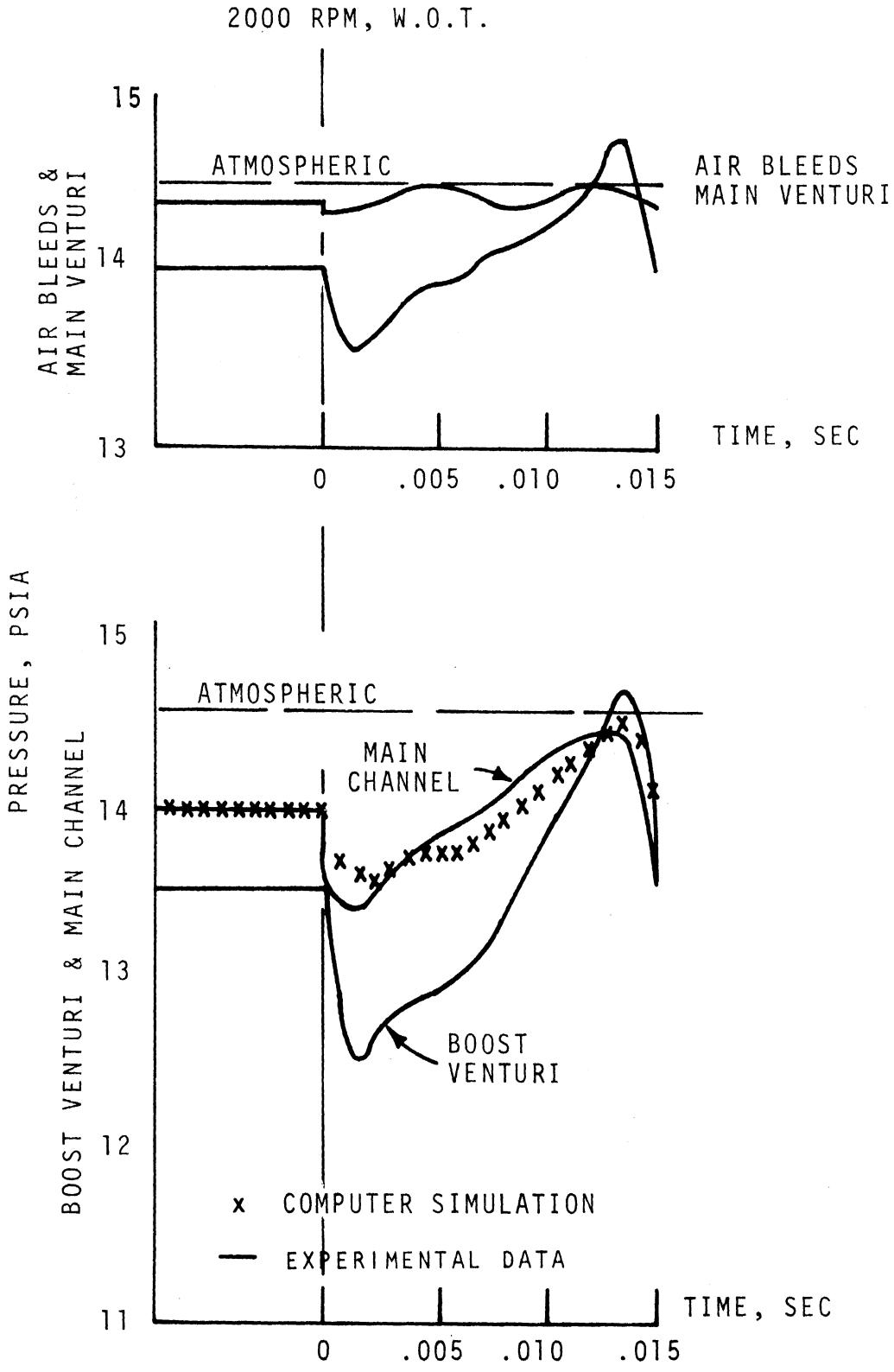

Figure 50. Simulated Transient Pressure for C8AF-L Carburetor, 2000 RPM.

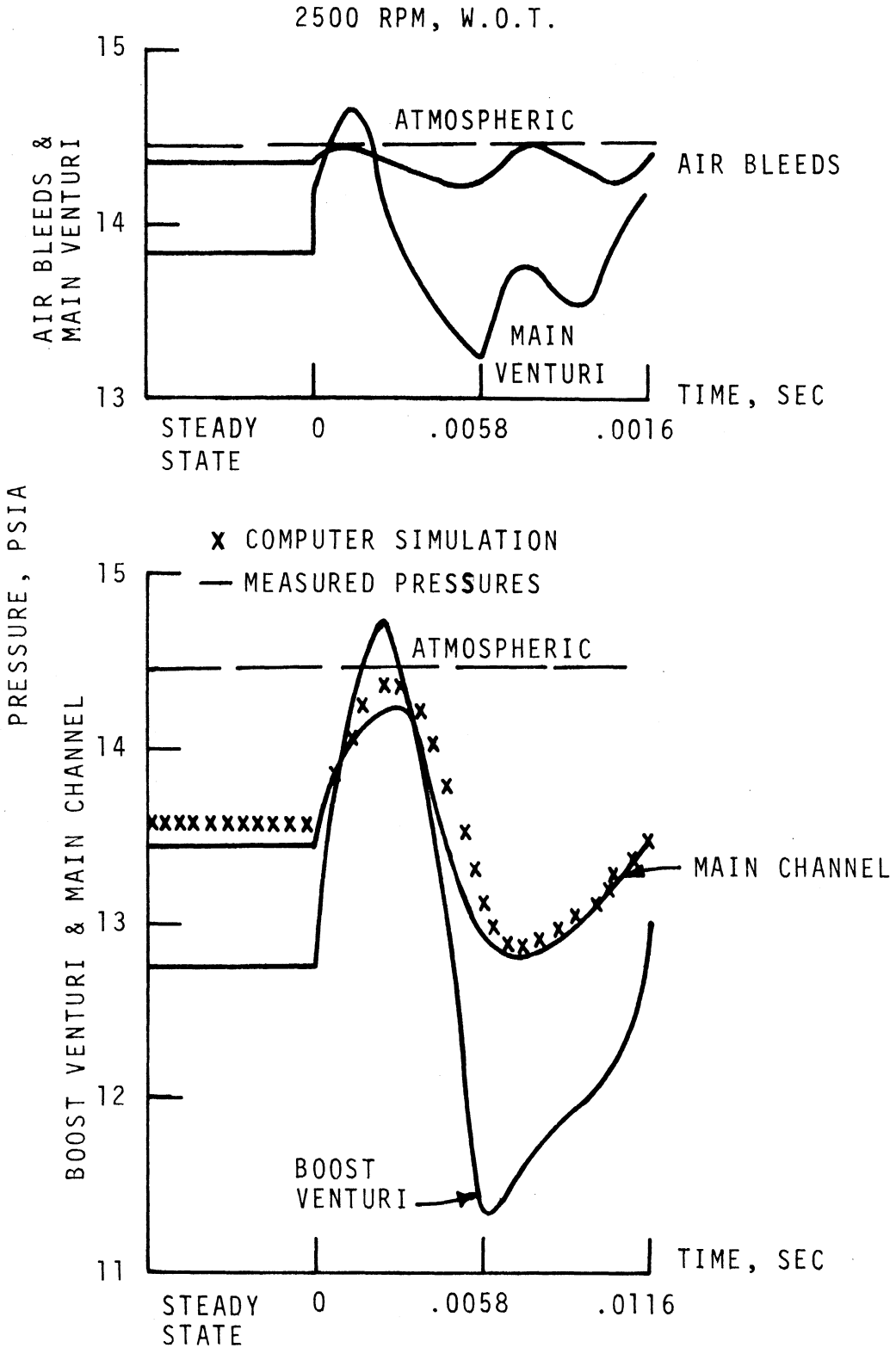

Figure 51. Simulated Transient Pressure for C8AF-L Carburetor, 2500 RPM.

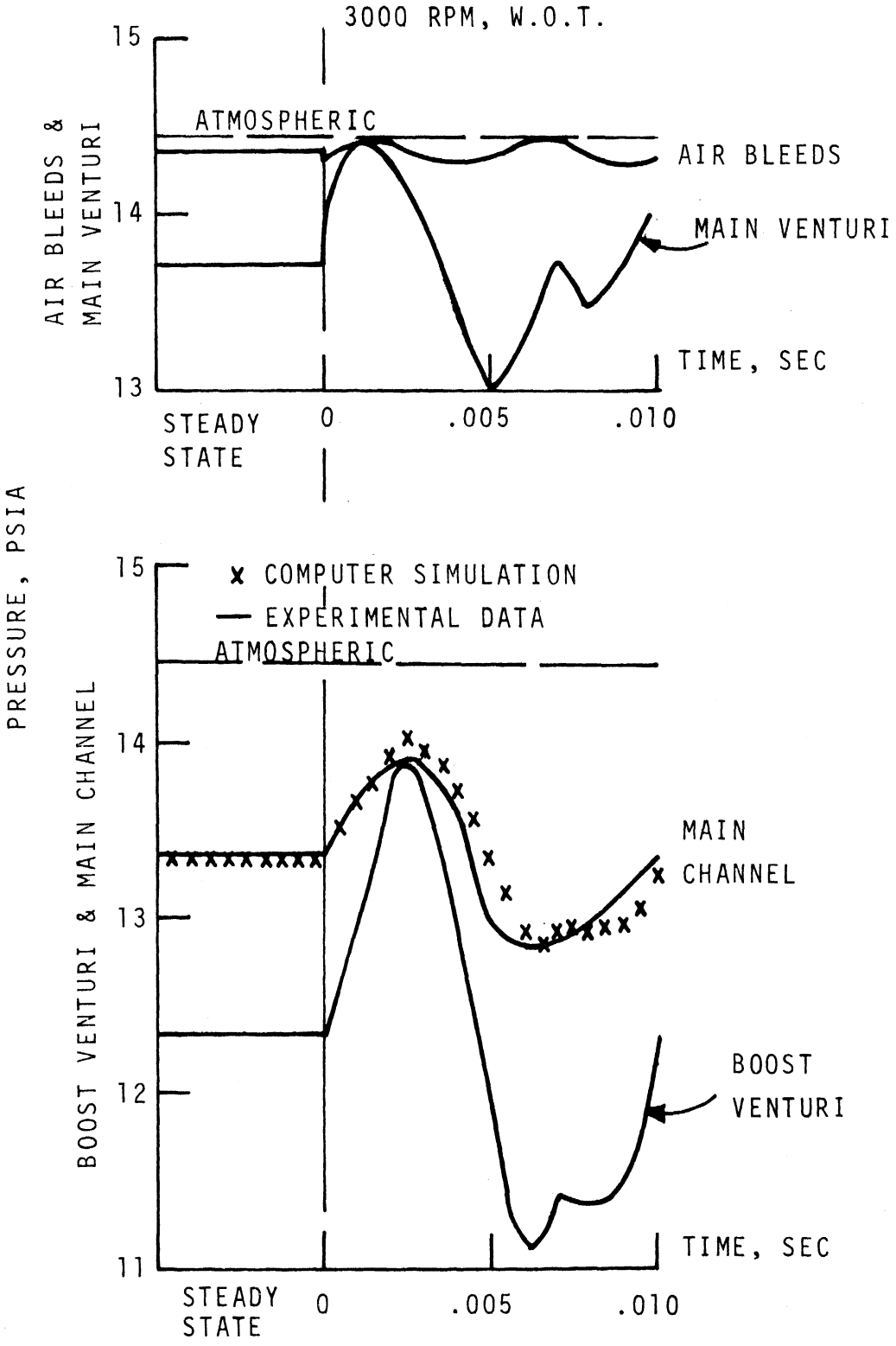

Figure 52. Simulated Transient Pressure for C8AF-L Carburetor, 3000 RPM.

Figures 53 and 54 illustrate the transient flows coming out of the boost venturi, and the air flow going into the air bleeds. These flows were calculated by the simulation program, and are assumed to be correct since the measured fuel channel pressure compares very well with the calculated fuel channel pressure as shown in Figures 49 through 52. Also, the measured average flow compares well with the calculated average flow as shown in Figure 48. Therefore, there is a great amount of confidence that the calculated flows are very close to the actual flows. It would be nearly impossible to measure the transient flows in the carburetor, therefore, the calculated flows are most valuable.

It is interesting to note in Figure 53 that the air bleed flow reverses for part of the cycle. This means that during part of the cycle air is actually coming out of the air bleed, rather than going into it. It is seen to only happen for a very short period, but the flow reversal does take place. Also, it is for this reason that the impedance method could not be successfully used in simulating the carburetor network. In the same Figure, the boost venturi flows have a large flow amplitude, which means that this flow might reverse if the engine speed were sufficiently reduced (lower boost-venturi average suction). However, for the high speed run (3000 rpm) of Figure 54, no flow reversal is seen to take place at any of the boundary points.

A multitude of plots could be made for flow and pressure in this metering network. However, the purpose here is not to study the transient flow in one particular carburetor, but merely to demonstrate a method by which the transient behavior can be accurately determined. The method used here can be applied to perform a detailed study of

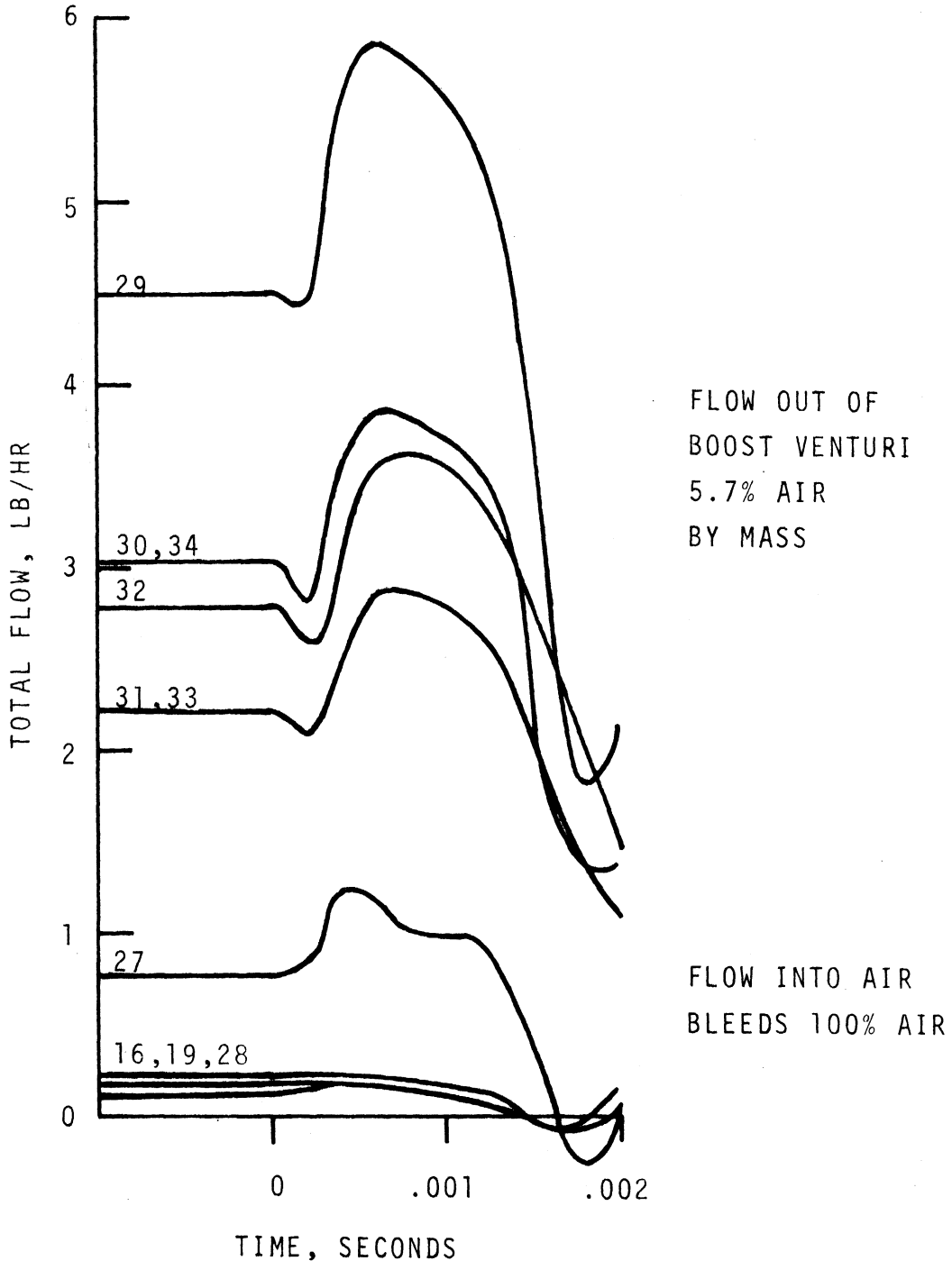

Figure 53. Simulated Transient Flow for C8AF-L Carburetor, 1500 RPM, W.O.T.

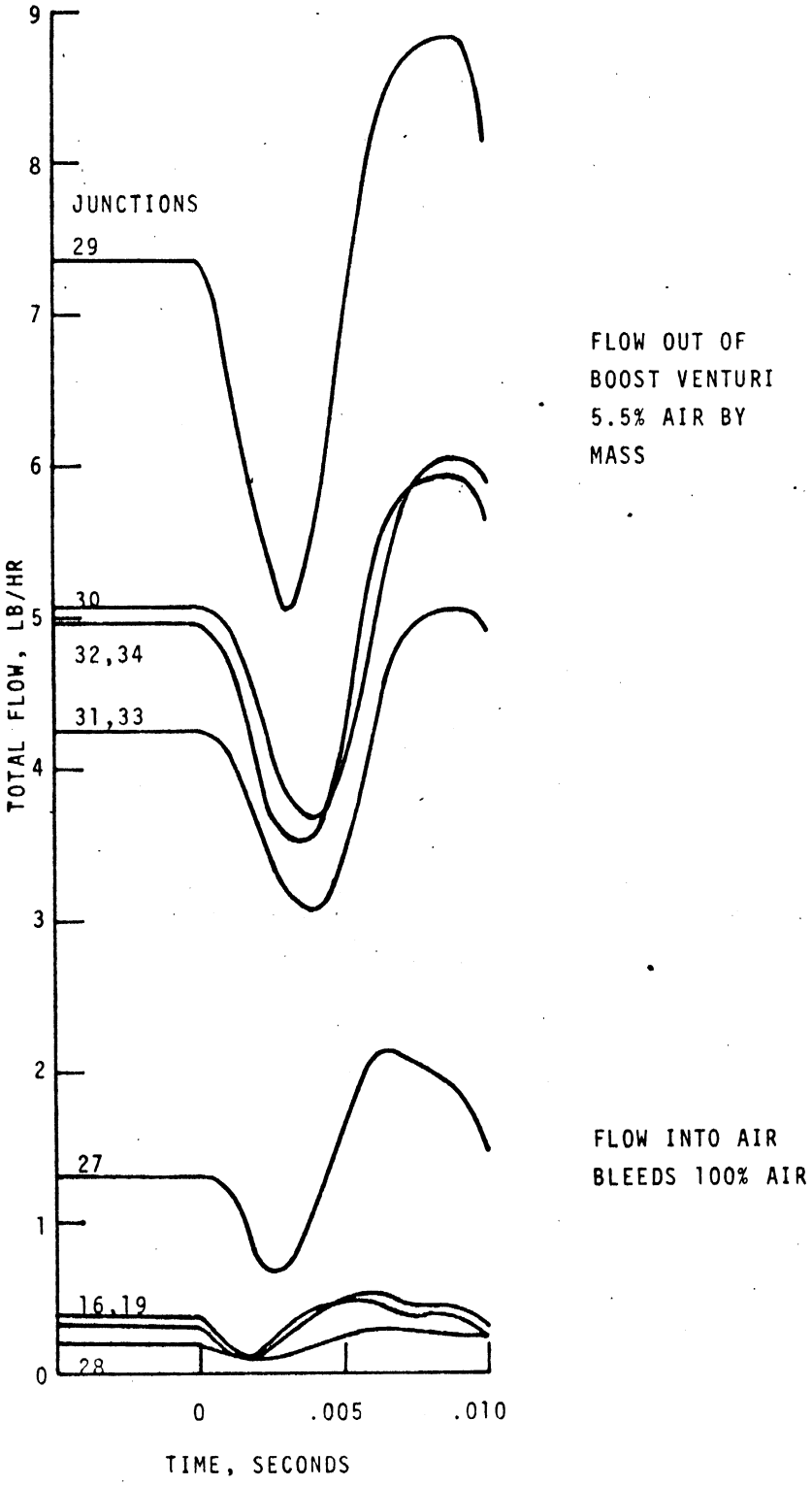

Figure 54. Simulated Transient Flow for C8AF-L Carburetor, 3000 RPM, W.O.T.

any carburetor network. Pressures at each junction and flows in each element are given as a function of time. The designer can study any or all of these points as he wishes, and the information provided for each run can be given a great amount of study.

CHAPTER V

COMMENTS AND RECOMMENDATIONS

The programming method of the simulation requires considerable computation time. One run for a single cycle requires up to ten minutes on the IBM 360 Computer. Double precision is also used which makes the storage also considerable. The long computation time is necessary because very small time steps are required to insure mathematical stability (10^{-5} seconds). Oyama (27) also needed the same time increment for his computer work on carburetor emulsion tubes. The simpler metering network used by Harrington (20) was used in order to limit the time, but the results were poor for the transient solution for several reasons. For steady-state flow, elements of a large diameter, which have little frictional force are justifiably ignored. However, for transient flow simulation, inertia is also important, so that large elements must be included in the network. Even if a large element contains only air (low inertia) its volume becomes important because of the amount of air which can be compressed, and thereby "soften" the system. Therefore, the metering network of 43 elements and 39 junctions is needed to simulate transient flow in the Ford C8AF carburetor, as compared to the network of 25 elements used by Harrington for steady flow simulation. However, the cost of the computing time is still much less than would be the cost of experimentally gathering the same information.

The method of solving the 39 simultaneous equations at each time increment is the Gauss elimination method (SUBROUTINE DGELG in the Scientific Subroutine Package). This method is quite wasteful

when the matrix for the solution has many zeros. (a sparse matrix) Methods do exist for solving sparse matrices as mentioned by Stoner (41) and this would be a logical approach to limiting the computer time if many runs were desired. Modification of the simulation would be very simple, once a subroutine for solving sparse matrices were developed.

The simulation could be greatly improved in the area of the friction factors. As mentioned earlier, the two phase-flow friction factors are not well known, especially for oscillatory flow. More data should be obtained and supplied via subroutine FRIC. It is a desirable feature of the simulation that the calculation of the friction factors is completely performed in subroutine FRIC. This makes adjustment of the friction factors easily done without disturbing the logic of the flow solution. The programming logic in FRIC is quite simple, whereas the logic of TFLOW, FLOW2, and QUAL is involved.

Another improvement would be to include the friction factors and coefficients as a function of time. This would be easily done by calling Subroutine FRIC at each time interval. The current flows would then be used to calculate current Reynolds numbers to give quasi-steady friction factors. The orifice data of Chapter III would be of great use in this respect since it can be used to give the coefficients of discharge as a function of time, and thereby eliminate the quais-steady assumption for the orifices.

The Ford carburetor has an enrichment valve which exposes a soft rubber diaphragm to the fuel channel. The simulation does not account for softness in the channel walls, hence, this unit was removed

from the carburetor in order to obtain comparable results between the simulation and the test. Including softness represents another improvement which could be made in the simulation. Such an improvement would be a major revision of subroutine TFLOW, and would be very difficult. Therefore, its advantage is in doubt since many carburetors do not have any soft channels.

For the simulation, it was assumed that the ratio of air and fuel in each channel remained constant during the transient flow. This, of course, is not true, but it is a good approximation if little or no flow reversal occurs. However, if a great amount of flow reverses for a large period of time, then the approximation is poor. This can be easily pictured if a condition of zero average flow is assumed. During part of the cycle, fuel will be entering the network from the float bowl, and tending to fill it. During the other part of the cycle, when the pressure at the boost venturi is positive, air will be entering the network and displacing the fuel. The inertia of the network will be greatly varying during the cycle, depending upon the proportion of fuel and air which it contains at each instant. Therefore, the simulation cannot be used to study transient flow when the average flow is zero. However, the simulation could easily be made to account for this phenomenon by using Subroutine QUAL to calculate the amount of air and fuel which is contained in each element at each instant in time.

Even though the simulation does contain limiting assumptions, it is accurate enough to closely simulate the one test carburetor for several frequencies (rpm) and average flows. It is also general enough to allow the user to specify the metering network via

the input data so that the simulation need not be changed in order to try different flow networks. It is, therefore, believed that the simulation can be successfully used for much further study of carburetion.

APPENDIX A

ENGINE-CARBURETOR TEST EQUIPMENT AND PROCEDURE

Figure 55 is a schematic of the overall test equipment arrangement which was used to run the engine to measure the pressure pulsations in the carburetor. The means of measuring the intake air flow is shown to be an orifice plate, which is the standard method used by the automotive industry. The pressure loss, which occurs across the orifice plate, is then recovered by the variable-speed air-pump so that atmospheric air pressure can be maintained at the inlet to the air cleaner. The air cleaner was in place during all tests because it probably has noticeable influence on the pressure pulsations in the carburetor.

The fuel-flow measuring equipment is also shown in Figure 55. This operated by recording the time necessary for a known volume of fuel to be used by the engine. An automatic stop-clock is started and stopped at the beginning and end of the known fuel-usage, and the total engine revolutions during this time is also recorded. This information is then used to calculate air flow, fuel flow, fuel-to-air ratio, and engine speed. Fuel temperature is also measured, and it is used to accurately obtain the density of the fuel from previously determined density-temperature relationships, which were made with a controlled-temperature bath and a hydrometer. Air temperature and barometric pressure were also needed to determine the inlet air density which is required to calculate the mass flow of air.

Figure 56 is a photograph of this test equipment. In it the air cleaner is removed and the air cart and fuel-flow measuring device are not visible, but the electronic equipment, which is used with the

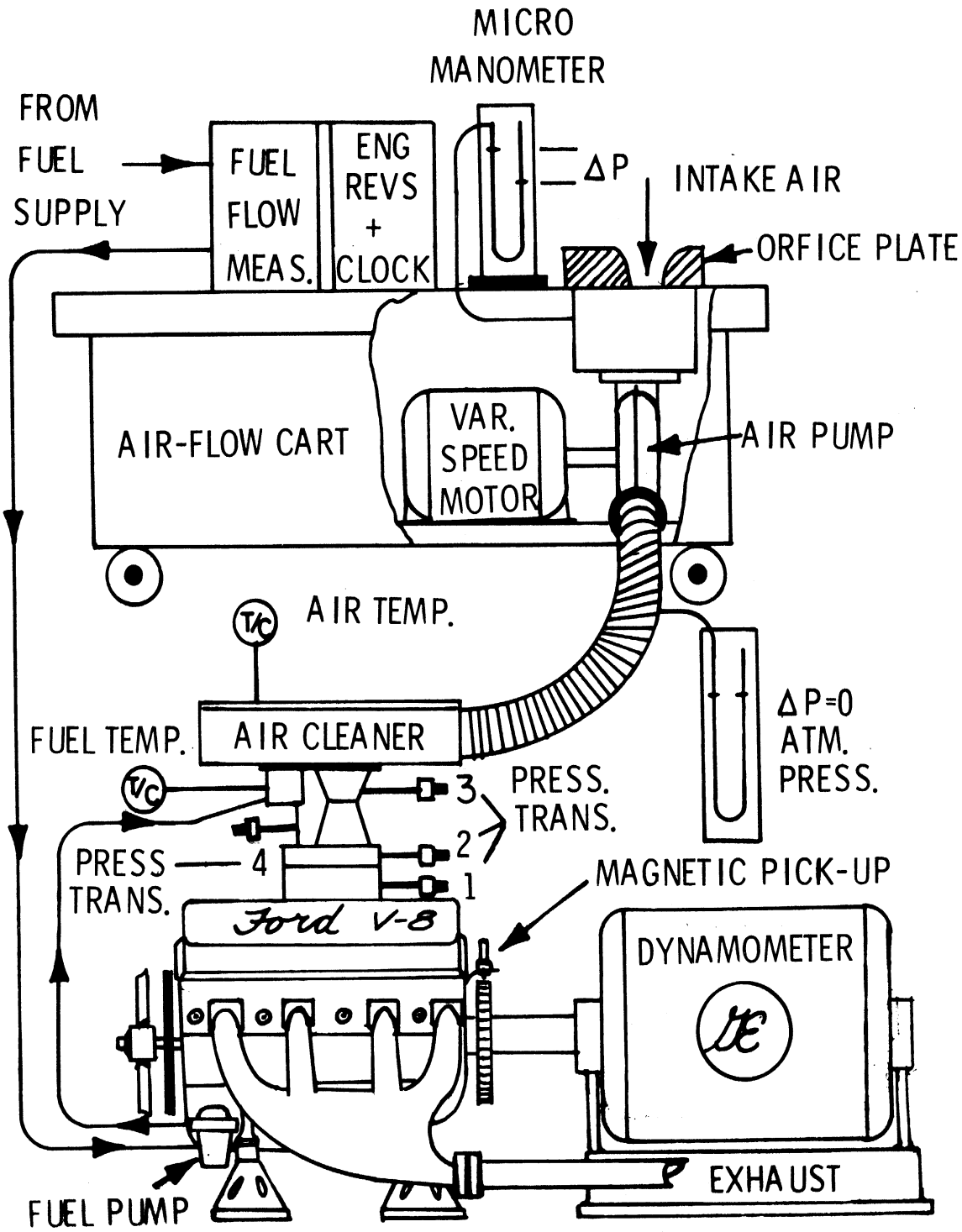

Figure 55. Schematic of Engine Testing Rig.

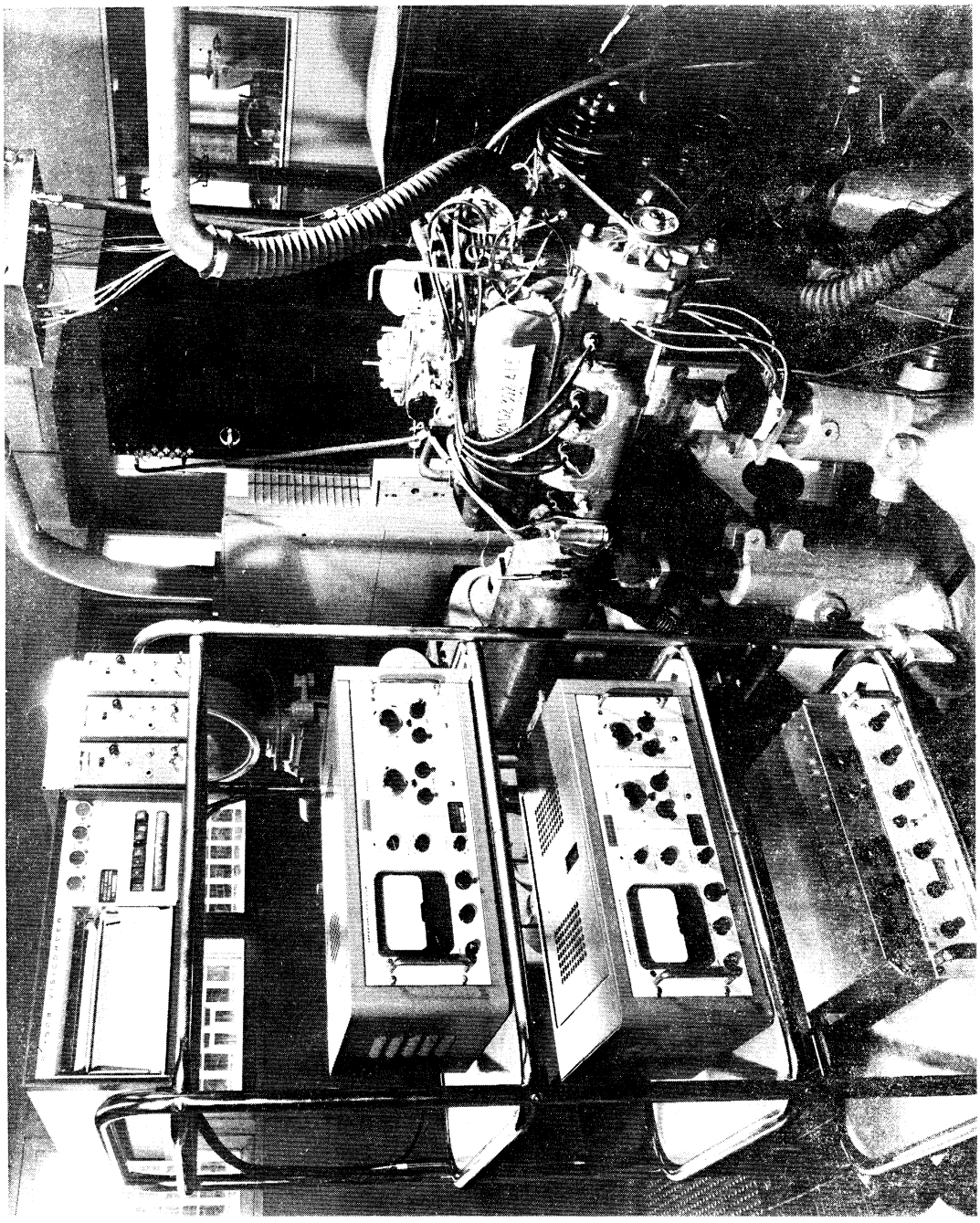

Figure 50. Engine Testing Rig.

pressure transducers to record the instantaneous pressures in the carburetor, is shown on the shelf cart. The top shelf contains the Visicorder, or the strip recorder, which made a permanent record of the pressure traces, the throttle angle, and the engine crankshaft angle. The middle-two shelves hold the Carrier amplifiers which are used to power the pressure transducers and magnify their signal. The bottom shelf contains the amplifier that is needed to record the crankshaft rotation signal, which is generated by the magnetic pick up and the flywheel.

Figure 57 is a close-up photograph of the carburetor, on the engine, and with the pressure transducers in position. Figure 11 also shows the location of the rotational potentiometer which is used to indicate the throttle angle. The location of the transducer which measures the main orifice pressure is on the other side of the carburetor beneath the float bowl, hence, it is not visible in the figure. Table VII summarizes all of the equipment which is used for the engine-carburetor tests.

Before the engine test was performed, the transducers were calibrated. This was done statically and a vacuum pump was used to provide the calibration pressures. Once a calibration pressure was reached, the pump was stopped and the pressure was measured with a mercury manometer. The corresponding inches of deflection on the strip recorder and the gain setting of the electronic amplifiers were also recorded. Several pressure points were recorded for each transducer and plotted as a function of inches deflection. This information was then used in the computer program which reduced the engine-carburetor data.

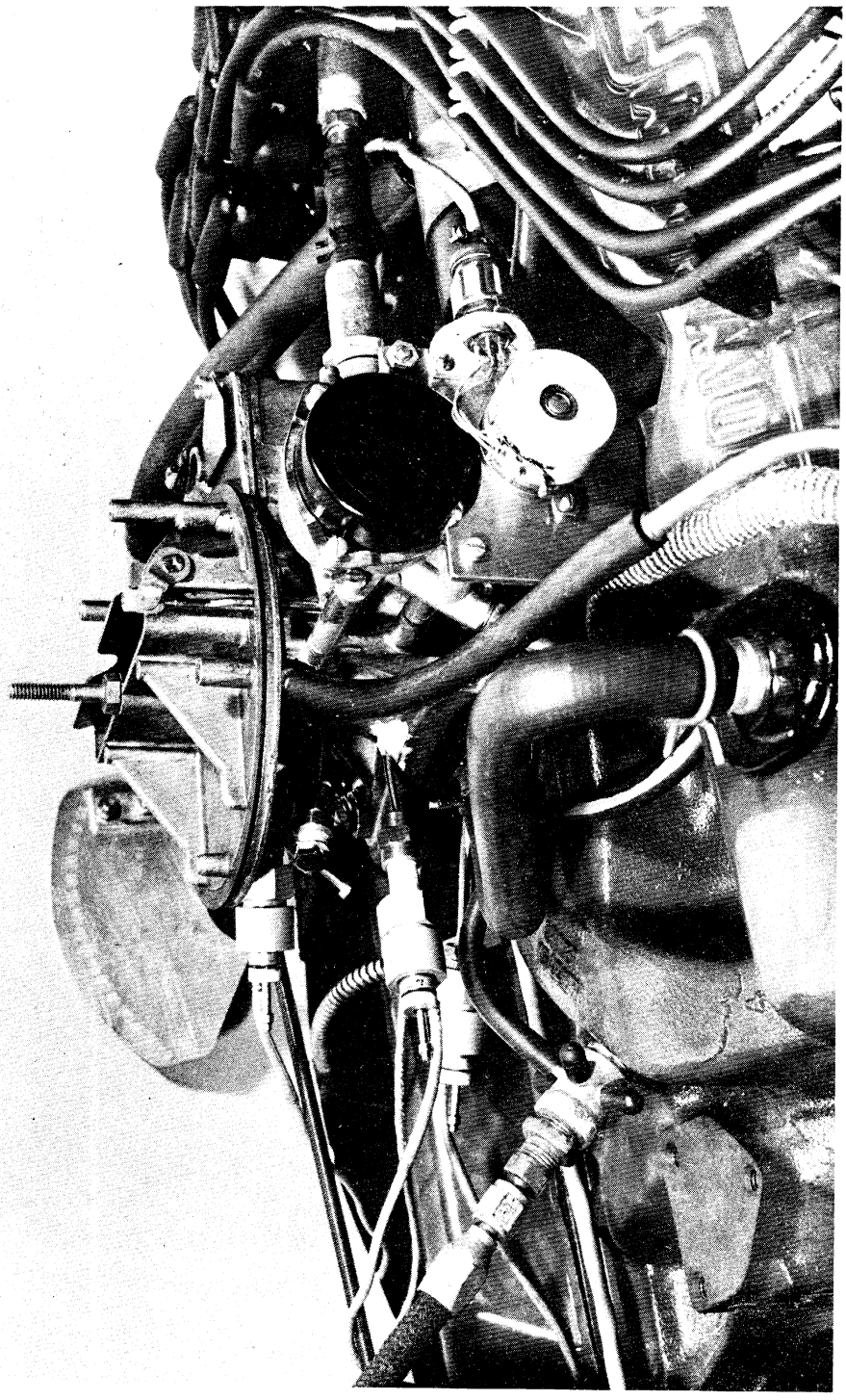

Figure 57. Carburetor on the Engine with Pressure Transducers.

TABLE VII

EQUIPMENT OF ENGINE-CARBURETOR TESTS

ITEM	DESCRIPTION	SIZE, CAPACITY
Carburetor	Ford C8AF-L	2-barrel
Engine	Ford V-8 302	302 cu. in.
Pressure Transducer	Statham PM 131, Ser. No. 34146	±2.5 psi
Pressure Transducer	Statham PM 131 Ser. No. 33658	±5.0 psi
Pressure Transducer	Statham PM 131 Ser. No. 34147	±15.0 psi
Pressure Transducer	CEC 4-312-0002 Ser. 34367	±5.0 psi
Rotary Potentiameter	Helipot 5403	10,000 ohm
Recorder	Honeywell visicorder, Model 508	8 inch paper width, 12 channels
Amplifier	Carrier strain gage amplifier	
Dynamometer	General Electric 26G51	
Fuel Flow Meter	Hewlett-Packard Model 521A	
Air Flow Meter	General Motors Standard Air Orifice Plate	
Manometer	Meriam Micromanometer Model A-750	10 inch

The test procedure is very simple. First, the electronic equipment is put into operation so that it can reach stable operating conditions. The gain settings for the transducers are then recorded, and the engine is started. Once the engine reaches stable operation, data points are taken. A set throttle angle is maintained, while engine speed is varied from 1000 to 3000 rpm in steps of 500 rpm. For each engine speed the strip recorder is run to obtain about 50 cycles of the pulsating pressures. The throttle angle is then re-set, and the process is repeated. This is done for throttle angles of 15, 30, 45, 60, 75, and 90 degrees, where 90 degrees is wide open throttle. All of the variables, which were recorded, are shown in Table VIII.

TABLE VIII

VARIABLES OF THE ENGINE-CARBURETOR TESTS

VARIABLE	RANGE FOR WHICH MEASURED
Engine Speed	1000-3000 rpm
Throttle Angle	10-90 degrees 90 = wide open throttle
Average Fuel Flow	0-65 lb/hr
Average Air Flow	0-900 lb/hr
Air Temperature	81-98°F
Barometric Pressure	29.04-29.08 in.hg.
Manifold Vacuum	0-22 in.hg.
Boost-Venturi Pressure	10-15 psia
Main-Venturi Pressure	12.5-15 psia
Manifold Pressure	0-15 psia
Main-Orifice Pressure	10-15 psia
Fuel	Standard Regular gasoline at air temperature

APPENDIX B

COEFFICIENTS OF DISCHARGE FOR OSCILLATING FLOW

Actual Orifice Flow-Data

The analysis of orifice flow for ideal conditions showed that the mean coefficient can be correlated with the velocity ratio and the mean Strouhal Number. However, the data does not correlate well when only these two variables are taken into account. Another dimensionless number, the Reynolds Number, is used to correlate the actual coefficient of discharge, and it is defined for oscillating flow as;

$$RE = V_M D/\nu$$

Therefore, the actual coefficient of discharge is given by the function;

$$C_{DM} = f(ST_M, V_R, RE)$$

The data for the orifices is put into four main divisions; 1) C_{DM} versus flow ratio, 2) C_{DM} versus head ratio; 3) C_{DA} versus flow ratio, and 4) C_{DA} versus head ratio.

MEAN COEFFICIENT OF DISCHARGE
VERSUS
FLOW RATIO

REYNOLDS NUMBER=1399-1849

TEST NUMBER 7770
ORIFICE: SQUARE EDGED
DIAMETER: 0.0518 in.
LENGTH: 0.3750 in.
L/D: 7.2394
FLUID: MINERAL SPIRITS
TEMP. RANGE: 88.8-89.2°F
VISCOSITY RANGE: 1.179-1.176 cp
SPECIFIC GRAVITY: .7786-.7788

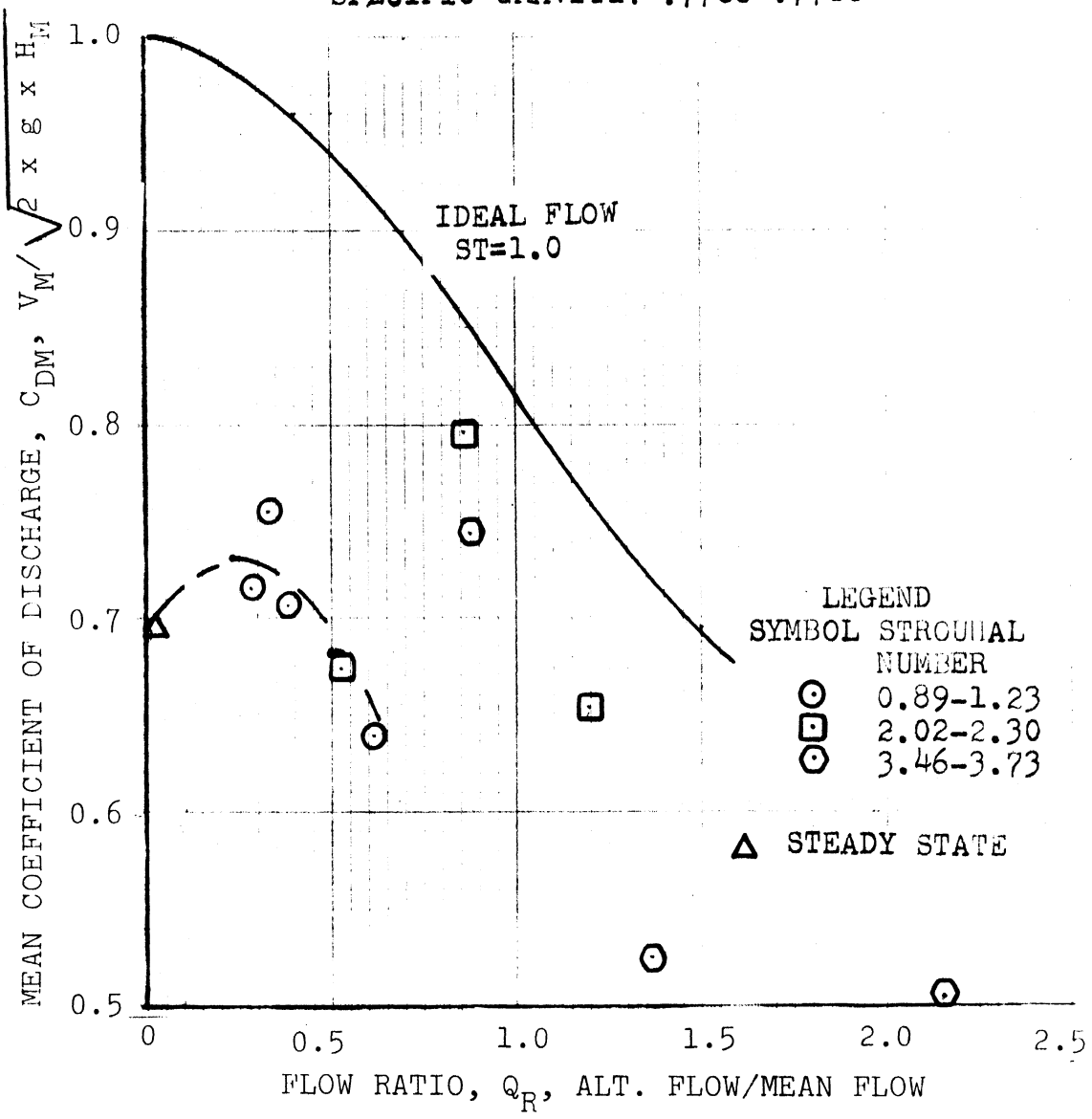

Figure 58. Mean Coefficient of Discharge versus Flow Ratio for L/D=7.24, RE=1399-1849.

MEAN COEFFICIENT OF DISCHARGE
VERSUS
FLOW RATIO

REYNOLDS NUMBER=2910-3320

TEST NUMBER 7770
ORIFICE: SQUARE EDGED
DIAMETER: 0.0518 in.
LENGTH: 0.3750 in.
L/D: 7.2394
FLUID: MINERAL SPIRITS
TEMP. RANGE: 88.8-89.2°F
VISCOSITY RANGE: 1.179-1.176 cp
SPECIFIC GRAVITY: .7786-.7788

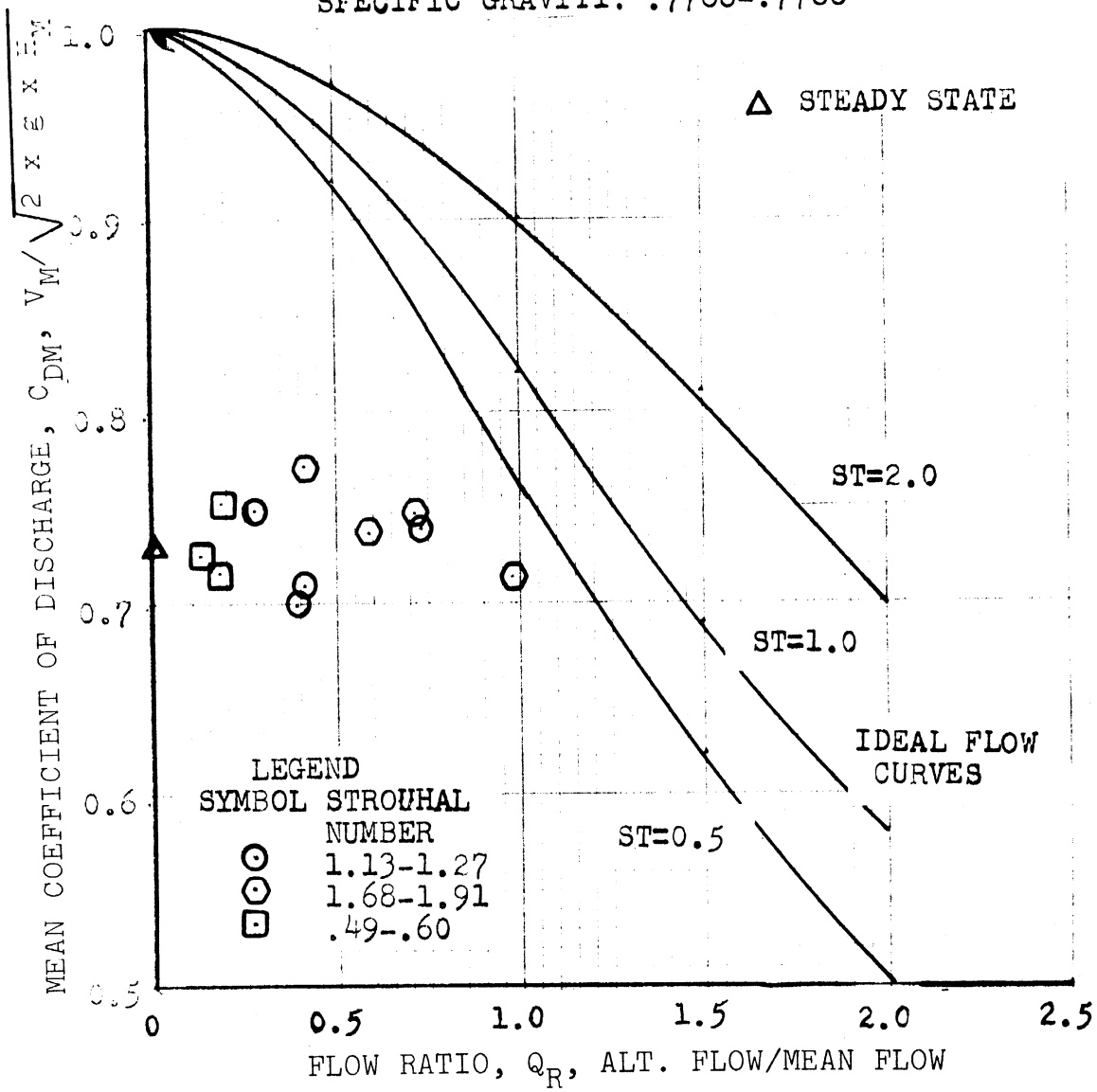

Figure 59. Mean Coefficient of Discharge versus Flow Ratio for L/D=7.24, RE=2910-3320.

MEAN COEFFICIENT OF DISCHARGE
VERSUS
FLOW RATIO

REYNOLDS NUMBER=4134-4393

TEST NUMBER 7770
ORIFICE: SQUARE EDGED
DIAMETER: 0.0518 in.
LENGTH: 0.3750 inc.
L/D: 7.2394
FLUID: MINERAL SPIRITS
TEMP. RANGE: 88.8-89.2°F
VISCOSITY RANGE: 1.179-1.176 cp
SPECIFIC GRAVITY: .7786-.7788

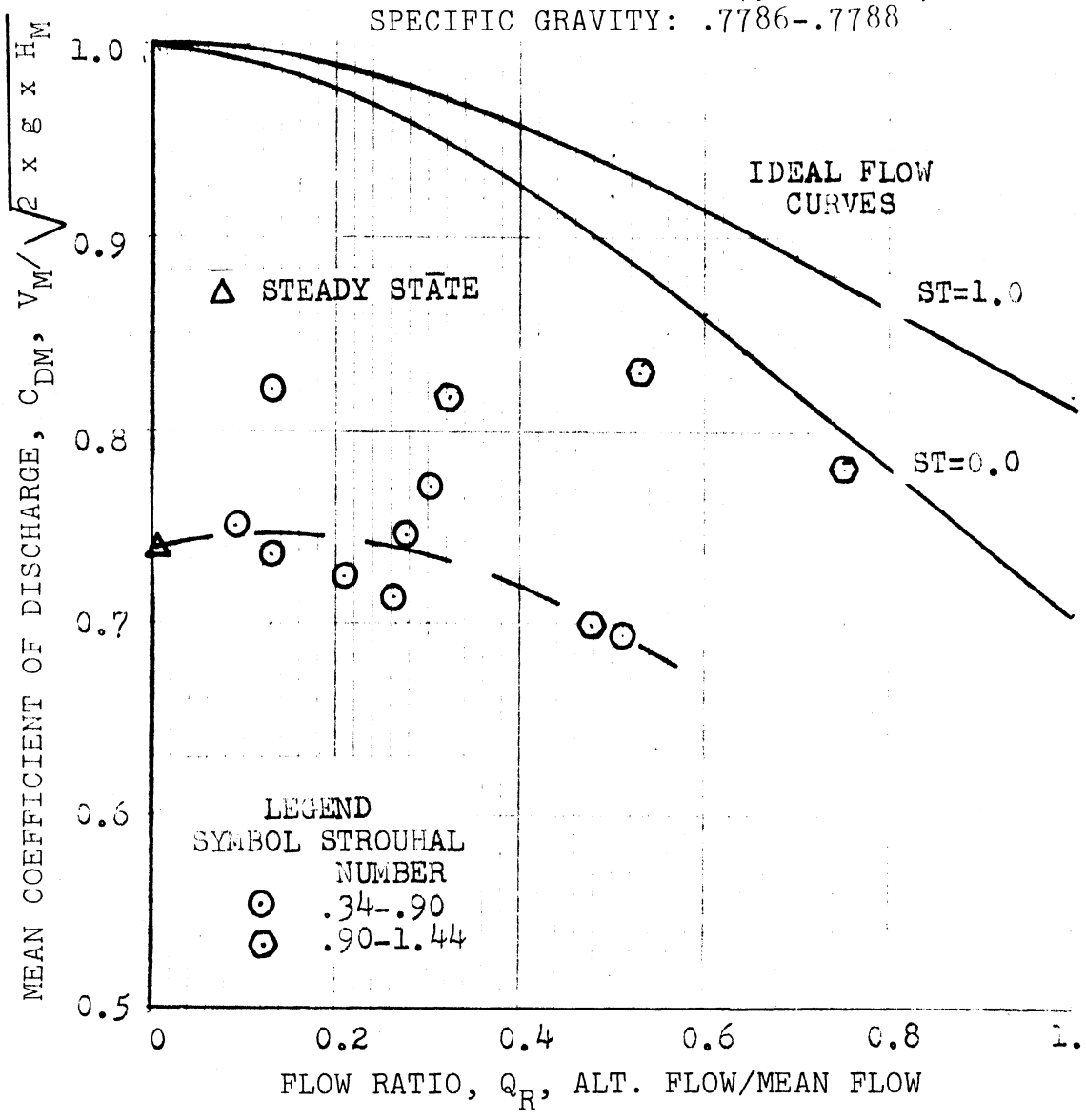

Figure 60. Mean Coefficient of Discharge versus Flow Ratio for L/D=7.24, RE=4134-4393.

MEAN COEFFICIENT OF DISCHARGE
VERSUS
FLOW RATIO

REYNOLDS NUMBER=5202-5554

TEST NUMBER 7770
ORIFICE: SQUARE EDGED
DIAMETER: 0.0518 in.
LENGTH: 0.3750 in.
L/D: 7.2394
FLUID: MINERAL SPIRITS
TEMP. RANGE: 88.8-89.2°F
VISCOSITY RANGE: 1.179-1.176 cp
SPECIFIC GRAVITY: .7786-.7788

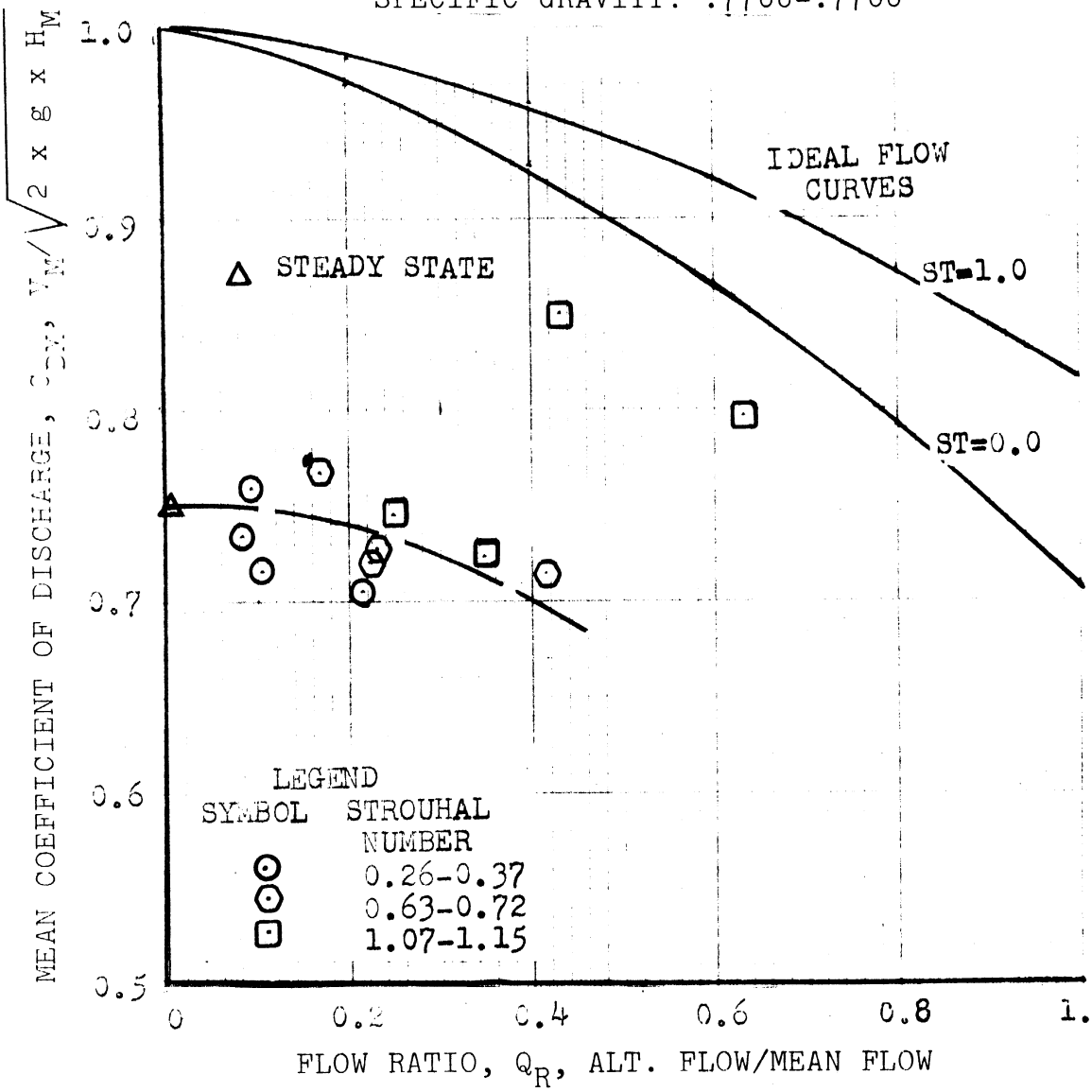

Figure 61. Mean Coefficient of Discharge versus Flow Ratio for L/D=7.24, RE=5202-5554.

MEAN COEFFICIENT OF DISCHARGE
VERSUS
FLOW RATIO

REYNOLDS NUMBER=1104-1218

TEST NUMBER 78701
ORIFICE: SQUARE EDGED
DIAMETER: 0.0518 in
LENGTH: 0.1880 in
L/D: 3.6293
FLUID: MINERAL SPIRITS
TEMPERATURE: 75.1-78.9°F
VISCOSITY: 1.307-1.269 cp
SPECIFIC GRAVITY: .7853-.7834

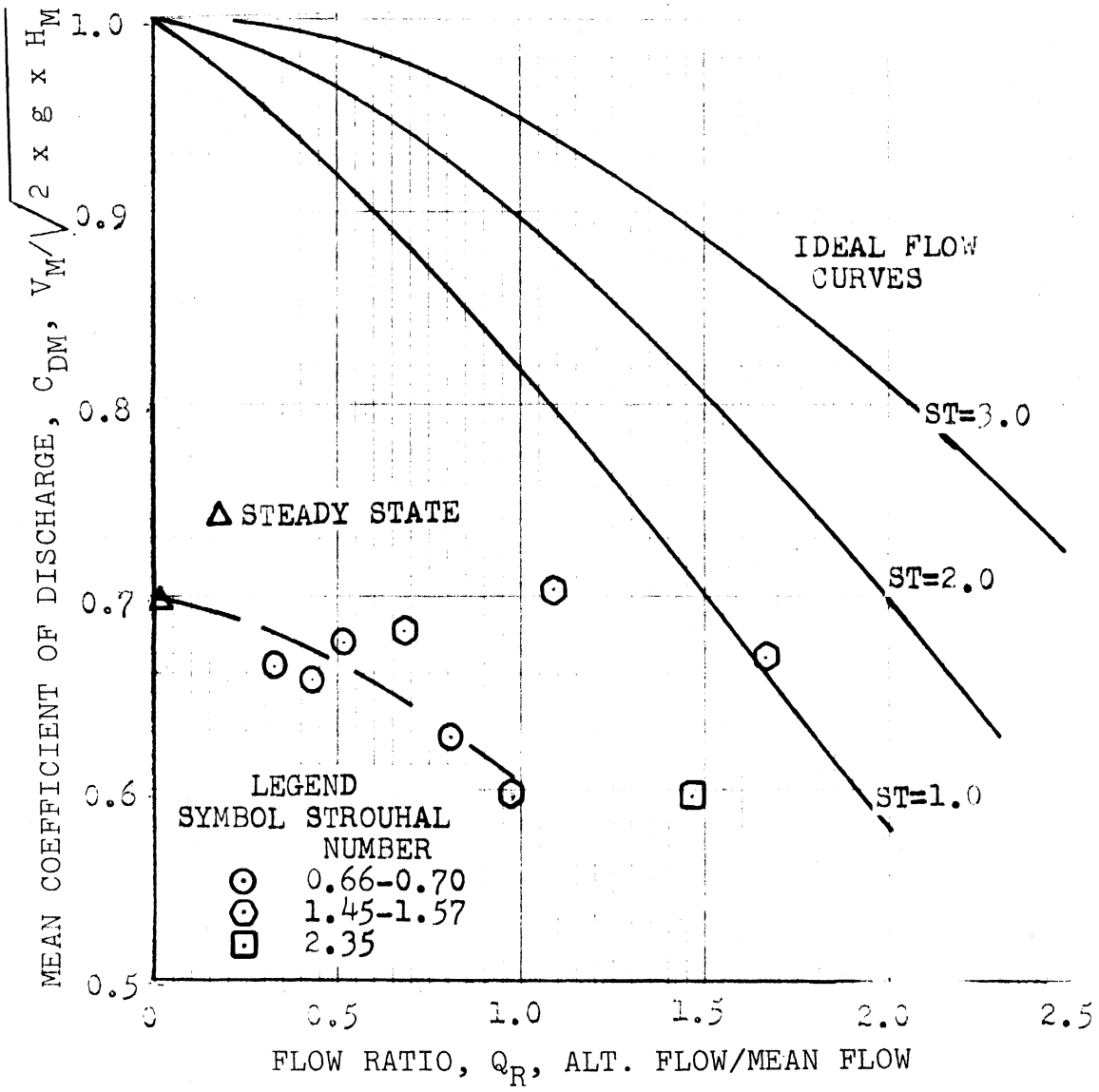

Figure 62. Mean Coefficient of Discharge versus Flow Ratio for L/D=3.63, RE=1104-1218.

MEAN COEFFICIENT OF DISCHARGE
VERSUS
FLOW RATIO

REYNOLDS NUMBER=2349-2638

TEST NUMBER 78701
ORIFICE: SQUARE EDGED
DIAMETER: 0.0518 inch
LENGTH: 0.1880 inch
L/D: 3.6293
FLUID: MINERAL SPIRITS
TEMPERATURE: 75.1-78.9°F
VISCOSITY: 1.307-1.269 cp
SPECIFIC GRAVITY: .7853-.7834

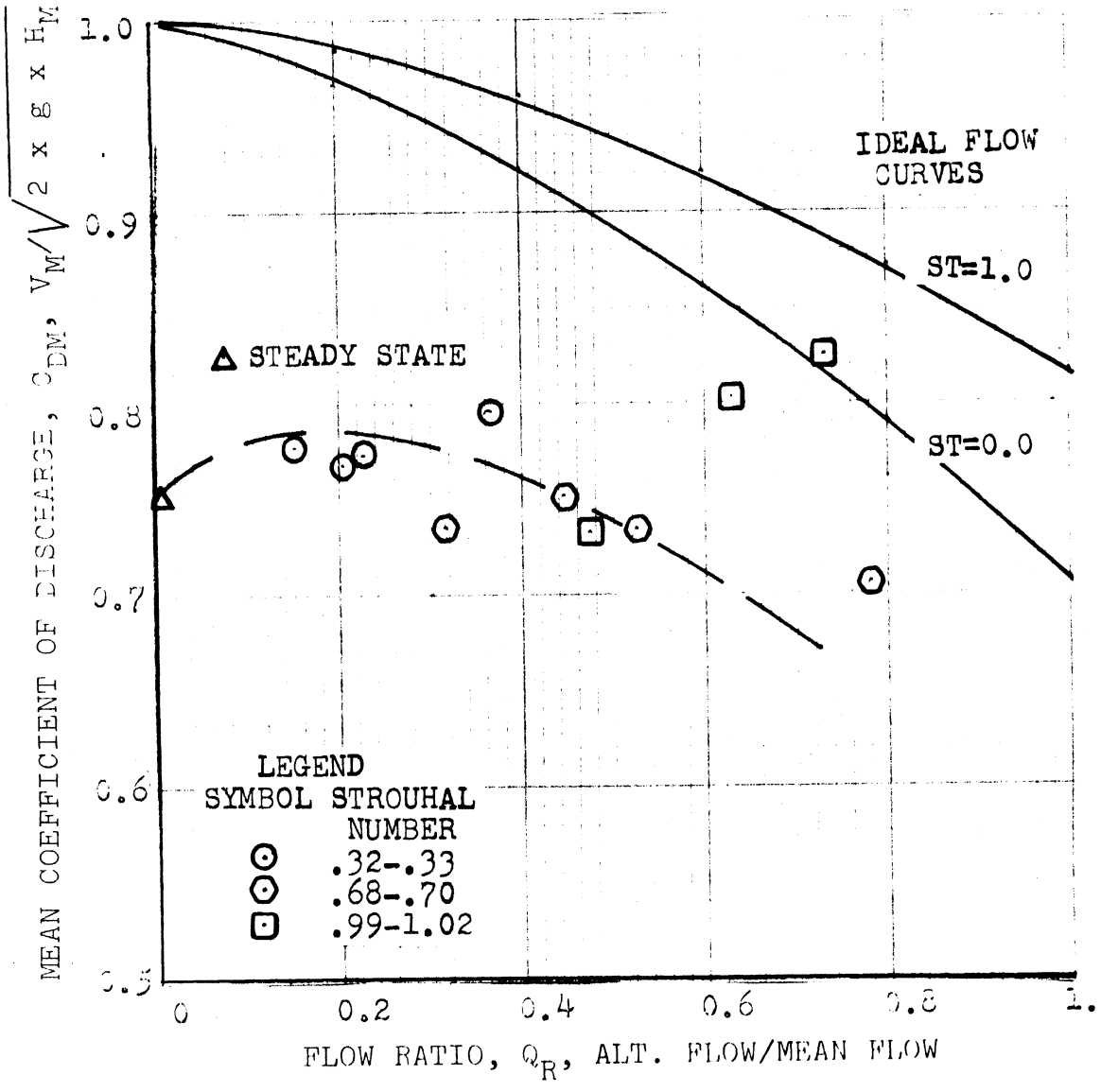

Figure 63. Mean Coefficient of Discharge versus Flow Ratio for L/D=3.63, RE=2349-2638.

MEAN COEFFICIENT OF DISCHARGE
VERSUS
FLOW RATIO

REYNOLDS NUMBER=3422-3751

TEST NUMBER 78701
ORIFICE: SQUARE EDGED
DIAMETER: 0.0518 inch
LENGTH: 0.1880 inch
L/D: 3.6293
FLUID: MINERAL SPIRITS
TEMPERATURE: 75.1-78.9°F
VISCOSITY: 1.307-1.269 cp
SPECIFIC GRAVITY: .7853-.7834

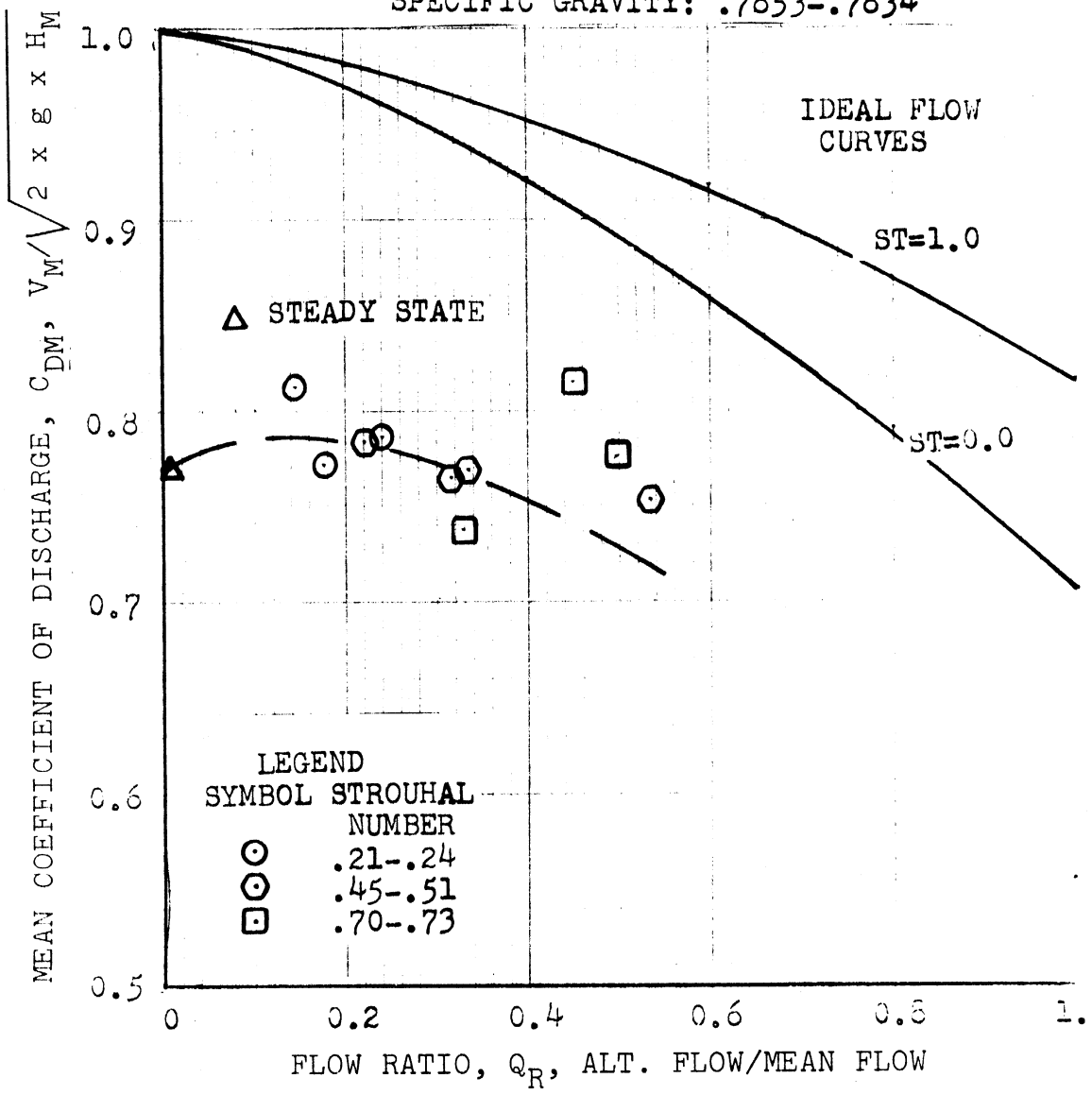

Figure 64. Mean Coefficient of Discharge versus Flow Ratio for L/D=3.63, RE=3422-3751.

MEAN COEFFICIENT OF DISCHARGE
VERSUS
FLOW RATIO

REYNOLDS NUMBER=4521-4751

TEST NUMBER 78701
ORIFICE: SQUARE EDGED
DIAMETER: 0.0518 in
LENGTH: 0.1880 in
L/D: 3.6293
FLUID: MINERAL SPIRITS
TEMPERATURE: 75.1-78.9°F
VISCOSITY: 1.307-1.269 cp
SPECIFIC GRAVITY: .7853-.7834

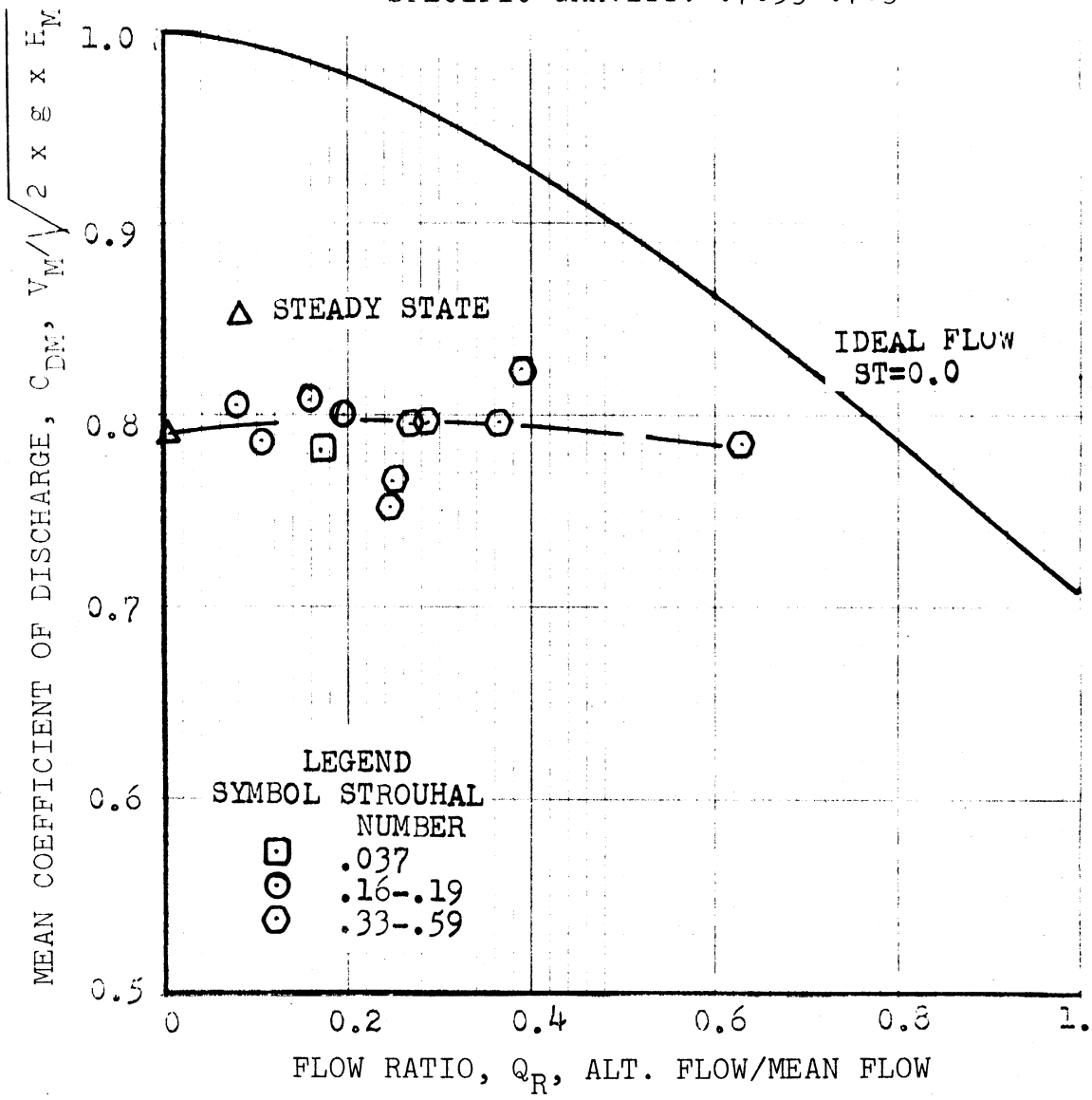

Figure 65. Mean Coefficient of Discharge versus Flow Ratio for L/D=3.63, RE=4521-4751.

MEAN COEFFICIENT OF DISCHARGE
VERSUS
FLOW RATIO

REYNOLDS NUMBER= 1099-1198
STROUHAL NUMBER=0.112-0.238
TEST NUMBER 78702
ORIFICE: SQUARE EDGED
DIAMETER: 0.0518 inch
LENGTH: 0.0319 inch
L/D; 0.6158
FLUID: MINERAL SPIRITS
TEMPERATURE: 75.2-75.7°F
SPECIFIC GRAVITY: .7852-.7850
VISCOSITY: 1.306-1.301 cp

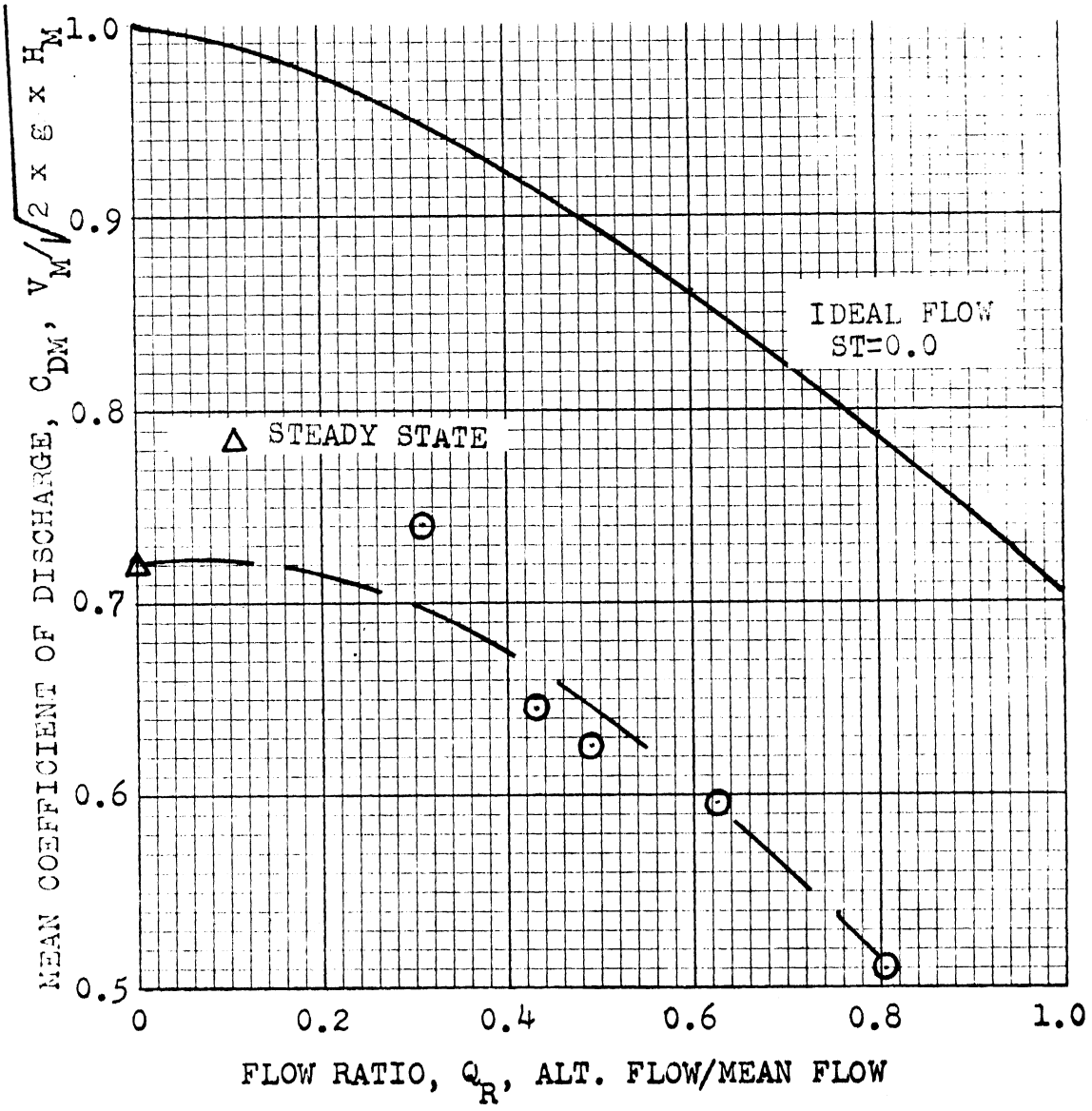

Figure 66. Mean Coefficient of Discharge versus Flow Ratio for L/D=0.62, RE=1099-1198.

MEAN COEFFICIENT OF DISCHARGE
VERSUS
FLOW RATIO

REYNOLDS NUMBER=2369-2612
STROUHAL NUMBER=0.0514-0.1834
TEST NUMBER 78702
ORIFICE: SQUARE EDGED
DIAMETER: 0.0518 inch
LENGTH: 0.0319 inch
L/D; 0.6158
FLUID: MINERAL SPIRITS
TEMPERATURE: 75.2-75.7°F
SPECIFIC GRAVITY: .7852-.7850
VISCOSITY: 1.306-1.301 cp

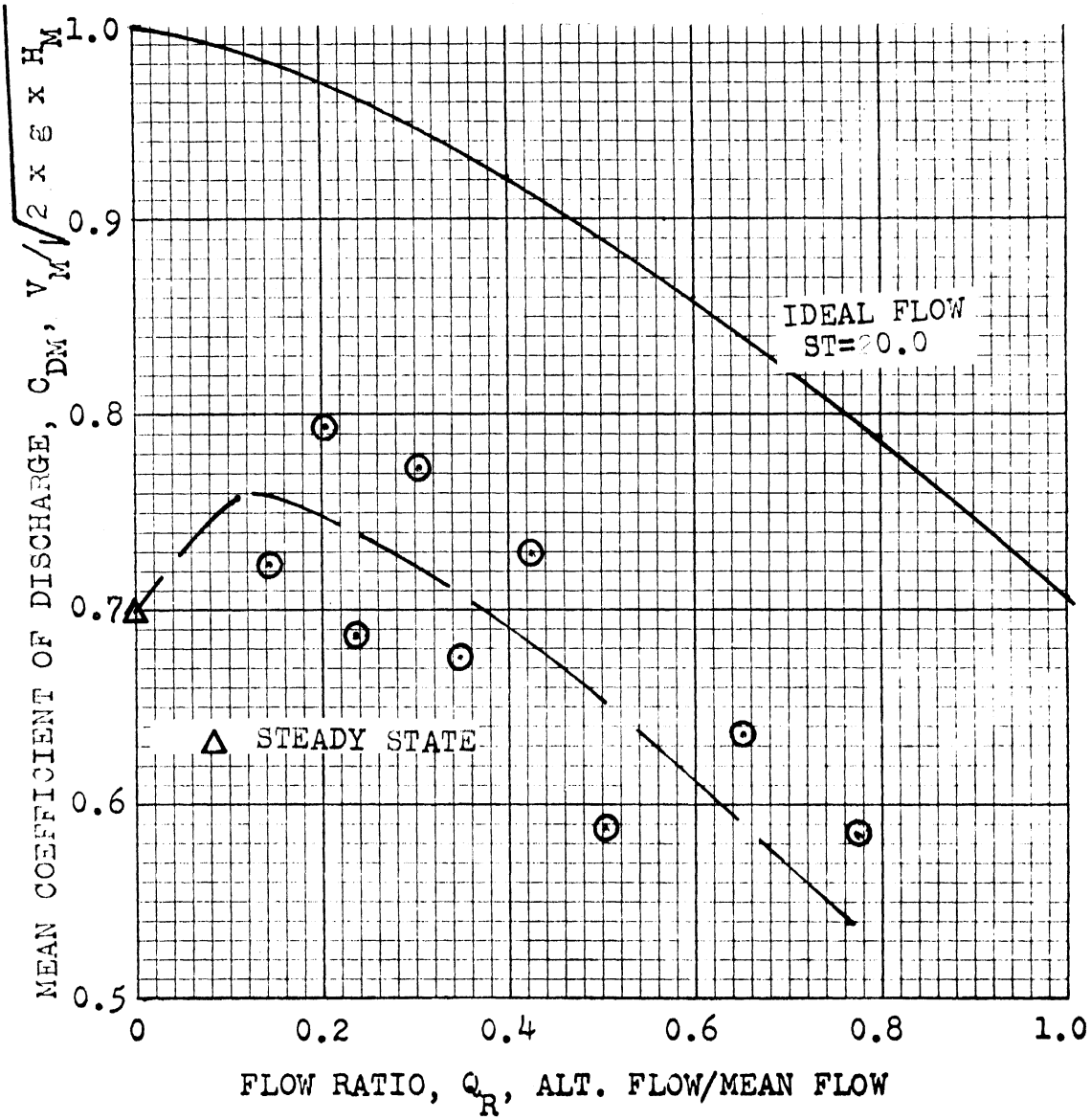

Figure 67. Mean Coefficient of Discharge versus Flow Ratio for L/D=0.62, RE=2369-2612.

MEAN COEFFICIENT OF DISCHARGE
VERSUS
FLOW RATIO

REYNOLDS NUMBER=3387-3713
STROUHAL NUMBER=0.0337-0.1313
TEST NUMBER 78702
ORIFICE: SQUARE EDGED
DIAMETER: 0.0518 inch
LENGTH: 0.0319 inch
L/D; 0.6158
FLUID: MINERAL SPIRITS
TEMPERATURE: 75.2-75.7°F
SPECIFIC GRAVITY: .7852-.7850
VISCOSITY: 1.306-1.301 cp

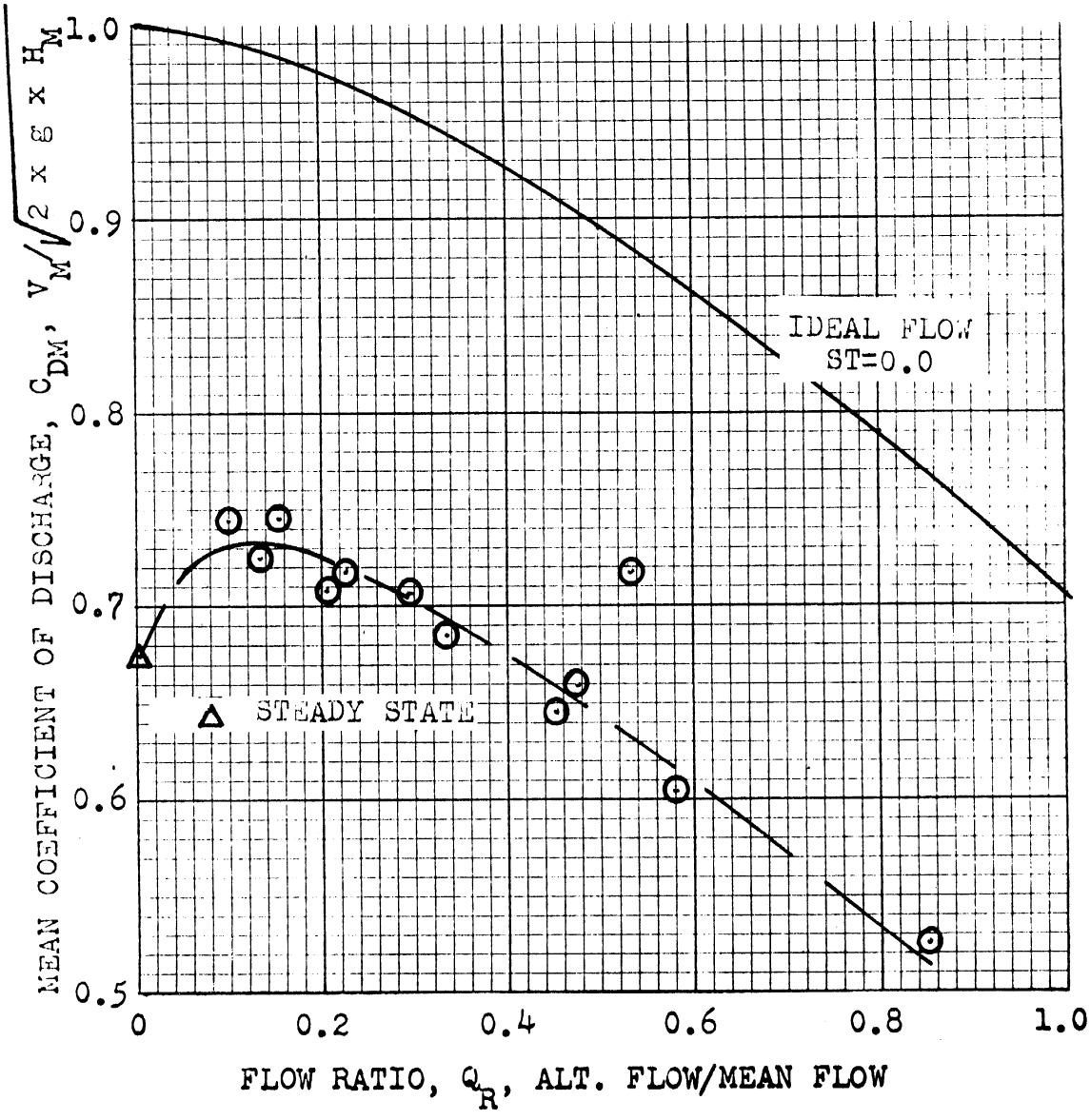

Figure 68. Mean Coefficient of Discharge versus Flow Ratio for L/D=0.62, RE=3387-3713.

MEAN COEFFICIENT OF DISCHARGE
VERSUS
FLOW RATIO

REYNOLDS NUMBER=4470-4721
STROUHAL NUMBER=0.0283-0.1044
TEST NUMBER 78702
ORIFICE: SQUARE EDGED
DIAMETER: 0.0518 inch
LENGTH: 0.0319 inch
L/D; 0.6158
FLUID: MINERAL SPIRITS
TEMPERATURE: 75.2-75.7°F
SPECIFIC GRAVITY: .7852-.7850
VISCOSITY: 1.306-1.301 cp

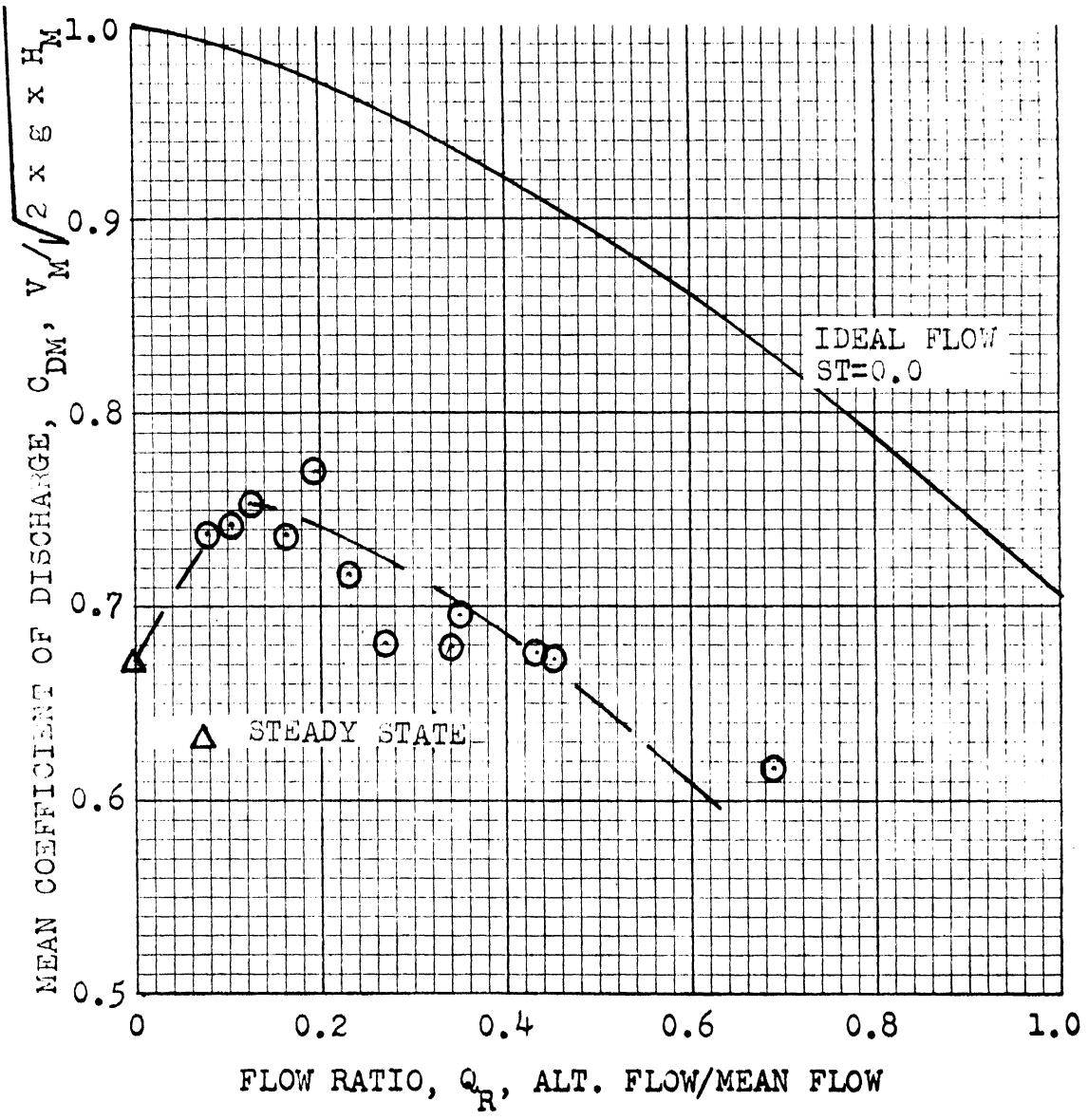

Figure 69. Mean Coefficient of Discharge versus Flow Ratio for L/D=0.62, RE=4470-4721.

MEAN COEFFICIENT OF DISCHARGE
VERSUS
FLOW RATIO
TEST 2470

REYNOLDS' NUMBER=1800-2200

ORIFICE: F-50
DIAM: .0497 in.
LENGTH: .1837 in.
FLUID: Mineral Spirits
TEMP: 77.8-84.2°F
SG: .7839-.7809
VISC: 1.280-1.219 cp

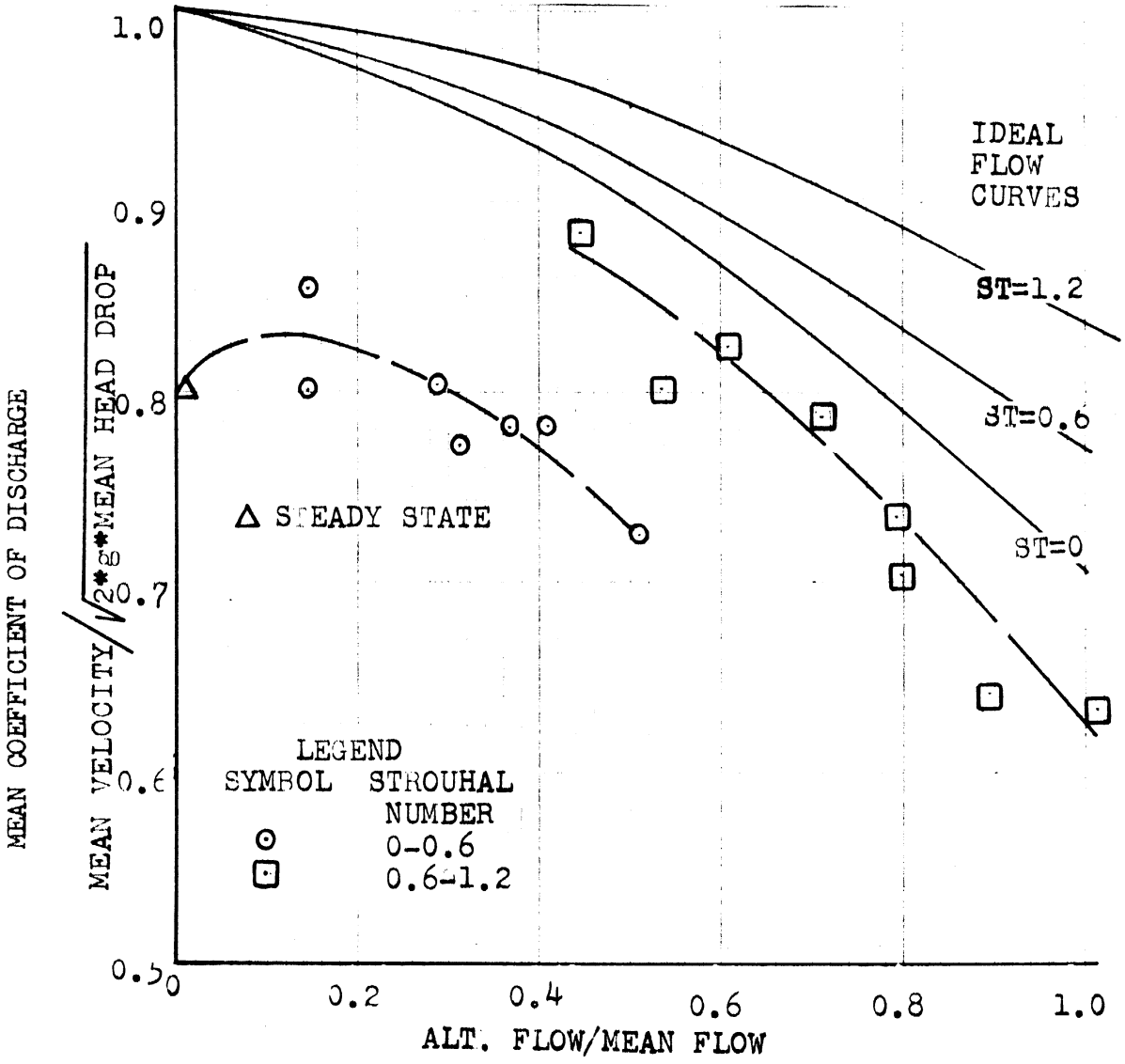

Figure 70. Mean Coefficient of Discharge versus Flow Ratio for F-50 Orifice, RE=1800-2200.

MEAN COEFFICIENT OF DISCHARGE
VERSUS
FLOW RATIO
TEST 2470

REYNOLDS' NUMBER=2800-3200

ORIFICE: F-50
DIAM: .0497 in.
LENGTH: .1837 in.
FLUID: Mineral Spirits
TEMP: 77.8-84.2 °F
SG: .7839-.7809
VISC: 1.280-1.219

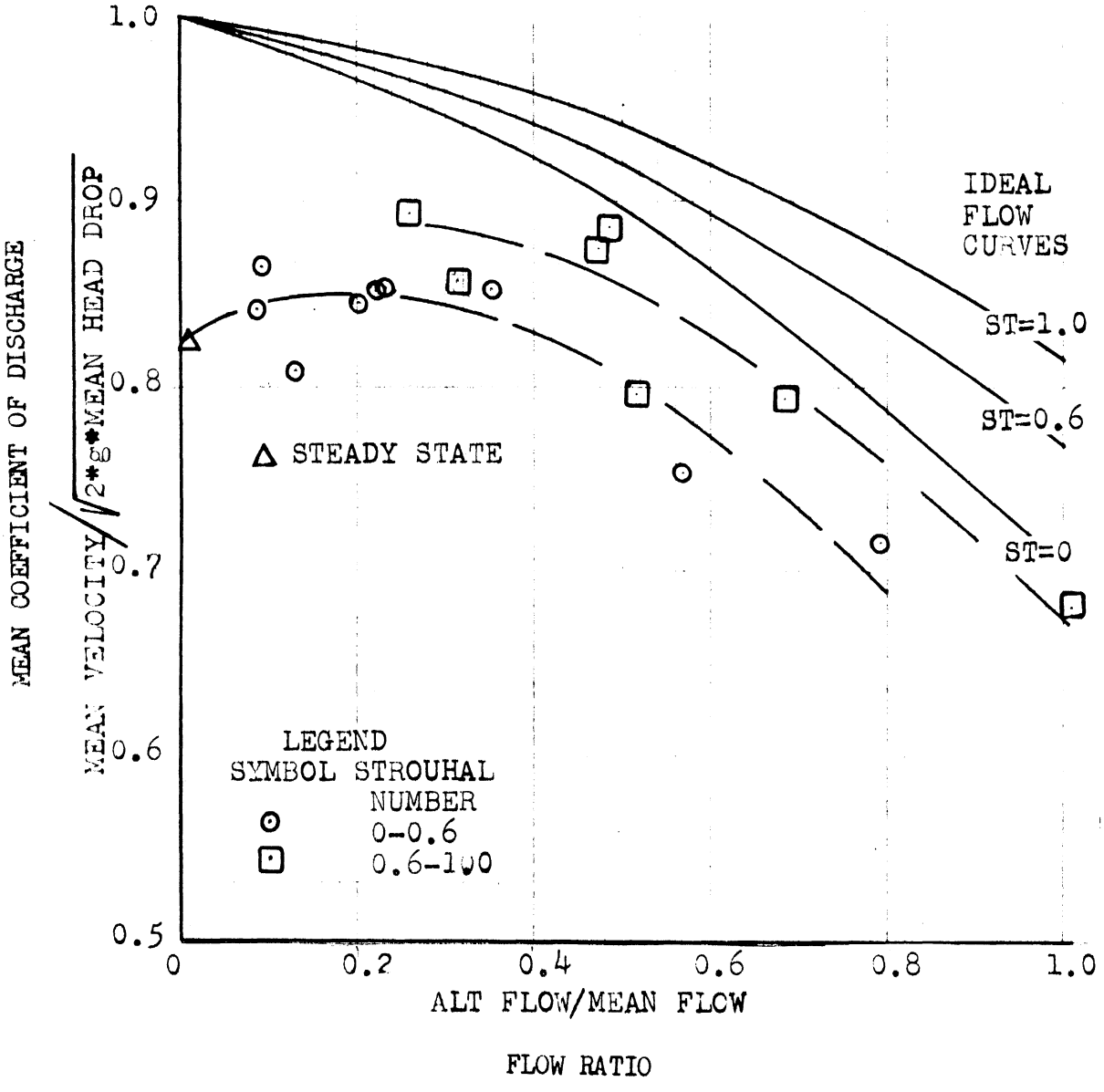

Figure 71. Mean Coefficient of Discharge versus Flow Ratio for F-50 Orifice, RE=2800-3200.

MEAN COEFFICIENT OF DISCHARGE
VERSUS
FLOW RATIO
TEST 2470

REYNOLDS' NUMBER=3800-4200

ORIFICE: F-50
DIAM: .0497 in.
LENGTH: .1837 in.
FLUID: Mineral Spirits
TEMP: 77.8-84.2 °F
SG: .7839-.7809
VISC: 1.280-1.219 cp.

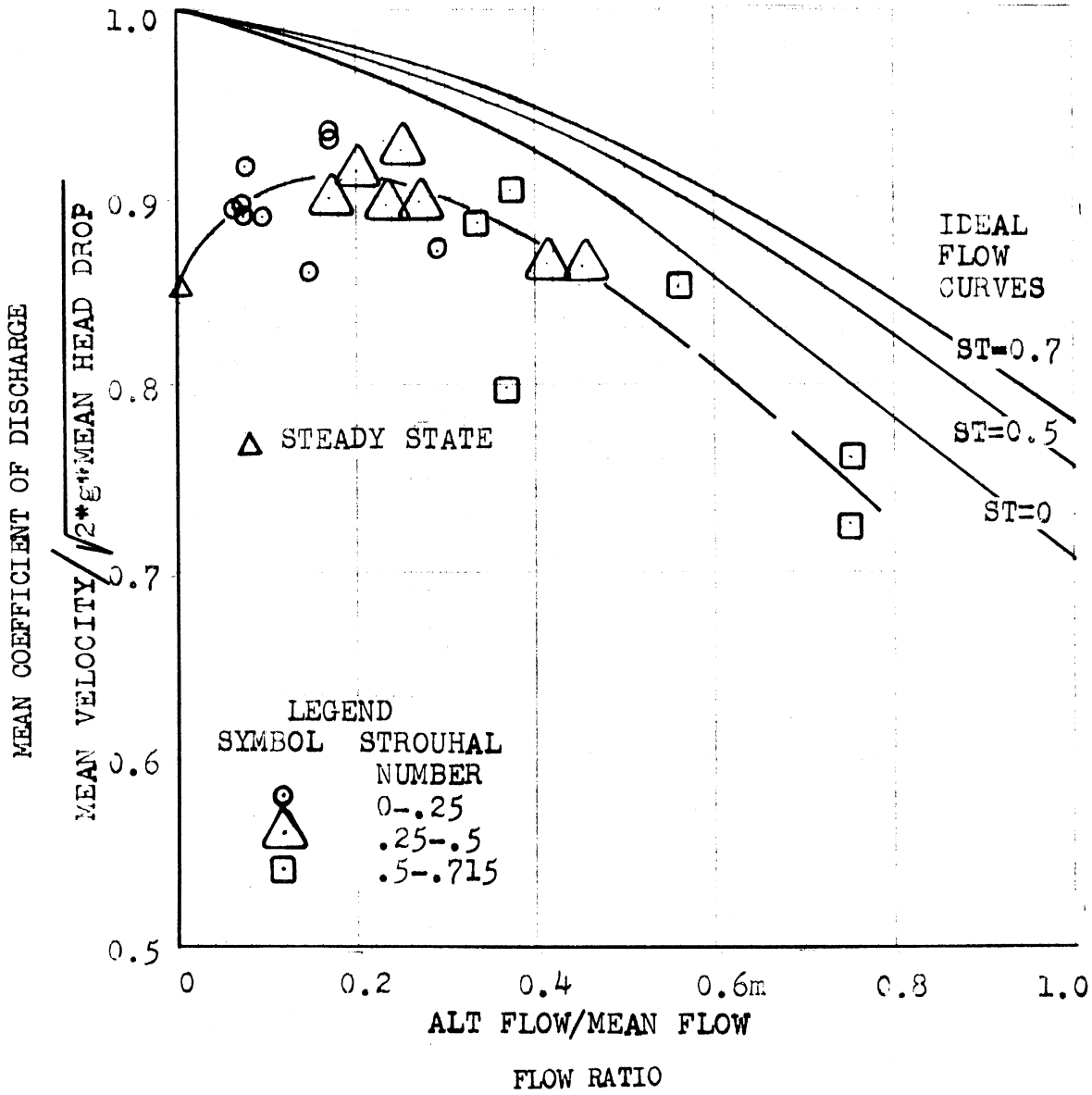

Figure 72. Mean Coefficient of Discharge versus Flow Ratio for F-50 Orifice, RE=3800-4200.

MEAN COEFFICIENT OF DISCHARGE
VERSUS
FLOW RATIO
TEST 2470

REYNOLDS' NUMBER=4800-5200
STROUHAL NUMBER=0-0.6

ORIFICE: F-50
DIAM: .0497 in.
LENGTH: .1837 in.
FLUID: Mineral Spirits
TEMP: 77.8-84.2 °F
SG: .7839-.7809
VISC: 1.280-1.219 cp

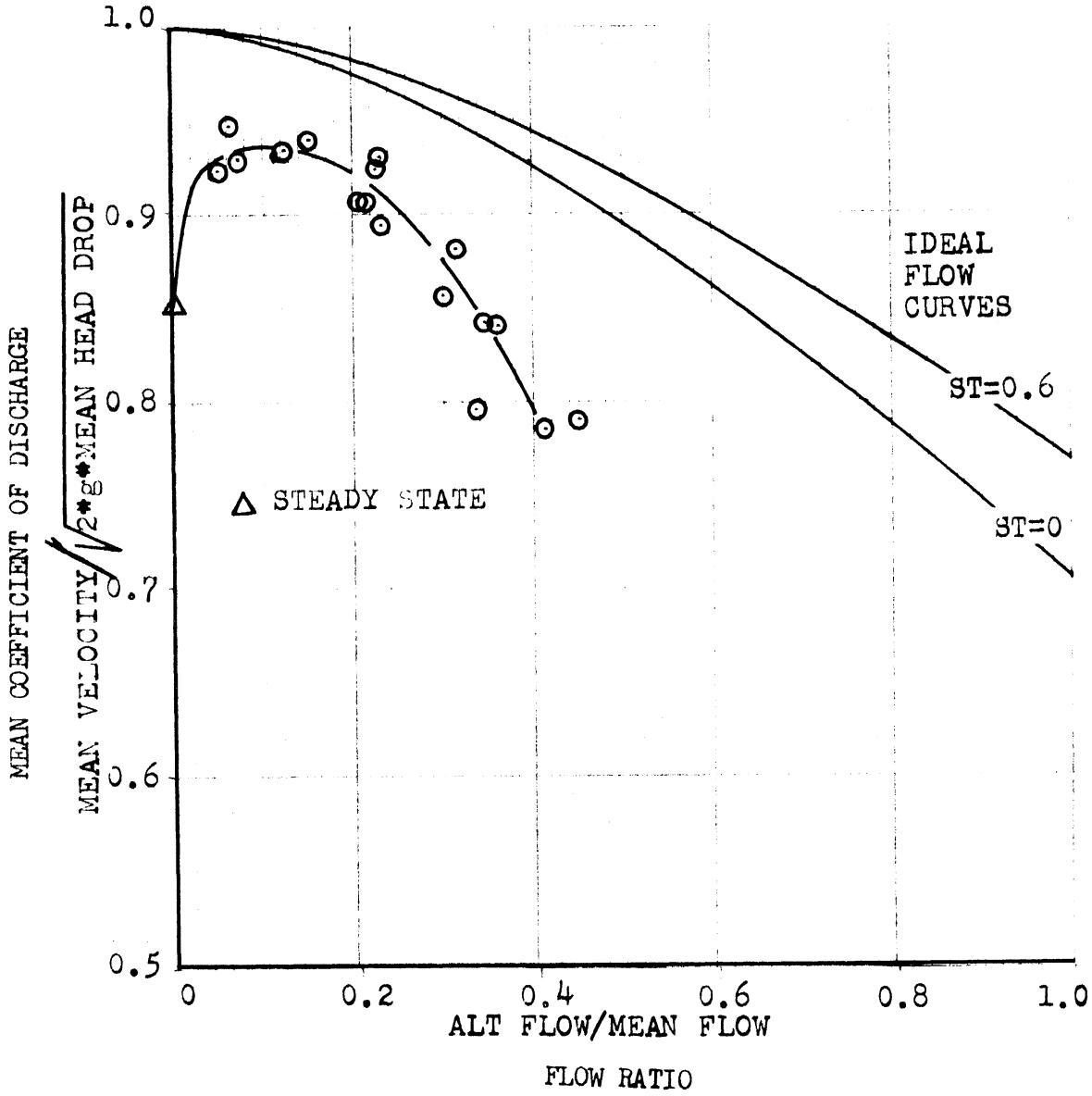

Figure 73. Mean Coefficient of Discharge versus Flow Ratio for F-50 Orifice, RE=4900-5200.

Coefficients as Functions of Head

As discussed in Chapter III, the data can be plotted as a function of head ratio instead of flow ratio. The following plots show the data of Figures 57 through 72 replotted as a function of head ratio.

MEAN COEFFICIENT OF DISCHARGE VERSUS HEAD RATIO

REYNOLDS NUMBER=1399-1849

STROUHAL NUMBER=0.89-2.21

TEST NUMBER 7770
ORIFICE: SQUARE EDGED
DIAMETER: 0.0518 in.
LENGTH: 0.3750 in.
L/D: 7.2394
FLUID: MINERAL SPIRITS
TEMP. RANGE: 88.8-89.2°F
VISCOSITY RANGE: 1.179-1.1.176 cp
SPECIFIC GRAVITY: .7786-.7788

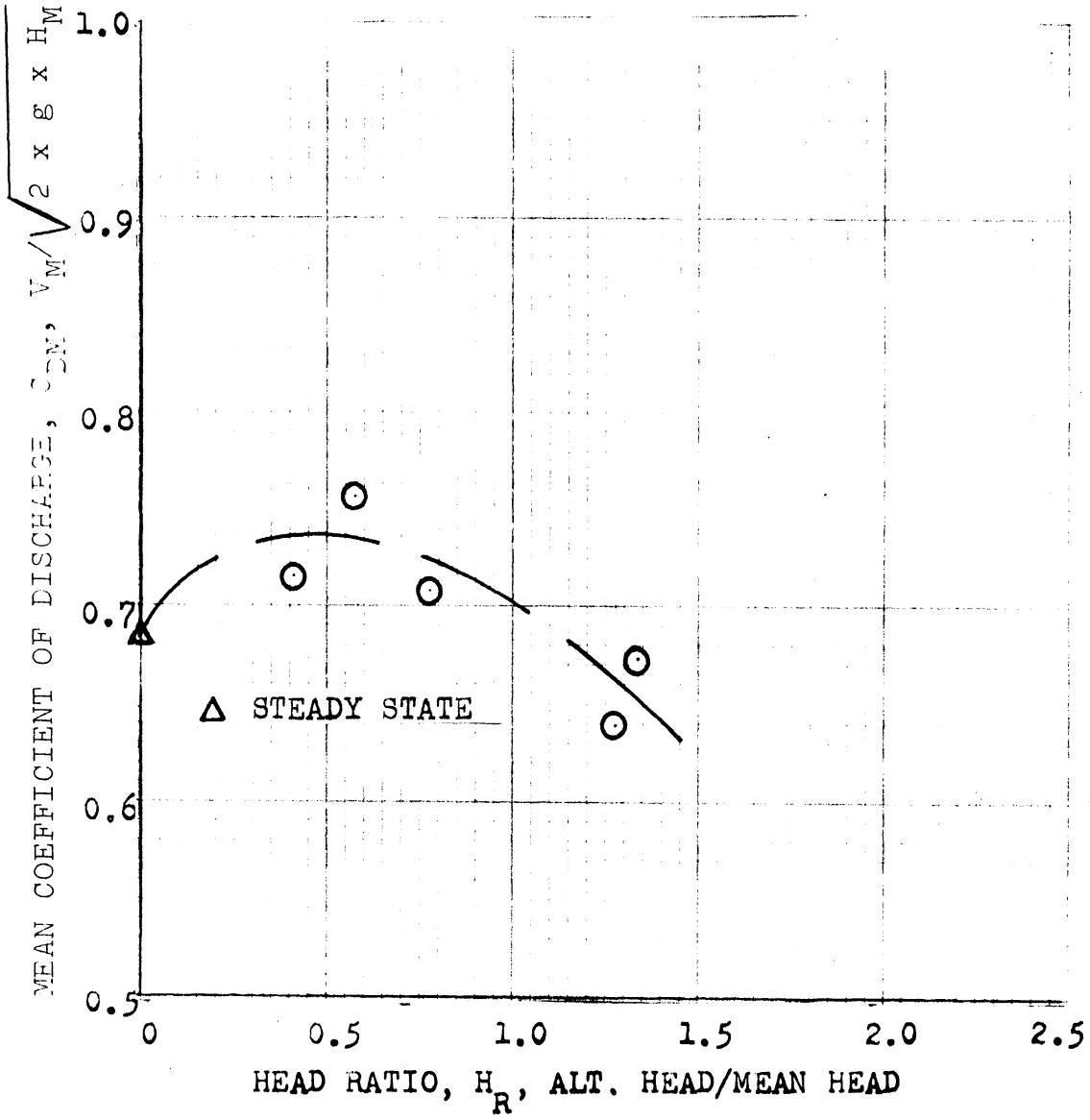

Figure 74. Mean Coefficient of Discharge versus Head Ratio for L/D=7.24, RE=1399-1849.

MEAN COEFFICIENT OF DISCHARGE VERSUS HEAD RATIO

REYNOLDS NUMBER=2910-3320

TEST NUMBER 7770
ORIFICE: SQUARE EDGED
DIAMETER: 0.0518 in.
LENGTH: 0.3750 inc.
L/D: 7.2394
FLUID: MINERAL SPIRITS
TEMP. RANGE: 88.8-89.2°F
VISCOSITY RANGE: 1.179-1.176 cp
SPECIFIC GRAVITY: .7786-.7788

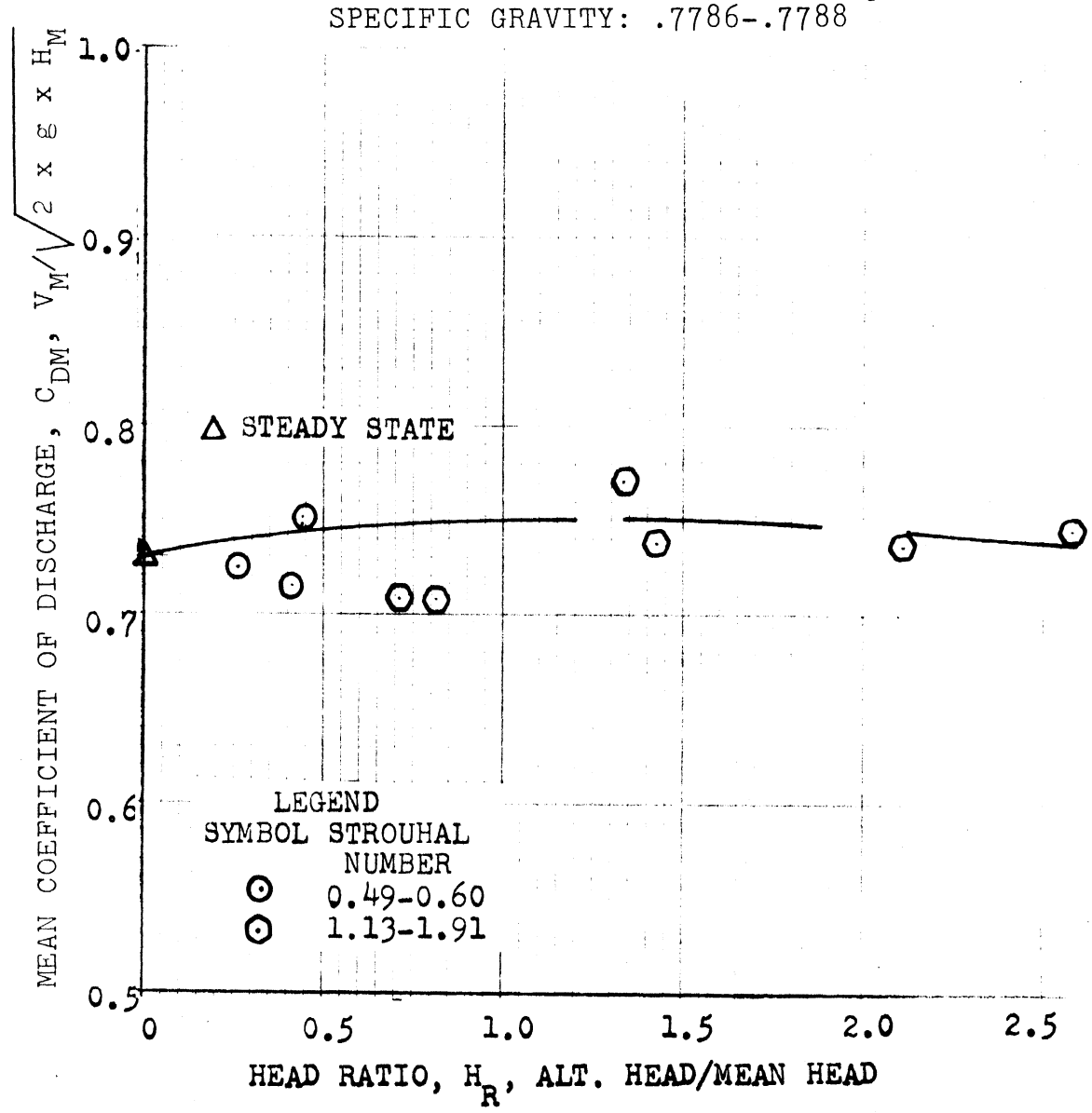

Figure 75. Mean Coefficient of Discharge versus Head Ratio for L/D=7.24, RE=2910-3320.

MEAN COEFFICIENT OF DISCHARGE VERSUS HEAD RATIO

STROUHAL NUMBER=0.34-0.90

REYNOLDS NUMBER=4134-4393

TEST NUMBER 7770
ORIFICE: SQUARE EDGED
DIAMETER: 0.0518 in.
LENGTH: 0.3750 in.
L/D: 7.2394
FLUID: MINERAL SPIRITS
TEMP. RANGE: 88.8-89.2°F
VISCOSITY RANGE: 1.179-1.176 cp
SPECIFIC GRAVITY: .7786-.7788

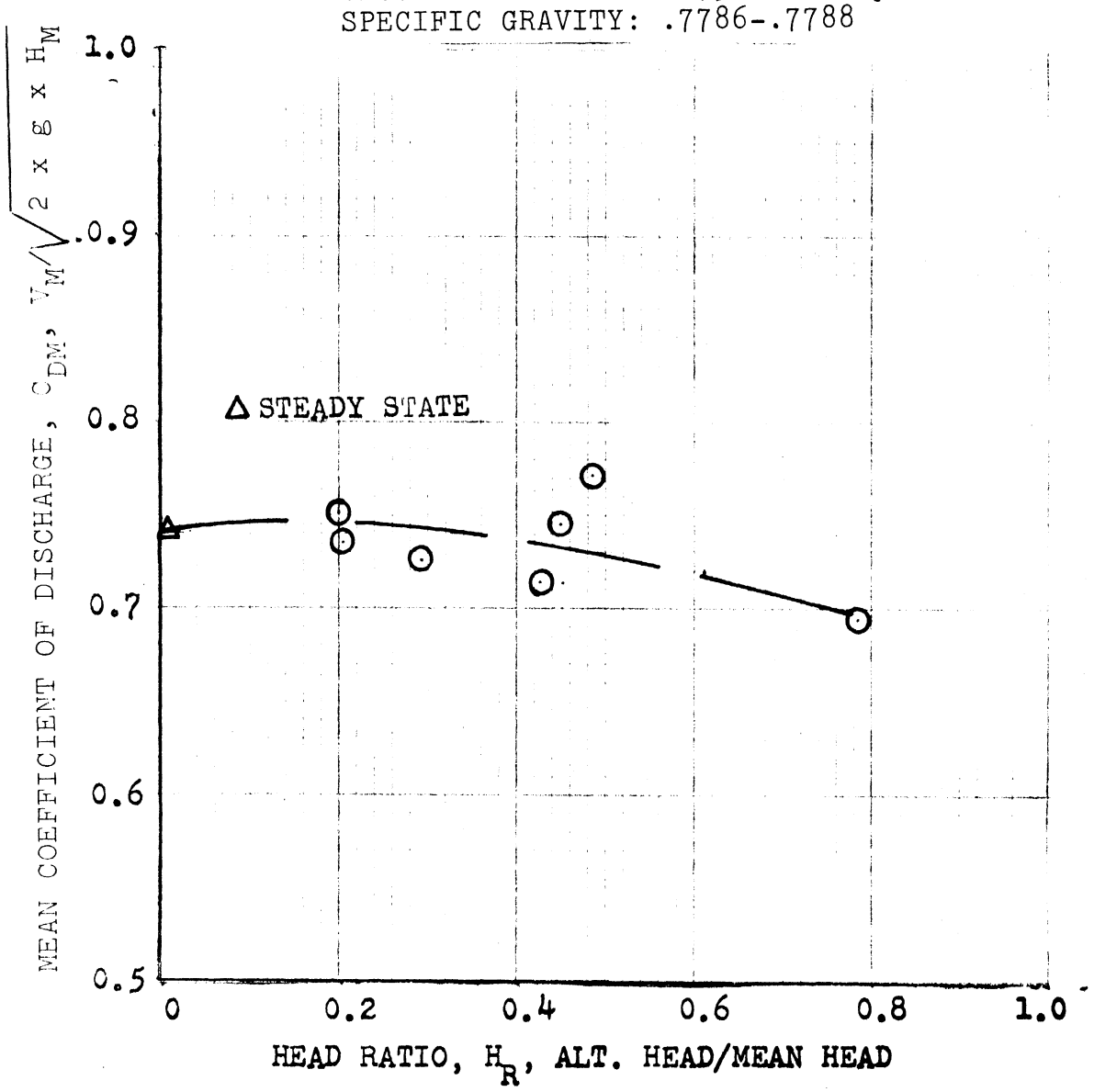

Figure 76. Mean Coefficient of Discharge versus Head Ratio for L/D=7.24, RE=4134-4393.

MEAN COEFFICIENT OF DISCHARGE VERSUS HEAD RATIO

REYNOLDS NUMBER=5202-5554

TEST NUMBER 7770
ORIFICE: SQUARE EDGED
DIAMETER: 0.0518 in.
LENGTH: 0.3750 in.
L/D: 7.2394
FLUID: MINERAL SPIRITS
TEMP. RANGE: 88.8-89.2°F
VISCOSITY RANGE: 1.179-1.176 cp
SPECIFIC GRAVITY: .7786-.7788

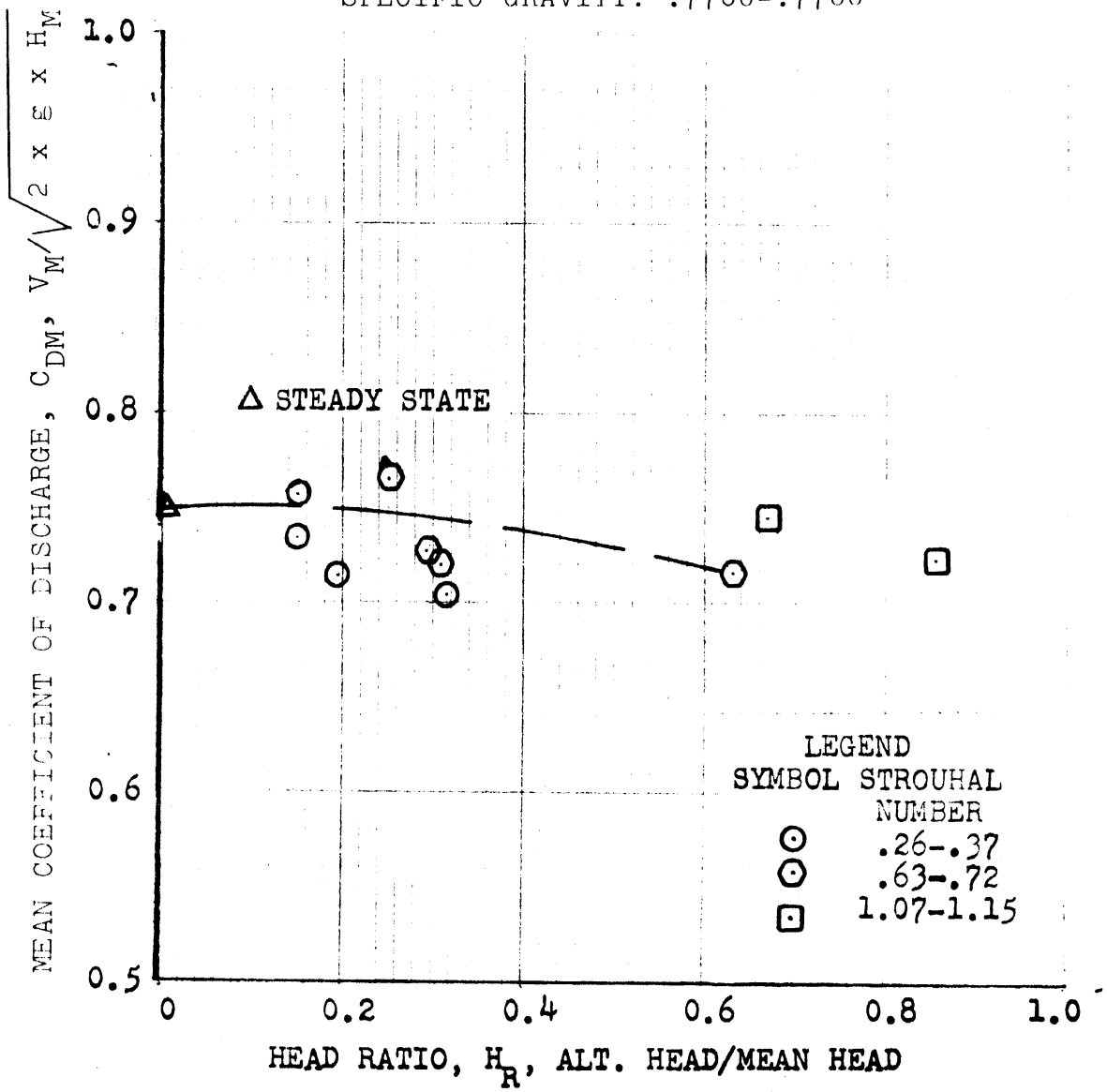

Figure 77. Mean Coefficient of Discharge versus Head Ratio for L/D=7.24, RE=5202-5554.

MEAN COEFFICIENT OF DISCHARGE VERSUS HEAD RATIO

REYNOLDS NUMBER=1104-1218

TEST NUMBER 78701
ORIFICE: SQUARE EDGED
DIAMETER: 0.0518 in.
LENGTH: 0.1880 in.
L/D: 3.6293
FLUID: MINERAL SPIRITS
TEMPERATURE: 75.1-78.9°F
VISCOSITY: 1.307-1.269 cp
SPECIFIC GRAVITY: .7853-.7834

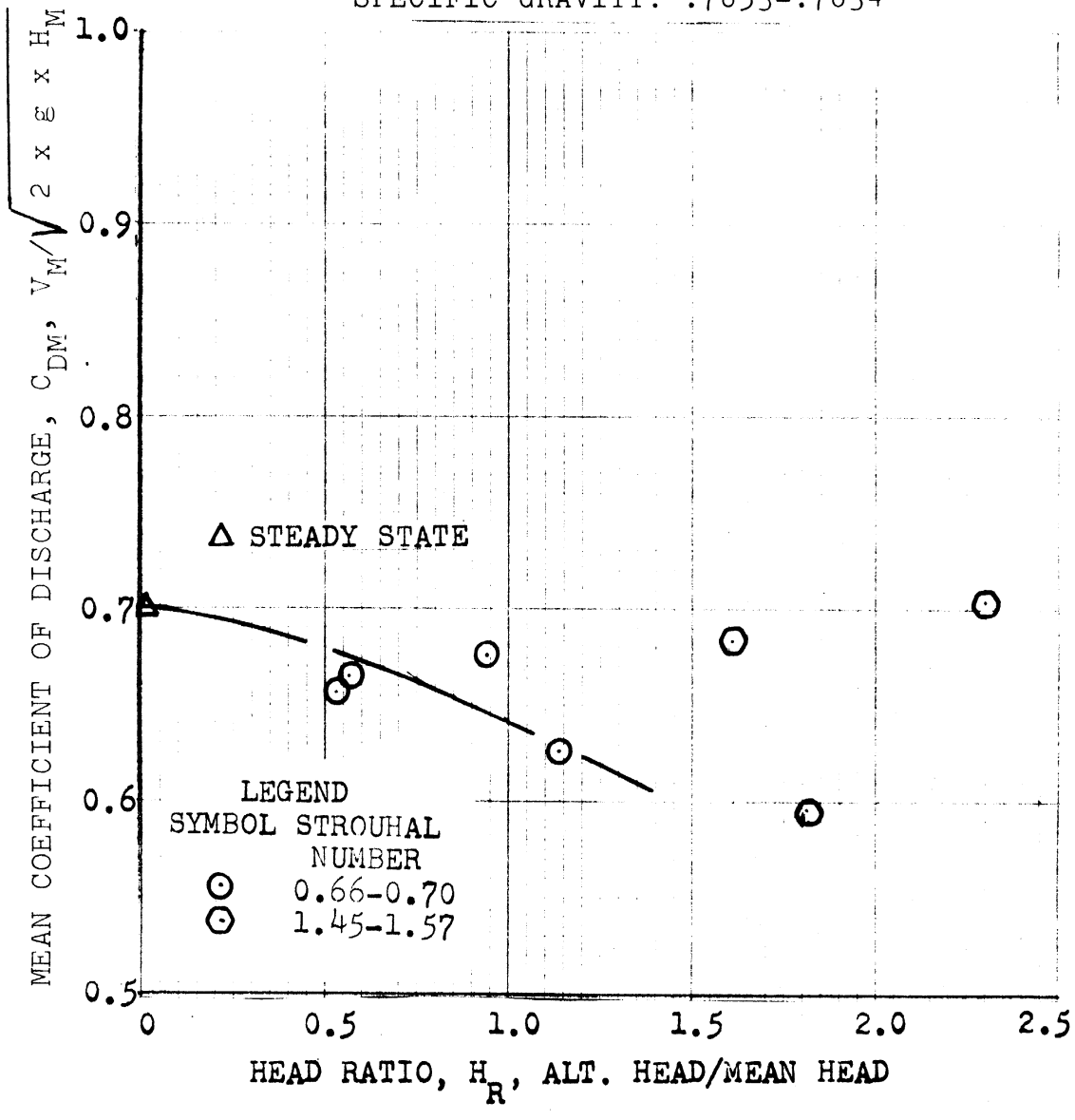

Figure 78. Mean Coefficient of Discharge versus Head Ratio for L/D=3.63, RE=1104-1218.

MEAN COEFFICIENT OF DISCHARGE VERSUS HEAD RATIO

REYNOLDS NUMBER=2349-2638

TEST NUMBER 78701
ORIFICE: SQUARE EDGED
DIAMETER: 0.0518 in.
LENGTH: 0.1880 in.
L/D: 3.6293
FLUID: MINERAL SPIRITS
TEMPERATURE: 75.1-78.9°F
VISCOSITY: 1.307-1.269 cp
SPECIFIC GRAVITY: .7853-.7834

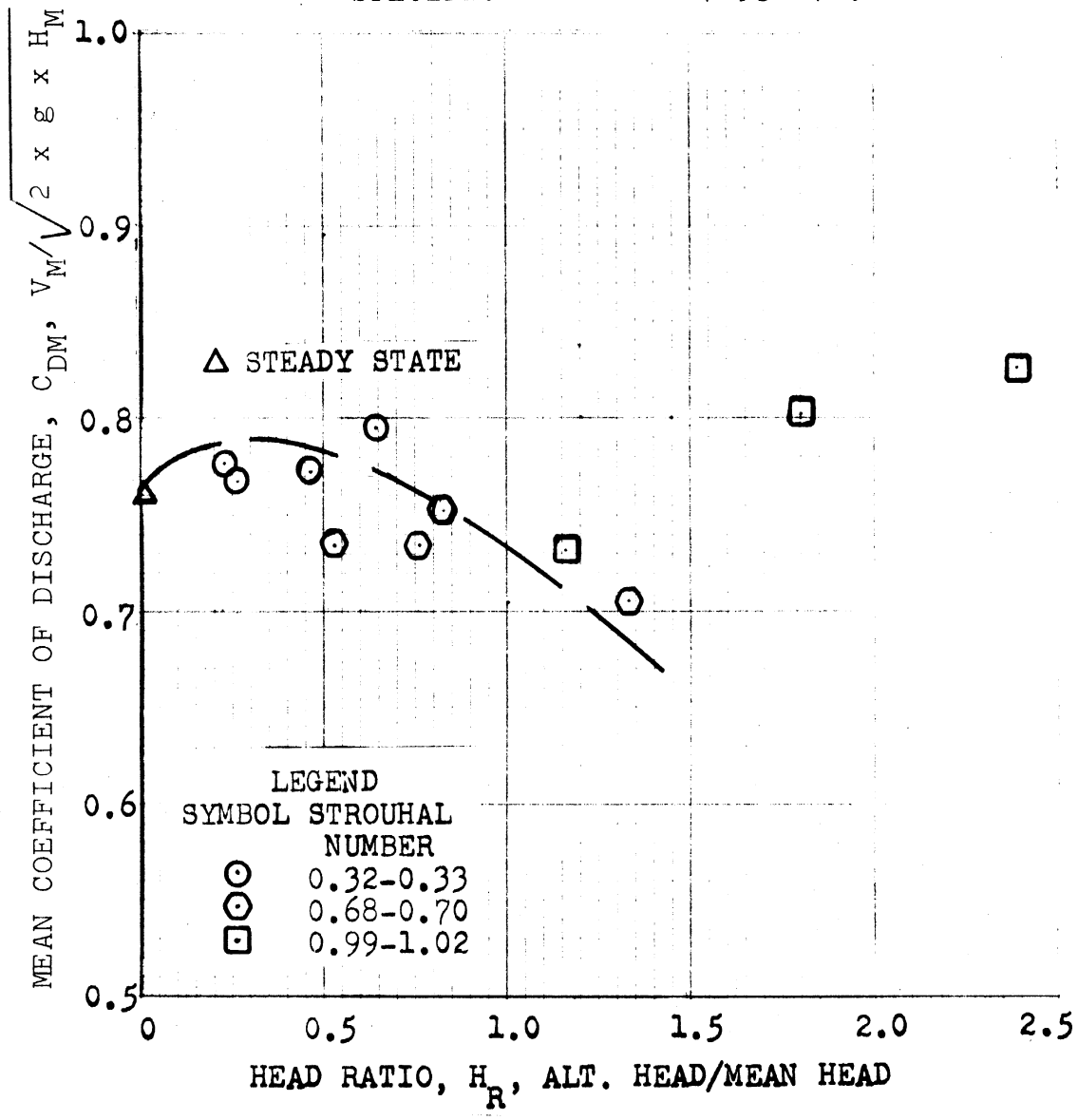

Figure 79. Mean Coefficient of Discharge versus Head Ratio for L/D=3.63, RE=2349-2638.

MEAN COEFFICIENT OF DISCHARGE VERSUS HEAD RATIO

REYNOLDS NUMBER=3422-3751

TEST NUMBER 78701
ORIFICE: SQUARE EDGED
DIAMETER: 0.0518 in.
LENGTH: 0.1880
L/D: 3.6293
FLUID: MINERAL SPIRITS
TEMPERATURE: 75.1-78.9°F
VISCOSITY: 1.307-1.269 cp
SPECIFIC GRAVITY: .7853-.7834

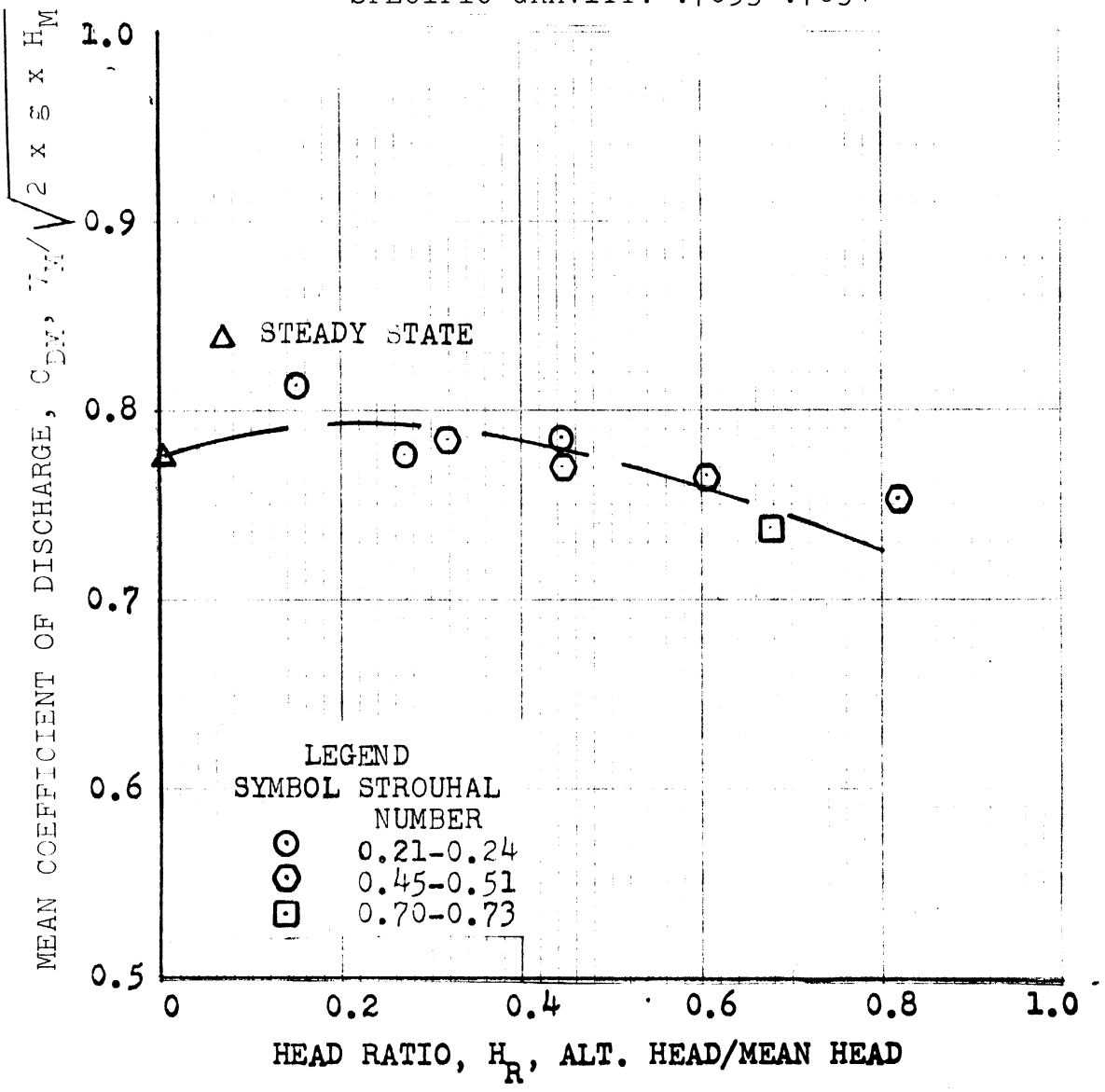

Figure 80. Mean Coefficient of Discharge versus Head Ratio for L/D=3.63, RE=3422-3751.

MEAN COEFFICIENT OF DISCHARGE VERSUS HEAD RATIO

REYNOLDS NUMBER=4521-4751

TEST NUMBER 78701
ORIFICE: SQUARE EDGED
DIAMETER: 0.0518 in.
LENGTH: 0.1880 in.
L/D: 3.6293
FLUID: MINERAL SPIRITS
TEMPERATURE: 75.1-78.9°F
VISCOSITY: 1.307-1.269 cp
SPECIFIC GRAVITY: .7853-.7834

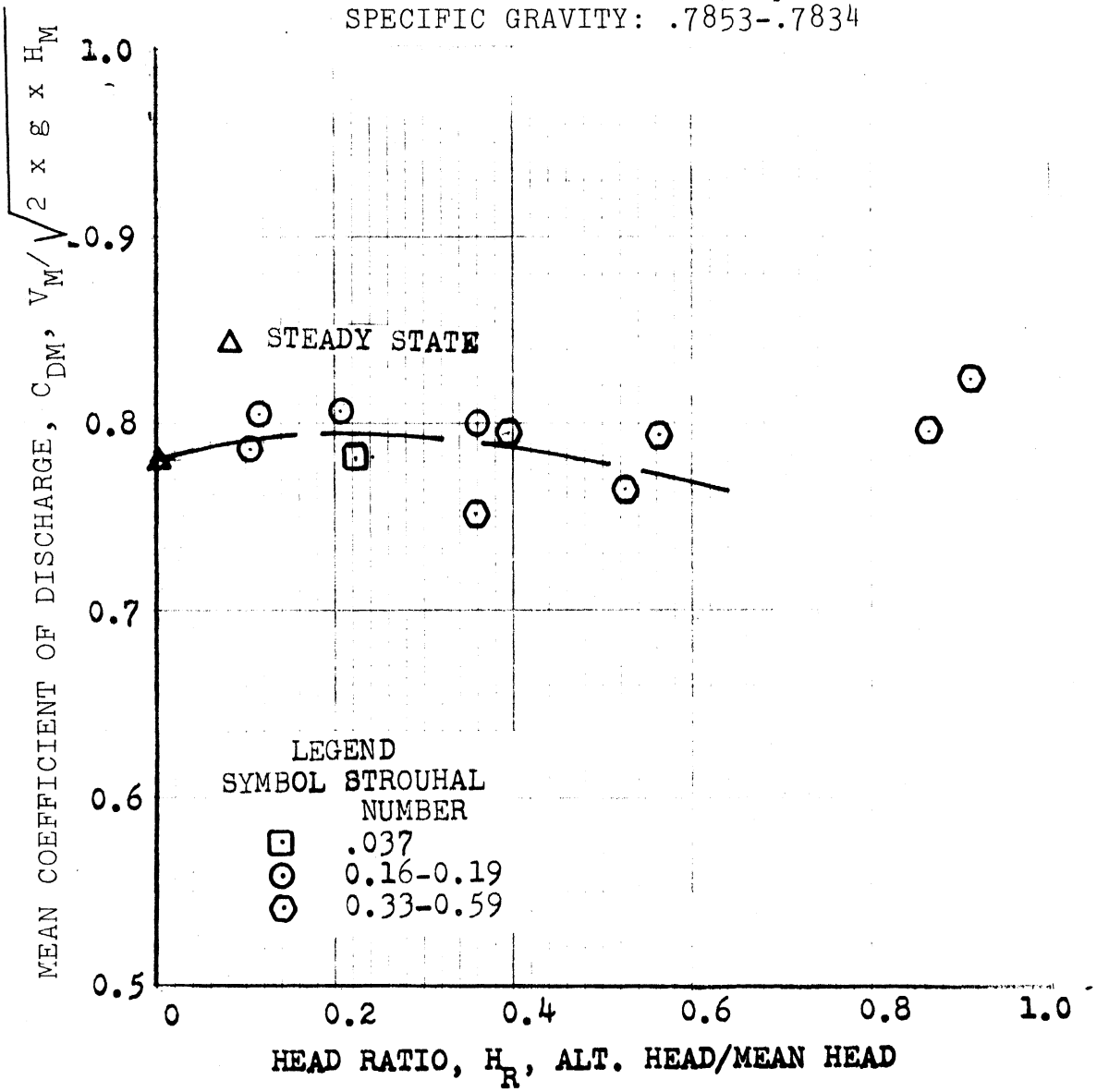

Figure 81. Mean Coefficient of Discharge versus Head Ratio for L/D=3.63, RE=4521-4751.

MEAN COEFFICIENT OF DISCHARGE
VERSUS
HEAD RATIO

REYNOLDS NUMBER= 1099-1198
STROUHAL NUMBER=0.112-0.238
TEST NUMBER 78702
ORIFICE: SQUARE EDGED
DIAMETER: 0.0518 inch
LENGTH: 0.0319 inch
L/D: 0.6158
FLUID: MINERAL SPIRITS
TEMPERATURE: 75.2-75.7°F
SPECIFIC GRAVITY: .7852-.7850
VISCOSITY: 1.306-1.301 cp

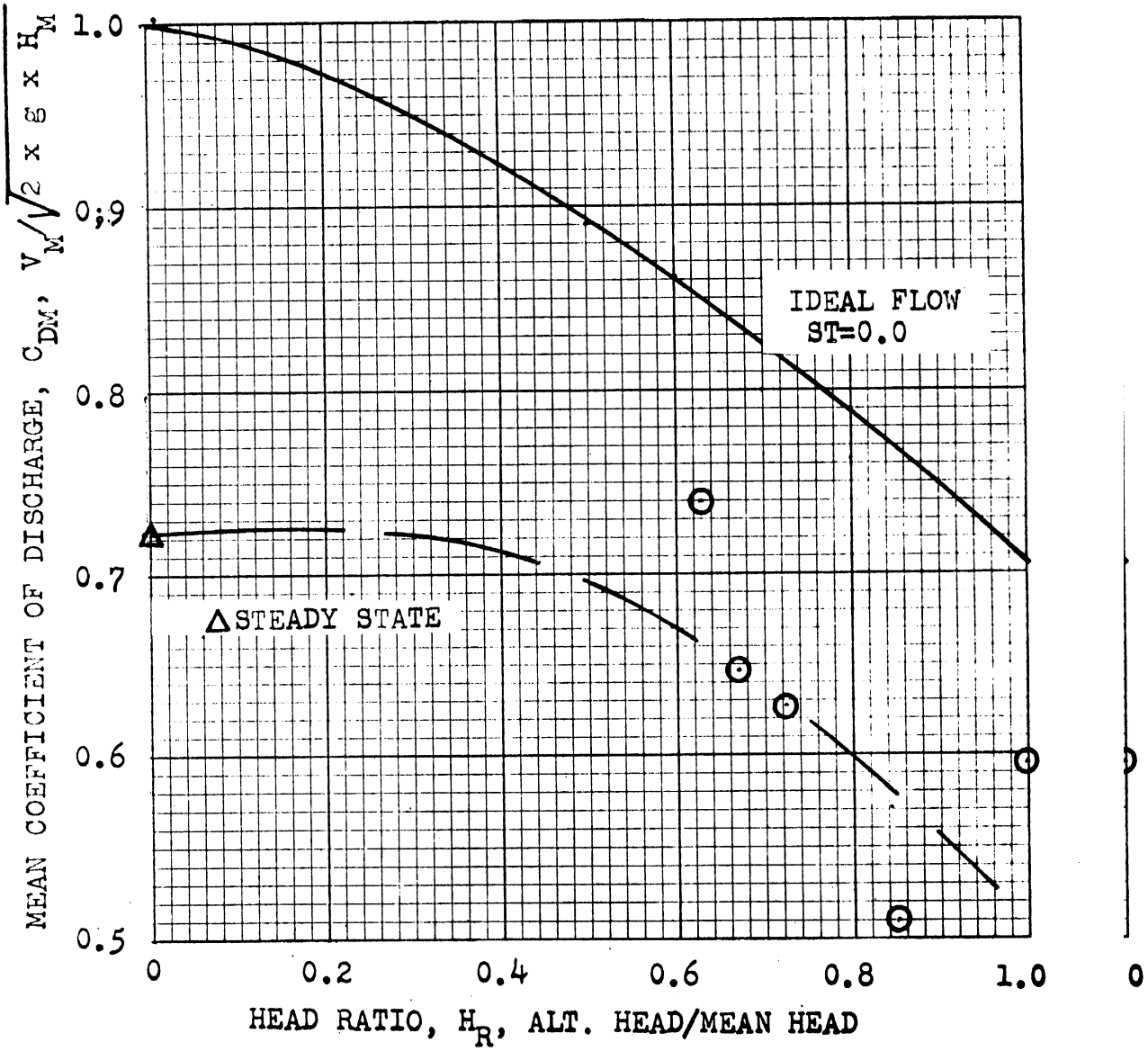

Figure 82. Mean Coefficient of Discharge versus Head Ratio for L/D=0.62, RE=1099-1198.

MEAN COEFFICIENT OF DISCHARGE
VERSUS
HEAD RATIO

REYNOLDS NUMBER=2369-2612
STROUHAL NUMBER=0.0514-0.1834
TEST NUMBER 78702
ORIFICE: SQUARE EDGED
DIAMETER: 0.0518 inch
LENGTH: 0.0319 inch
L/D: 0.6158
FLUID: MINERAL SPIRITS
TEMPERATURE: 75.2-75.7°F
SPECIFIC GRAVITY: .7852-.7850
VISCOSITY: 1.306-1.301 cp

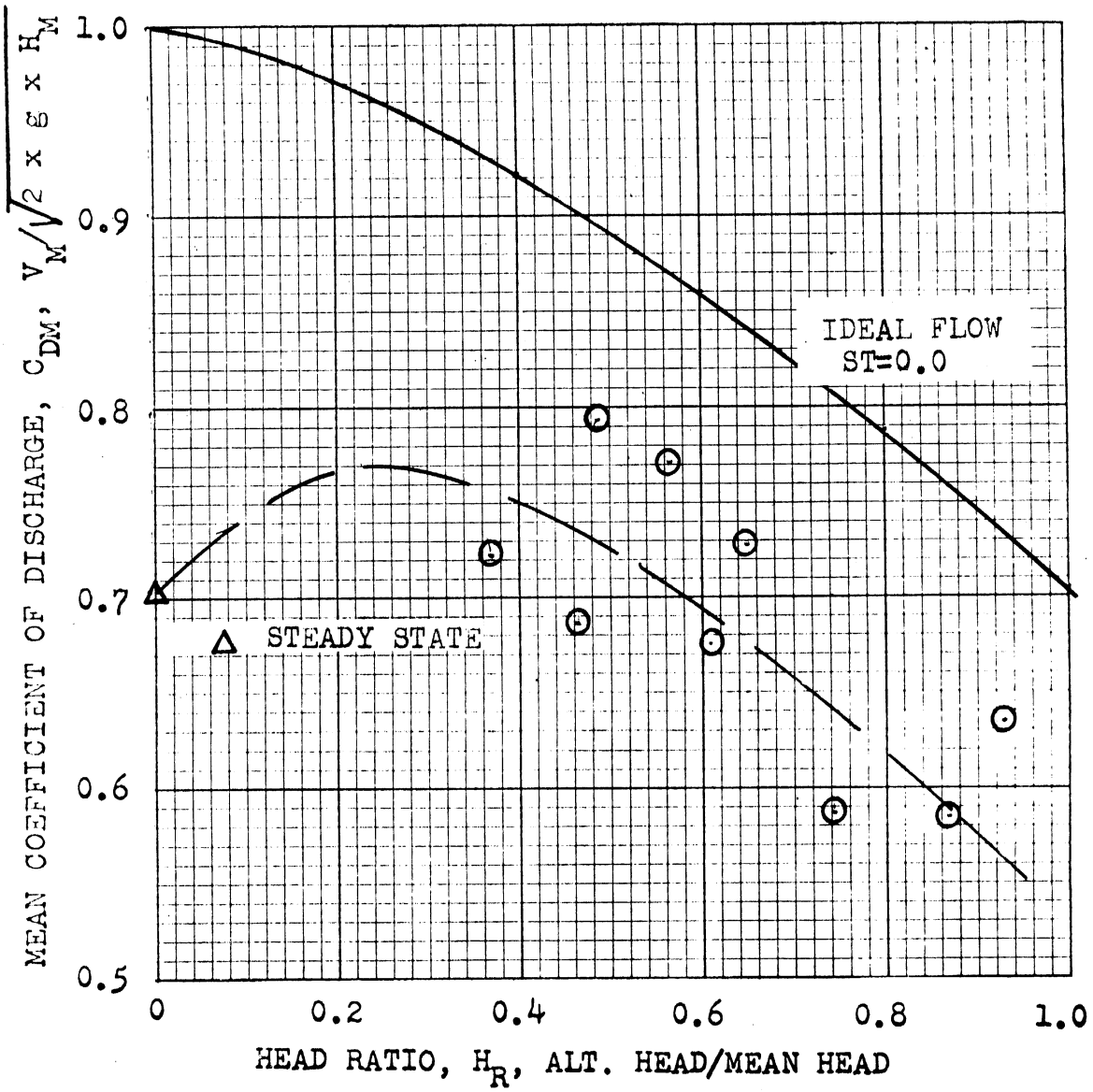

Figure 83. Mean Coefficient of Discharge versus Head Ratio for L/D=0.62, RE=2369-2612.

MEAN COEFFICIENT OF DISCHARGE
VERSUS
HEAD RATIO

REYNOLDS NUMBER= 3387-3713
STROUHAL NUMBER=0.0337-0.1313
TEST NUMBER 78702
ORIFICE: SQUARE EDGED
DIAMETER: 0.0518 inch
LENGTH: 0.0319 inch
L/D: 0.6158
FLUID: MINERAL SPIRITS
TEMPERATURE: 75.2-75.7°F
SPECIFIC GRAVITY: .7852-.7850
VISCOSITY: 1.306-1.301 cp

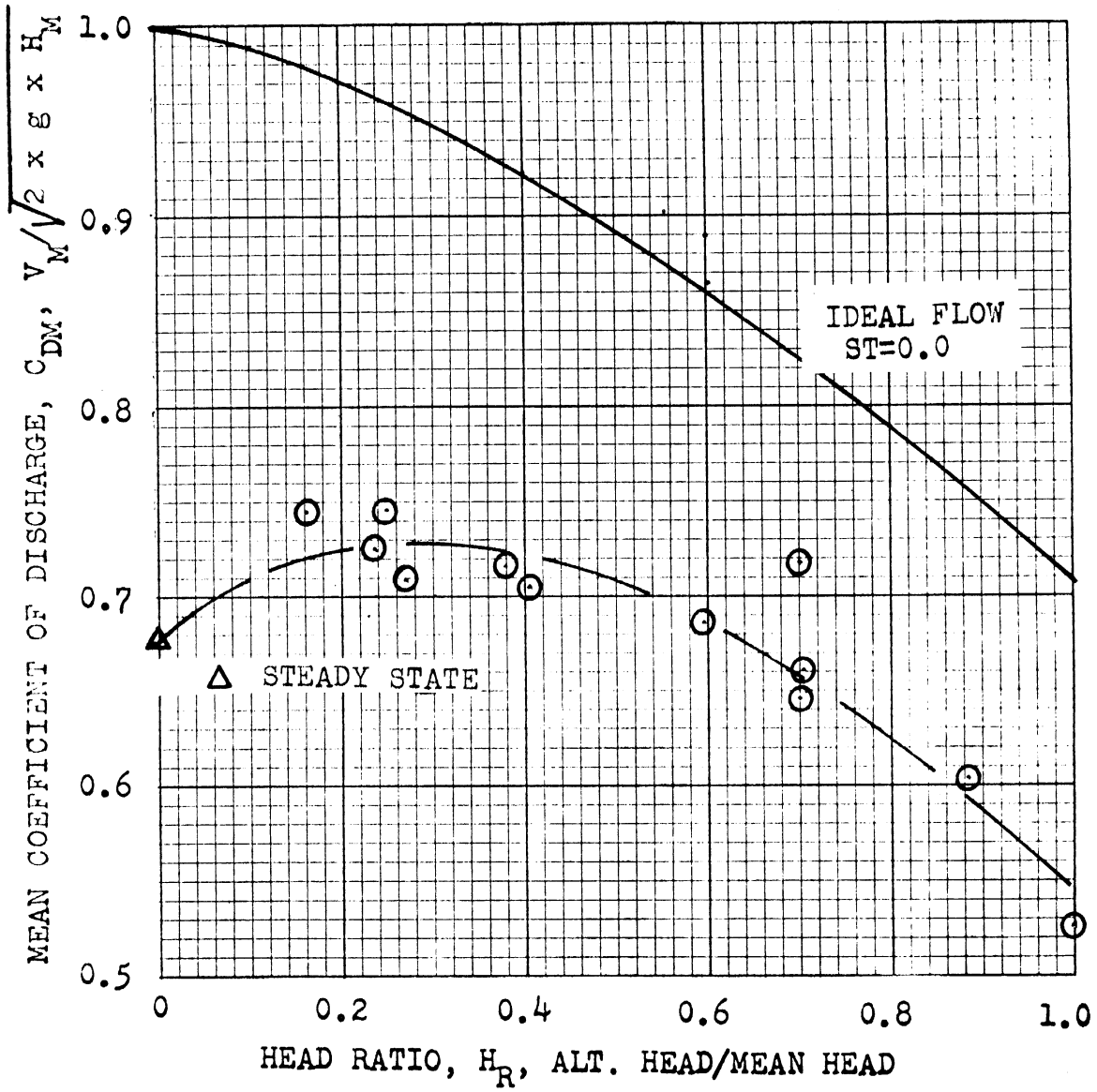

Figure 84. Mean Coefficient of Discharge versus Head Ratio for L/D=0.62, RN=3387-3713.

MEAN COEFFICIENT OF DISCHARGE VERSUS HEAD RATIO

REYNOLDS NUMBER= 4470-4721
STROUHAL NUMBER= 0.0283-0.1044
TEST NUMBER 78702
ORIFICE: SQUARE EDGED
DIAMETER: 0.0518 in.
LENGTH: 0.0319 in.
L/D: 0.6158
FLUID: MINERAL SPIRITS
TEMPERATURE: 75.2-75.7°F
SPECIFIC GRAVITY: .7852-.7850
VISCOSITY: 1.306-1.301 cp

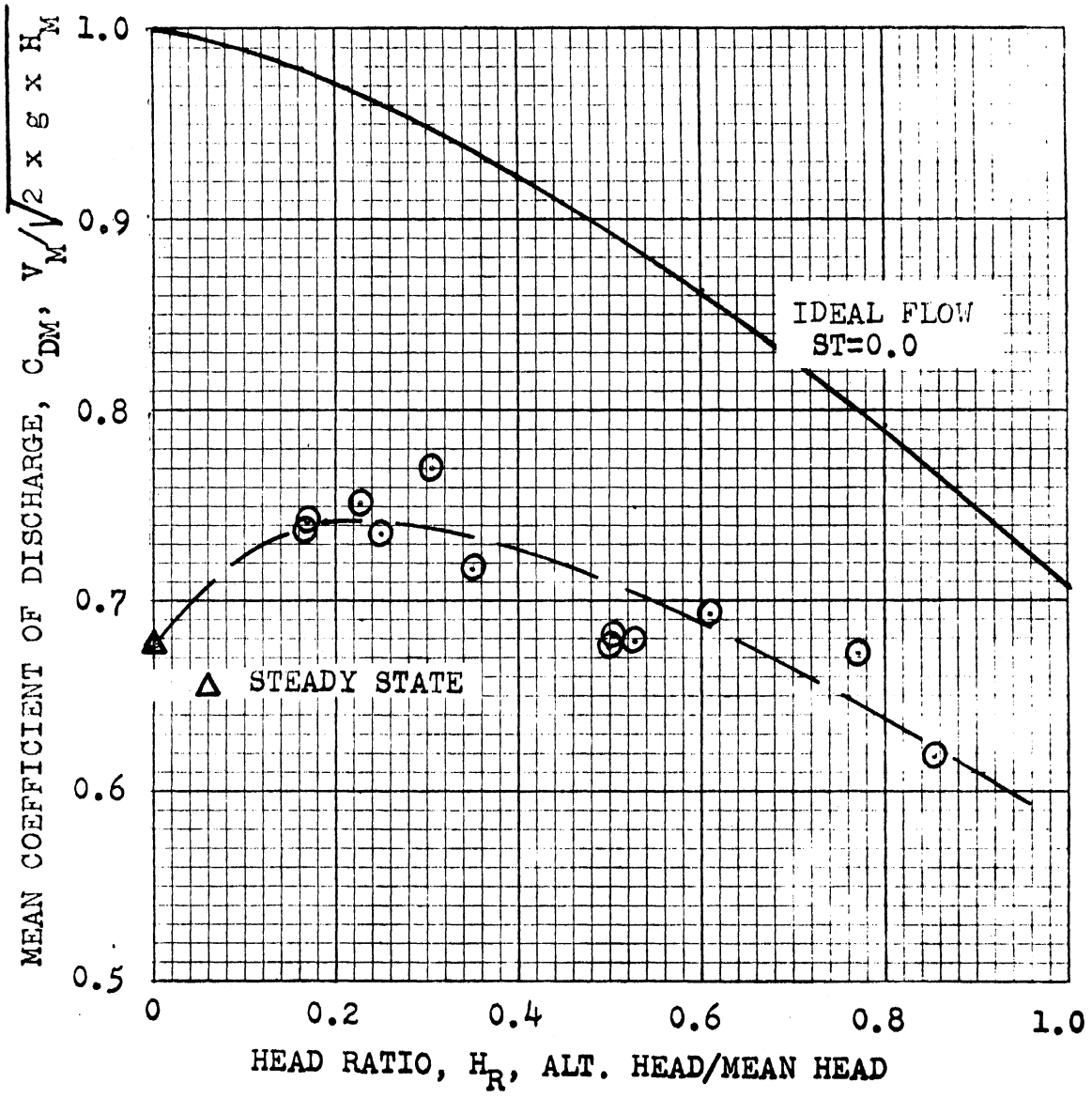

Figure 85. Mean Coefficient of Discharge versus Head Ratio for L/D=0.62, RE=4470-4721.

MEAN COEFFICIENT OF DISCHARGE
VERSUS
HEAD RATIO

REYNOLDS NUMBER=1800-2200

ORIFICE: F-50
DIAM: .0497 in.
LENGTH: .1837 in.
FLUID: Mineral Spirits
TEMP: 77.8-84.2 °F
SG: .7839-.7809
VISC: 1.280-1.219 cp

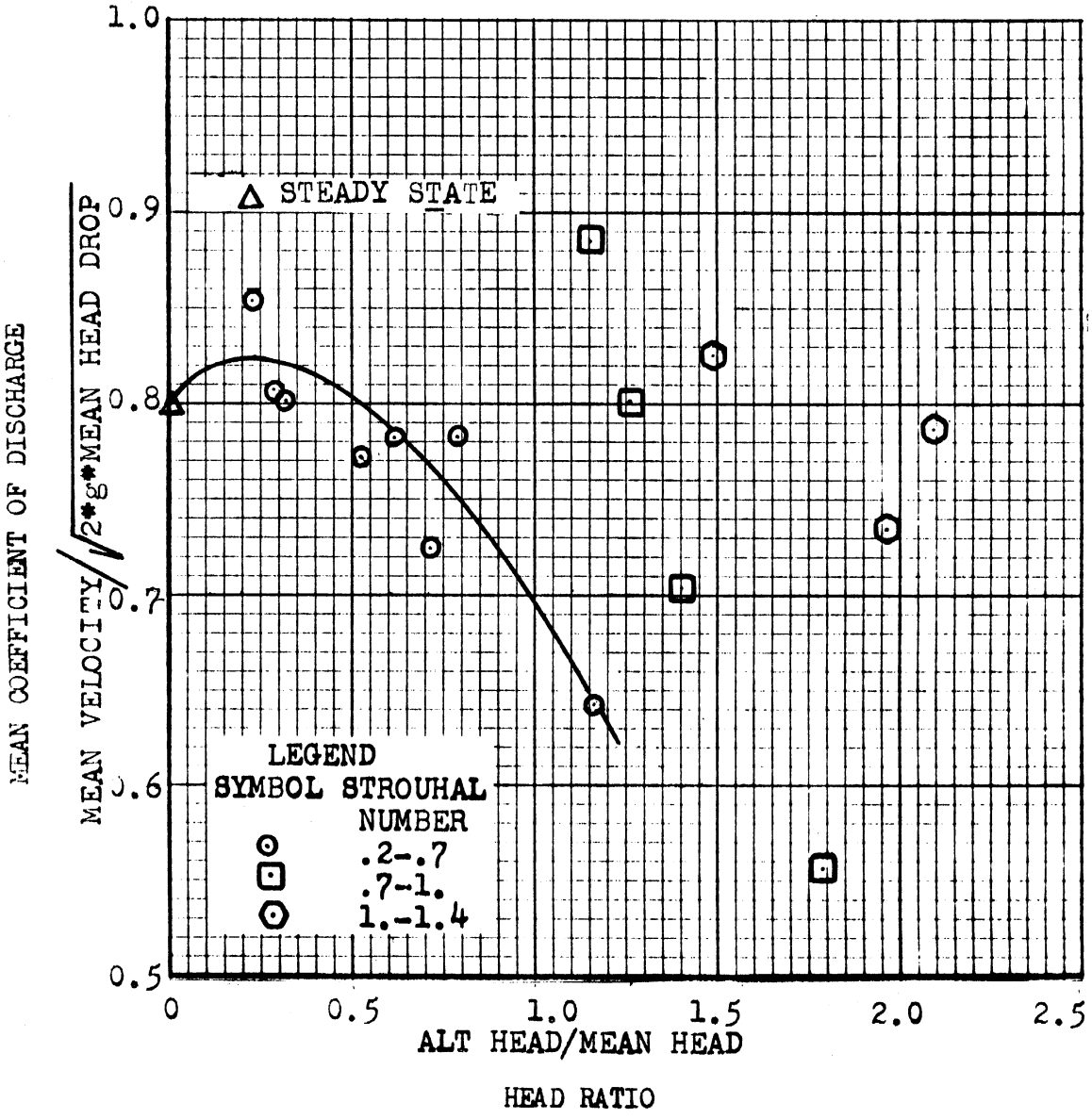

Figure 86. Mean Coefficient of Discharge versus Head Ratio for F-50 Orifice, RE=1800-2200.

MEAN COEFFICIENT OF DISCHARGE
VERSUS
HEAD RATIO
TEST 2470

REYNOLDS NUMBER=2800-3200

ORIFICE: F-50
DIAM: .0497 in.
LENGTH: .1837 in.
FLUID: Mineral Spirits
TEMP: 77.8-84.2 °F
SG: .7839-.7809
VISC: 1.280-1.219 cp

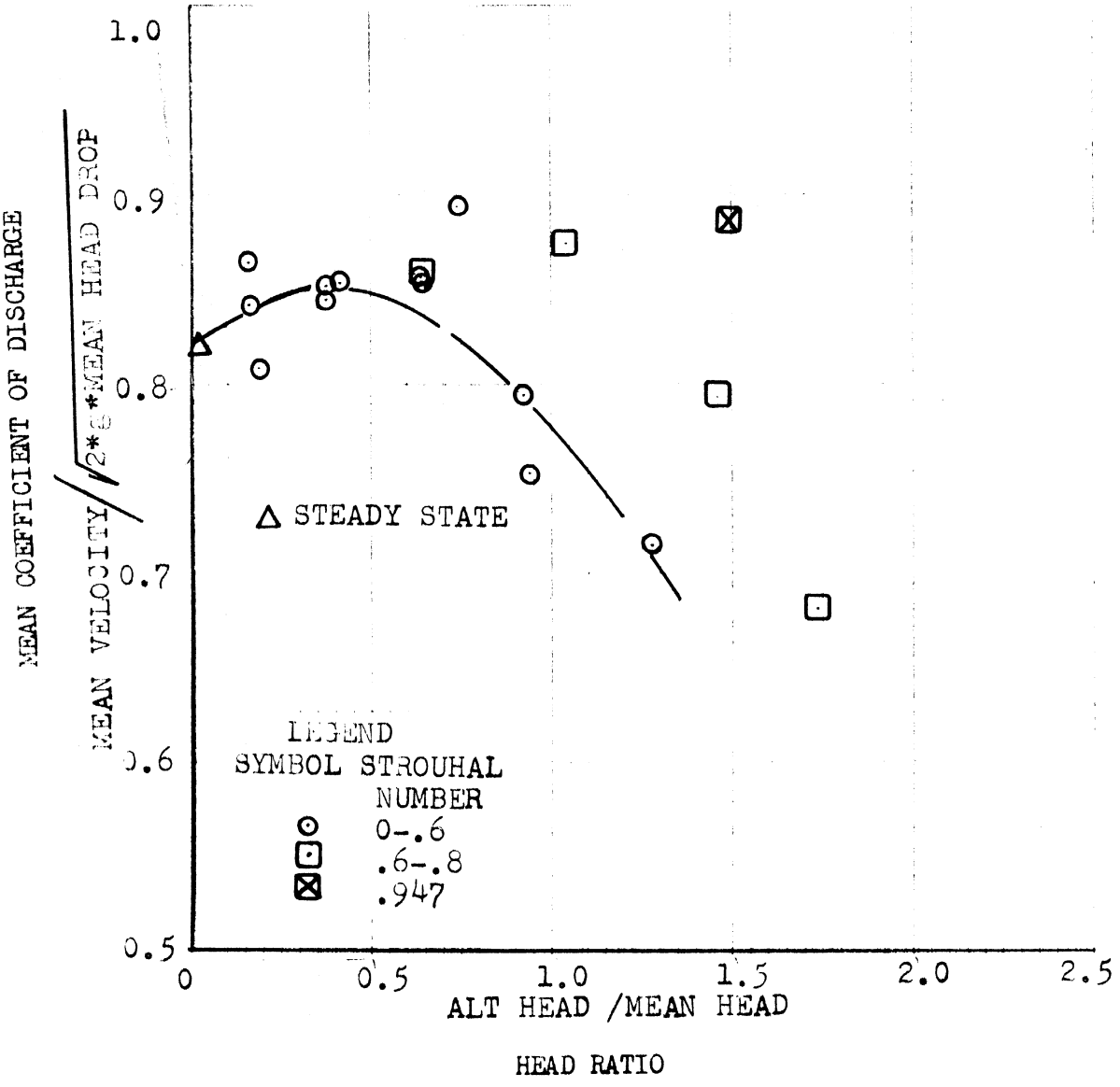

Figure 87. Mean Coefficient of Discharge versus Head Ratio for F-50 Orifice, RE=2800-3200.

MEAN COEFFICIENT OF DISCHARGE
VERSUS
HEAD RATIO
TEST 2470

REYNOLDS NUMBER=3800-4200

ORIFICE: F-50
DIAM: .0497 in.
LENGTH: .1837 in.
FLUID: Mineral Spirits
TEMP: 77.8-84.2 °F
SG: .7839-.7809
VISC: 1.280-1.219 cp

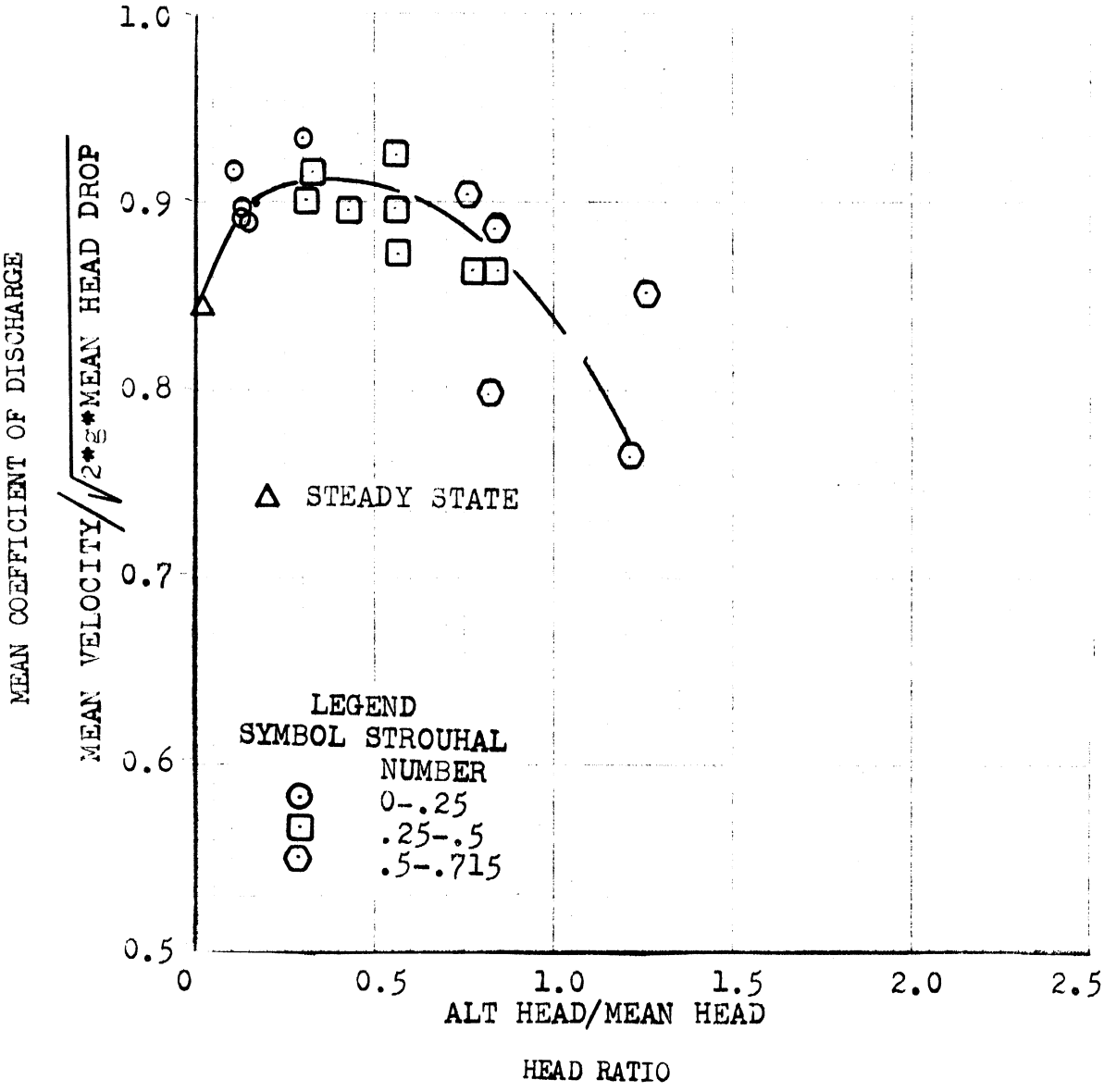

Figure 88. Mean Coefficient of Discharge versus Head Ratio for F-50 Orifice, RE=3800-4200.

MEAN COEFFICIENT OF DISCHARGE
VERSUS
HEAD RATIO
TEST 2470

REYNOLDS NUMBER=4800-5200
STROUHAL NUMBER= 0-0.6

ORIFICE: F-50
DIAM: .0497 in.
LENGTH: .1837 in.
FLUID: Mineral Spirits
TEMP: 77.8-84.2 °F
SG: .7839-.7809
VISC: 1.219-1.280 cp

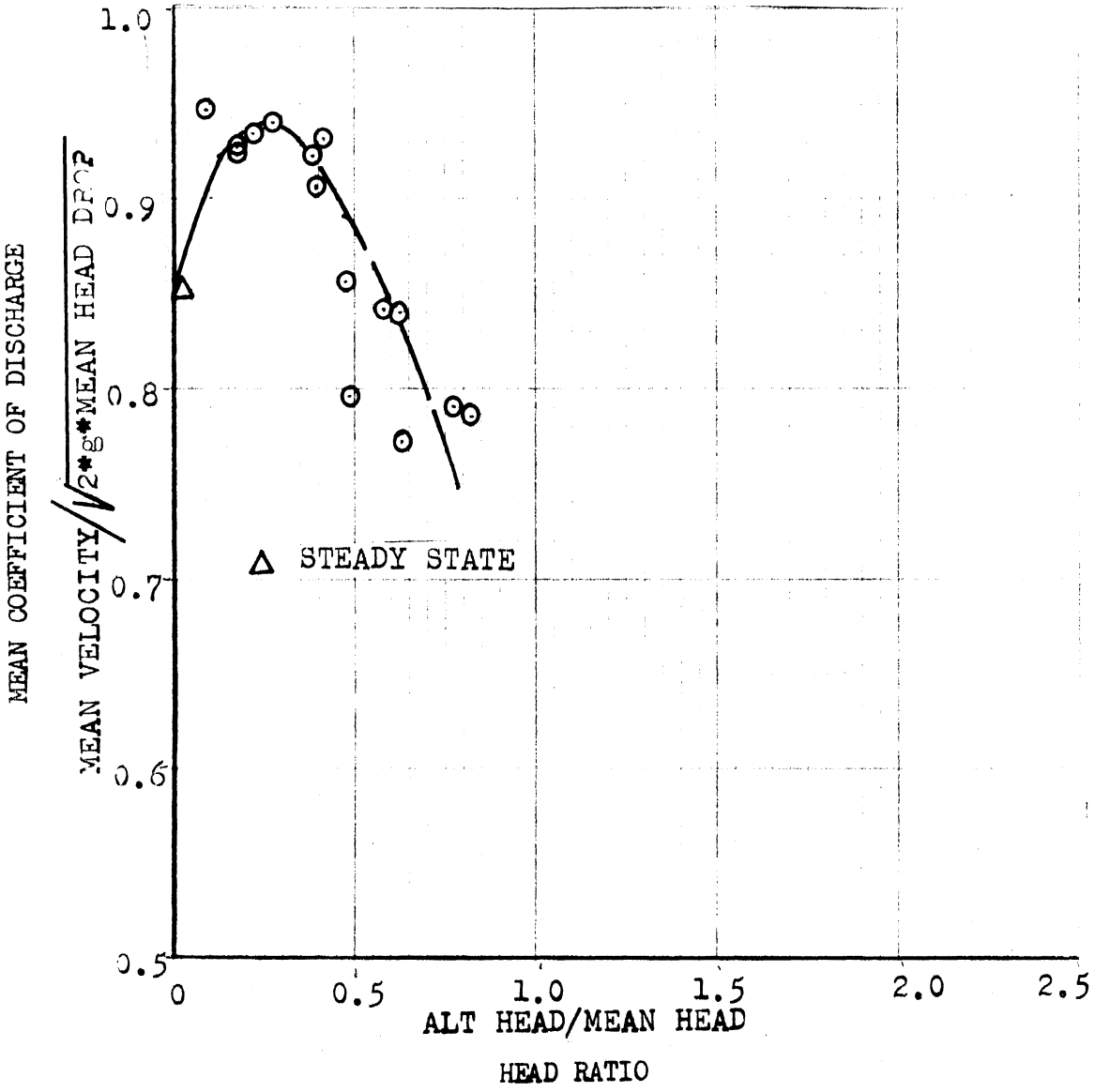

Figure 89. Mean Coefficient of Discharge versus Head Ratio for F-50 Orifice, RE=4800-5200.

Alternating Coefficient of Discharge

Figures 89 through 104 show the alternating coefficient of discharge versus the velocity ratio and Figures 105 through 120 show C_{DA} vs H_R. Each curve is for a constant alternating Strouhal Number, and no account is made for the Reynolds Number. That is, the actual alternating coefficient data is plotted in terms of the same independent variables as the ideal alternating coefficient data. Most of the actual coefficients are lower than the ideal coefficients, as shown by the solid curve in the figures. However, at low velocity ratios the actual coefficient is equal to the ideal coefficient.

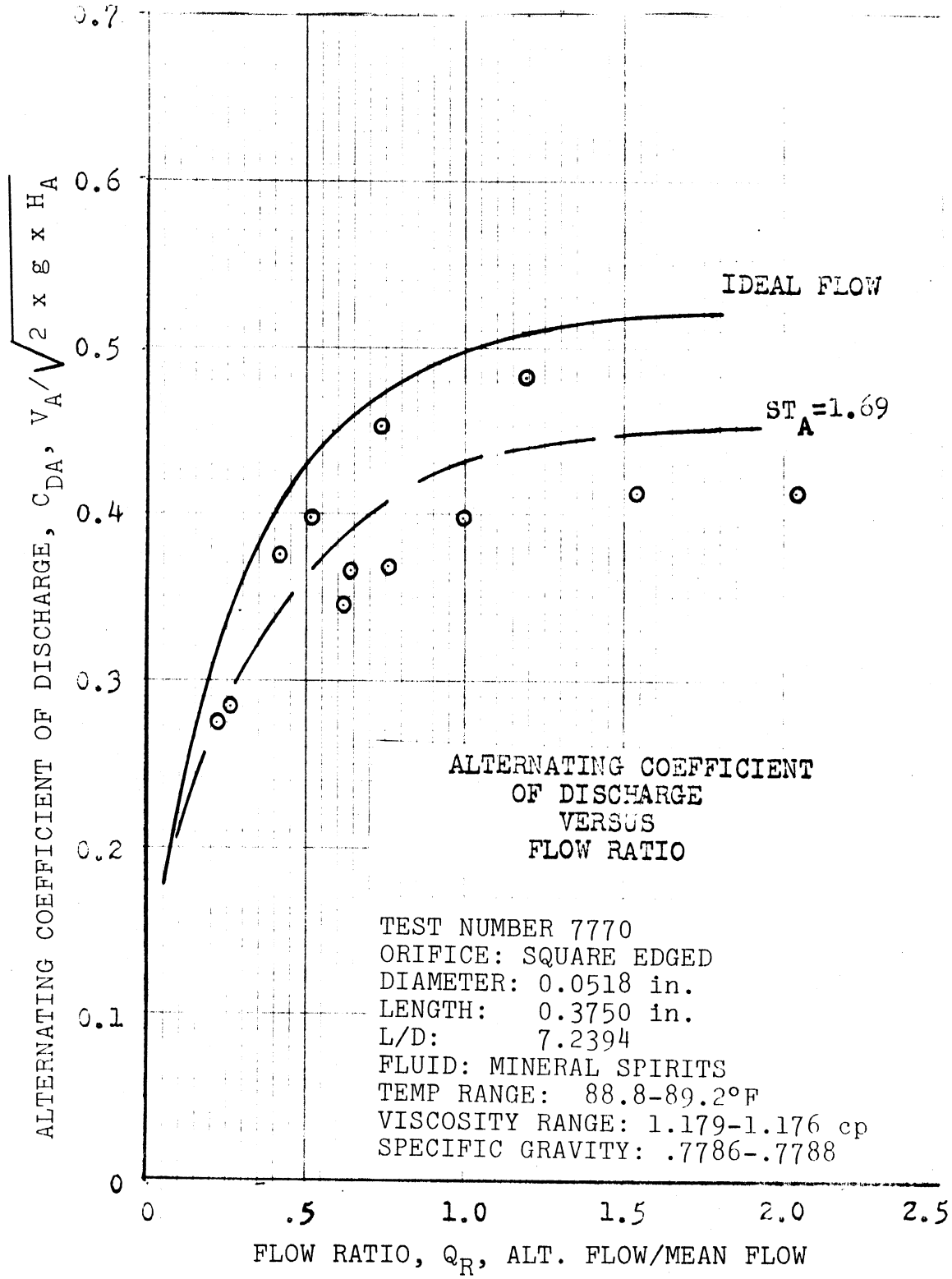

Figure 90. Alternating Coefficient of Discharge versus Flow Ratio for L/D=7.24, ST_A=1.69.

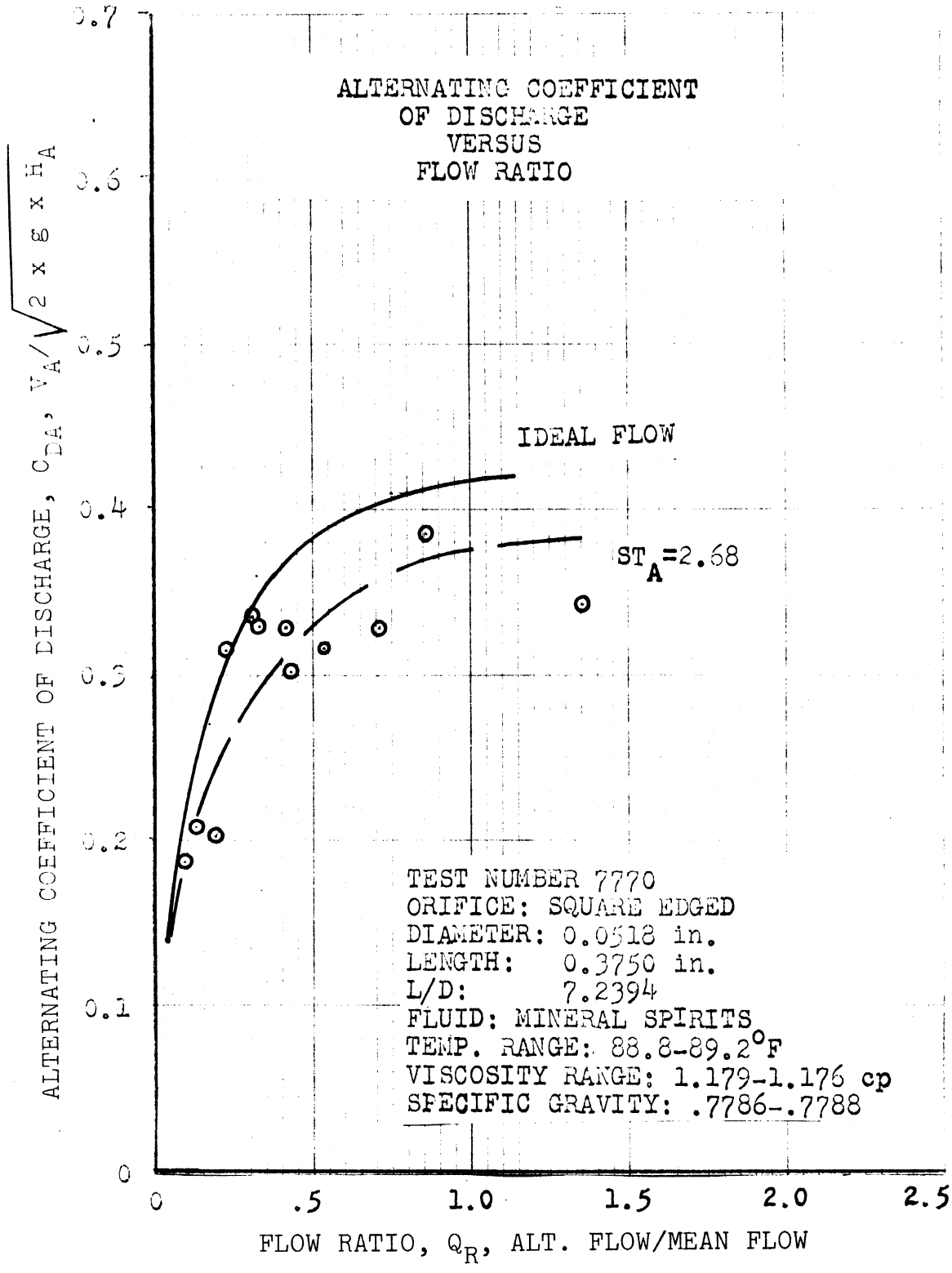

Figure 91. Alternating Coefficient of Discharge versus Flow Ratio for L/D=7.24, ST_A=2.68.

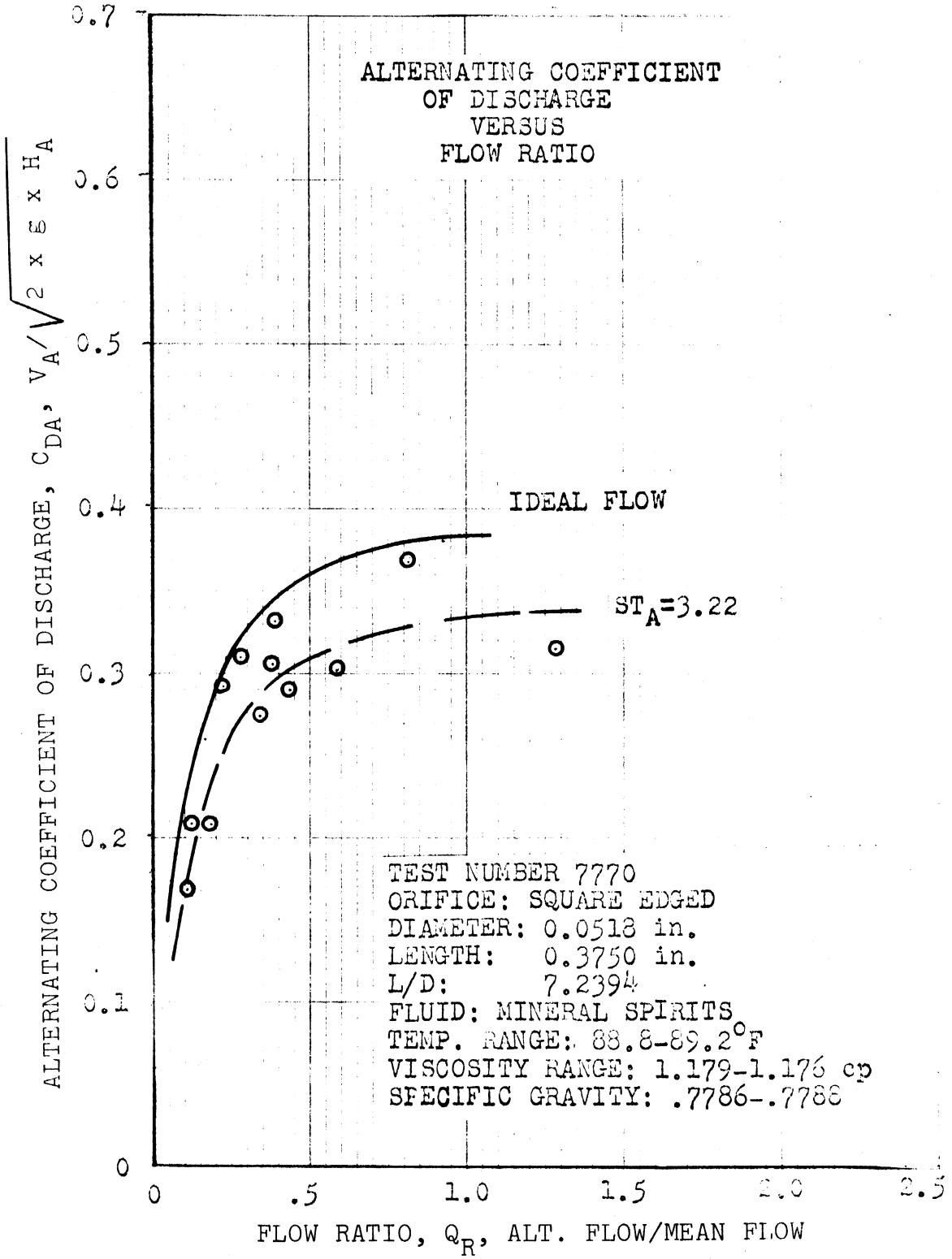

Figure 92. Alternating Coefficient of Discharge versus Flow Ratio for L/D=7.24, ST_A=3.22.

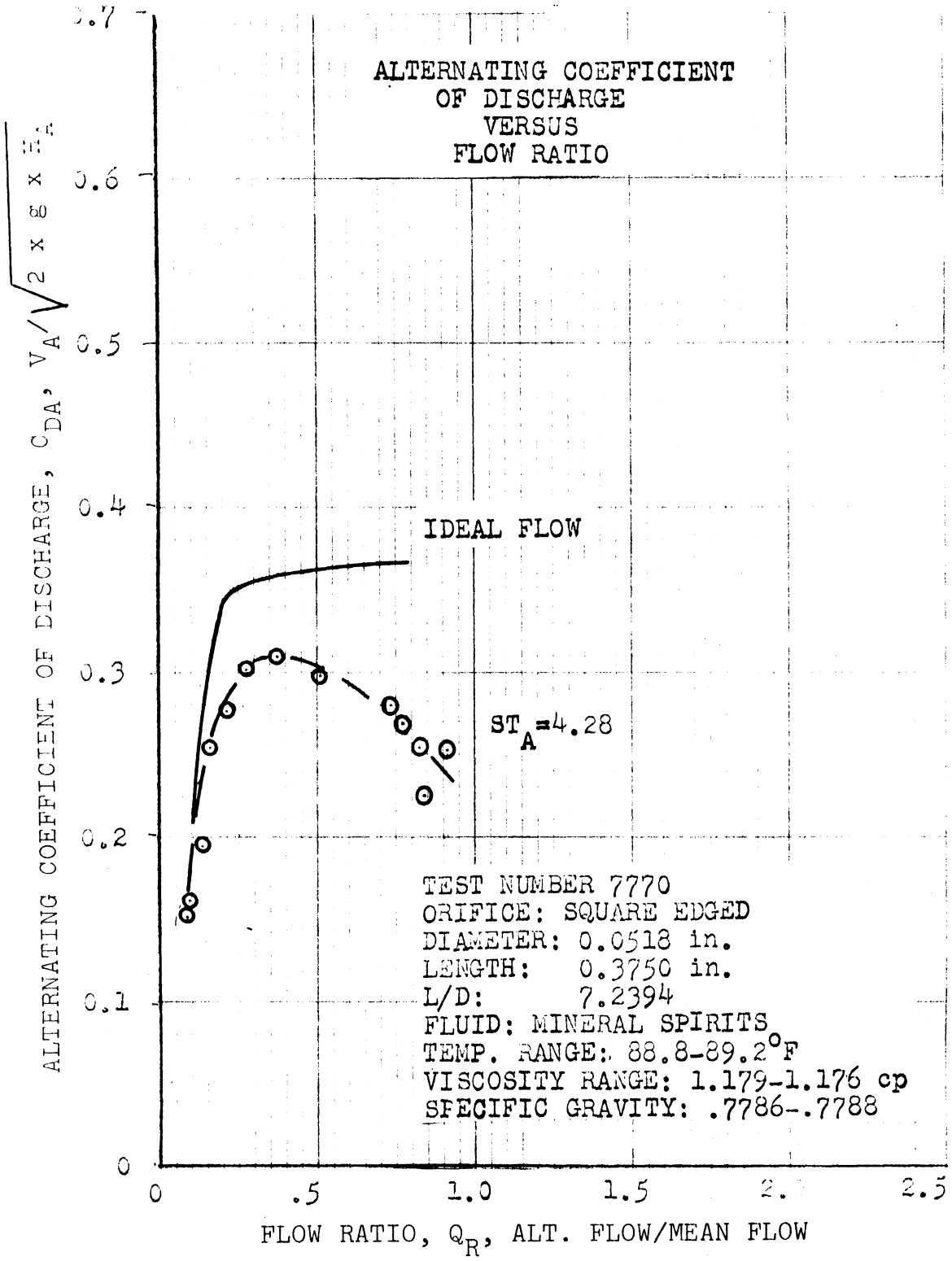

Figure 93. Alternating Coefficient of Discharge versus Flow Ratio for L/D=7.24, ST_A=4.28.

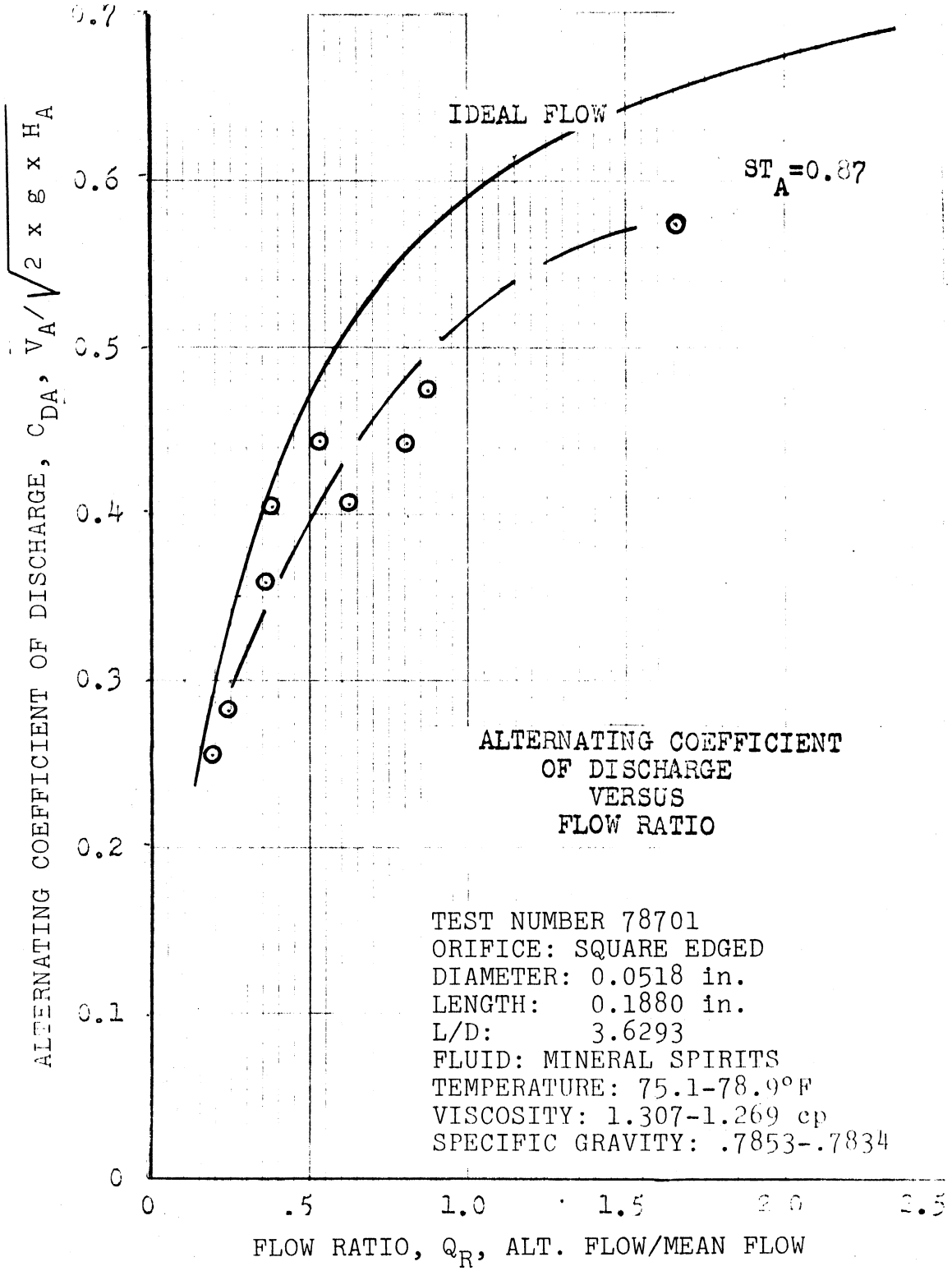

Figure 94. Alternating Coefficient of Discharge versus Flow Ratio for L/D=3.63, ST_A=0.87.

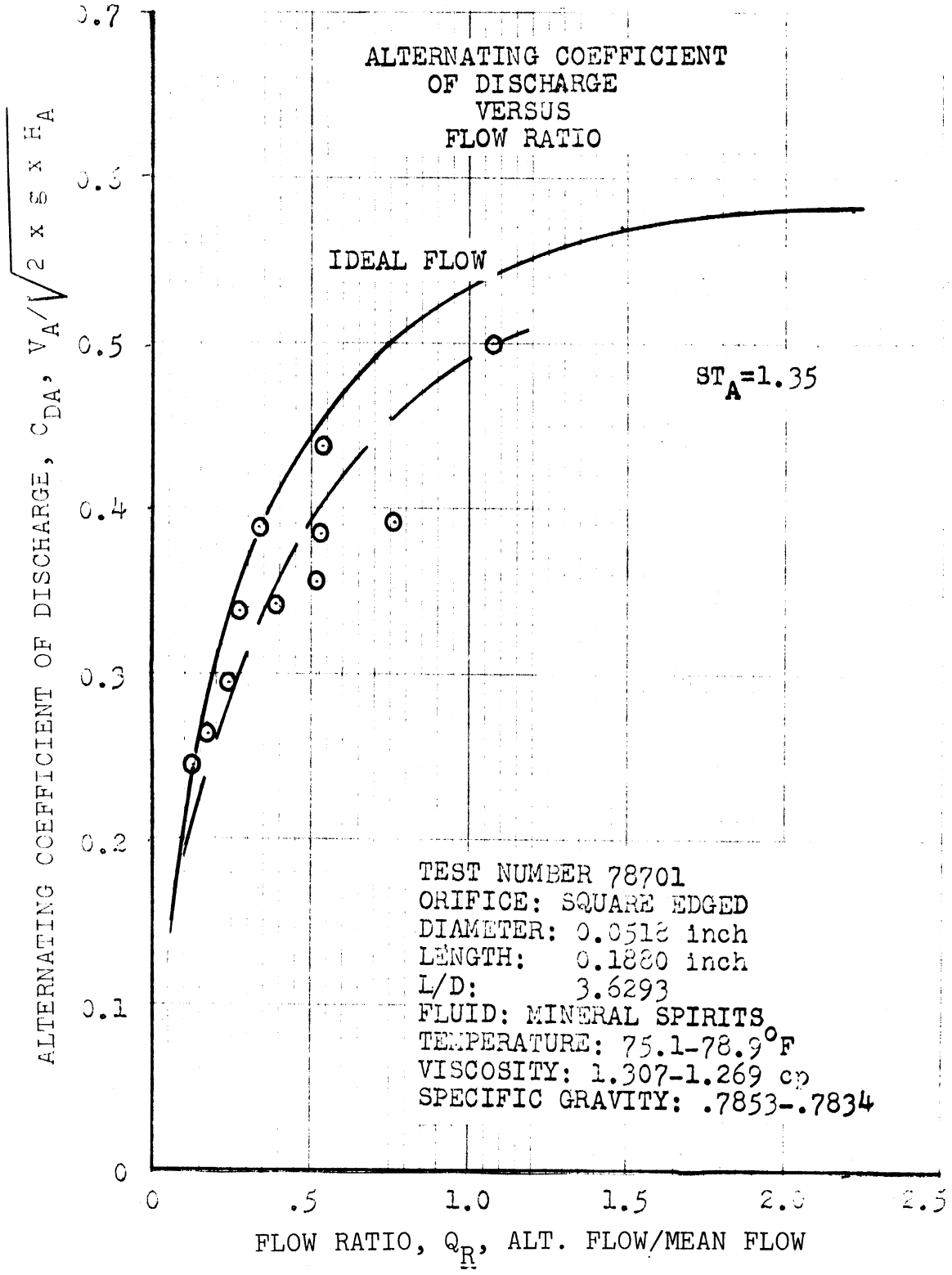

Figure 95. Alternating Coefficient of Discharge versus Flow Ratio for L/D=3.63, ST_A=1.35.

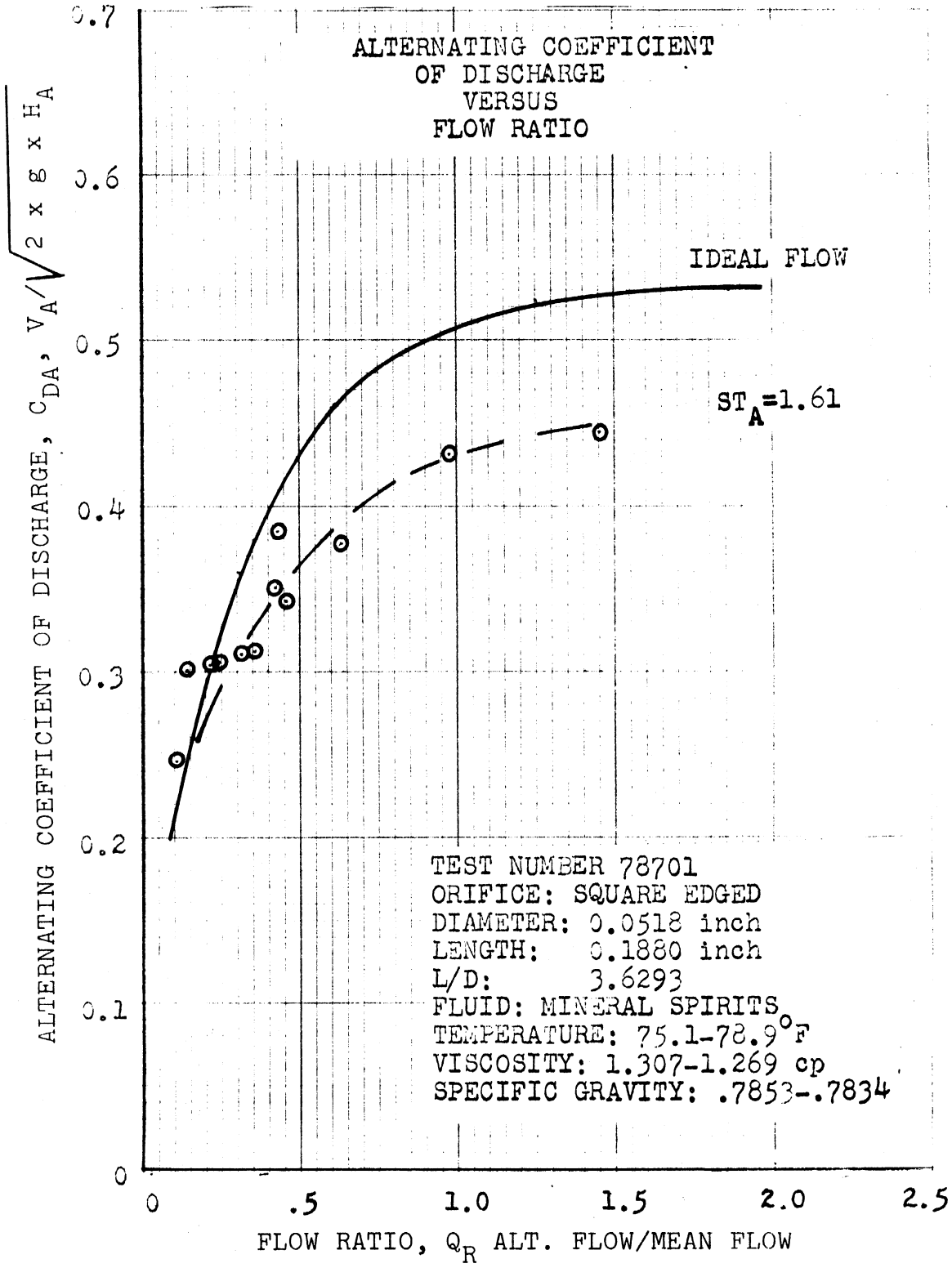

Figure 96. Alternating Coefficient of Discharge versus Flow Ratio for L/D=3.63, ST_A=1.61.

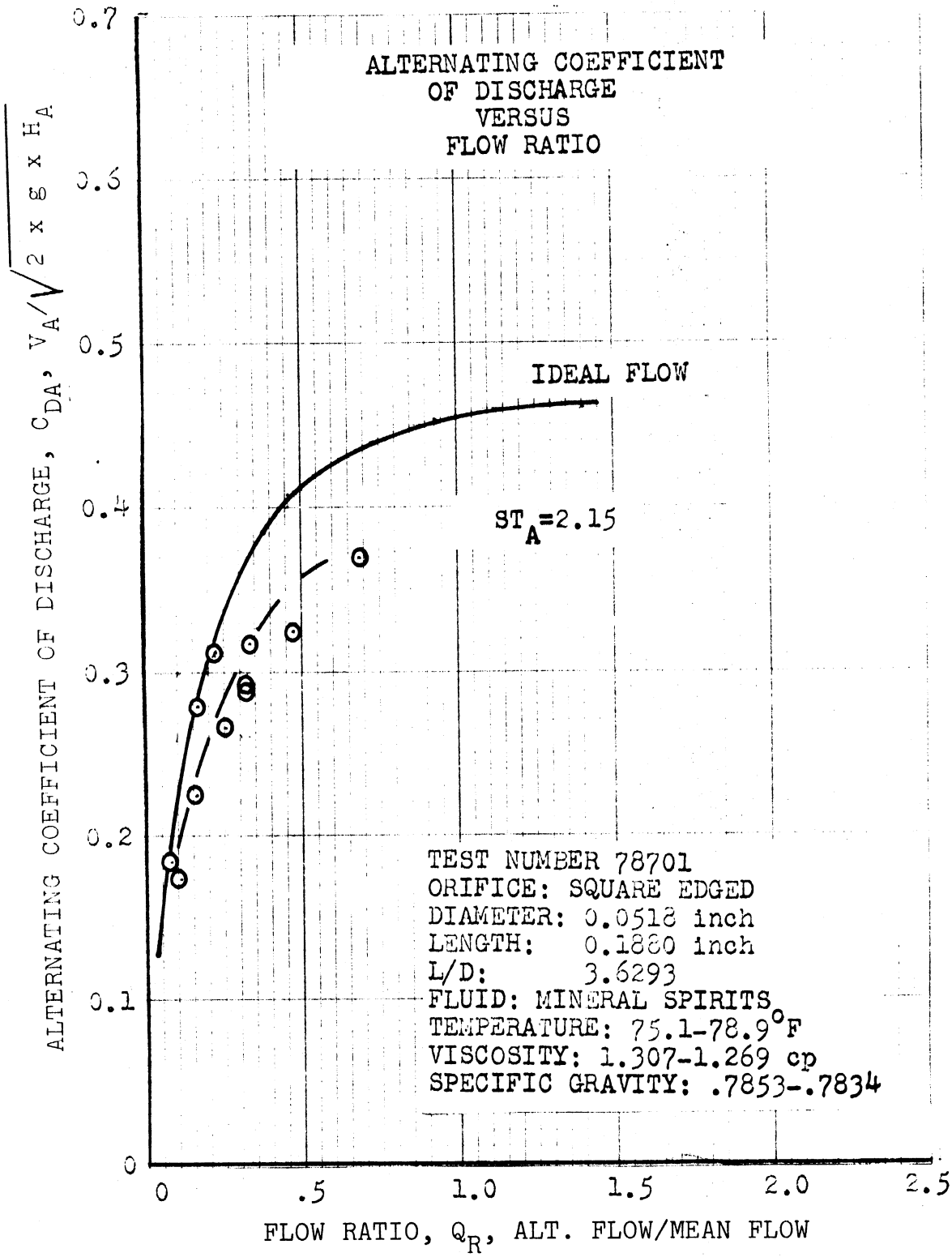

Figure 97. Alternating Coefficient of Discharge versus Flow Ratio for L/D=3.63, ST_A=2.15.

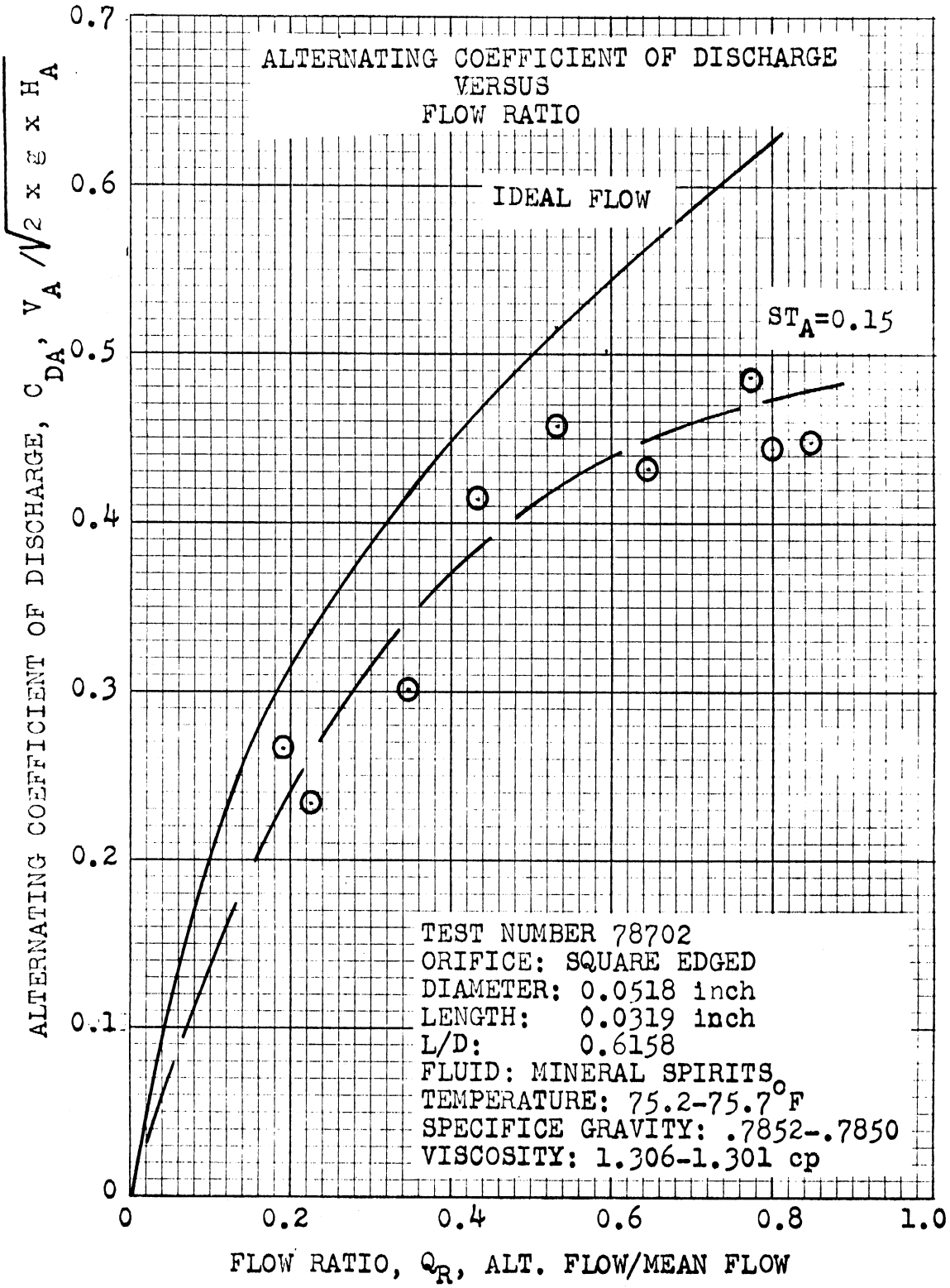

Figure 98. Alternating Coefficient of Discharge versus Flow Ratio for L/D=0.62, ST_A=0.15.

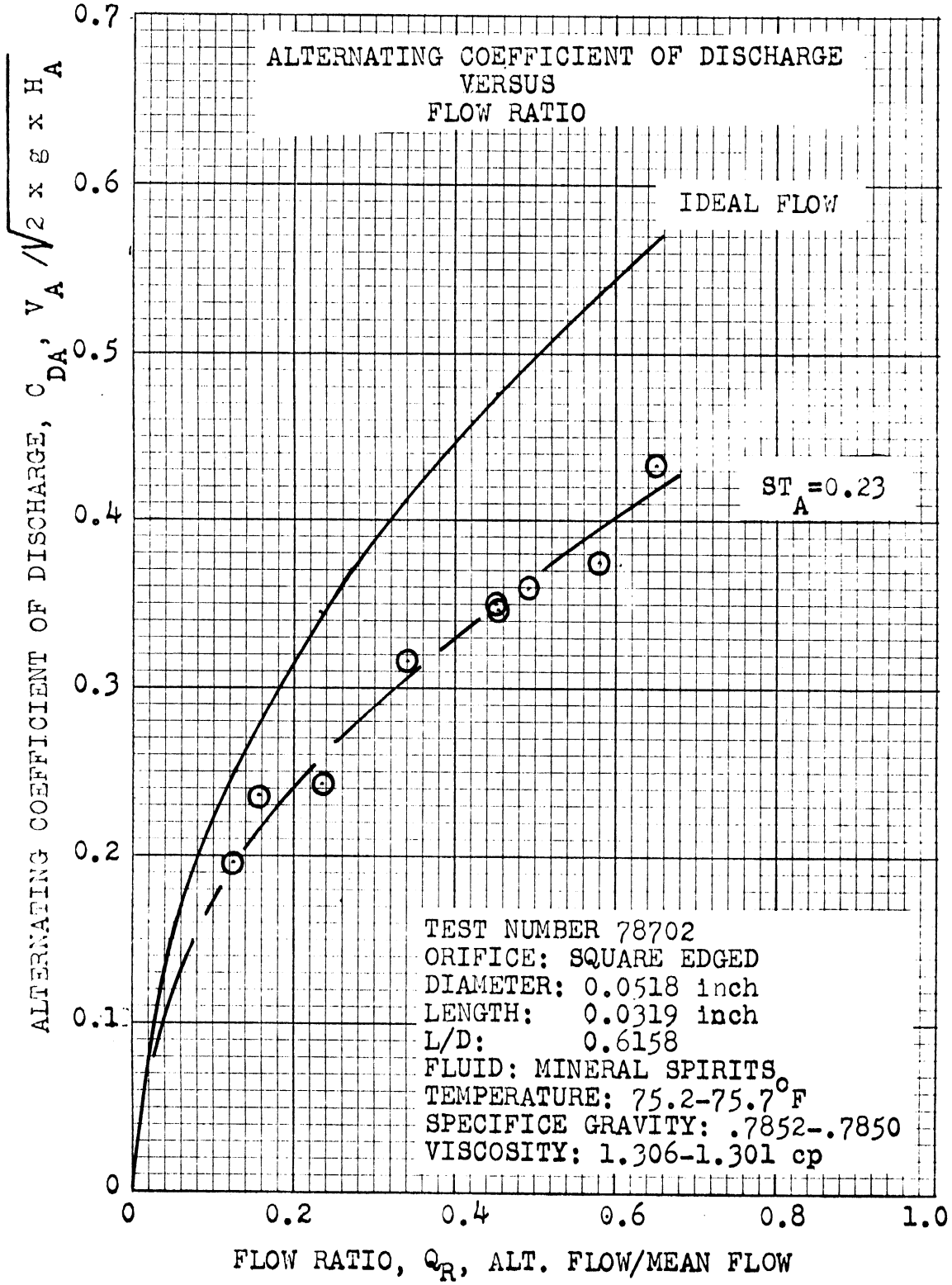

Figure 99. Alternating Coefficient of Discharge versus Flow Ratio for L/D=0.62, ST_A=0.23.

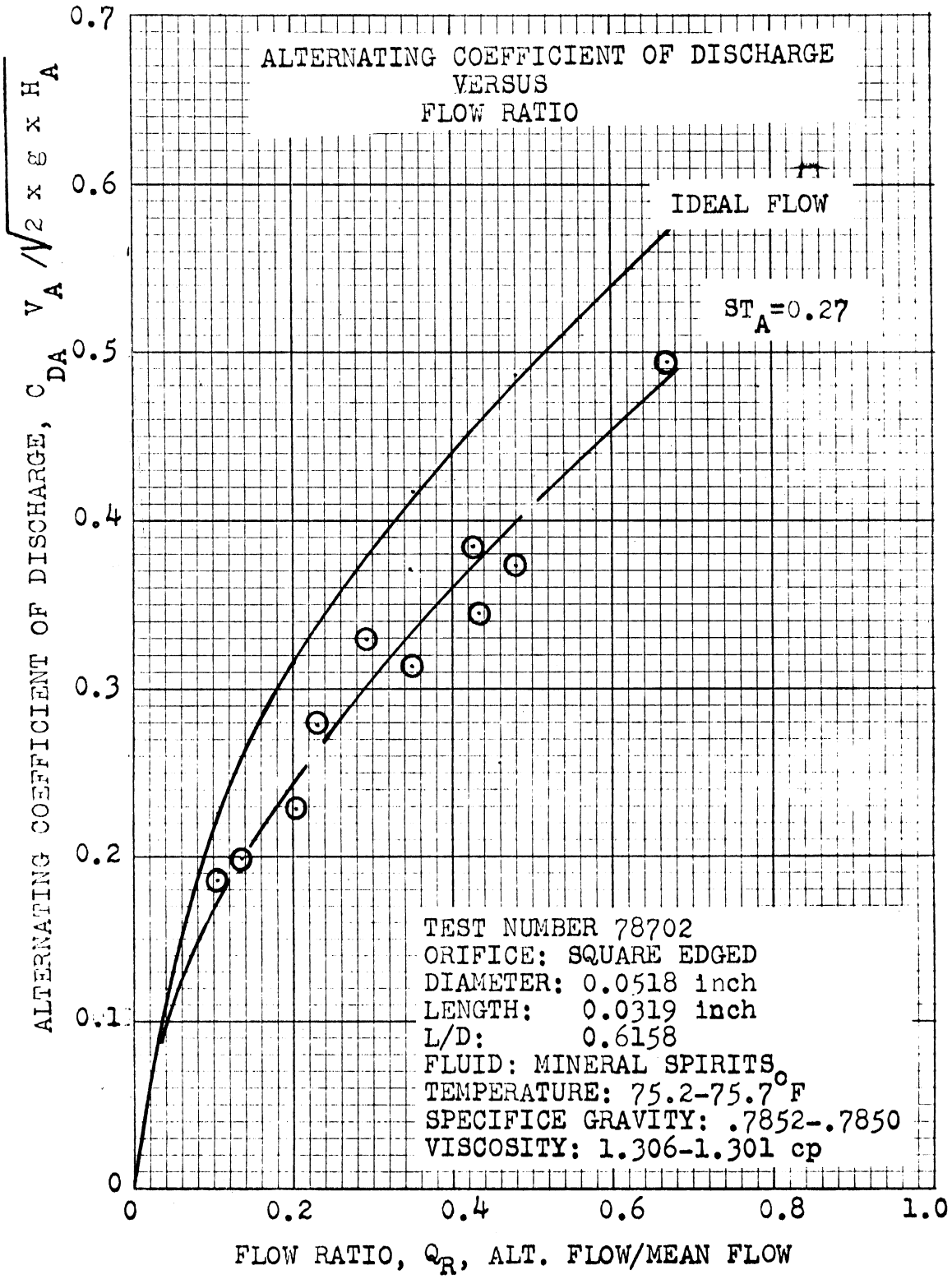

Figure 100. Alternating Coefficient of Discharge versus Flow Ratio for L/D=0.62, ST_A=0.27.

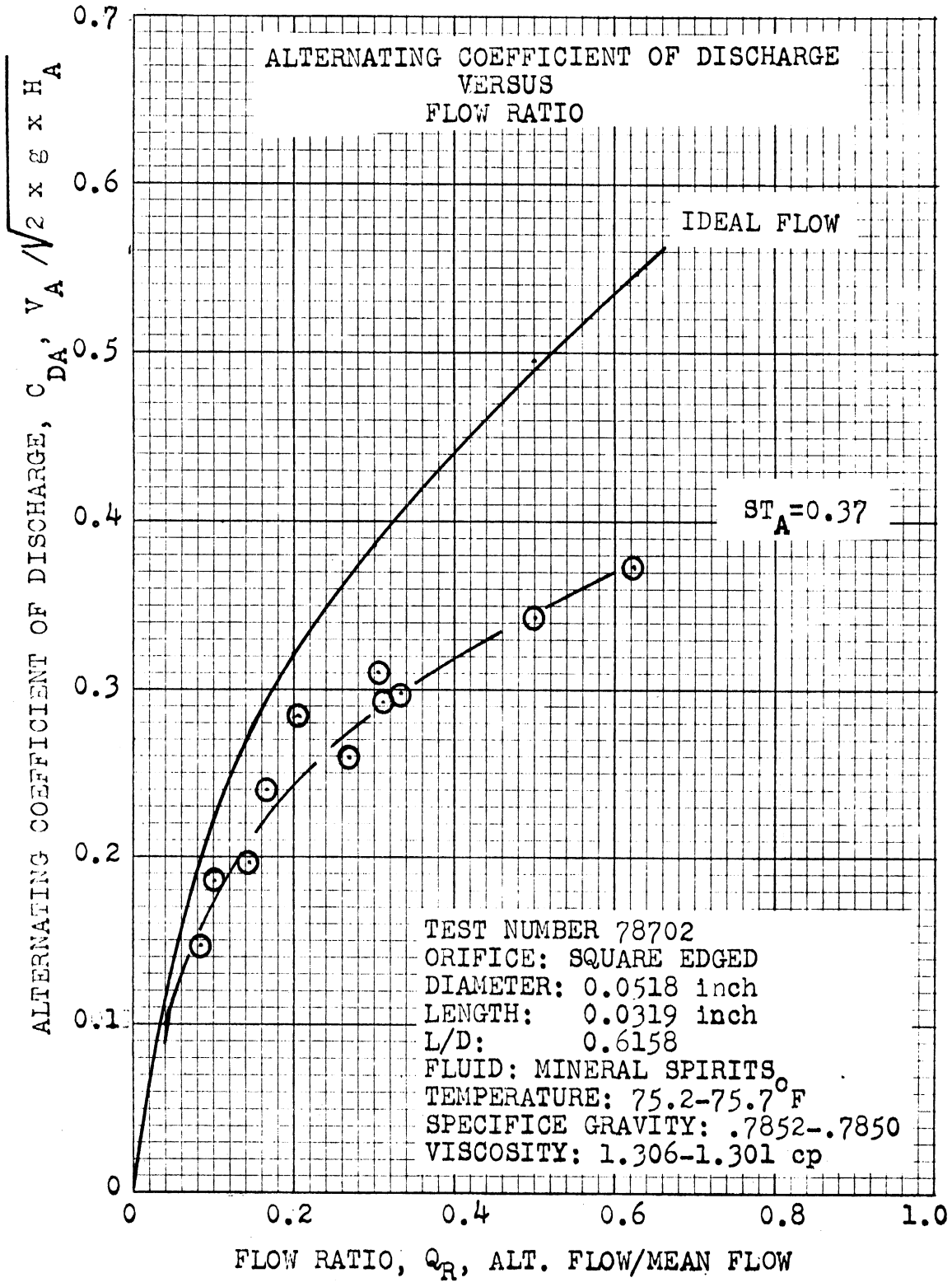

Figure 101. Alternating Coefficient of Discharge versus Flow Ratio for L/D=0.62, ST_A=0.37.

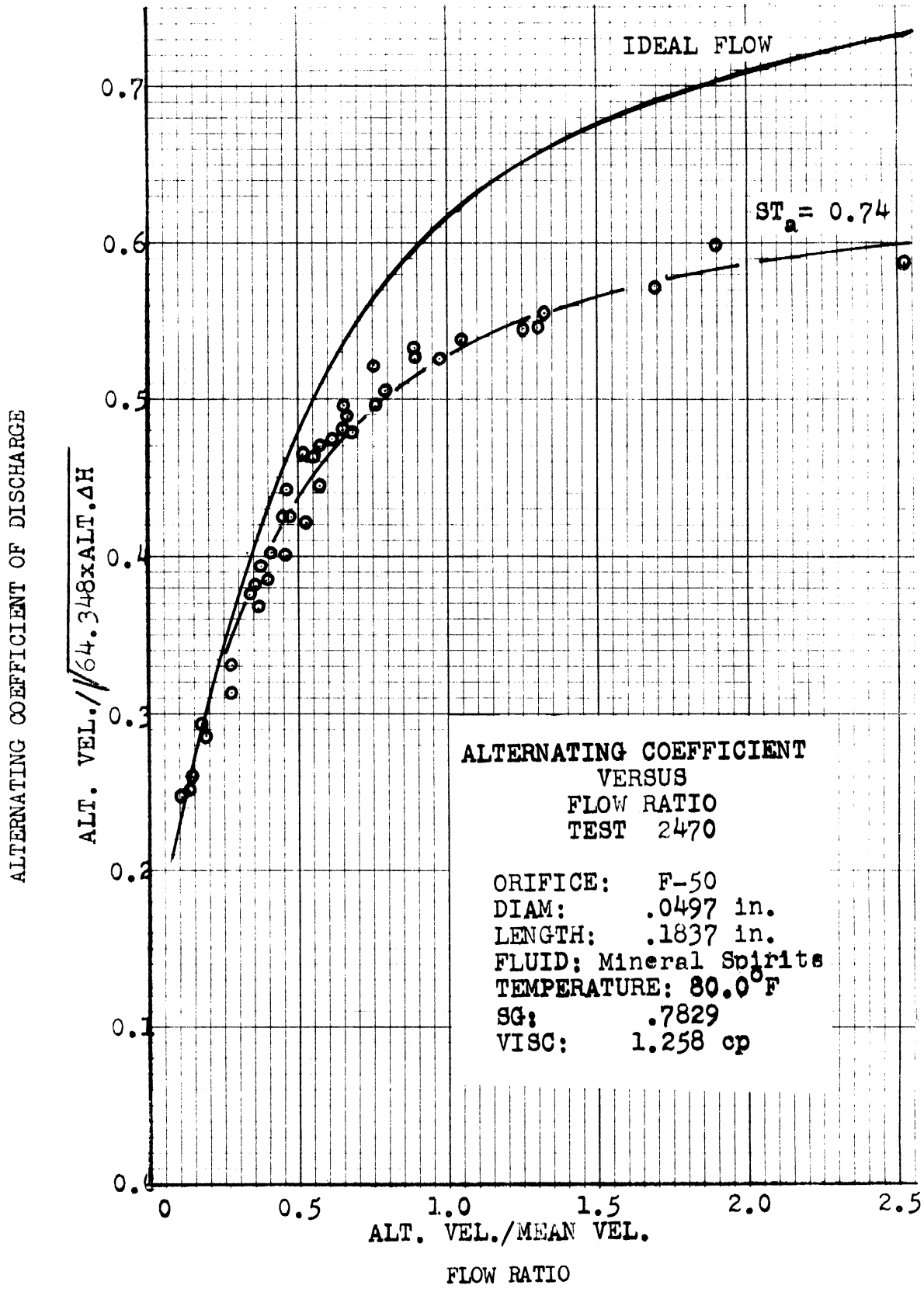

Figure 102. Alternating Coefficient of Discharge versus Flow Ratio for F-50 Orifice, ST_A=0.74.

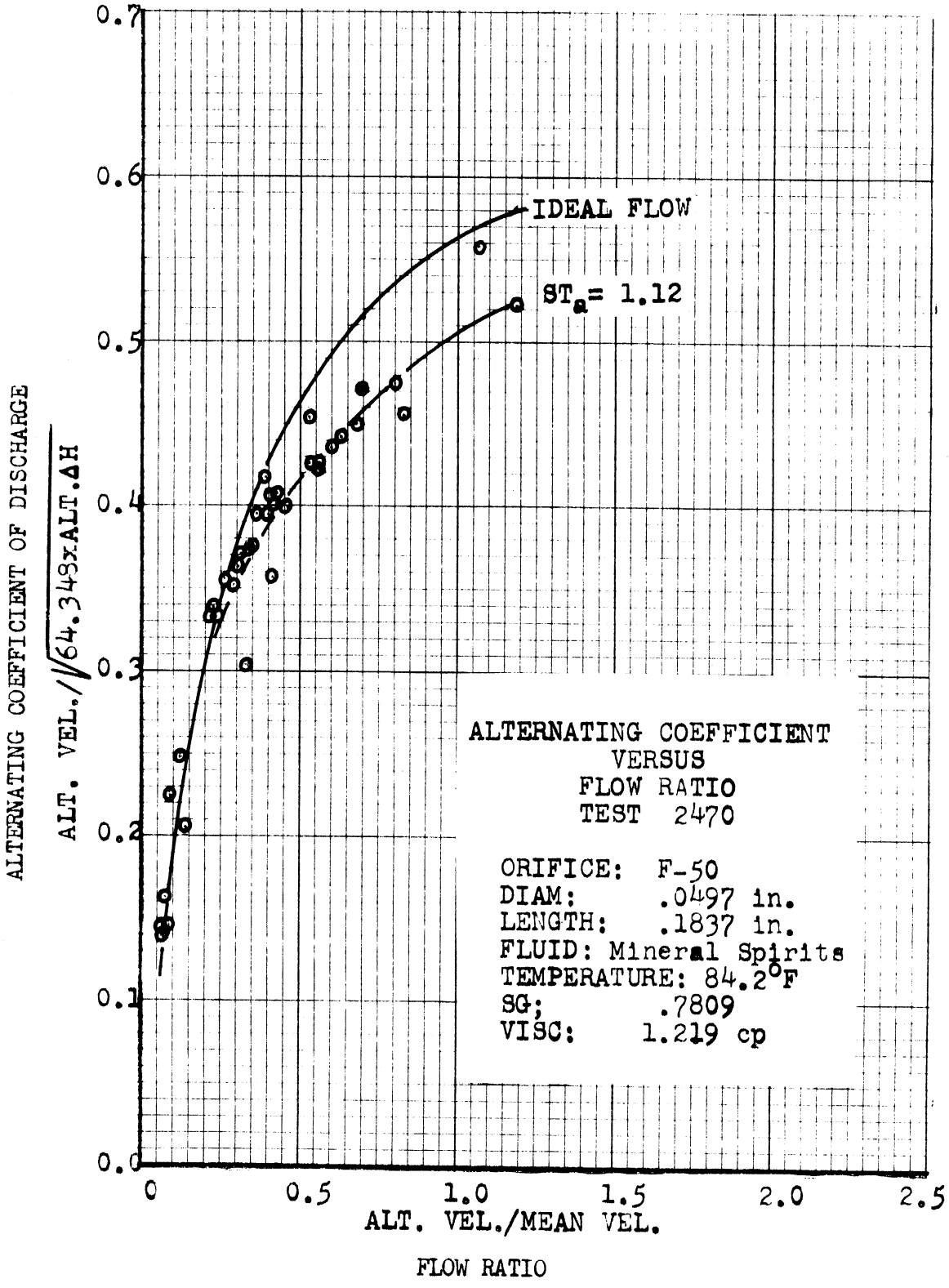

Figure 103. Alternating Coefficient of Discharge versus Flow Ratio for F-50 Orifice, ST_A=1.12.

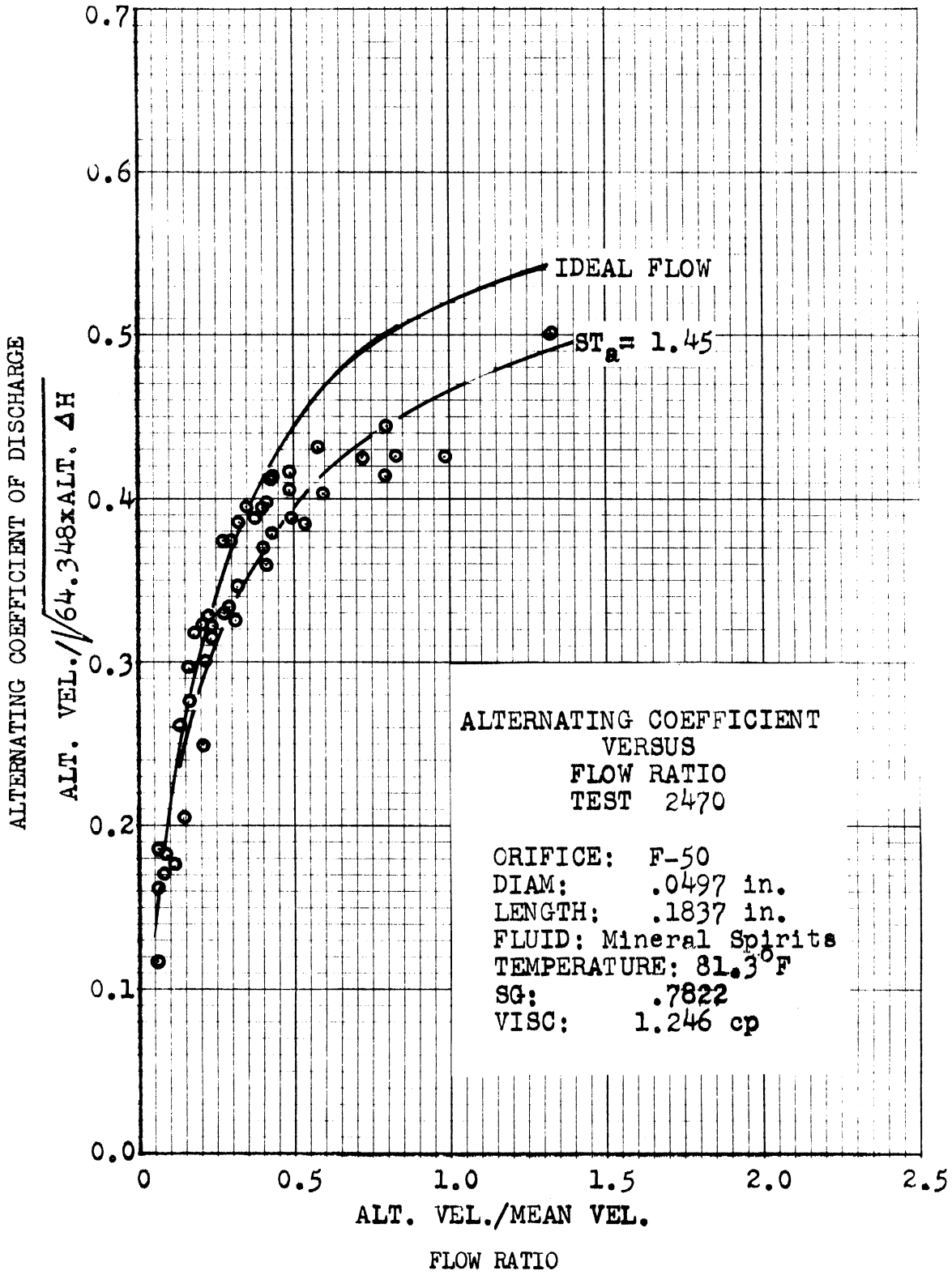

Figure 104. Alternating Coefficient of Discharge versus Flow Ratio for F-50 Orifice, ST_A=1.45.

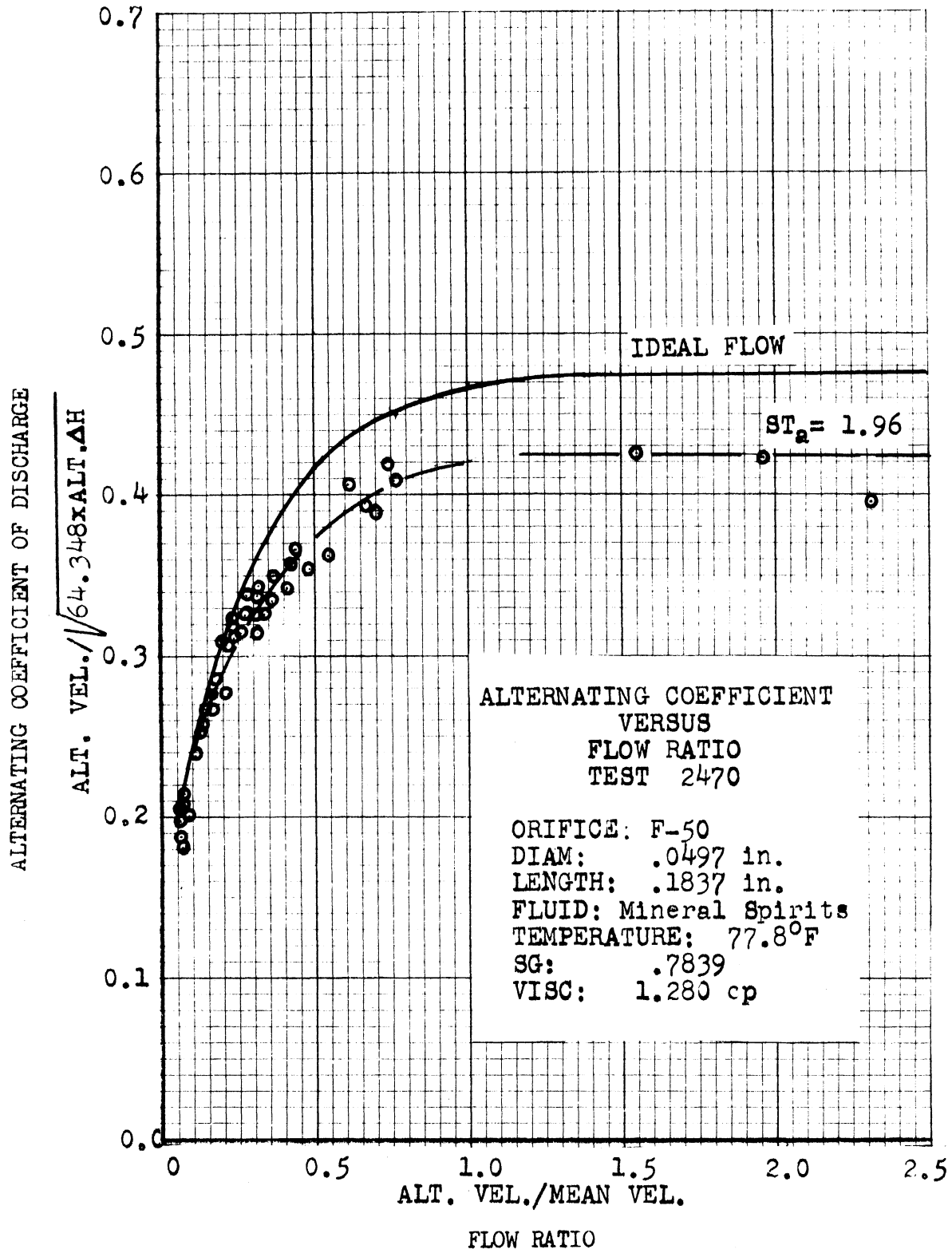

Figure 105. Alternating Coefficient of Discharge versus Flow Ratio for F-50 Orifice, ST_A=1.96.

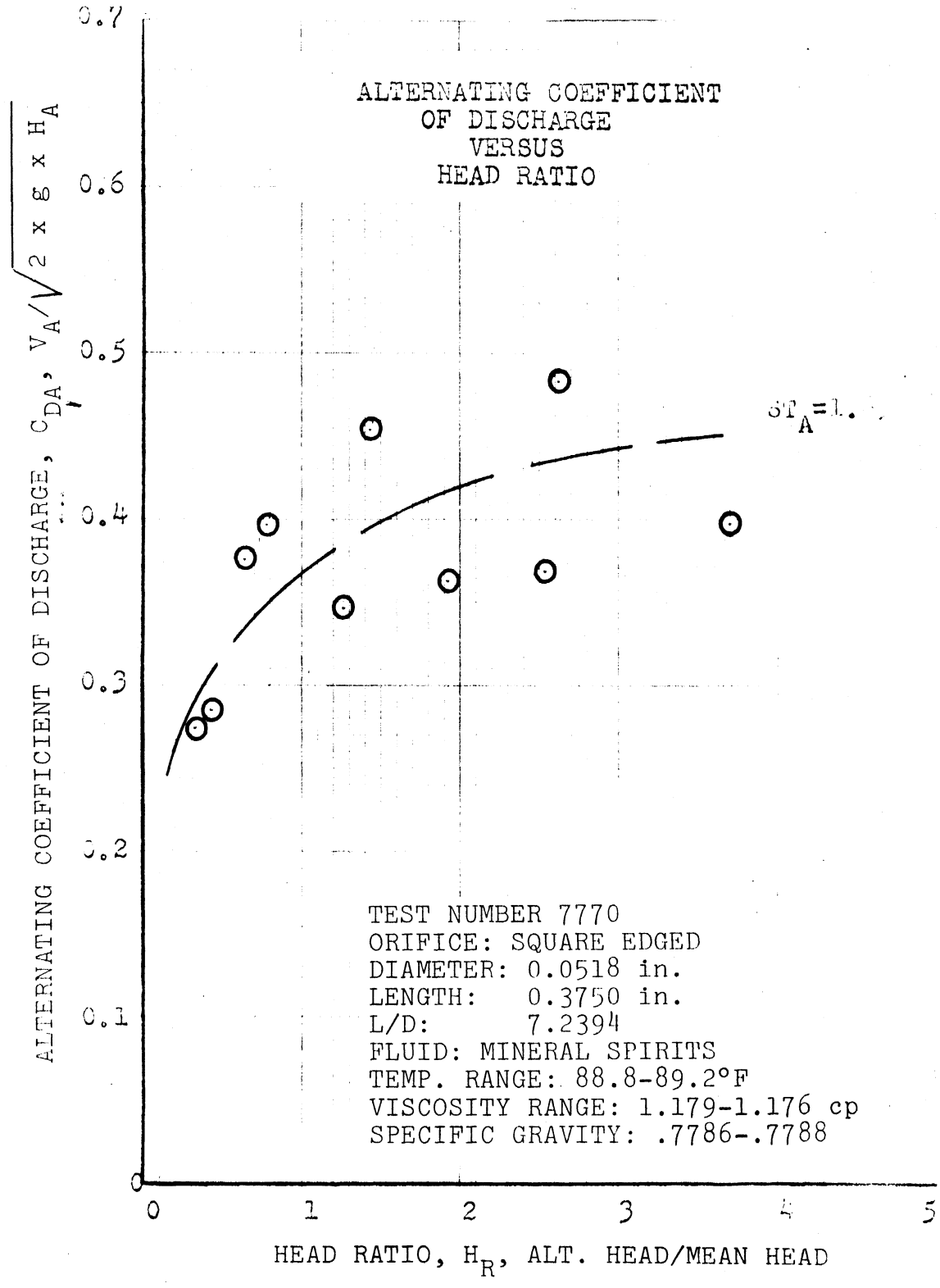

Figure 106. Alternating Coefficient of Discharge versus Head Ratio for L/D=7.24, ST_A=1.69.

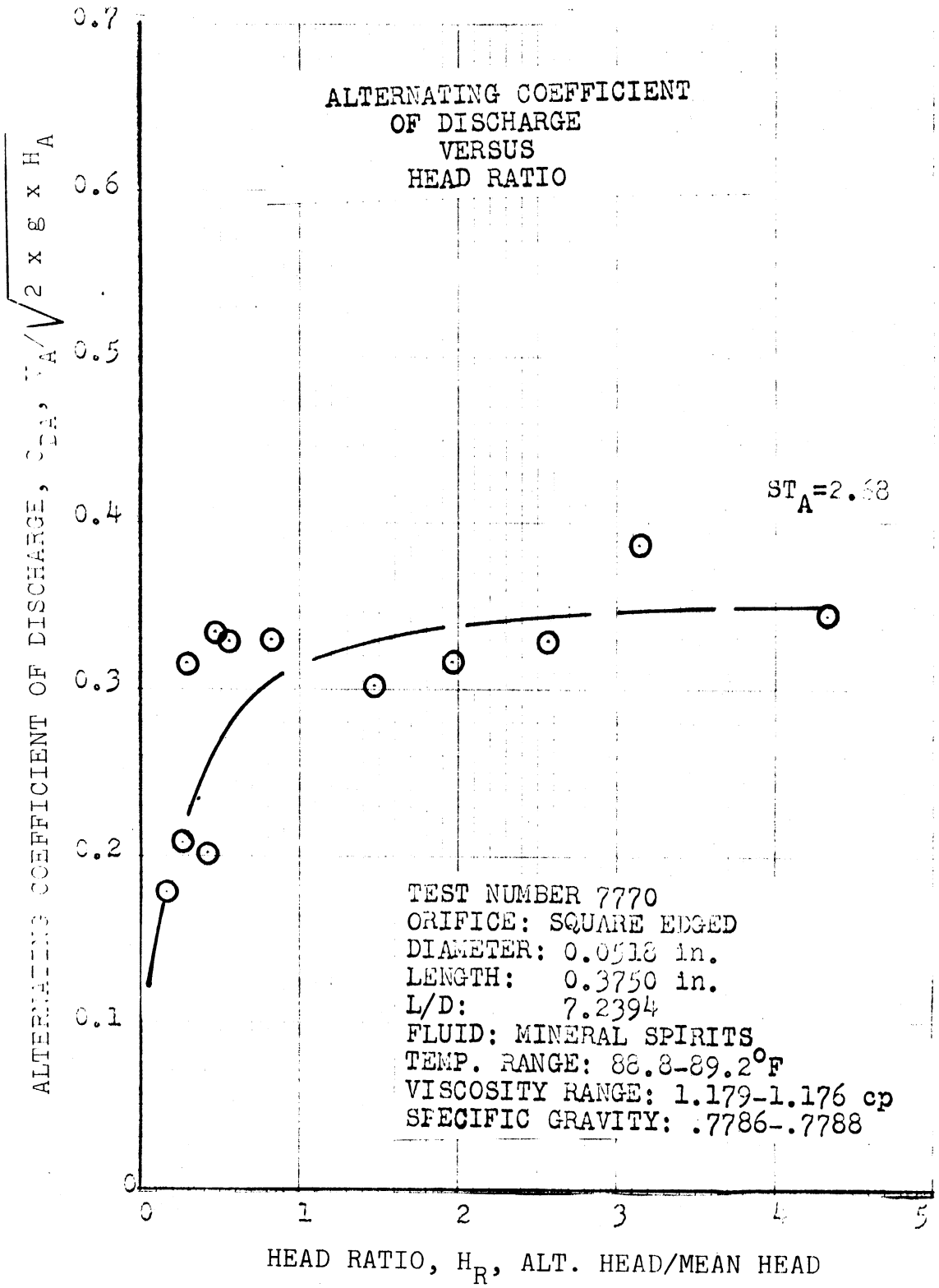

Figure 107. Alternating Coefficient of Discharge versus Head Ratio for L/D=7.24, ST_A=2.68.

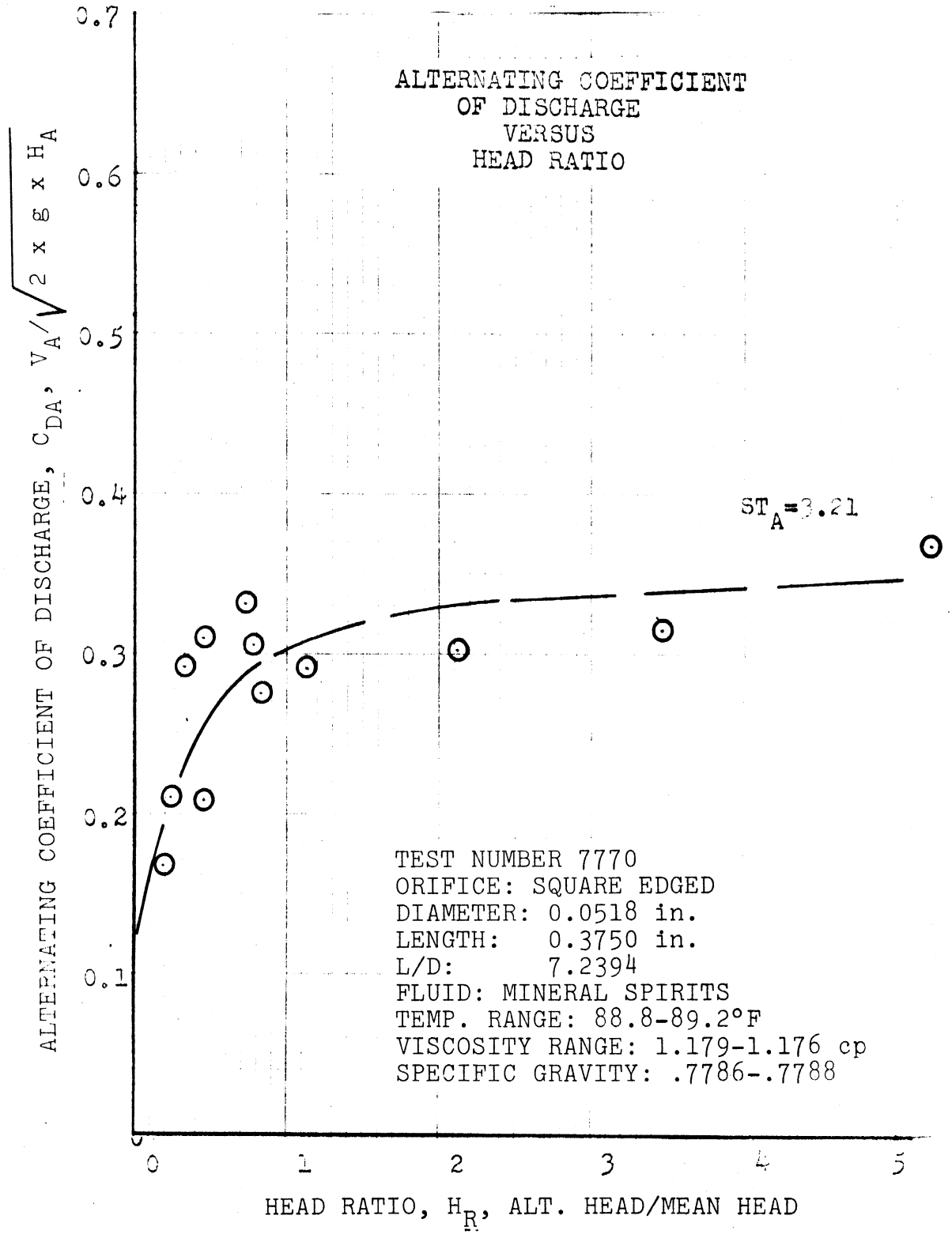

Figure 108. Alternating Coefficient of Discharge versus Head Ratio for L/D=7.24, ST_A=3.21.

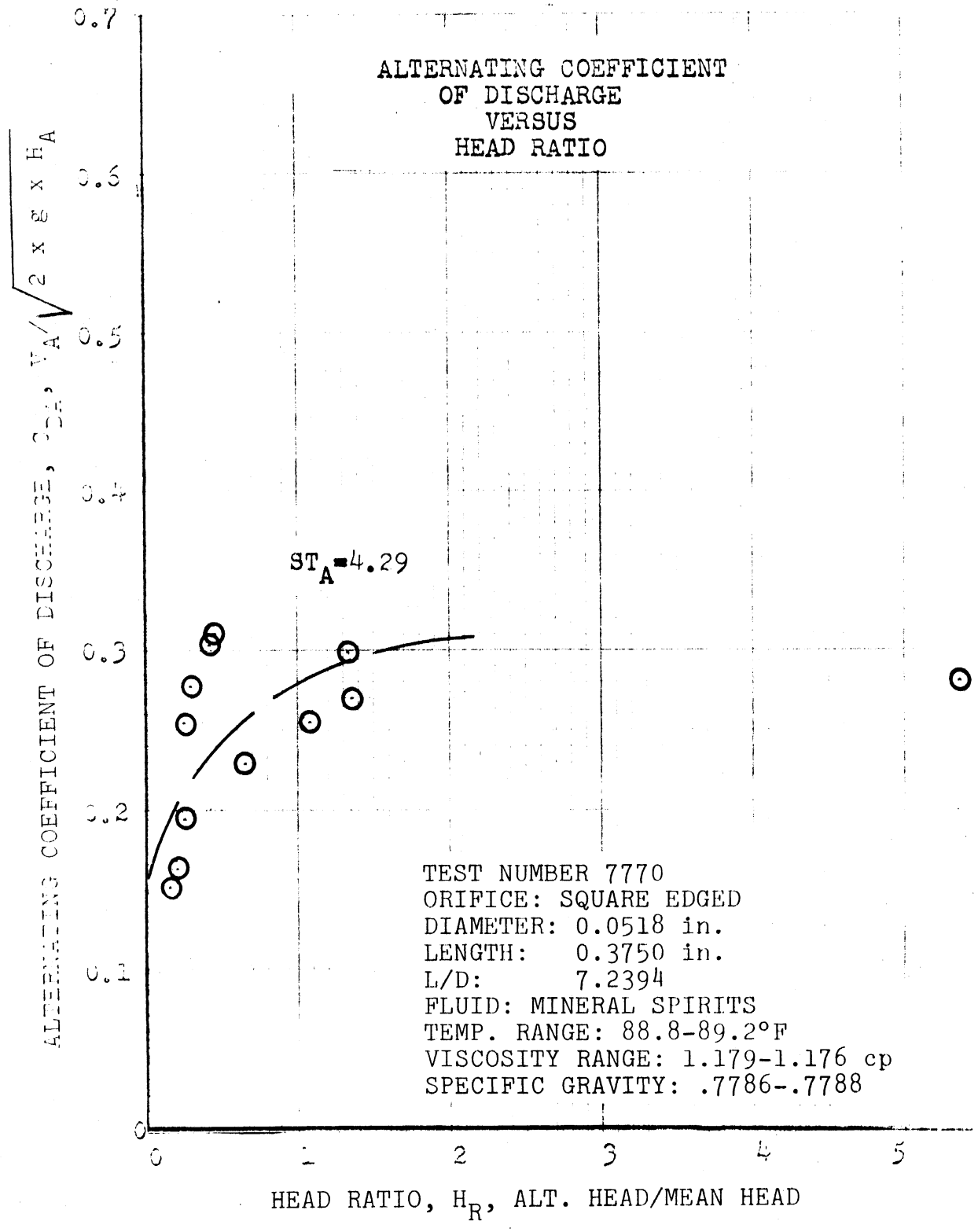

Figure 109. Alternating Coefficient of Discharge versus Head Ratio for L/D=7.24, ST_A=4.29.

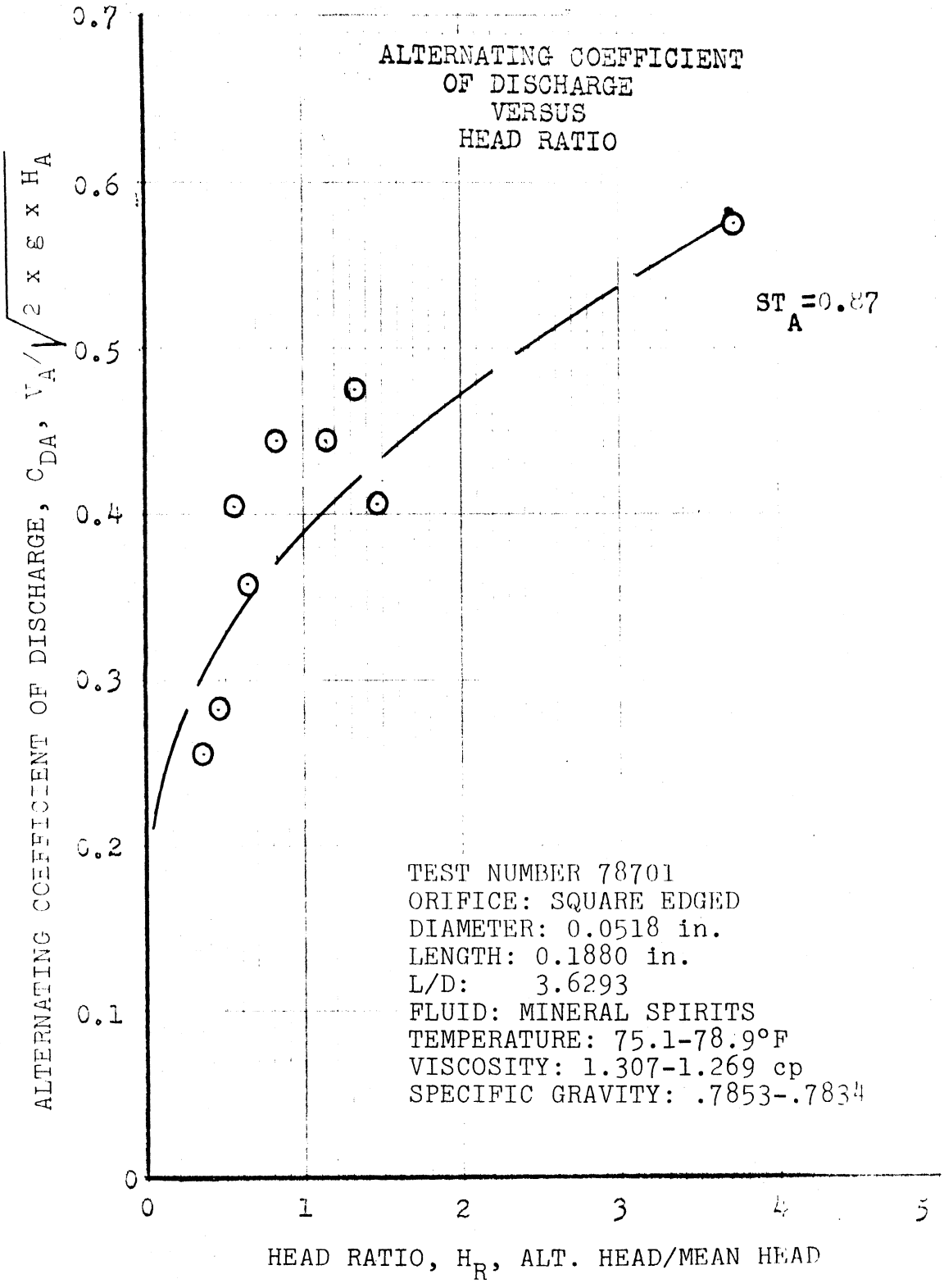

Figure 110. Alternating Coefficient of Discharge versus Head Ratio for L/D=3.63, ST_A=0.87.

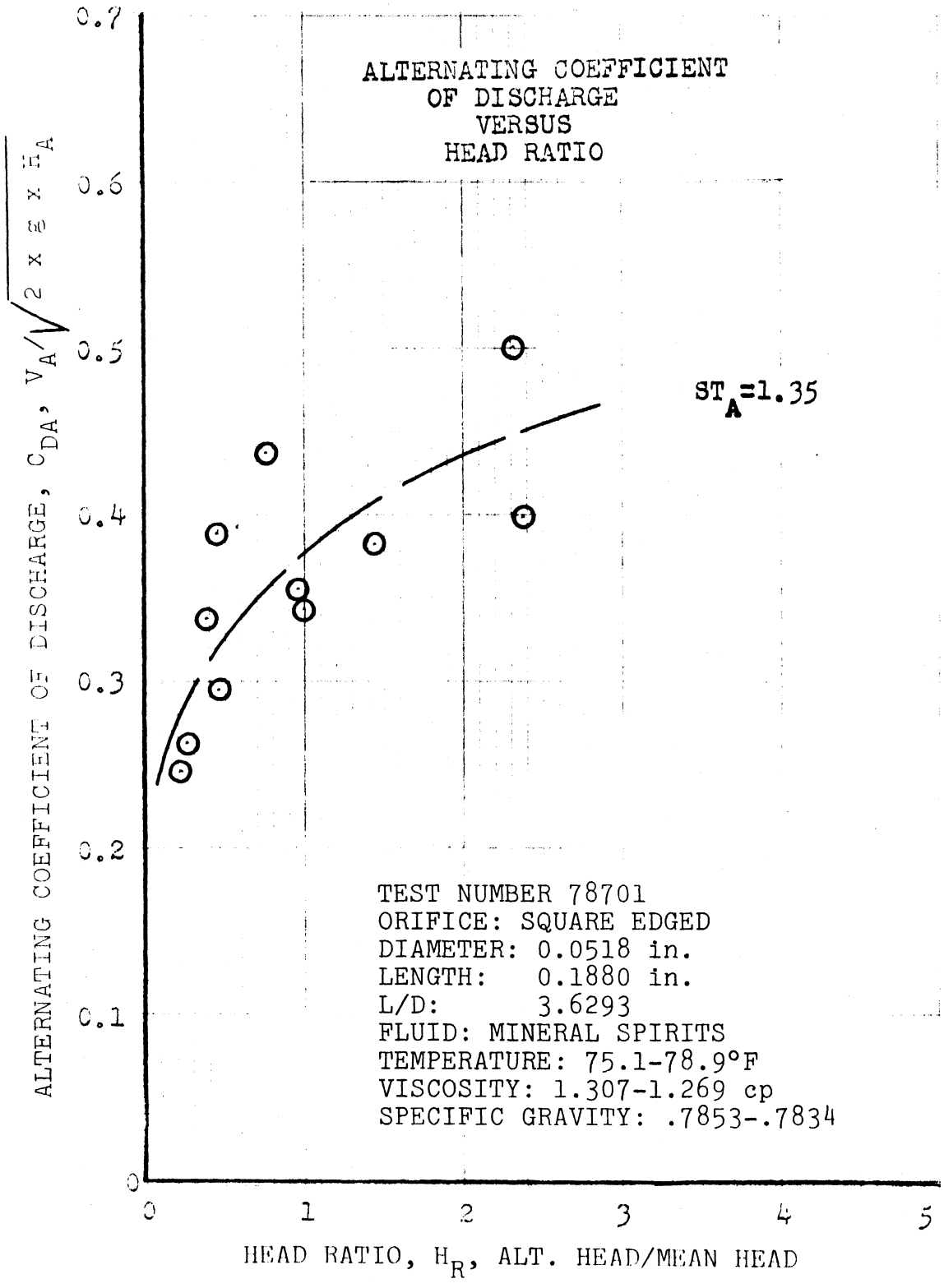

Figure 111. Alternating Coefficient of Discharge versus Head Ratio for L/D=3.63, ST_A=1.35.

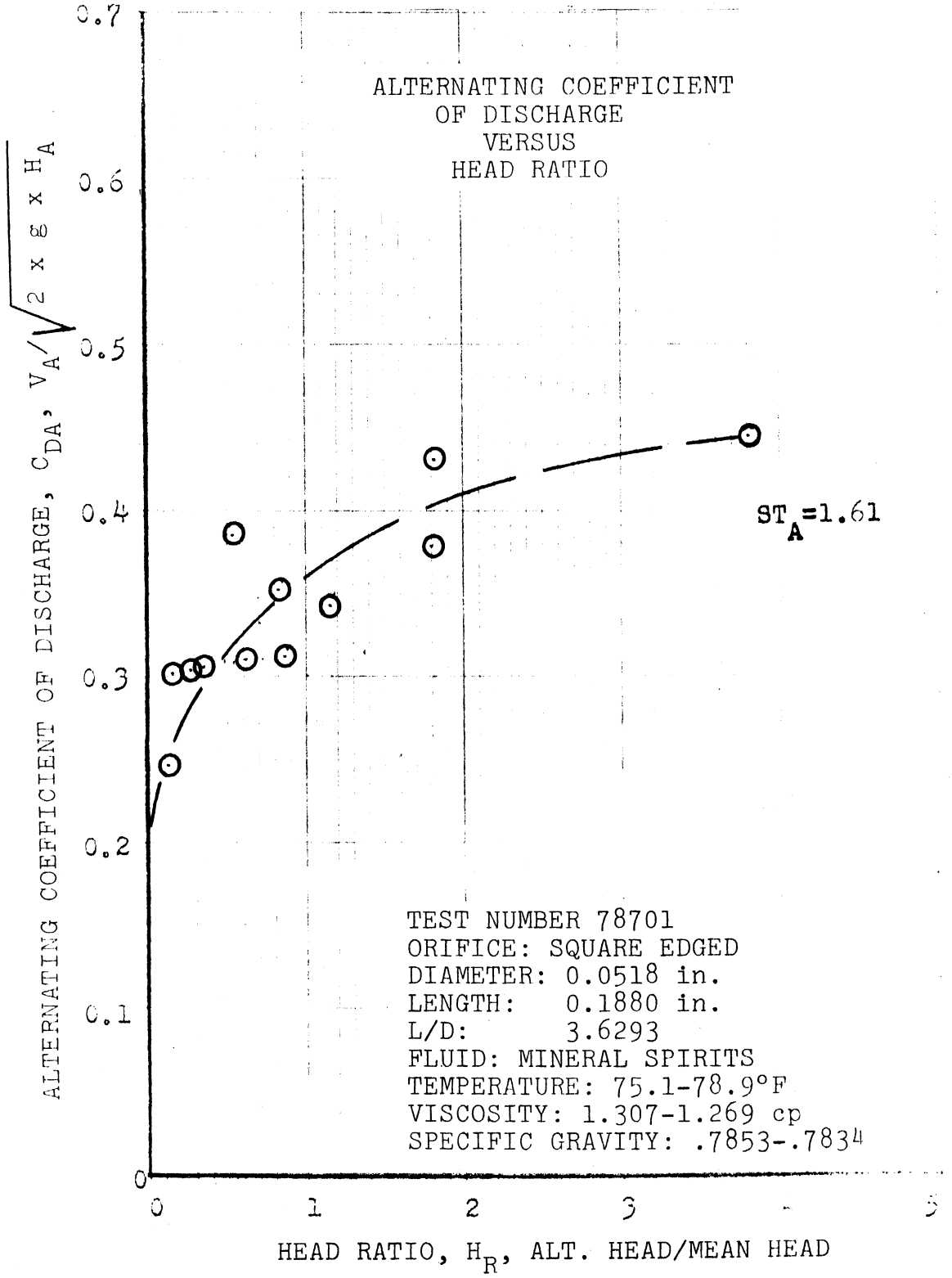

Figure 112. Alternating Coefficient of Discharge versus Head Ratio for L/D=3.63, ST_A=1.61.

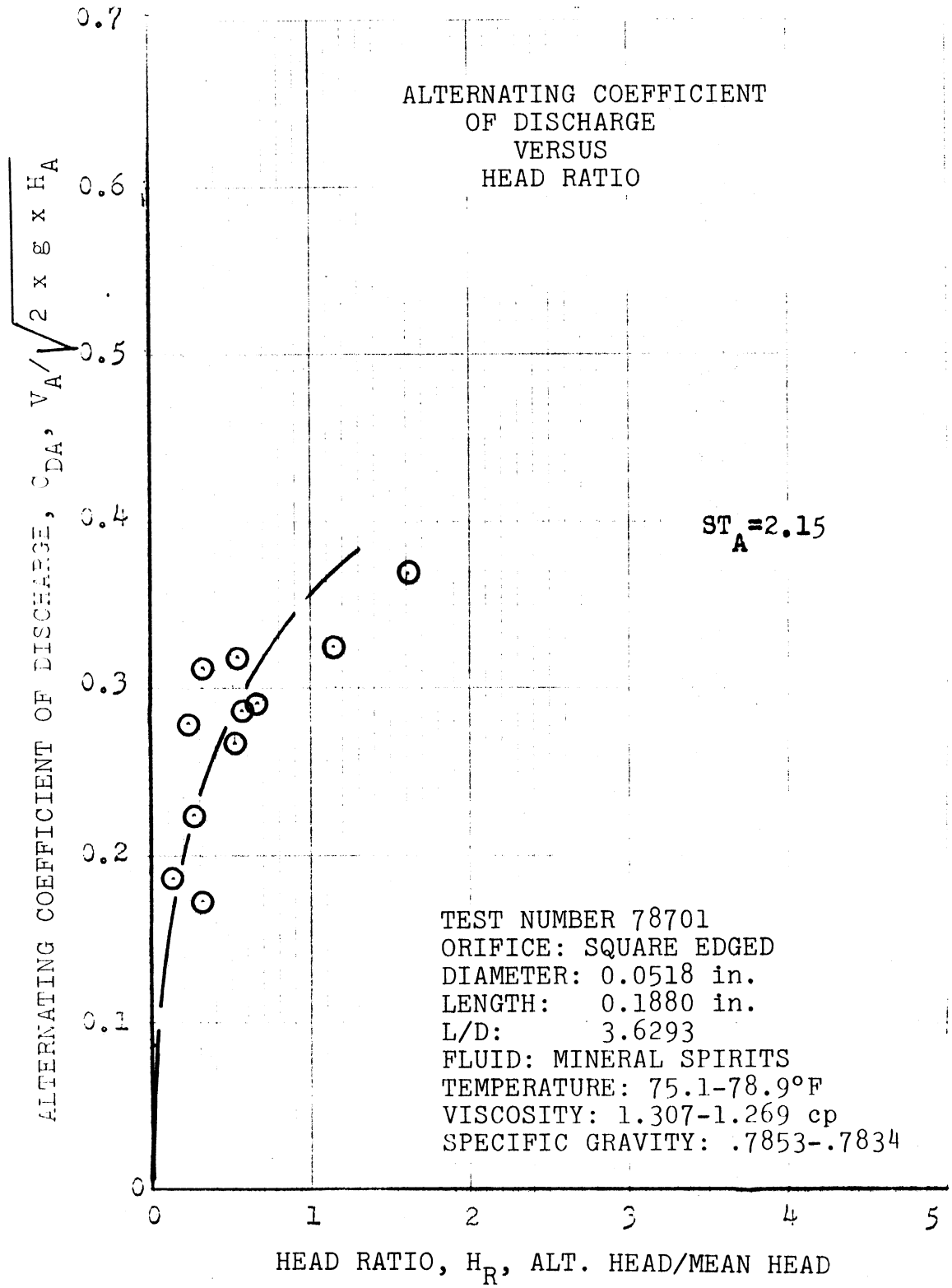

Figure 113. Alternating Coefficient of Discharge versus Head Ratio for L/D=3.63, ST_A=2.15.

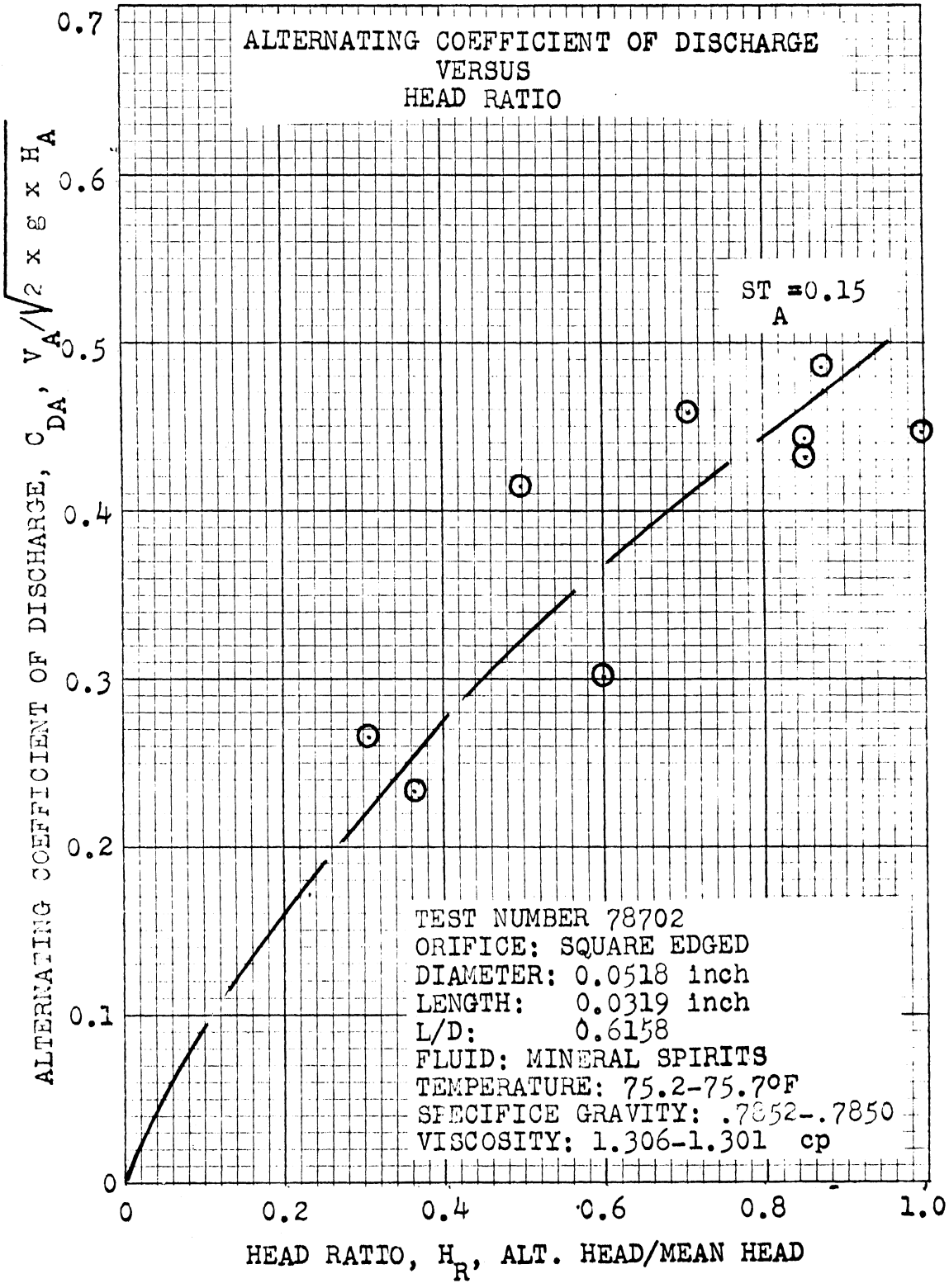

Figure 114. Alternating Coefficient of Discharge versus Head Ratio for L/D=0.62, ST_A=0.15.

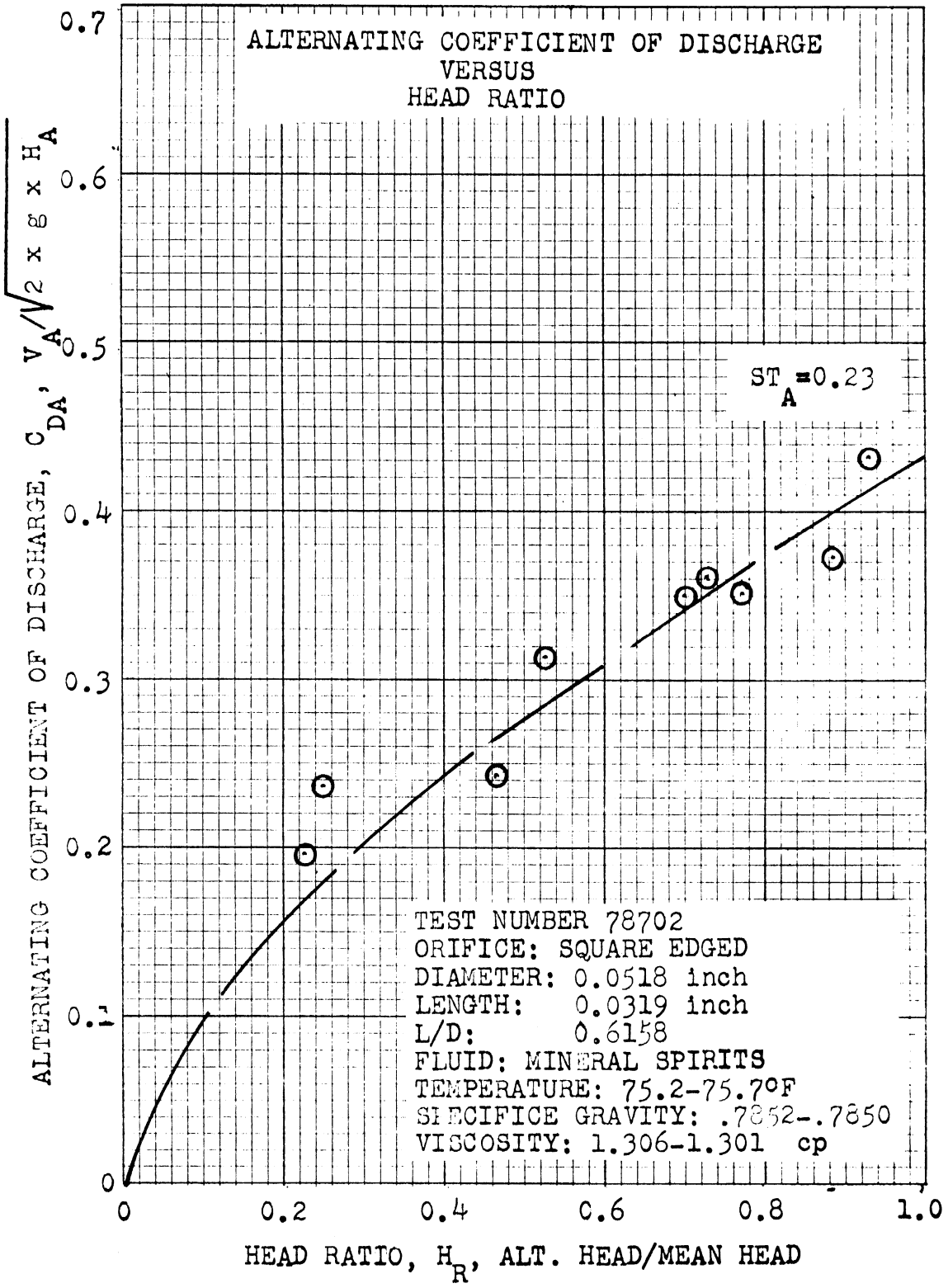

Figure 115. Alternating Coefficient of Discharge versus Head Ratio for L/D=0.62, ST_A=0.23.

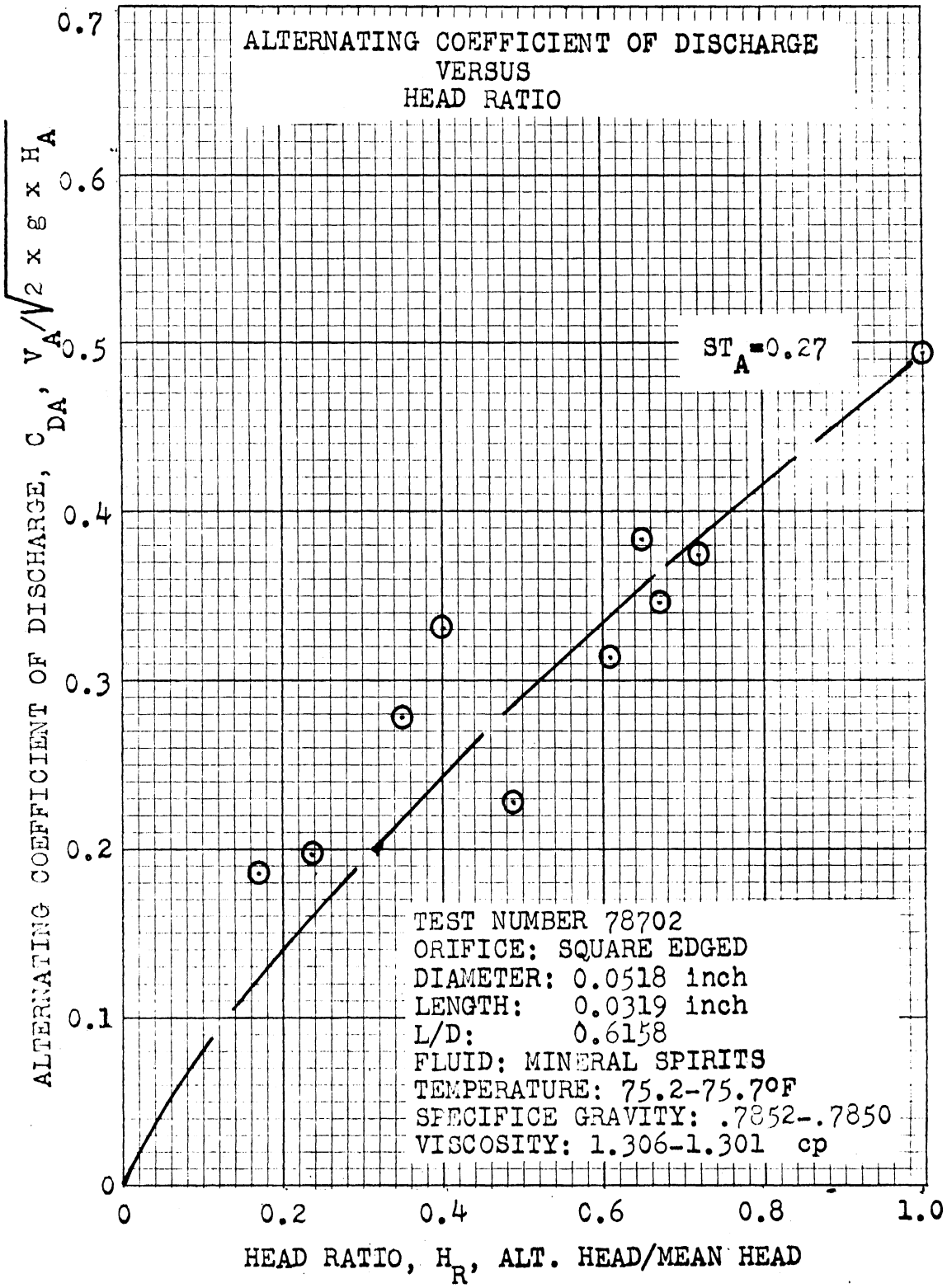

Figure 116. Alternating Coefficient of Discharge versus Head Ratio for L/D=0.62, ST_A=0.27.

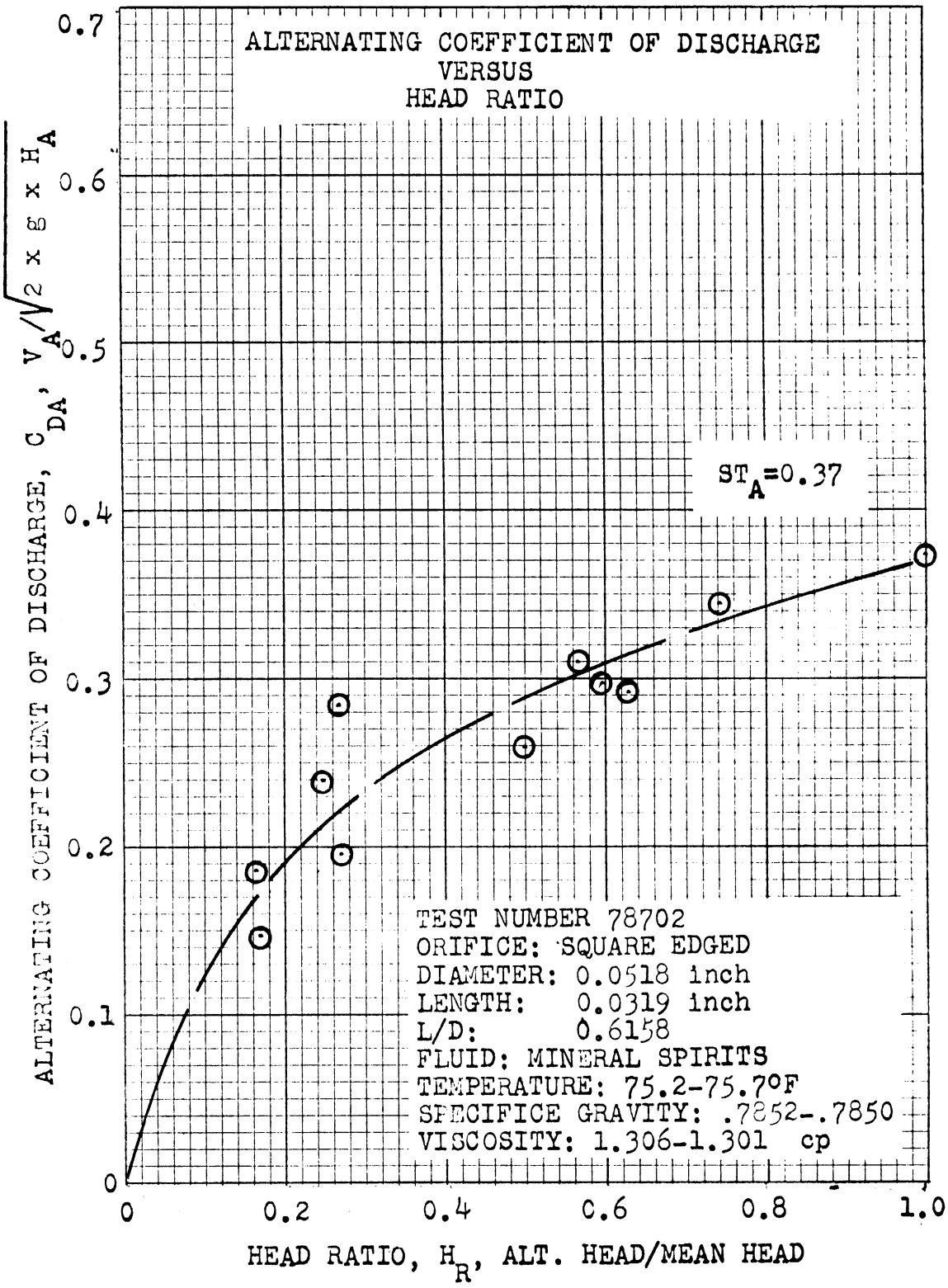

Figure 117. Alternating Coefficient of Discharge versus Head Ratio for L/D=0.62, ST_A=0.37.

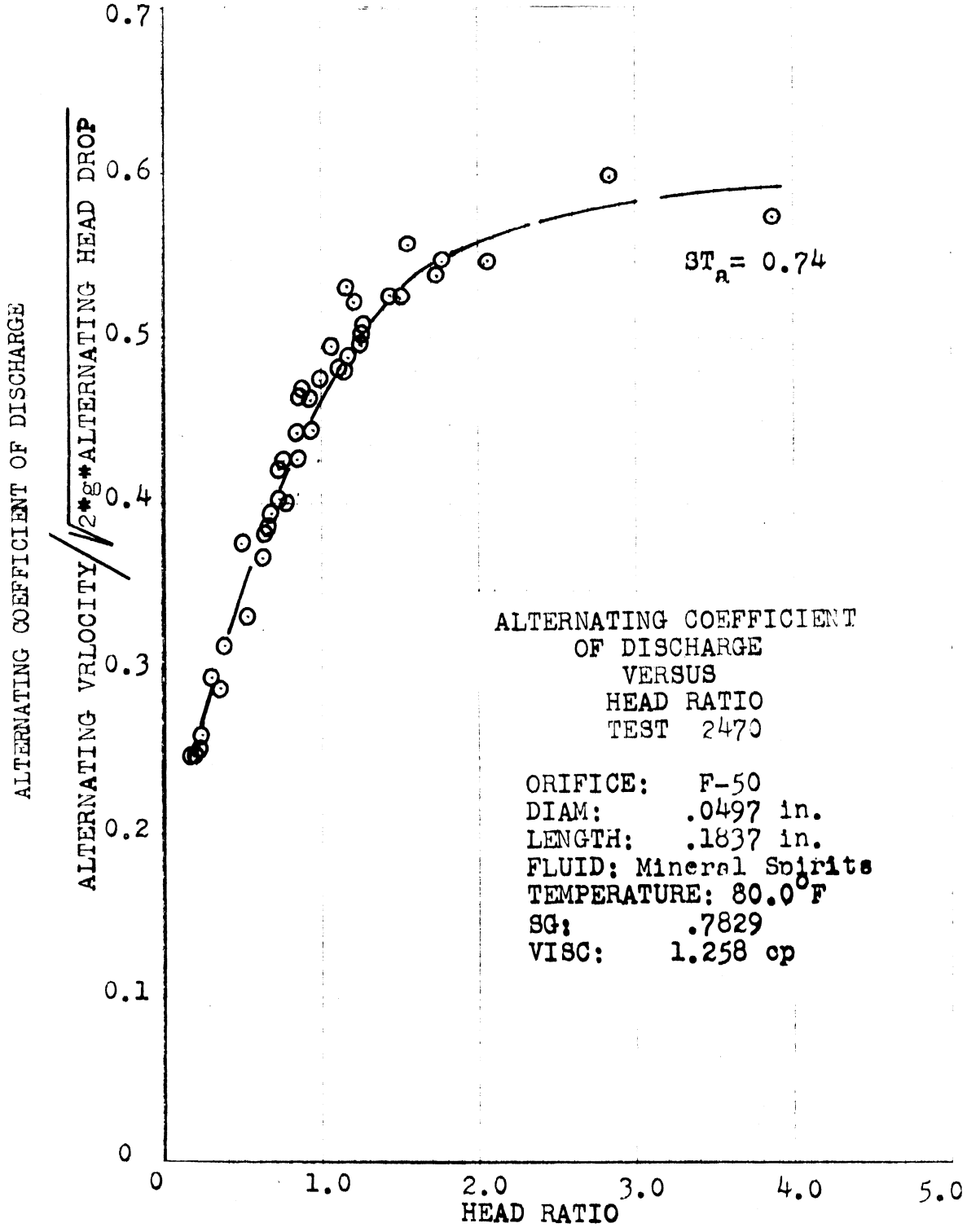

Figure 118. Alternating Coefficient of Discharge versus Head Ratio for F-50 Orifice, ST_A=0.74.

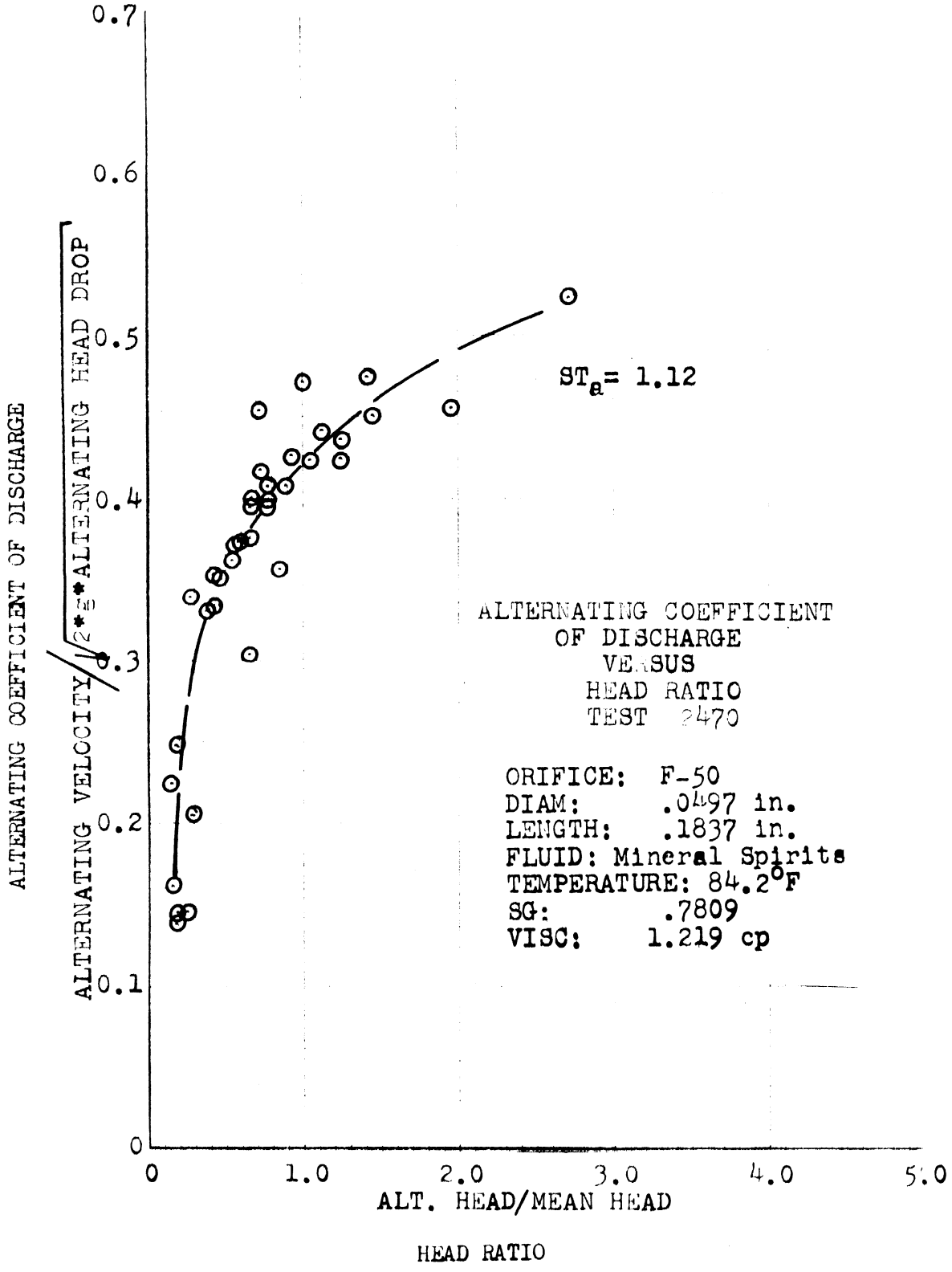

Figure 119. Alternating Coefficient of Discharge versus Head Ratio for F-50 Orifice, ST_A=1.12.

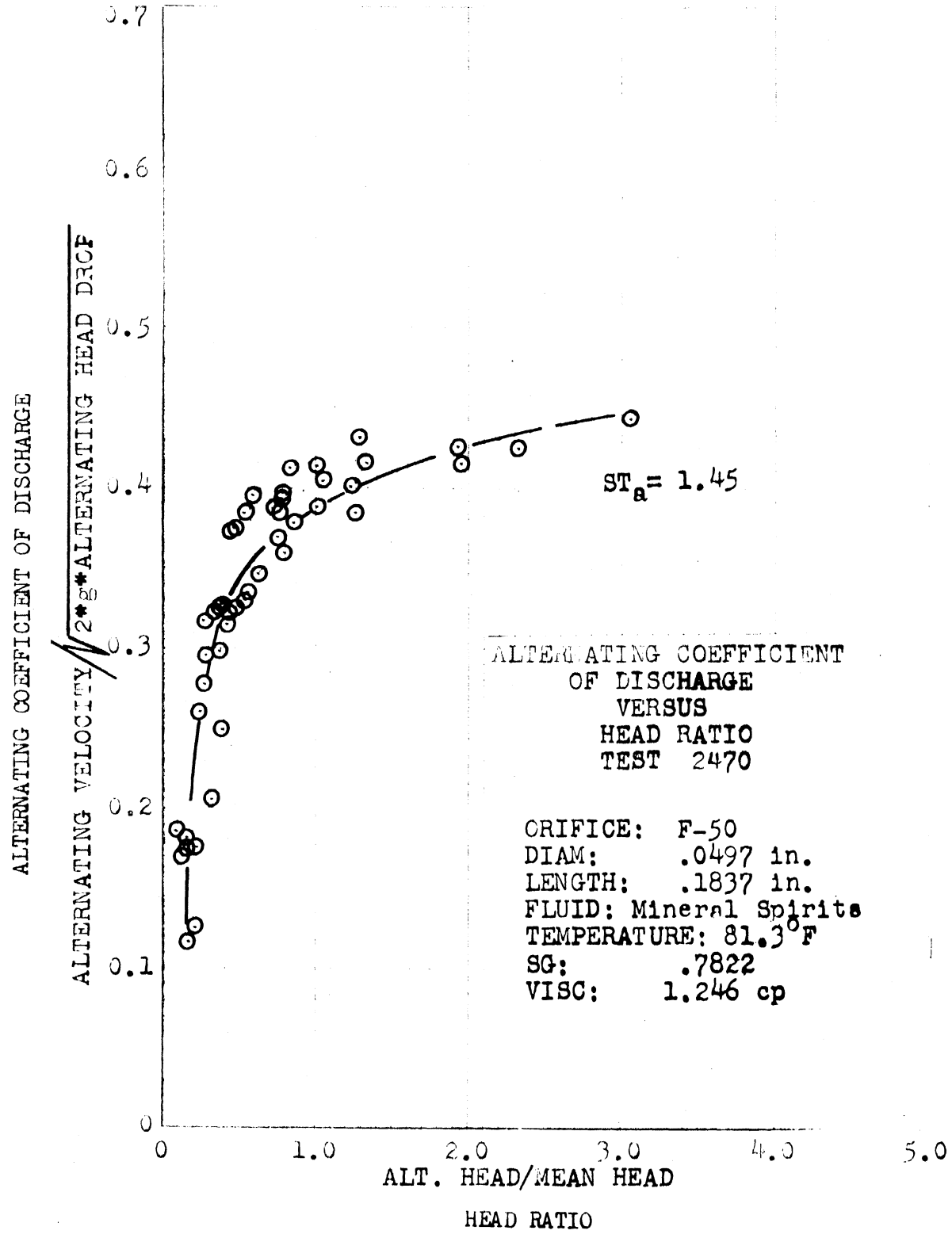

Figure 120. Alternating Coefficient of Discharge versus Head Ratio for F-50 Orifice, ST_A=1.45.

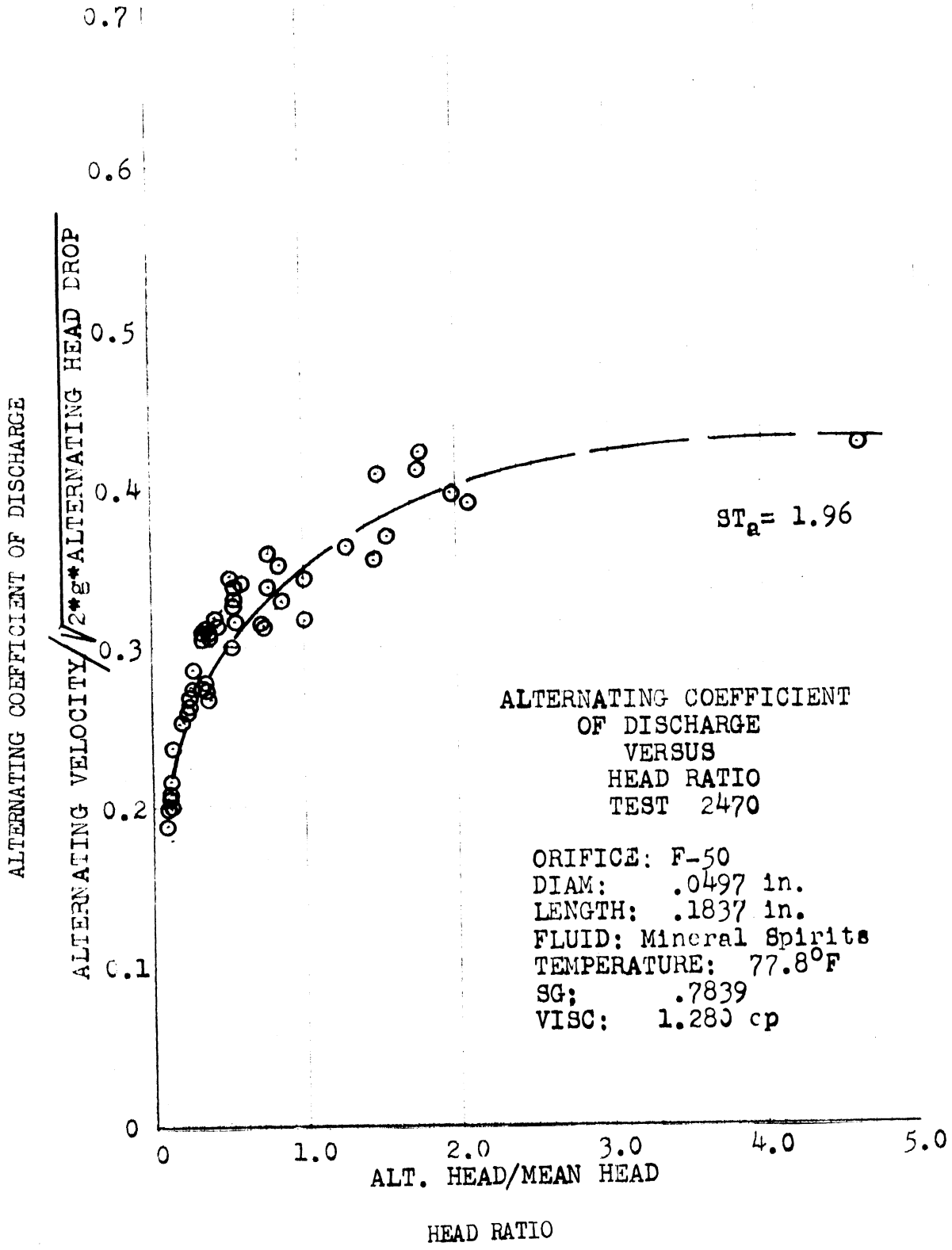

Figure 121. Alternating Coefficient of Discharge versus Head Ratio for F-50 Orifice, ST_A=1.96.

TABLE IX

F-50 ORIFICE DATA

UNIVERSITY OF MICHIGAN

MECHANICAL ENGINEERING DOCTORAL THESIS

ORIFICE DISCHARGE COEFFICIENTS FOR OSCILLATORY FLOW

STEPHEN J. DEREZINSKI

TEST NUMBER= 2470
MINERAL SPIRITS AT TEMPERATURE OF 77.8
SPECIFIC GRAVITY=.7839
VISCOSITY, CENTISTOKES 1.280
ORIFICE DIAMETER IN INCHES=.0497
ORIFICE LENGTH IN INCHES= 0.1837
ORIFICE LENGTH/DIAMETER= 3.6962
CAM DISPLACEMENT=.007400
08:40.57 MAR 31, 1970

PRESSURE DROPS INCHES WATER			FLOWS CU FEET/HOUR			FREQ CPS	COEFF
ALT	MEAN	RATIO	ALT	MEAN	RATIO		
*****	*****	*****	*****	*****	*****	***	*****
1.215	1.215	1.000	0.0444	0.1090	0.4069	18.7	0.7791
1.735	4.898	0.354	0.0465	0.2290	0.2032	19.6	0.8152
2.121	9.448	0.224	0.0477	0.3333	0.1431	20.1	0.8543
2.275	14.423	0.158	0.0455	0.4190	0.1085	19.1	0.8692
3.278	19.938	0.164	0.0459	0.4895	0.0938	19.3	0.8636
2.873	23.081	0.124	0.0449	0.5710	0.0786	18.9	0.9363
3.006	28.461	0.106	0.0472	0.6210	0.0760	19.9	0.9170
4.184	33.416	0.125	0.0467	0.6565	0.0711	19.6	0.8947
3.664	37.755	0.097	0.0458	0.7166	0.0639	19.3	0.9187
3.548	43.964	0.081	0.0492	0.7971	0.0617	20.7	0.9470
3.567	50.230	0.071	0.0475	0.8500	0.0558	20.0	0.9448
3.587	2.044	1.755	0.1011	0.1378	0.7334	42.5	0.7594
5.129	6.633	0.773	0.1026	0.2452	0.4183	43.1	0.7499
6.247	11.685	0.535	0.1044	0.3349	0.3117	43.9	0.7719
6.922	16.216	0.427	0.1043	0.4284	0.2435	43.9	0.8381
8.699	22.849	0.381	0.1030	0.5125	0.2010	43.3	0.8446
9.583	24.546	0.390	0.1045	0.5780	0.1808	44.0	0.9191
9.275	30.485	0.304	0.1057	0.6307	0.1676	44.5	0.8999
9.506	34.457	0.276	0.1067	0.6889	0.1548	44.9	0.9245
9.757	37.523	0.260	0.1064	0.7164	0.1485	44.7	0.9213
10.316	44.754	0.231	0.1069	0.7551	0.1415	45.0	0.8892
10.779	49.189	0.219	0.1048	0.8314	0.1260	44.1	0.9339
7.848	1.176	6.672	0.1499	0.0764	1.9615	63.1	0.5552
9.294	4.705	1.975	0.1522	0.2307	0.6596	64.0	0.8379
10.335	8.947	1.155	0.1495	0.3356	0.4456	62.9	0.8839
11.434	13.710	0.834	0.1504	0.4235	0.3550	63.2	0.9011
12.533	19.591	0.640	0.1517	0.4815	0.3151	63.8	0.8570
13.461	23.736	0.565	0.1575	0.5777	0.2726	66.2	0.9341
13.748	32.298	0.426	0.1522	0.6464	0.2354	64.0	0.8961
14.269	37.909	0.376	0.1472	0.6845	0.2150	61.9	0.8758

TABLE IX (CONT'D)
F-50 ORIFICE DATA

UNIVERSITY OF MICHIGAN
MECHANICAL ENGINEERING DOCTORAL THESIS
ORIFICE DISCHARGE COEFFICIENTS FOR OSCILLATORY FLOW
STEPHEN J. DEREZINSKI

TEST NUMBER= 2470
MINERAL SPIRITS AT TEMPERATURE OF 77.8
SPECIFIC GRAVITY=.7839
VISCOSITY, CENTISTOKES 1.280
ORIFICE DIAMETER IN INCHES=.0497
ORIFICE LENGTH IN INCHES= 0.1837
ORIFICE LENGTH/DIAMETER= 3.6962
CAM DISPLACEMENT=.07400
08:40.57 MAR 31, 1970

PRESSURE DROPS INCHES WATER			FLOWS CU FEET/HOUR			FREQ CPS	COEFF
ALT	MEAN	RATIO	ALT	MEAN	RATIO		
*****	*****	*****	*****	*****	*****	***	*****
14.018	44.214	0.317	0.1473	0.7389	0.1993	62.0	0.8754
14.886	43.501	0.342	0.1503	0.7709	0.1949	63.2	0.9208
16.795	63.766	0.263	0.1485	0.8451	0.1757	62.5	0.8337
13.131	2.834	4.633	0.1944	0.1251	1.5549	81.8	0.5852
13.016	7.501	1.735	0.1875	0.2455	0.7635	78.8	0.7062
13.729	9.178	1.496	0.1911	0.3170	0.6030	80.4	0.8242
13.729	17.663	0.777	0.1580	0.4354	0.3628	66.4	0.8162
14.404	28.596	0.504	0.1653	0.5240	0.3154	69.5	0.7720
16.139	30.601	0.527	0.1664	0.6003	0.2771	70.0	0.8549
17.817	32.047	0.556	0.1684	0.6643	0.2535	70.8	0.9244
18.048	43.848	0.412	0.1719	0.7494	0.2293	72.3	0.8916
18.916	47.608	0.397	0.1698	0.7935	0.2140	71.4	0.9059
19.398	53.450	0.363	0.1727	0.8417	0.2051	72.6	0.9070
20.439	3.664	5.579	0.2252	0.0970	2.3218	93.1	0.3992
20.671	9.873	2.094	0.2241	0.3142	0.7134	94.3	0.7877
24.257	18.820	1.289	0.2254	0.4105	0.5492	94.8	0.7455
26.320	17.759	1.482	0.2291	0.4744	0.4828	96.3	0.8868
27.419	27.419	1.000	0.2267	0.5519	0.4108	95.4	0.8303
31.122	38.102	0.817	0.2277	0.6251	0.3642	95.8	0.7977
29.232	34.631	0.844	0.2239	0.6624	0.3380	94.2	0.8868
32.568	45.410	0.717	0.2266	0.7351	0.3082	95.3	0.8594
31.739	43.925	0.723	0.2231	0.7018	0.2929	93.9	0.9056
35.557	67.527	0.527	0.2265	0.8039	0.2818	95.3	0.7706

TABLE IX (CONT'D)
F-50 ORIFICE DATA
UNIVERSITY OF MICHIGAN
MECHANICAL ENGINEERING DOCTORAL THESIS
ORIFICE DISCHARGE COEFFICIENTS FOR OSCILLATORY FLOW
STEPHEN J. DEREZINSKI

TEST NUMBER= 2470
MINERAL SPIRITS AT TEMPERATURE OF 81.3
SPECIFIC GRAVITY=.7822
VISCOSITY, CENTISTOKES 1.246
ORIFICE DIAMETER IN INCHES=.0497
ORIFICE LENGTH IN INCHES= 0.1837
ORIFICE LENGTH/DIAMETER= 3.6962
CAM DISPLACEMENT=.010000
08:40.57 MAR 31, 1970

PRESSURE DROPS INCHES WATER			FLOWS CU FEET/HOUR			FREQ	COEF
ALT	MEAN	RATIO	ALT	MEAN	RATIO	CPS	
*****	*****	*****	*****	*****	*****	***	*****
2.217	5.650	0.392	0.0472	0.2290	0.2060	14.7	0.7580
2.738	8.658	0.317	0.0431	0.2992	0.1442	13.4	0.8010
3.683	15.715	0.234	0.0431	0.4191	0.1030	13.4	0.8320
3.104	19.957	0.156	0.0407	0.4777	0.0851	12.7	0.8415
3.702	23.447	0.158	0.0425	0.5521	0.0770	13.2	0.8972
3.633	31.141	0.118	0.0415	0.6331	0.0655	12.9	0.8928
7.115	34.843	0.204	0.0427	0.6924	0.0617	13.3	0.9231
3.201	38.969	0.082	0.0422	0.7419	0.0569	13.1	0.9350
8.059	46.046	0.176	0.0427	0.7954	0.0536	13.3	0.9224
5.843	5.843	1.000	0.1194	0.2394	0.4987	37.2	0.7792
7.154	9.043	0.791	0.1225	0.2989	0.4098	38.1	0.7821
8.484	18.665	0.455	0.1207	0.3970	0.3041	37.6	0.7231
7.906	19.244	0.411	0.1124	0.4756	0.2364	35.0	0.8532
8.369	23.447	0.357	0.1200	0.5496	0.2182	37.3	0.8932
8.561	26.725	0.320	0.1202	0.6011	0.1999	37.4	0.9151
8.831	33.358	0.265	0.1202	0.6706	0.1793	37.4	0.9137
10.702	37.697	0.284	0.1232	0.7425	0.1659	38.3	0.9517
12.109	42.575	0.284	0.1220	0.7792	0.1565	38.0	0.9398
13.575	56.459	0.240	0.1218	0.8504	0.1432	37.9	0.8907
10.605	5.515	1.923	0.1768	0.2120	0.8339	55.0	0.7104
12.668	10.003	1.266	0.1731	0.3221	0.5374	53.9	0.8013
13.555	15.985	0.848	0.1775	0.4062	0.4371	55.3	0.7994
14.732	19.745	0.746	0.1803	0.5042	0.3576	56.1	0.8936
16.216	25.780	0.629	0.1770	0.5538	0.3195	55.1	0.8564
17.566	30.871	0.569	0.1777	0.6158	0.2884	55.4	0.8721
17.720	31.835	0.557	0.1764	0.6441	0.2740	54.9	0.8983
18.665	44.156	0.423	0.1768	0.7388	0.2393	55.0	0.8749
17.260	44.118	0.390	0.1734	0.7789	0.2225	54.0	0.9229
20.921	55.244	0.379	0.1734	0.8272	0.2097	54.0	0.8758
15.222	7.848	2.322	0.2302	0.2324	0.9902	71.6	0.6529

TABLE IX (CONT'D)
F-50 ORIFICE DATA
UNIVERSITY OF MICHIGAN
MECHANICAL ENGINEERING DOCTORAL THESIS
ORIFICE DISCHARGE COEFFICIENTS FOR OSCILLATORY FLOW
STEPHEN J. DEREZINSKI

TEST NUMBER= 2470
MINERAL SPIRITS AT TEMPERATURE OF 81.3
SPECIFIC GRAVITY=.7822
VISCOSITY, CENTISTOKES 1.246
ORIFICE DIAMETER IN INCHES=.0497
ORIFICE LENGTH IN INCHES= 0.1837
ORIFICE LENGTH/DIAMETER= 3.6962
CAM DISPLACEMENT=.010000
08:40.57 MAR 31, 1970

PRESSURE DROPS INCHES WATER			FLOWS CU FEET/HOUR			FREQ CPS	COEFF
ALT	MEAN	RATIO	ALT	MEAN	RATIO		
*****	*****	*****	*****	*****	*****	***	*****
19.340	9.853	1.963	0.2314	0.2926	0.7908	72.0	0.7335
21.191	17.335	1.222	0.2351	0.3946	0.5956	73.2	0.7459
20.690	19.726	1.049	0.2345	0.4935	0.4752	73.0	0.8744
21.635	27.458	0.788	0.2351	0.5603	0.4195	73.2	0.8414
22.057	29.637	0.764	0.2344	0.6252	0.3749	72.9	0.9038
22.580	38.854	0.581	0.2382	0.6816	0.3495	74.1	0.8605
23.062	43.115	0.535	0.2340	0.7376	0.3173	72.8	0.8840
25.028	52.949	0.473	0.2376	0.7918	0.3002	74.0	0.8563
23.775	54.280	0.438	0.2309	0.8507	0.2714	71.9	0.9086
23.177	4.204	5.514	0.3064	0.2310	1.3268	95.4	0.8865
30.273	9.950	3.043	0.3101	0.3877	0.7998	96.5	0.9672
34.207	26.417	1.295	0.3203	0.5689	0.5631	99.7	0.8710
32.780	24.758	1.324	0.3132	0.6143	0.4936	94.4	0.9715
35.672	35.672	1.000	0.3144	0.6769	0.4644	97.9	0.8916
35.807	43.906	0.816	0.3133	0.7329	0.4275	97.5	0.8704
39.124	44.523	0.879	0.3140	0.7868	0.3991	97.7	0.9279
40.281	56.159	0.717	0.3127	0.8577	0.3645	97.3	0.9006

CAM DISPLACEMENT=.012900
08:40.57 MAR 31, 1970

PRESSURE DROPS INCHES WATER			FLOWS CU FEET/HOUR			FREQ CPS	COEFF
ALT	MEAN	RATIO	ALT	MEAN	RATIO		
*****	*****	*****	*****	*****	*****	***	*****
34.920	23.929	1.459	0.3379	0.4931	0.6853	91.5	0.7926
37.157	29.714	1.250	0.3369	0.5621	0.5993	91.3	0.8108
39.355	31.295	1.258	0.3393	0.6062	0.5597	91.9	0.8520
41.245	38.969	1.058	0.3446	0.6494	0.5307	93.2	0.8180
44.638	54.781	0.815	0.3038	0.7385	0.4113	73.3	0.7845
43.192	48.457	0.892	0.3411	0.7964	0.4283	92.3	0.8997
46.972	60.778	0.773	0.3442	0.8627	0.3990	93.1	0.8700

TABLE IX (CONT'D)
F-50 ORIFICE DATA
UNIVERSITY OF MICHIGAN
MECHANICAL ENGINEERING DOCTORAL THESIS
ORIFICE DISCHARGE COEFFICIENTS FOR OSCILLATORY FLOW
STEPHEN J. DERLZINSKI

TEST NUMBER= 2470
MINERAL SPIRITS AT TEMPERATURE OF 84.2
SPECIFIC GRAVITY=.7809
VISCOSITY, CENTISTOKES 1.219
ORIFICE DIAMETER IN INCHES=.0497
ORIFICE LENGTH IN INCHES= 0.1837
ORIFICE LENGTH/DIAMETER= 3.6962
CAM DISPLACEMENT=.012900
08:40.57 MAR 31, 1970

PRESSURE DROPS INCHES WATER			FLOWS CU FEET/HOUR			FREQ CPS	COEFF
ALT	MEAN	RATIO	ALT	MEAN	RATIO		
*****	*****	*****	*****	*****	*****	***	*****
2.719	4.184	0.650	0.0636	0.1935	0.3287	15.3	0.7437
2.352	8.176	0.288	0.0661	0.2927	0.2258	15.9	0.8048
4.801	16.641	0.289	0.0568	0.4043	0.1403	13.7	0.7802
3.278	18.588	0.176	0.0571	0.4434	0.1288	13.8	0.8086
4.126	29.463	0.140	0.0578	0.6140	0.0942	14.0	0.8893
8.812	35.344	0.249	0.0549	0.6891	0.0797	13.2	0.9113
6.749	40.686	0.166	0.0531	0.7535	0.0705	12.8	0.9288
9.043	47.261	0.191	0.0554	0.8009	0.0691	13.4	0.9160
9.680	51.059	0.190	0.0549	0.8824	0.0622	13.2	0.9710
5.862	5.662	1.035	0.1451	0.2076	0.6988	35.0	0.6749
8.234	11.589	0.710	0.1658	0.3134	0.5289	40.0	0.7239
10.933	16.563	0.660	0.1683	0.3981	0.4226	40.6	0.7691
12.995	20.131	0.646	0.1725	0.4882	0.3533	41.6	0.8556
14.115	25.084	0.550	0.1728	0.5632	0.3068	41.7	0.8738
14.944	31.642	0.472	0.1724	0.5821	0.2962	41.6	0.8137
15.754	38.458	0.410	0.1782	0.6840	0.2605	43.0	0.8671
16.126	38.959	0.414	0.1705	0.7389	0.2307	41.1	0.9309
19.359	48.784	0.397	0.1856	0.7930	0.2340	44.8	0.8927
14.076	5.206	2.704	0.2492	0.2093	1.1906	60.1	0.7211
17.773	12.688	1.401	0.2544	0.3186	0.7986	61.4	0.7033
20.767	17.990	1.154	0.2557	0.4065	0.6291	61.7	0.7536
22.271	23.891	0.932	0.2557	0.4946	0.5171	61.7	0.7956
25.048	31.835	0.787	0.2537	0.5592	0.4537	61.2	0.7793
24.758	32.047	0.773	0.2574	0.6221	0.4137	62.1	0.8640
26.602	40.956	0.654	0.2594	0.7075	0.3667	62.6	0.8692
28.403	47.569	0.597	0.2527	0.7389	0.3419	61.0	0.8423
28.653	51.252	0.559	0.2524	0.8019	0.3148	60.9	0.8807
23.852	33.069	0.721	0.2596	0.6548	0.3965	62.6	0.8952
21.784	14.963	1.456	0.3316	0.3118	1.0635	80.0	0.6337
34.303	17.528	1.957	0.3385	0.4049	0.8359	81.7	0.7605

TABLE IX (CONT'D)
F-50 ORIFICE DATA
UNIVERSITY OF MICHIGAN
MECHANICAL ENGINEERING DOCTORAL THESIS
ORIFICE DISCHARGE COEFFICIENTS FOR OSCILLATORY FLOW
STEPHEN J. DEREZINSKI

TEST NUMBER= 2470
MINERAL SPIRITS AT TEMPERATURE OF 80.0
SPECIFIC GRAVITY=.7829
VISCOSITY, CENTISTOKES 1.255
ORIFICE DIAMETER IN INCHES=.0497
ORIFICE LENGTH IN INCHES= 0.1837
ORIFICE LENGTH/DIAMETER= 3.6962
CAM DISPLACEMENT=.01970
08:40.57 MAR 31, 1970

PRESSURE DROPS INCHES WATER			FLOWS CU FEET/HOUR			FREQ CPS	COEFF
ALT	MEAN	RATIO	ALT	MEAN	RATIO		
*****	*****	*****	*****	*****	*****	***	*****
4.878	6.807	0.717	0.1180	0.2240	0.5270	18.6	0.6758
5.650	9.198	0.614	0.1107	0.3012	0.3674	17.5	0.7819
6.691	12.938	0.517	0.1086	0.3927	0.2766	17.2	0.8596
7.482	19.699	0.376	0.1086	0.4823	0.2252	17.2	0.8511
8.619	24.255	0.356	0.1075	0.5595	0.1922	17.0	0.8947
8.041	26.861	0.299	0.1058	0.6140	0.1724	16.7	0.9327
8.368	36.405	0.230	0.0955	0.6582	0.1451	15.1	0.8587
9.217	42.344	0.218	0.0966	0.7037	0.1373	15.3	0.8514
6.708	42.633	0.159	0.0819	0.7344	0.1115	12.9	0.8855
8.735	53.894	0.162	0.0930	0.8360	0.1112	14.7	0.8965
14.385	9.294	1.548	0.2583	0.2031	1.3208	42.4	0.5246
16.660	14.307	1.164	0.2756	0.3081	0.8944	43.5	0.6413
20.536	20.536	1.000	0.2736	0.4469	0.6122	43.2	0.7764
23.216	24.643	0.942	0.2710	0.4744	0.5713	42.8	0.7523
24.758	32.703	0.757	0.2685	0.5586	0.4806	42.4	0.7690
27.342	32.394	0.844	0.2826	0.6239	0.4529	44.6	0.8630
29.733	41.303	0.720	0.2734	0.6907	0.4031	44.0	0.8461
32.666	47.145	0.680	0.2830	0.7465	0.3791	44.7	0.8559
32.240	48.360	0.667	0.2770	0.7087	0.3908	43.8	0.8023
32.047	51.098	0.627	0.2743	0.7627	0.3596	43.3	0.8400
34.741	66.408	0.493	0.2743	0.8230	0.3333	43.3	0.7951
27.342	9.641	2.836	0.3978	0.2086	1.9071	62.9	0.5289
34.240	19.244	1.780	0.4060	0.3098	1.3105	64.1	0.5559
35.387	24.585	1.439	0.4032	0.4126	0.9774	63.7	0.6553
37.118	29.174	1.272	0.3917	0.4921	0.7960	61.9	0.7172
38.815	33.570	1.156	0.3794	0.5581	0.6798	59.9	0.7583
38.642	34.901	1.107	0.3797	0.5831	0.6512	60.0	0.7771
40.435	44.021	0.919	0.3731	0.6753	0.5526	59.0	0.8014
39.162	46.046	0.851	0.3699	0.7251	0.5101	58.4	0.8412
43.809	51.214	0.855	0.3717	0.8059	0.4612	58.7	0.8866

TABLE IX (CONT'D)
F-50 ORIFICE DATA
UNIVERSITY OF MICHIGAN
MECHANICAL ENGINEERING DOCTORAL THESIS
ORIFICE DISCHARGE COEFFICIENTS FOR OSCILLATORY FLOW
STEPHEN J. DEREZINSKI

TEST NUMBER= 2470
MINERAL SPIRITS AT TEMPERATURE OF 80.0
SPECIFIC GRAVITY=.7829
VISCOSITY, CENTISTOKES 1.258
ORIFICE DIAMETER IN INCHES=.0497
ORIFICE LENGTH IN INCHES= 0.1837
ORIFICE LENGTH/DIAMETER= 3.6962
CAM DISPLACEMENT=.019700
08:40.57 MAR 31, 1970

PRESSURE DROPS INCHES WATER			FLOWS CU FEET/HOUR			FREQ CPS	COEFF
ALT	MEAN	RATIO	ALT	MEAN	RATIO		
*****	*****	*****	*****	*****	*****	***	*****
54.241	68.086	0.797	0.3746	0.8281	0.4524	59.2	0.7901
41.534	5.322	7.804	0.4797	0.1891	2.5364	75.8	0.6454
43.212	11.293	3.857	0.4779	0.2820	1.6947	75.5	0.6633
45.506	22.620	2.067	0.4678	0.3728	1.2548	73.9	0.6255
49.073	28.287	1.735	0.4791	0.4598	1.0420	75.7	0.6806
53.161	37.041	1.435	0.4834	0.5458	0.8947	77.2	0.7061
52.795	43.899	1.205	0.4813	0.6402	0.7519	76.1	0.7615
53.040	47.049	1.234	0.4737	0.6307	0.7591	75.6	0.7238
58.078	49.478	1.174	0.4734	0.7089	0.6678	74.8	0.7934
58.001	55.649	1.042	0.4737	0.7412	0.6459	75.6	0.7822
67.584	76.493	0.884	0.4895	0.8620	0.5679	77.3	0.7759

TABLE X
ORIFICE DATA, L/D = 7.23
UNIVERSITY OF MICHIGAN
MECHANICAL ENGINEERING DOCTORAL THESIS
ORIFICE DISCHARGE COEFFICIENTS FOR OSCILLATORY FLOW
STEPHEN J. DEREZINSKI

TEST NUMBER= 777C
MINERAL SPIRITS AT TEMPERATURE OF 89.1
SPECIFIC GRAVITY=.7786
VISCOSITY, CENTISTOKES 1.177
ORIFICE DIAMETER IN INCHES=.0518
ORIFICE LENGTH IN INCHES= 0.3745
ORIFICE LENGTH/DIAMETER= 7.2297
CAM DISPLACEMENT=.CC75OC
11:41.53 JUL 30, 197C

PRESSURE DROPS INCHES WATER			FLOWS CU FEET/HOUR			FREQ CPS	COEFF
ALT	MEAN	RATIO	ALT	MEAN	RATIO		
*****	*****	*****	*****	*****	*****	***	*****
28.969	5.395	5.369	C.2C83	C.2392	C.8708	86.5	0.7444
28.3C5	21.084	1.343	C.1969	C.4897	C.4021	81.7	0.7708
36.6C6	33.701	1.C86	C.2114	0.6575	C.3215	87.7	C.8186
44.243	66.738	C.663	C.21C4	C.8426	C.2497	87.3	0.7454
2.181	5.292	C.412	C.C617	C.2271	C.2717	25.6	0.7136
5.549	21.C72	C.263	C.C629	0.4596	C.1368	26.1	0.7236
8.227	41.070	C.200	C.C64C	C.6662	0.096)	26.5	0.7513
9.478	62.719	C.151	C.C641	0.8C37	C.0798	26.6	0.7334
10.C23	7.457	1.344	C.1310	C.2543	C.5153	54.4	0.6729
9.638	21.826	0.442	0.1332	C.4842	C.2751	55.3	0.7491
12.268	41.551	0.295	0.1342	C.6466	C.2076	55.7	0.7250
15.251	6C.314	0.253	C.137C	C.8228	0.1665	56.9	0.7657

CAM DISPLACEMENT=.C1CCOC
11:41.53 JUL 30, 197C

PRESSURE DROPS INCHES WATER			FLOWS CU FEET/HOUR			FREQ CPS	COEFF
ALT	MEAN	RATIO	ALT	MEAN	RATIO		
*****	*****	*****	*****	*****	*****	***	*****
3.824	4.853	C.788	C.C827	C.2159	C.3832	25.7	0.7083
8.388	18.672	0.449	C.C839	C.4491	0.1868	26.1	0.7511
8.227	40.621	0.2C3	C.C835	C.6480	C.1289	26.0	0.7348
12.655	66.170	C.194	C.0833	C.8C28	0.1038	25.9	C.7133
12.373	2.378	5.2C3	C.1795	C.2238	0.802C	55.9	1.0491
15.988	22.576	C.708	C.1836	C.4661	0.3939	57.1	0.7090
17.643	39.175	C.45C	C.18C1	C.6466	C.2786	56.1	0.7466
2C.262	66.765	C.3C3	0.1819	C.8142	0.2234	56.6	C.7202
43.184	12.418	3.477	C.2865	C.2231	1.2842	89.2	0.4576
46.269	21.913	2.112	C.2836	C.4774	0.5940	88.3	0.7371
51.677	42.463	1.217	C.2833	C.6536	C.4335	88.2	0.7249
56.CC3	67.541	C.829	C.2849	C.8215	C.3469	88.7	0.7224

TABLE X (CONT'D)
ORIFICE DATA, L/D = 7.23
UNIVERSITY OF MICHIGAN
MECHANICAL ENGINEERING DOCTORAL THESIS
ORIFICE DISCHARGE COEFFICIENTS FOR OSCILLATORY FLOW
STEPHEN J. CEREZINSKI

TEST NUMBER= 777C
MINERAL SPIRITS AT TEMPERATURE OF 89.0
SPECIFIC GRAVITY=.7787
VISCOSITY, CENTISTOKES 1.178
ORIFICE DIAMETER IN INCHES=.0518
ORIFICE LENGTH IN INCHES= C.3745
ORIFICE LENGTH/DIAMETER= 7.2297
CAM DISPLACEMENT=.C120CC
11:41.53 JUL 30, 197C

PRESSURE DROPS INCHES WATER			FLOWS CU FEET/HOUR			FREQ CPS	COEFF
ALT	MEAN	RATIO	ALT	MEAN	RATIO		
*****	*****	*****	*****	*****	*****	***	*****
3.876	6.730	0.576	C.C857	C.2715	C.3303	23.3	0.7565
9.313	22.271	0.418	C.C849	C.4666	0.1819	22.0	0.7147
8.561	33.320	C.257	C.C843	C.6568	0.1283	21.9	0.8225
10.220	66.587	0.153	C.C831	C.8584	C.0968	21.6	0.7560
13.363	4.261	3.136	C.1953	0.2282	0.8559	50.7	0.7990
18.125	22.136	0.819	C.194C	C.4618	C.4201	50.3	0.7094
17.354	35.595	C.488	C.1918	C.6464	0.2967	49.8	C.7631
19.089	64.557	0.296	C.1912	0.8095	0.2362	49.6	0.7282
50.078	11.681	4.338	0.337C	C.2482	1.3578	87.4	0.5249
97.238	22.194	2.579	C.3441	C.4856	C.7085	89.2	0.7451
62.225	31.404	1.981	0.3457	C.6441	0.5366	89.7	0.8308
72.064	48.791	1.477	0.3535	0.8217	C.4302	91.7	0.8503

CAM DISPLACEMENT=.C19CC0
11:41.53 JUL 30, 197C

PRESSURE DROPS INCHES WATER			FLOWS CU FEET/HOUR			FREQ CPS	COEFF
ALT	MEAN	RATIO	ALT	MEAN	RATIO		
* *****	*****	*****	*****	*****	*****	***	*****
84.902	12.413	6.840	C.5254	C.2444	2.1500	86.1	0.5014
87.055	27.805	3.131	0.5107	C.5198	C.9825	83.7	0.7126
100.626	39.224	2.565	C.5117	C.6775	C.7553	83.8	0.7819
107.908	56.271	1.918	C.5223	C.8270	0.6316	85.6	0.7968
13.381	10.496	1.275	C.1752	C.2862	0.6122	28.7	C.6386
20.246	47.529	0.426	0.1775	C.6799	C.2610	29.1	0.7129
22.261	72.206	C.308	C.1793	C.8280	0.2165	29.4	0.7043
24.677	9.488	2.601	0.3320	C.2782	1.1931	54.4	0.6529
29.612	20.645	1.434	C.3414	C.4644	0.7352	55.9	C.7388
38.475	48.555	C.792	C.3416	C.6689	C.5107	56.0	0.6938
42.420	67.167	0.632	0.3384	C.8116	C.4169	55.4	0.7158

TABLE XI
ORIFICE DATA, L/D = 3.63

UNIVERSITY OF MICHIGAN
MECHANICAL ENGINEERING DOCTORAL THESIS
ORIFICE DISCHARGE COEFFICIENTS FOR OSCILLATORY FLOW
STEPHEN J. DEREZINSKI

TEST NUMBER= 7E7C1
MINERAL SPIRITS AT TEMPERATURE OF 75.8
SPECIFIC GRAVITY=.7843
VISCOSITY, CENTISTOKES 1.300
ORIFICE DIAMETER IN INCHES=.0518
ORIFICE LENGTH IN INCHES= 0.1880
ORIFICE LENGTH/DIAMETER= 3.6293
CAM DISPLACEMENT=.CC75CC
11:41.53 JUL 30, 197C

PRESSURE DROPS INCHES WATER			FLOWS CU FEET/HOUR			FREQ CPS	COEFF
ALT	MEAN	RATIO	ALT	MEAN	RATIO		
*****	*****	*****	*****	*****	*****	***	*****
2.409	4.234	C.569	C.C614	C.1884	C.3261	25.5	C.6643
3.957	13.963	C.283	C.C613	C.4CC6	C.1531	25.4	C.7780
6.643	21.549	C.3C8	C.C612	C.5952	C.1028	25.4	C.9304
5.854	5C.C19	C.117	C.C612	C.7845	C.C780	25.4	C.8050

CAM DISPLACEMENT=.CC75CC
11:41.53 JUL 30, 197C

PRESSURE DROPS INCHES WATER			FLOWS CU FEET/HOUR			FREQ CPS	COEFF
ALT	MEAN	RATIO	ALT	MEAN	RATIO		
*****	*****	*****	*****	*****	*****	***	*****
6.47C	4.026	1.6C7	C.1293	C.1884	C.6863	53.7	C.6815
8.553	15.884	C.538	C.1284	C.4028	C.3189	53.3	C.7333
9.534	3C.8C6	C.3C9	C.1322	C.5996	C.2205	54.9	C.7840
11.397	51.617	C.221	C.13CC	C.7732	C.1681	53.9	C.7810
18.227	15.824	1.152	C.19C6	C.4C1C	C.4753	79.1	C.7316
23.996	35.453	C.677	C.1959	C.6C56	C.3234	81.3	C.7380
28.142	53.5CC	C.526	C.1944	C.7710	C.2522	8C.7	C.7649

CAM DISPLACEMENT=.C185CC
11:41.53 JUL 30, 197C

PRESSURE DROPS INCHES WATER			FLOWS CU FEET/HOUR			FREQ CPS	COEFF
ALT	MEAN	RATIO	ALT	MEAN	RATIO		
*****	*****	*****	*****	*****	*****	***	*****
5.769	5.048	1.143	C.1467	C.1942	C.7553	24.7	C.6273
8.953	13.841	C.647	C.1481	C.4C75	C.3635	24.9	C.7950
15.163	33.991	C.446	C.1515	C.6217	C.2399	25.5	C.7864
18.5C8	51.396	C.36C	C.1519	C.7898	C.1923	25.5	C.7996
16.204	4.346	3.728	C.3188	C.1923	1.658C	53.6	C.6694
23.435	17.586	1.333	C.3168	C.4C86	C.7753	53.3	C.7073
27.281	33.33C	C.819	C.3192	C.5989	C.5330	53.7	C.7530
29.464	52.418	C.562	C.3C28	C.7923	C.3822	5C.9	C.7942
8C.86C	54.461	1.485	C.5C36	C.8CC4	C.6291	84.7	C.7872

TABLE XI (CONT'D)
ORIFICE DATA, L/D = 3.63
UNIVERSITY OF MICHIGAN
MECHANICAL ENGINEERING DOCTORAL THESIS
ORIFICE DISCHARGE COEFFICIENTS FOR OSCILLATORY FLOW
STEPHEN J. CEREZINSKI

TEST NUMBER= 7E7C1
MINERAL SPIRITS AT TEMPERATURE OF 77.5
SPECIFIC GRAVITY=.7841
VISCOSITY, CENTISTOKES 1.283
ORIFICE DIAMETER IN INCHES=.0518
ORIFICE LENGTH IN INCHES= 0.1880
ORIFICE LENGTH/DIAMETER= 3.6293
CAM DISPLACEMENT=.C12CCC
11:41.53 JUL 30, 197C

PRESSURE DROPS INCHES WATER			FLOWS CU FEET/HOUR			FREQ CPS	COEFF
ALT	MEAN	RATIO	ALT	MEAN	RATIO		
*****	*****	*****	*****	*****	*****	***	*****
3.999	4.217	C.948	C.C979	C.1917	C.5109	25.4	0.6771
5.983	12.949	C.462	C.C991	C.4CC1	C.2476	25.7	0.8065
8.56C	31.865	C.269	C.1063	C.6010	0.1768	27.6	0.7722
1C.C75	48.563	0.207	C.1C75	C.7766	C.1384	27.9	0.8083
9.C6C	3.936	2.302	0.2C75	C.1923	1.C789	53.8	0.7030
13.C74	17.104	0.764	C.2182	C.4182	C.5218	56.6	0.7333
13.043	29.413	C.443	C.1935	C.5759	0.3360	5C.2	0.7702
2C.15C	51.C47	0.395	0.2C9C	C.7829	C.2670	54.2	0.7947
32.381	13.511	2.397	C.3C74	C.4188	C.7341	79.7	0.8263
39.441	33.818	1.166	C.3C43	C.6213	0.4898	78.9	0.7748
45.533	49.938	C.912	C.31C9	C.8C19	C.3878	80.7	0.8230

CAM DISPLACEMENT=.C10000
11:41.53 JUL 30, 197C

PRESSURE DROPS INCHES WATER			FLOWS CU FEET/HOUR			FREQ CPS	COEFF
ALT	MEAN	RATIO	ALT	MEAN	RATIO		
*****	*****	*****	*****	*****	*****	***	*****
2.702	5.014	C.539	C.C873	C.2C29	C.4302	27.2	0.6569
4.374	16.714	C.262	C.C874	C.4333	C.2017	27.2	C.7683
4.592	30.147	C.152	C.C885	C.6148	0.1446	27.7	0.8117
5.496	53.202	C.103	0.C797	0.7911	C.1007	24.8	0.7863
9.950	5.483	1.815	C.1877	C.1927	C.9743	58.4	0.5966
14.839	17.932	C.828	0.1864	C.4393	C.4244	58.0	0.7521
2C.759	34.349	C.604	C.1945	C.6181	0.3147	6C.5	0.7646
19.6C3	54.749	C.358	C.1867	C.7666	C.2436	58.1	0.7511
19.447	5.1C8	3.8C7	C.27C6	C.1857	1.4571	84.2	0.5958
27.273	15.152	1.800	C.2721	C.4286	0.6348	84.7	C.7983
35.614	3C.834	1.155	C.2827	C.6246	C.4526	88.0	0.8155
42.C49	48.672	C.864	C.2785	C.7665	0.3633	86.7	0.7965

TABLE XII
ORIFICE DATA, L/D = 0.62
UNIVERSITY OF MICHIGAN
MECHANICAL ENGINEERING DOCTORAL THESIS
ORIFICE DISCHARGE COEFFICIENTS FOR OSCILLATORY FLOW
STEPHEN J. DEBEZIASKI

TEST NUMBER= 78702
MINERAL SPIRITS AT TEMPERATURE OF 75.2
SPECIFIC GRAVITY=.7852
VISCOSITY, CENTISTOKES 1.306
ORIFICE DIAMETER IN INCHES=.0518
ORIFICE LENGTH IN INCHES= 0.0319
ORIFICE LENGTH/DIAMETER= 0.6158
CAM DISPLACEMENT=.CC75CC
11:41.53 JUL 30, 197C

PRESSURE DROPS INCHES WATER			FLOWS CU FEET/HOUR			FREQ CPS	COEFF
ALT	MEAN	RATIO	ALT	MEAN	RATIO		
*****	*****	*****	*****	*****	*****	***	*****
2.471	3.929	C.629	C.0629	0.2022	0.3113	26.1	0.7404
5.455	20.205	0.271	C.0637	C.4476	0.1424	26.5	0.7216
6.237	38.5C4	C.162	C.0637	C.6362	C.1001	26.4	0.7441
10.733	63.332	0.169	C.0664	C.8C90	0.0821	27.6	0.7378
6.251	6.251	1.COC	0.1277	C.2052	0.6224	53.0	0.5957
8.249	14.594	C.565	C.1225	C.4060	C.3017	5C.8	0.7713
10.666	40.C7U	0.266	C.1272	C.6187	C.2056	52.8	0.7094
14.621	58.769	0.249	C.1263	0.7761	0.1627	52.4	0.7348
19.104	25.773	C.741	C.2C63	C.41C8	C.5023	85.6	0.5873
25.976	43.446	C.598	C.2C92	C.6223	0.3362	86.8	0.6853
34.792	66.976	C.5C4	C.21C3	C.7781	C.2702	87.3	0.6800

CAM DISPLACEMENT=.C1CCCC
11:41.53 JUL 30, 197C

PRESSURE DROPS INCHES WATER			FLOWS CU FEET/HOUR			FREQ CPS	COEFF
ALT	MEAN	RATIO	ALT	MEAN	RATIO		
*****	*****	*****	*****	*****	*****	***	*****
2.984	4.442	C.672	C.C819	C.1879	C.4357	25.5	C.6471
6.8C4	13.933	C.488	C.C821	C.4C77	0.2015	25.6	0.7928
8.911	37.478	C.238	0.C818	C.61C8	0.1339	25.5	0.7241
9.923	59.12C	0.168	C.C811	C.7853	C.1033	25.3	C.7412
6.737	6.737	1.CUC	C.1766	C.2642	0.6684	55.0	0.7387
11.435	17.619	0.649	0.1792	C.4219	C.4249	55.8	0.7294
15.728	39.CC4	C.403	C.18C2	C.6CE7	C.296C	56.1	0.7074
21.C75	59.876	C.352	C.1768	C.7640	C.2314	55.0	0.7166
29.225	4C.57C	C.72C	C.2774	C.5789	0.4792	86.3	0.6596
41.758	66.49C	C.61C	C.2779	C.7912	C.3512	86.5	0.6938

TABLE XII (CONT'D)
ORIFICE DATA, L/D = 0.62

UNIVERSITY OF MICHIGAN
MECHANICAL ENGINEERING DOCTORAL THESIS
ORIFICE DISCHARGE COEFFICIENTS FOR OSCILLATORY FLOW
STEPHEN J. DEREZINSKI

TEST NUMBER= 787C2
MINERAL SPIRITS AT TEMPERATURE OF 75.5
SPECIFIC GRAVITY=.7851
VISCOSITY CENTISTOKES 1.303
ORIFICE DIAMETER IN INCHES=.0518
ORIFICE LENGTH IN INCHES= 0.0319
ORIFICE LENGTH/DIAMETER= 0.6158
CAM DISPLACEMENT=.C185CC
11:41.53 JUL 3C, 197C

PRESSURE DROPS INCHES WATER			FLOWS CU FEET/HOUR			FREQ CPS	COEFF
ALT	MEAN	RATIO	ALT	MEAN	RATIO		
*****	*****	*****	*****	*****	*****	***	*****
6.786	7.944	C.854	C.1588	C.1980	0.8017	26.7	0.5099
12.785	21.060	C.6C7	C.1485	C.4274	0.3474	25.0	0.6758
15.555	4C.838	C.382	0.1437	C.6317	0.2275	24.2	0.7174
16.757	54.616	C.3C7	C.15C4	C.7839	0.1919	25.3	C.7698
14.171	11.027	1.285	0.3117	C.1939	1.6076	52.4	0.4238
22.55C	25.984	C.868	C.3183	C.4111	0.7743	53.6	0.5853
25.281	35.955	C.7C3	C.3173	C.5925	0.5355	53.4	C.7171
34.487	69.1CC	0.499	C.3356	C.7731	C.4341	56.5	0.6747
66.477	66.477	1.CCC	C.51C3	C.5983	C.8529	85.9	C.5247
71.539	83.496	C.857	C.5026	C.7787	C.6455	84.6	0.6134

CAM DISPLACEMENT=.C12CCC
11:41.53 JUL 3C, 197C

PRESSURE DROPS INCHES WATER			FLOWS CU FEET/HOUR			FREQ CPS	COEFF
ALT	MEAN	RATIO	ALT	MEAN	RATIO		
*****	*****	*****	*****	*****	*****	***	*****
3.827	5.275	C.725	C.C972	C.1984	C.4900	25.2	0.6267
8.71C	18.888	C.461	C.C979	C.41C9	C.2384	25.4	0.6861
9.268	37.114	C.25C	C.C990	C.6254	C.1583	25.7	C.7450
12.744	55.899	C.228	0.C965	C.7745	C.1245	25.0	C.7517
12.CC1	7.592	1.589	C.C272	C.1948	0.1394	7.C	C.5131
19.881	21.371	C.93C	C.2654	C.4048	0.6555	68.8	0.6355
31.983	45.679	C.7CC	C.2727	C.6CC8	C.4539	70.7	C.6450
3C.886	65.914	C.528	C.2657	C.7825	C.3396	68.9	0.6791
46.696	52.746	C.885	C.3505	C.6C42	C.58C2	90.9	C.6037
51.724	66.52C	C.773	C.3470	C.7587	C.4573	90.0	0.6730

APPENDIX C

LISTING OF MAIN PROGRAM AND SUBROUTINES

MAIN	
FLOW2	Steady-State Solution
TFLOW	Transient Solution
FRIC	Friction Factors
OVAL	Quality of Fluid in Each Element
CDMEAN	Coefficient of Discharge, F-50 Orifice
CDSQ	Coefficient of Discharge, Square-Edged Orifices for Pulsating Head
CDSS	Coefficient of Discharge, Square-Edged Orifices for Steady Flow
FPROP	Fluid Properties
CI	Parabolic Interpolation of Tabular Points

```
            INTEGER*2 X
            REAL*8 L
            DOUBLE PRECISION VISCF,VISCA,PG,PT,PZ,RJ,DR,FL,CSH,CSG,PDROP,
           1RI,PV,AA,F,FA,FB,V,AR,CD,F2
            DOUBLE PRECISION D,A,RLD,RE,FT,CS,RHC,RHOA,VR,VISC,RHOF,DP,DZ,
           1FLO,HP,TOLP,PPOT
            NAMELIST/DIN/X,D,L,NELS,    CS,JT,NL,LT,JO,RJ,FT,F2/
           1DIN2/ELZER,PBAR ,PZ,NPOINT,NDIV,NCYC,PT,CSG,G,T,NFLO,ISOL,NSPACE,
           2ITP,NJUNC
            DIMENSION PG(50),PI(50),PDROP(50),FL(50),PZ(50),RE(50),RJ(50),
           1CSG(2),AR(50),F(50),FA(50),FB(50),DR(50),CD(50),V(50)
            COMMON X(750),L(50),D(50),A(50),RLD(50),RL(50),FT(50),JT(50),
           1JO(50),CS(2,50),LT(50),RHO(50),RHOA(50),NL(50),VR(50),
           2VISC(50),RHOF,DP(50),DZ(50),FLO(50),HR(50),TR,NELS,AA(2500),NJUNC
            COMMON/DIMP/PV(50,3),RHOT(50,2),XJ(50,50),PB(50,50),J1(50),J2(50)
            COMMON/DATA/TOLP,LIM,ITIME
            LIM=10
            LPT=10
            TOLP=1.
            READ(5,DIN)
   13       DO 5 I=1,50
            DO 5 II=1,50
    5       PB(I,II)=0.
            READ(5,DIN2,END=99)
            NJUNC=NELS+1
            NP1=NPOINT+1
            PBAR=PBAR*144.
            DO 4 I=1,NJUNC
            IF(JT(I).EQ.0) GO TO 4
            DO 4 J=1,NPOINT
            XJ(I,J)=PB(J,I)*144.
    4       CONTINUE
            DO 7 I=1,NJUNC
            IF(JT(I).EQ.0) GO TO 7
            DO 6 II=1,NPOINT
    6       PB(I,II+1)=XJ(I,II)+PBAR
            PB(I,1)=XJ(I,NPOINT)+PBAR
    7       CONTINUE
      C
      C
      C     FIND THE JUNCTIONS AT THE ENDS OF EACH ELEMENT
      C
            I=1
            DO 80 J=1,NJUNC
            IF(JT(J).NE.0) GO TO 80
            NUMLS=NL(J)
            DO 79 K=1,NUMLS
            LNUM=X(I-1+2*K)
            J1(LNUM)=J0(LNUM)
            J2(LNUM)=X(I+2*K)
   79       IF(J2(LNUM).EQ.J1(LNUM)) J2(LNUM)=J
   80       I=I+1+2*NL(J)
            TR=T+459.69
            [illegible]=2.[illegible]/(1545.*32.174*TR)
            CALL [illegible](NFLO,1,SG,VF)
```

```
      CALL FPROP(8,T,SGA,VA)
      RHOF=SGF*1.939
      VISCF=VF*.00001076
      VISCA=VA*.00001076
      PG(1)=PT(1)*144.
      PZ(1)=0.
      DO 100 I=2,NJUNC
      LL=I-1
      HP(LL)=0.
      RLP(LL)=L(LL)/D(LL)
      PG(I)=PT(I)*144.
      DP(I)=0.
      IF(JT(I).NE.0) DP(I)=(PT(I)-PT(1))*144.
      FL(I)=0.
      CSH=CSG(1)*CS(1,LL)+CSG(2)*CS(2,LL)+CSG(3)*CS(3,LL)
  100 PZ(LL)=L(LL)*CSH*G/12.
      DO 10 J=1,NJUNC
      D(J)=D(J)/12.
      A(J)=D(J)*D(J)*.7854
      L(J)=L(J)/12.
   10 PT(J)=PT(J)*144.
      CALL FLOW2(PG,PT,PZ,FL,RJ,PDROP,RL,III ,VISCA,VISCF)
   30 DO 20 K=1,LFT
      WRITE(6,14) ITIME
      CALL FRIC(F,FA,FB,V,AR,CD,RL,VISCF,F2)
      CALL FLOW2(PG,PT,PZ,FL,RJ,PDROP,RL,III ,VISCA,VISCF)
      IF(ITIME.EQ.1) K=LFT+1
   20 CONTINUE
      WRITE(6,9)
    9 FORMAT(1H1,30X,'JUNCTIONS')
      WRITE(6,15)
      WRITE(6,16)
   15 FORMAT(1H0,6X,'PRESSURE, LB/SQ-IN',18X,'FLOW, LB/HR')
   16 FORMAT(2X,'J',2X,'TOTAL',4X,'GRADE',3X,'HEAD',7X,
     1'TOTAL',6X,'AIR',5X,'FUEL',4X,'AIR/TOT')
   14 FORMAT(1H0,'ITERATIONS IN FLOW2 ARE 'I4)
      DO 11 J=1,NJUNC
      IF(J.EQ.26) WRITE(6,9)
      IF(J.EQ.26) WRITE(6,15)
      IF(J.EQ.26) WRITE(6,16)
      PV(J,1)=PT(J)
      PV(J,2)=PT(J)
      PV(J,3)=PT(J)
      FLT=FL(J)*3600.*32.174
      FLA=RJ(J)*FLT
      FLF=(1.-RJ(J))*FLT
      P1=PT(J)/144.
      P2=PG(J)/144.
      P3=PZ(J)/144.
   11 WRITE(6,12) J,P1,P2,P3,FLT,FLA,FLF,RJ(J)
   12 FORMAT(1H0,I2,1X,2(F8.3,1X),F8.5,1X,3(F7.5,1X),F8.6)
      WRITE(6,19)
      WRITE(6,22)
      WRITE(6,23)
   19 FORMAT(1H1,41X,'ELEMENTS'/)
```

```
  22   FORMAT('1',1X,'DIFFERENTIAL',2X,'PRESS',9X,
      1'FLOW, LB/HR',14X,'DP',5X,'FRICT',4X,'DENSITY',4X,'VOLUME')
  23   FORMAT(3X,'DIAM.',1X,'LENGTH',2X,'DROP',4X,'TOTAL',
      14X,'AIR',5X,'FUEL',1X,'AIR/TOT',3X,'NUM',12X,'LB/CU-FT',4X,'RATIO
      2')
       DO 25 J=1,NELS
       IF(J.EQ.1) WRITE(6,19)
       IF(J.EQ.26) WRITE(6,22)
       IF(J.EQ.26) WRITE(6,23)
       I1=J1(J)
       I2=J2(J)
       PDOT(J,1)=(1.-V2(J))*PAIR+V2(J)*SCON*PT(I1)
       PDOT(J,2)=(1.-V2(J))*PAIR+V2(J)*SCON*PT(I2)
       X1=D(J)*12.
       X2=L(J)*12.
       X3=PDROP(J)/144.
       X4=FLO(J)*3600.*32.174
       X5=X4*PI(J)
       X6=X4*(1.-PI(J))
       X7=RHO(J)*32.174
  25   WRITE(6,21)J,X1,X2,X3,X4,X5,X6,PI(J),RE(J),FT(J),X7,VR(J)
  21   FORMAT(1H0,I2,1X,2(F5.3,1X),F7.5,1X,2F8.4,F7.3,F7.4,
      1F7.0,1X,F7.3,F10.4,F10.3)
       IF(ISOL.EQ.0) GO TO 13
       CALL TFLOW(NPOINT,NDIV,NCYC,FREQ,ITP ,NSPACE)
       WRITE(6,40)(HR(I),I=1,NELS)
  40   FORMAT(1H ,(1H ,5F10.6)/)
  41   FORMAT(1H0,'PRESSURE, PSI, AT JUNCTION ',I2)
  42   FORMAT(1H0,'MASS FLOW, LB/HR, IN ELEMENT 'I2)
       ISOL=0
       GO TO 30
  99   CALL SYSTEM
       END
```

TOTAL MEMORY REQUIREMENTS 002858 BYTES

```
FORTRAN IV G COMPILER        FLOW2          09-25-71        12:08.31        PAGE 000

0001                 SUBROUTINE FLOW2(PG,PT,PZ,FL,RJ,PDROP,RL,III,VISCA,VISCF)
0002                 INTEGER X
0003                 REAL*8 L
0004                 DOUBLE PRECISION D,A,RID,RE,FT,CS,RHO,RHOA,VR,VISC,RHOF,DP,DZ,
                    1FLO,HR,TOLP
0005                 DOUBLE PRECISION PRESS,DPZ,B,R,AA,EP,AX,PGJ,PZJ,DR,SUM,FLOIN
0006                 DOUBLE PRECISION PG,PT,PZ,FL,RJ,PDROP,RL,VISCA,VISCF
0007                 DIMENSION PG(50),PT(50),PDROP(50),FL(50),PZ(50),RL(50),
                    1RJ(50),DR(50),B(50),R(50,50),DPZ(50)
0008                 COMMON X(750),L(50),Z(50),A(50),RID(50),RE(50),FT(50),JT(50),
                    1JG(50),CS(3,50),LI(50),RHO(50),RHOA(50),MI(50),VR(50),
                    2VISC(50),RHOF,DP(50),DZ(50),FLO(50),HR(50),TR,NELS,AA(2500),NJUNC
0009                 COMMON/DATA/TOLP,LIM,ITIME
0010                 ITIME=0
0011                 DO 1000 IV=1,LIM
0012                 DO 5 II=1,2500
0013               5 AA(II)=0.
0014                 DO 6 II=1,50
0015               6 B(II)=0.
0016                 ITIME=ITIME+1
0017                 ITRY=0
                C
                C
                C    CALCULATE THE DENSITY AND VISCOSITY IN EACH OF THE ELEMENTS
                C    ***********************************************************
0018                 I=4
0019                 DO 130 II=2, NJUNC
0020                 NUMLS=NL(II)
0021                 IF(JT(II).NE.0) GO TO 130
0022                 DO 129 J=1,NUMLS
0023                 LNUM=X(I-1+2*J)
0024                 JATOE=X(I+2*J)
0025                 PRESS=2000.
0026                 IF(IV.EQ.1) PDROP(LNUM)=PG(JATOE)-PG(II)
0027                 RHOA(LNUM)=PRESS/(53.34*TR*32.174)
0028                 RL(LNUM)=RJ(II)
0029                 IF(PG(JATOE).GT.PG(II)) RL(LNUM)=RJ(JATOE)
0030                 VR(LNUM)=RL(LNUM)*RHOF/(RL(LNUM)*RHOF+RHOA(LNUM)*(1.-RL(LNUM)))
0031                 RHO(LNUM)=RHOA(LNUM)*VR(LNUM)+(1.-VR(LNUM))*RHOF
0032                 VISC(LNUM)=VR(LNUM)*VISCA+(1.-VR(LNUM))*VISCF
0033                 DPZ(LNUM)=RHO(LNUM)*LZ(LNUM)
0034             129 CONTINUE
0035             130 I=I+1+2*NUMLS
                C
                C
                C    SET UP THE MATRIX OF EQUATIONS FOR CONTINUITY AT EACH INTERIOR JUI
                C    ******************************************************************
0036                 I=4
0037                 DO 20 J=1,NELS
0038                 B(J)=DP(J+1)
0039                 NUMLS=NL(J+1)
0040                 DO 19 LL=1,NELS
0041                 R(J,II)=0.
0042                 DO 17 J1=1,NUMLS
0043                 LNUM=X(I-1+2*J1)
```

```
FORTRAN IV G COMPILER        FLOW2          09-25-71        12:08.31        PAGE 000.

0044                  IF(II.NE.LNUM) GO TO 17
0045                  JATOE=X(I+2*J1)
0046             9    R(J,LL)=DSQRT(DABS(PDROP(LL)))
0047                  IF(X(I+2*J1).NE.JO(LNUM)) R(J,LL)=-R(J,LL)
0048                  IF(J1(J+1).NE.0) GO TO 16
0049                  IF(FI(LNUM).GT.100.) FI(LNUM)=100.
0050                  R(J,LL)=A(LNUM)*DSQRT(DABS(2.*RHO(LNUM)/FI(LNUM)))
0051                  IF(JO(LNUM).EQ.J+1) R(J,LL)=-R(J,LL)
0052            16    J1=NUMLS
0053            17    CONTINUE
0054            19    AA((II-1)*NELS+J)=R(J,LL)
0055            20    I=I+1+2*NUMLS
                C
                C
                C     SOLVE THE MATRIX FOR THE ELEMENT PRESSURE DROPS
                C     ***********************************************
0056                  CONS=.0000001
0057                  CALL DGELG(B,AA,NELS,1,CONS,IER)
0058                  DO 30 LL=1,NELS
0059                  EP=DABS(PDROP(LL))-DABS(B(LL)*B(LL))
0060                  IF(EP.GT.TOLP) LIMY=1
0061            30    PDROP(LL)=B(LL)*DSQRT(DABS(PDROP(LL)))
                C
                C
                C     SOLVE FOR FLOWS THROUGH ELEMENTS AND OUT OF JUNCTIONS
                C     *****************************************************
0062                  I=4
0063                  DO 40 II=2,NJUNC
0064                  NUMLS=NL(II)
0065                  IF(J1(II).GT.0) GO TO 40
0066                  DO 41 J=1,NUMLS
0067                  LNUM=X(I-1+2*J)
0068                  AX=1.
0069                  IF(JO(LNUM).EQ.II) AX=-1.
0070                  FLO(LNUM)=AX*R(II-1,LNUM)*B(LNUM)
0071                  IF(FLO(LNUM).EQ.0.) PDROP(LNUM)=0.
0072            41    CONTINUE
0073            40    I=I+1+2*NUMLS
                C
                C
                C     CALCULATE THE PRESSURE AT EACH JUNCTION
                C     ***************************************
0074                  LNUM=X(2)
0075                  FI(1)=-DABS(FLO(LNUM))
0076                  I=4
0077                  DO 50 II=2,NJUNC
0078                  NUMLS=NL(II)
0079                  IF(J1(II).EQ.0) GO TO 50
0080                  PGJ=PG(1)
0081                  PZJ=0.
0082                  DO 49 J=1,NUMLS
0083                  LNUM=X(I-1+2*J)
0084                  JATOE=X(I+2*J)
0085                  AX=1.
0086                  IF(JO(LNUM).NE.JATOE) AX=-1.
```

```
FORTRAN IV G COMPILER        FLOW2          09-25-71        12:08.31        PAGE 000

0087                PZ(JATOE)=PZJ+AX*DPZ(LNUM)
0088                PZJ=PZ(JATOE)
0089                IF(J.EQ.NUMLS) GO TO 48
0090                PG(JATOE)=PGJ+AX*PDROP(LNUM)
0091                PT(JATOE)=PG(JATOE)-PZ(JATOE)
0092                PGJ=PG(JATOE)
0093                GO TO 49
0094          48    PG(JATOE)=PT(JATOE)+PZ(JATOE)
0095                DP(II)=PG(JATOE)-PG(1)
0096                PL(JATOE)=-AX*PLG(LNUM)
0097          49    CONTINUE
0098          50    I=I+1+2*NUMLS
                C
                C
                C     CALCULATE THE AIR TO FUEL RATIO AT EACH OF THE JUNCTIONS
                C     ********************************************************
0099                CALL QUAL(EJ)
0100                IF(ITRY.EQ.0) IV=LIM+1
0101          1000  CONTINUE
0102                RETURN
0103                END

 TOTAL MEMORY REQUIREMENTS 005F5E BYTES
```

```
FORTRAN IV G COMPILER        IFLOW              10-08-71          09:14.14        PAGE 0001

            SUBROUTINE IFLOW(NPOINT,NDIV,NCYC,FREQ,ITP ,NSPACE)
            REAL*8 L
            INTEGER X
            DOUBLE PRECISION D,A,RLD,RE,FT,CS,RHO,RHOA,VR,VISC,RHOF,DP,DZ,
           1FLO,HR
            DOUBLE PRECISION  F2   ,C4,C5,DT,PT,AA,R,CONS,A1,V,FF,FF1,FACT
           1,C6,C7,    P1,P2,P3,[illegible],DIM,[illegible],        RV
            CONS=.[illegible]
            COMMON X(7[illegible]),L([illegible]),D([illegible]),A([illegible]),RLD(50),RE(50),FT(50),JT(50),
           1JR(50),CS(3,50),LT(50),RHO(50),RHOA(50),NL(50),VR(50),
           2VISC(50),RHOF,DP(50),DZ(50),FLO(50),HR(50),TR,NELS,AA(2500),NJUNC
            COMMON/DUMP/PT(50,3),RHOT(50,2),XJ(50,50),PB(50,50),J1(50),J2(50)
            DIMENSION PM(50),PN(50),IR(50),FF(50),
           1P(50),R(50),C4(50),C5(50),F2(50),
           2 V(50,2),C6(50),C7(50),C8(50),RV(50,2)
       100  FORMAT(1H1)
       200  FORMAT(1H ,10E13.6)
       202  FORMAT(1H0,'T=',F7.5,I5)
       203  FORMAT(1H ,'VELOCITY, FEET/SEC=' 10F10.5)
       204  FORMAT(1H ,'MASS FLOW, LB/HOUR=' 10F10.5)
       205  FORMAT(1H ,'PRESSURE,PSIA='10F10.5)
       206  FORMAT(1H ,'FRICTION FORCE,PSIA='10F10.5)
            FACT=.5
            PER=1./FREQ
            DT=PER/NDIV
            GCON=28.96/(1545.*32.174*TR)
            NP1=NPOINT+1
            XD=PER/NPOINT
            NINTJ=0
            DO 10 I=1,NJUNC
            IF(I.GT.NELS) GO TO 6
            FF(I)=0.
            C8(I)=A(I)/L(I)
            C4(I)=(1.-VR(I))*RHOF*C8(I)
            C5(I)=V2(I)*GCON*C8(I)
            C6(I)=C5(I)*L(I)*L(I)/(DT*DT)*C8(I)
            C7(I)=DT/L(I)
            RV(I,1)=FLO(I)/A(I)
            RV(I,2)=RV(I,1)
            V(I,1)=RV(I,1)/RHOT(I,1)
            V(I,2)=RV(I,2)/RHOT(I,2)
         6  CONTINUE
            IF(JT(I).NE.0) GO TO 10
            NINTJ=NINTJ+1
            IR(I)=NINTJ
        10  CONTINUE
            NINTJ2=NINTJ*NINTJ
            IF(ITP.GT.NDIV) GO TO 80
            T=0.
            IT=0
            WRITE(6,100)
            WRITE(6,200)(C4(I),I=1,NELS)
            WRITE(6,200)(C5(I),I=1,NELS)
            WRITE(6,200)(C6(I),I=1,NELS)
            WRITE(6,200)(C7(I),I=1,NELS)
```

```
0050                WRITE(6,200)(CB(I),I=1,NELS)
0051                WRITE(6,202)T,IT
0052                WRITE(6,200)(A(I),I=1,NELS)
0053                WRITE(6,200)(V(I,1),I=1,NELS)
0054                WRITE(6,200)(V(I,2),I=1,NELS)
0055                WRITE(6,200)(RV(I,1),I=1,NELS)
0056                WRITE(6,200)(RV(I,2),I=1,NELS)
0057                WRITE(6,200)(PT(I,1),I=1,NJUNC)

                C
                C       MAIN LOOP OF THE PROGRAM
                C*************************************************************************
0058             90 DO 100 LOOP=1,NCYC
0059                DO 100 IT=1,NDIV
0060                IF(IT.EQ.1) T=0.
0061                T=T+DT
                C
                C       DETERMINE THE NEW BOUNDARY PRESSURES
                C
0062                DO 14 J=1,NJUNC
0063                PT(J,1)=PT(J,2)
0064                PT(J,2)=PT(J,3)
0065                IF(JT(J).EQ.0) GO TO 14
0066                PT(J,3)=CI(T,PB,XD,PER,NP1,50,J)
0067             14 CONTINUE
                C
                C       CALCULATE THE FRICTION FORCE TERM
                C
0068                DO 16 J=1,NELS
0069                FF1=FF(J)
0070                FF(J)=.25*FT(J)*CB(I)*(RV(J,1)*DABS(V(J,1))+RV(J,2)*DABS(V(J,2)))
0071                FF(J)=(FF(J)-FF1)*FACT+FF(J)
0072                IF(LOOP.EQ.1.AND.IT.EQ.1) FR(J)=FF(J)
0073             16 CONTINUE
                C
                C       SET UP THE COEFFICIENTS OF THE INDEPENDENT VARIABLES
                C       AND OF THE RIGHT SIDE OF THE EQUATIONS
                C
0074                DO 15 J=1,NINTJ2
0075             15 AA(J)=0.
0076                I=1
0077                DO 20 J=1,NJUNC
0078                IF(JT(J).NE.0) GO TO 20
0079                II=IR(J)
0080                R(II)=0.
0081                IDUM=IR(J)+(IR(J)-1)*NINTJ
0082                NUMLS=NL(J)
0083                DO 10 K=1,NUMLS
0084                LNUM=X(I-1+2*K)
0085                II=JO(LNUM)
0086                JATOE=X(I+2*K)
0087                IF(JT(JATOE).EQ.0) JDUM=IR(J)+(IR(JATOE)-1)*NINTJ
0088                IF(J.EQ.II) GO TO 11
                C
                C       POSITIVE FLOW IS INTO THE JUNCTION
```

```
C
0089            IF(JT(II).NE.0) GO TO 18
C
C     CALCULATE THE COEFFICIENTS
C
0090            AA(IDUM)=C8(LNUM)-C6(LNUM)/6.+C5(LNUM)*V(LNUM,1)*DABS(V(LNUM,1))
0091     12     AA(IDUM)=AA(IDUM)-C3(LNUM)-C6(LNUM)/3.-C5(LNUM)*V(LNUM,2)*
              1DABS(V(LNUM,2))
C
C     CALCULATE THE RIGHT HAND SIDE
C
0092            R(II)=R(III)+
              1   FR(LNUM)          +.5*C6(LNUM)*(-4.*PT(J,2 )/3.+2./3.*PT(J,1 )
              2-2./3.*PT(II,2 )+1./3.*PT(II,1 ))-C4(LNUM)      *(V(LNUM,1)*DABS
              3(V(LNUM,1))-V(LNUM,2)*DABS(V(LNUM,2)))
0093            IF(JT(II).EQ.0) GO TO 19
0094            R(II)=R(III)-PT(II,3 )*(C8(LNUM)-C6(LNUM)/6.+C5(LNUM)*V(LNUM,1)*
              1DABS(V(LNUM,1)))
0095            GO TO 19
C
C     POSITIVE FLOW IS OUT OF THE JUNCTION, J
0096     11     IF(JT(JATOE).NE.0) GO TO 17
C
C
C     CALCULATE THE COEFFICIENTS
C
0097            AA(JDUM)=C8(LNUM)-C6(LNUM)/6.+C5(LNUM)*V(LNUM,2)*DABS(V(LNUM,2))
0098     17     AA(IDUM)=AA(IDUM)-C3(LNUM)-1./3.*C6(LNUM)-C5(LNUM)*V(LNUM,1)*
              1DABS(V(LNUM,1))
C
C     CALCULATE THE RIGHT HAND SIDE
C
0099            R(II)=R(III)-FR(LNUM)
              1                  +.5*C6(LNUM)*(-4./3.*PT(I1,2 )+2./3.*PT(I1,1 )
              2-2./3.*PT(JATOE,2 )+1./3.*PT(JATOE,1 ))+C4(LNUM)*
              3(V(LNUM,1)*DABS(V(LNUM,1))-V(LNUM,2)*DABS(V(LNUM,2)))
0100            IF(JT(JATOE).EQ.0) GO TO 19
0101            R(II)=R(III)-PT(JATOE,3 )*(C8(LNUM)-C6(LNUM)/6.+C5(LNUM)*V(LNUM,2)
              1*DABS(V(LNUM,2)))
0102     18     CONTINUE
0103     20     I=I+1+2*NL(J)
C
C
C     CALCULATE THE PRESSURES AT THE INTERIOR JUNCTIONS
C
0104            CALL DOFLG(R,AA  ,MINTJ,1,COMS,IER)
0105            DO 45 I=1,NJUNC
0106            IF(JT(I).NE.0) GO TO 45
0107            J=IR(I)
0108            PT(I,2)=P(J)
0109     45     CONTINUE
C
C     CALCULATE THE INSTANTANEOUS MASS FLUX IN EACH ELEMENT
C
0110            DO 60 LNUM=1,NELS
```

```
OPTRAN IV G COMPILER        TFLOW          10-06-71        09:14.14        PAGE 0004

0111                I1=J1(LNUM)
0112                I2=J2(LNUM)
0113                RHOT(LNUM,1)=(C4(LNUM)+C5(LNUM)*PT(I1,3 ))/C8(LNUM)
0114                RHOT(LNUM,2)=(C4(LNUM)+C5(LNUM)*PT(I2,3 ))/C8(LNUM)
0115                P1=C7(LNUM)*(PT(I1,3 )-PT(I2,3 )-FR(LNUM)/C8(LNUM))
0116                P2=(RHOT(LNUM,1)*(V(LNUM,1)*DABS(V(LNUM,1)))-RHOT(LNUM,2)*
                   1(V(LNUM,2)*DABS(V(LNUM,2))))*C7(LNUM)
0117                RV(LNUM,1)=RV(LNUM,1)+P1+P2*C6(LNUM)/4.*C7(LNUM)*(2.*
                   1PT(I1,3 )-4.*PT(I1,2 )+3.*PT(I1,1 )+   PT(I2,3 )-2.*PT(I2,2 )
                   2   +PT(I2,1 ))/C8(LNUM)
0118                RV(LNUM,2)=RV(LNUM,2)+P1+P2-C7(LNUM)*C6(LNUM)/4.*(2.*PT(I2,3 )-4.
                   1  *PT(I2,2 )+3.*PT(I2,1 )+PT(I1,3 )-2.*PT(I1,2 )+PT(I1,1 ))
                   2/C8(LNUM)
0119                V(LNUM,1)=RV(LNUM,1)/RHOT(LNUM,1)
0120                V(LNUM,2)=RV(LNUM,2)/RHOT(LNUM,2)
0121          99    CONTINUE
0122                DO 96 I=1,NELS
0123                I1=J1(I)
0124                I2=J2(I)
0125                PTRY1=DABS(PT(I1,3)-PT(I2,3))
0126                IF(LOOP.EQ.1.AND.IT.EQ.1)PN(I)=PTRY1
0127                PTRY2=PN(I)
0128                PN(I)=AMAX1(PTRY1,PTRY2)
0129                PTRY2=PN(I)
0130          96    PN(I)=AMIN1(PTRY1,PTRY2)
0131                IF(IT/ITP*ITP-IT) 100,97,100
0132          97    WRITE(6,202)I,IT
0133                DO 94 I=1,NJUNC
0134                PT(I,3)=PT(I,3)/144.
0135                RV(I,1)=RV(I,1)*32.2*3600.*A(I)
0136                RV(I,2)=RV(I,2)*32.2*3600.* A(I)
0137          94    FR(I)=FR(I)/144.
0138                WRITE(6,203)(V(I,1),I=1,NELS)
0139                WRITE(6,203)(V(I,2),I=1,NELS)
0140                WRITE(6,204)(RV(I,1),I=1,NELS)
0141                WRITE(6,204)(RV(I,2),I=1,NELS)
0142                WRITE(6,205)(PT(I,3 ),I=1,NJUNC)
0143                WRITE(6,206)(FR(I),I=1,NELS)
0144                DO 93 I=1,NJUNC
0145                PT(I,3)=PT(I,3)*144.
0146                IF(A(I).EQ.0.) GO TO 93
0147                RV(I,1)=RV(I,1)/(32.2*3600.*A(I))
0148                RV(I,2)=RV(I,2)/(32.2*3600.*A(I))
0149          93    FR(I)=FR(I)*144.
0150          100   CONTINUE
                  C
                  C      END OF THE MAIN LOOP OF THE PROGRAM
                  C*****************************************************************
                  C
                  C      CALCULATE THE HEAD RATIOS FOR EACH ELEMENT
                  C
0151                DO 121 I=1,NELS
0152          121   HR(I)=(PN(I)-PN(I))/(PN(I)+PN(I))
0153                RETURN
0154                END
```

```
CRTRAN IV G COMPILER        FRIC          09-29-71        13:47.07        PAGE 0001

0001                SUBROUTINE FRICTF,FA,FB,V,AR,CC,RL,VISCF,F2)
0002                REAL*8 L
0003                INTEGER X
0004                DOUBLE PRECISION F,FA,FB,V,AR,CC,D,A,RLD,RE,FT,CS,RFC,RFCA,
                   1VR,VISC,RFCF,DP,DZ,FLC,HR,AX,AIN,ACUT,CC,W,U,ANG,A1,A2,A3,
                   2ANG1,ANG2,AA
0005                DOUBLE PRECISION AI,RL,VISCF,F2
0006                DIMENSION F(50),FA(50),FB(50),V(50),AR(50),CC(50),RL(50)
0007                COMMON X(750),L(50),D(50),A(50),RLD(50),RE(50),FT(50),JT(50),
                   1JC(50),CS(3,50),LT(50),RFC(50),RFCA(50),NL(50),VR(50),
                   2VISC(50),RFCF,DP(50),DZ(50),FLC(50),HR(50),TR,NELS,AA(2500),NJUNC
0008                DO 1 I=1,NELS
0009                V(I)=0.
0010                IF(A(I).EQ.0..OR.RFC(I).EQ.0.) GO TO 2
0011                V(I)=DABS(FLC(I)/(A(I)*RFC(I)))
0012              2 RE(I)=0.
0013                IF(VISC(I).EQ.0.) GO TO 3
0014                RE(I)=V(I)*D(I)/VISC(I)
0015              3 F(I)=0.
0016                FT(I)=0.
0017                FA(I)=0.
0018                FB(I)=0.
0019                CC(I)=0.
0020              1 AR(I)=1.0
                C
                C
                C       AREA CHANGE LOSS FACTORS, FA
                C       ****************************
0021                I=4
0022                LNUM=X(2)
0023                IF(LT(LNUM).EQ.0) FA(LNUM)=.5
0024                DO 10 II=2,NJUNC
0025                NUMLS=NL(II)
0026                IF(JT(II).NE.0) GO TO 5
0027                IF(NUMLS.NE.2) GO TO 10
0028                IF(JT(II).NE.0) GO TO 5
0029                DO 9 LL=1,NUMLS
0030                LNUM=X(I-1+2*LL)
0031                IF(LT(LNUM).NE.0) GO TO 10
0032                AX=1.
0033                IF(JC(LNUM).EQ.II) AX=-1.
0034                IF(AX*FLC(LNUM).GT.0.) AIN=A(LNUM)
0035                IF(AX*FLC(LNUM).LE.0.) ACUT=A(LNUM)
0036              9 IF(AX*FLC(LNUM).LE.0.) LREF=LNUM
0037                AR(II)=1.
0038                IF(ACUT.EQ.0.) GO TO 8
0039                AR(II)=AIN/ACUT
0040                IF(AR(II)-1.)7,7,8
0041              7 CC=.618+.0375*(AR(II)+.6)**5
0042                IF(CC.GT.1.) CC=1.
0043                FA(LREF)=(1./CC-1.)*(1./CC-1.)
0044                GO TO 10
0045              8 FA(LREF)=(AR(II)-1.)*(AR(II)-1.)
0046                GO TO 10
0047              5 LNUM=X(I-1+2*NUMLS)
```

```
FORTRAN IV G COMPILER        FRIC            09-29-71        13:47.07       PAGE 0002

0048                IF(LT(LNUM).NE.0) GO TO 10
0049                AX=1.
0050                IF(JC(LNUM).EQ.II) AX=-1.
0051                IF(AX*FLO(LNUM).LE.0.) FA(LNUM)=0.5
0052             10 I=I+1+2*NUMLS
0053                I=4
                 C
                 C
                 C      BEND LOSS FACTORS, FB
                 C      *********************
0054                DO 20 II=2,NJUNC
0055                NUMLS=NL(II)
0056                IF(JT(II).NE.0) GO TO 20
0057                IF(NUMLS-3)12,13,20
                 C
                 C
                 C      ELBOWS
                 C      ******
0058             12 L1=X(I+1)
0059                L2=X(I+3)
0060                AX=1.
0061                IF(JC(L1).EQ.JC(L2)) AX=-1.
0062                H=(CS(1,L1)*CS(1,L2)+CS(2,L1)*CS(2,L2)+CS(3,L1)*CS(3,L2))*AX
0063                U=DSQRT(DABS(1.-H*H))
0064                ANG=DABS(57.2*DATAN2(U,H))
0065                IF(ANG.LT.10.) ANG=0.
0066                LREF=L1
0067                AX=1.
0068                IF(JC(L1).NE.II) AX=-1.
0069                IF(AX*FLO(LREF).LE.0.) LREF=L2
0070                FB(LREF)=.01222*ANG
0071                GO TO 20
                 C
                 C
                 C      TEES
                 C      ****
0072             13 L1=X(I+1)
0073                L2=X(I+3)
0074                L3=X(I+5)
0075                IF(FLO(L1).EQ.0.) GO TO 20
0076                IF(FLO(L2).EQ.0.) GO TO 20
0077                IF(FLO(L3).EQ.0.) GO TO 20
0078                A1=1.
0079                A2=1.
0080                A3=1.
0081                IF(JC(L1).NE.II) A1=-1.
0082                IF(JC(L2).NE.II) A2=-1.
0083                IF(JC(L3).NE.II) A3=-1.
0084                N1=A1*FLO(L1)/DABS(A1*FLO(L1))
0085                N2=A2*FLO(L2)/DABS(A2*FLO(L2))
0086                N3=A3*FLO(L3)/DABS(A3*FLO(L3))
0087                IF(N1-N2)14,15,14
0088             14 IF(N2-N3)16,17,16
0089             15 LS1=L1
0090                LS2=L2
```

```
FORTRAN IV G COMPILER        FRIC          09-29-71        13:47.07       PAGE 0003

0091                LC=L3
0092                NC=N3
0093                GO TO 18
0094           16   LS1=L1
0095                LS2=L3
0096                LC=L2
0097                NC=N2
0098                GO TO 18
0099           17   LS1=L2
0100                LS2=L3
0101                LC=L1
0102                NC=N1
0103           18   A1=1.
0104                IF(JC(LC).EQ.JC(LS1)) A1=-1.
0105                W=(CS(1,LS1)*CS(1,LC)+CS(2,LS1)*CS(2,LC)+CS(3,LS1)*CS(3,LC))*A1
0106                U=DSQRT(DABS(1.-W*W))
0107                ANG1=DABS(57.2*DATAN2(U,W))
0108                IF(ANG1.LT.10.) ANG1=0.
0109                A2=1.
0110                IF(JC(LC).EQ.JC(LS2)) A2=-1.
0111                W=(CS(1,LS2)*CS(1,LC)+CS(2,LS2)*CS(2,LC)+CS(3,LS2)*CS(3,LC))*A2
0112                U=DSQRT(DABS(1.-W*W))
0113                ANG2=DABS(57.2*DATAN2(U,W))
0114                IF(ANG2.LT.10.) ANG2=0.
0115                IF(ANG1.EQ.90..AND.ANG2.EQ.90.)  FB(LC)=1.8
0116                IF(FB(LC).EQ.1.8) GO TO 20
0117                FB(LS1)=.01222*ANG1+FB(LS1)
0118                FB(LS2)=.01222*ANG2+FB(LS2)
0119           20   I=I+1+2*NLNLS
                C
                C
                C       FRICTIONAL LOSS FACTORS, PIPE AND ORIFICES, F
                C       LT=0; PIPE
                C       LT=1; MAIN METERING ORIFICE
                C       LT=2; SQUARE EDGED ORIFICE
                C       ******************************************
0120                    DO 100 I=1,NELS
0121                    IF(LT(I)-1)110,120,120
0122           110      F(I)=(.64-.0064*(RE(I)-100.))*RLD(I)
0123                    IF(RE(I).LE.100.) GO TO 100
0124                    F(I)=.3164/(RE(I)**.25)
0125                    IF(RE(I).LT.1187.382) F(I)=64./RE(I)
0126                    F(I)=F(I)*RLD(I)
0127                    IF(VR(I).LE..0001.OR.VR(I).GT..9999) GO TO 100
0128                    F(I)=F2*F(I)
0129                    GO TO 100
0130           120      RX=RE(I)
0131                    HX=HR(I)
0132                    IF(LT(I)-1)130,130,140
0133           130      CD(I)=CDMEAN(RX,HX)
0134                    GO TO 150
0135           140      RLDX=RLD(I)
0136                    CD(I)=CDSQ(RX,HX,RLDX)
0137           150      IF(CD(I).LE.0.) CD(I)=.05
0138                    F(I)=1./(CD(I)*CD(I))
```

```
FORTRAN IV G COMPILER        FRIC          09-29-71        13:47.07        PAGE 0004

 0139          100   FT(I)=FA(I)+FB(I)+F(I)
 014C                RETURN
 0141                END

  TOTAL MEMORY REQUIREMENTS 0012B4 BYTES
```

```
ORTRAN IV G COMPILER        QUAL          09-25-71        12:08.38        PAGE 0001

0001                SUBROUTINE QUAL(Q)
0002                INTEGER X
00                  REAL*8 L
0004                DOUBLE PRECISION D,A,RLD,RE,FT,CS,RHO,RHOA,VR,VISC,RHOF,DP,DZ,
                   1FLO,HF,TOLP,AA,FLOW,C,E,CONS
0005                DIMENSION Q(50),B(50),IB(50)
0006                COMMON X(750),L(50),D(50),A(50),RLD(50),RE(50),FT(50),JT(50),
                   1JC(50),CS(3,50),LT(50),RHO(50),RHOA(50),NI(50),VR(50),
                   2VISC(50),RHOF,DP(50),DZ(50),FLO(50),HR(50),TR,NELS,AA(2500),NJUNC
0007                CONS=.000C0000001
0008                NINTJ=0
0009                DO 5 J=1,NJUNC
0010                IF(JT(J).NE.0) GO TO 5
0011                NINTJ=NINTJ+1
0012                IB(J)=NINTJ
0013           5    CONTINUE
0014                DO 6 I=1,NINTJ
0015                B(I)=0.
0016                DO 6 J=1,NINTJ
0017           6    AA(I+(J-1)*NINTJ)=0.
0018                I=4
0019                DO 10 J=2,NJUNC
0020                IF(JT(J).NE.0) GO TO 10
0021                IJ=IB(J)
0022                NUMLS=NL(J)
0023                DO 20 I1=1,NUMLS
0024                JATCE=X(I+2*I1)
0025                LNUM=X(I-1+2*I1)
002                 FLOW=DABS(FLO(LNUM))
0027                IF(JC(LNUM).EQ.J.AND.FLO(LNUM).GT.0.) GO TO 20
0028                IF(JC(LNUM).NE.J.AND.FLO(LNUM).LE.0.) GO TO 20
0029                IF(JT(JATCE).NE.0) GO TO 18
0030                II=IB(JATCE)
0031                AA(IJ+(II-1)*NINTJ)=-FLOW
0032                GO TO 19
0033           18   IF(JT(JATCE).EQ.1)  GO TO 19
0034                B(IJ)=B(IJ)+FLOW
0035           19   AA(IJ+(IJ-1)*NINTJ)=AA(IJ+(IJ-1)*NINTJ)+FLOW
0036           20   CONTINUE
0037           10   I=I+1+2*NL(J)
0038                CALL DGELG(B,AA,NINTJ,1,CONS,IER)
0039                I=4
0040                DO 30 J=2,NJUNC
0041                NUMLS=NI(J)
0042                IF(JT(J).NE.0) GO TO 30
0043                IJ=IB(J)
0044                Q(J)=B(IJ)
0045                DO 28 I1=1,NUMLS
0046                JATCE=X(I+2*I1)
0047                IF(JT(JATCE).EQ.0) GO TO 28
0048                LNUM=X(I-1+2*I1)
0049                IF(J.EQ.JC(LNUM).AND.FLO(LNUM).LT.0.) GO TO 29
0050                IF(J.NE.JC(LNUM).AND.FLO(LNUM).GE.0.) GO TO 29
005                 Q(JATCE)=Q(J)
0052                GO TO 28
```

```
0053          29    IF(JT(JATOE).EQ.2) Q(JATOE)=1.
0054                IF(JT(JATOE).EQ.1) Q(JATOE)=0.
0055          28    CONTINUE
0056          30    I=I+1+2*NUMLS
0057                RETURN
0058                END
```

TOTAL MEMORY REQUIREMENTS 000950 BYTES

```
FORTRAN IV G COMPILER        CDMEAN          09-13-71        14:54.09        PAGE 0001

0001                 FUNCTION CDMEAN(RE,HR)
0002                 DIMENSION C(11,4),CS(1,11),XR(11),XH(11),CD(4,11),CH(1,6),XCH(6)
0003                 DATA C/.739,.805,.825,.820,.805,.785,.760,
                    1.732,.702,.670,.636,.784,.829,.850,.860,.855,
                    2.845,.828,.805,.780,.754,.722,.820,.880,.910,
                    3.915,.911,.902,.885,.861,.835,.805,.770,
                    4.853,.920,.940,.925,.893,.850,.775,.720,.665,.610,
                    5.555/,CS/0.,.05,.733,.734,.820,.840,.858,.870,
                    6.875,.880,.885/,XR/0.,1000.,2000.,3000.,4000.,5000.,
                    76000.,7000.,8000.,9000.,10000./,XH/0.,.125,.25,
                    8.375,.500,.625,.750,.875,1.,1.125,1.25/,XCH/0.,1000.,
                    92000.,3000.,4000.,5000./
0004                 R=ABS(RE)
0005                 H=ABS(HR)
0006                 IF(H.LT..01) GO TO 100
0007                 IF(R.GT.5000.) R=5000.
0008                 IF(H.GT.1.25) H=1.25
0009                 CH(1,1)=0.
0010                 DO 10 I=1,4
0011                 DO 9 J=1,11
0012           9     CD(I,J)=C(J,I)
0013                 K=I+2
0014          10     CH(1,K)=CI(H,CD,.125,1.25,11,4,I)
0015                 CH(1,2)=CH(1,3)*.943
0016                 Y=CI(R,CH,1000.,5000.,6,1,1)
0017                 GO TO 200
0018          100    IF(R.GT.10000.) R=10000.
0019                 Y=CI(R,CS,1000.,10000.,11,1,1)
0020          200    IF(Y.LE.0.) Y=.05
0021                 IF(Y.GT.1.) Y=1.
0022                 CDMEAN=Y
0023                 RETURN
0024                 END

 TOTAL MEMORY REQUIREMENTS 000586 BYTES
```

```
AN IV G COMPILER        CDSQ            09-16-70        08:54.18        PAGE 0001

      FUNCTION CDSQ(X1,X2,X3)
      DIMENSION RE(4,3),A(4,3),B(4,3),C(4,3),RLD(3),CD(5),CD1(5)
      H=ABS(X2)
      IF(H.GT.1.) H=1.
      R=ABS(X1)
      YLD=ABS(X3)
      DATA RE/1148.,2491.,3550.,4595.,1161.,2493.,3586.,4636.,
     1  1625.,3115.,4263.,5277./,A/.273,.012,.556,.587,.0217,.329,
     2.247,.221,.2035,.3625,.1851,.13/,B/.16,.25,.3,.32,.04,.26,.26,.22,
     3.55,.4,.2,.1/,C/.726,.77,.73,.74,.7,.796,.797,.8,.745,.73,.75,.75
     4/,RLD/.6159,3.6293,7.2304/
      IF(H.GE..01) GO TO 4
      CDSQ=CDSS(R,YLD)
      GO TO 70
    4 LD2=3
      LD1=3
      DO 5 LD=1,3
      IF(YLD.GT.RLD(LD)) GO TO 5
      LD1=LD-1
      LD2=LD
      LD=3
    5 CONTINUE
      IF(LD1.EQ.0) LD1=1
      DO 10 LD=LD1,LD2
      DO 10 I2=1,5
      IF(I2.EQ.5) GO TO 30
      IF(R.GT.RE(I2,LD)) GO TO 10
      IF(I2.EQ.1) GO TO 20
      I1=I2-1
      DO 40 J=I1,I2
   40 CD(J)=-A(J,LD)*(H-B(J,LD))*(H-B(J,LD))+C(J,LD)
      SLOPE=0.
      IF(RE(I2,LD).EQ.RE(I1,LD)) GO TO 41
      SLOPE=(CD(I2)-CD(I1))/(RE(I2,LD)-RE(I1,LD))
   41 CD1(LD)=SLOPE*(R-RE(I1,LD))+CD(I1)
      I2=5
      GO TO 10
   20 XLD=RLD(LD)
      CDSS1=CDSS(R,XLD)
      XR=RE(1,LD)
      CDSS2=CDSS(XR,XLD)
      CD(1)=-A(1,LD)*(H-B(1,LD))*(H-B(1,LD))+C(1,LD)
      CD1(LD)=CD(1)*CDSS1/CDSS2
      I2=5
      GO TO 10
   30 CD1(LD)=-A(4,LD)*(H-B(4,LD))*(H-B(4,LD))+C(4,LD)
   10 CONTINUE
      SLOPE=0.
      IF(RLD(LD2).EQ.RLD(LD1)) GO TO 69
      SLOPE=(CD1(LD2)-CD1(LD1))/(RLD(LD2)-RLD(LD1))
   69 CDSQ=CD1(LD1)+SLOPE*(YLD-RLD(LD1))
   70 IF(CDSQ.LT.0.) CDSQ=0.
      IF(CDSQ.GT.1.) CDSQ=1.
      RETURN
      END
```

```
ORTRAN IV G COMPILER        CDSS            09-13-71        16:30.33        PAGE 0001

0001                FUNCTION CDSS(RE,RLD)
0002                DIMENSION Y1(1,21),Y2(1,21 ),Y3(1,21),Y4(1,21)
0003                DATA Y1/0.,.662,.665,.6575,.65,.645,.64,
                   1.638,.636,.635,.633,.632,.631,.63,.63,6*.63/,
                   2Y2/0.,.682,.72,.685,.675,.698,.685,.675,.675,.67,.68,.70,
                   3.685,.685,7*.7/,Y3/0.,.67,.72,.75,.76,.77,.776,
                   4.78,.783,.785,.786,.787,.788,.788,.789,.789,
                   55*.79/,Y4/0.,.55,.65,.69,.72,.735,.74,.74,.74,.742,.745,
                   6.746,.748,.750,.753,.755,.757,.758,.759,.76,
                   7.761/
0004                XV=ABS(RE)
0005                ZV=ABS(RLD)
0006                IF(XV.LT.500.) GO TO 80
0007                IF(ZV.LE..1) GO TO 30
0008                IF(ZV.LT..616) GO TO 40
0009                IF(ZV.LE.3.63) GO TO 50
0010                IF(ZV.LE.7.2297) GO TO 60
0011                GO TO 70
0012          30    CDSS=CI(XV,Y1,500.,10000.,21,1,1)
0013                RETURN
0014          40    C1=CI(XV,Y1,500.,10000.,21,1,1)
0015                C2=CI(XV,Y2,500.,10000.,21,1,1)
0016                CDSS=C2-(.616-RLD)*(C2-C1)*1.936
0017                RETURN
0018          50    C1=CI(XV,Y2,500.,10000.,21,1,1)
0019                C2=CI(XV,Y3,500.,10000.,21,1,1)
0020                CDSS=C2-(3.63-RLD)*(C2-C1)*.332
0021                RETURN
0022          60    C1=CI(XV,Y3,500.,10000.,21,1,1)
0023                C2=CI(XV,Y4,500.,10000.,21,1,1)
0024                CDSS=C2-(7.2297-RLD)*(C2-C1)*.278
0025                RETURN
0026          70    CMAX=.827-.0085*RLD
0027                CM7RE=CI(XV,Y4,500.,10000.,21,1,1)
0028                CDSS=CMAX*CM7RE*1.314
0029                RETURN
0030          80    IF(XV.GT.1.) GO TO 90
0031                CDSS=.05
0032                RETURN
0033          90    CMAX=.827-.0085*ZV
0034                IF(ZV.LT.2.) CMAX=.73+.045*ZV
0035                IF(ZV.LT.1.) CMAX=.6+.175*ZV
0036                C=1./CMAX+20./XV*(1.+2.25*ZV)-.005*ZV/(1.+7.5*ALOG10(.00015*XV)*
                   1ALOG10(.00015*XV))
0037                CDSS=1./C
0038                RETURN
0039                END

 TOTAL MEMORY REQUIREMENTS 000604 BYTES
```

```
IV G COMPILER        FPROP          08-20-70        16:21.26        PAGE 0001

      SUBROUTINE FPROP(FLUNC, TEMP, SG, VISC)
    1   IF(FLUNC.NE.C.0) GC TC  2                                    ISO OCT
        SG=0.7219-0.CCC43826*TEMP                                    ISO OCT
        VISC=-0.4378+313.3462/(TEMP+200.0)                           ISO OCT
        RETURN
    2   IF(FLUNC.NE.1.C) GC TC  3                                    STD REG
        SG=24720.0/(TEMP+6270.0)-3.172                               STD REG
        VISC=135.79/(TEMP+132.5)-0.0830                              STD REG
        RETURN
    3   IF(FLUNC.NE.2.0) GC TC  4                                    WATER
        SG=1.0-C.000133*TEMP                                         WATER
        VISC=-C.1570+102.C/(TEMP+20.0)                               WATER
        RETURN
    4   IF(FLUNC.NE.3.C) GC TC  5                                    ETH ALC
        SG=0.830-C.0C0340*TEMP                                       ETH ALC
        VISC=-0.C890+346.C/(TEMP+190.0)                              ETH ALC
        RETURN
    5   IF(FLUNC.NE.4.C) GC TC  6                                    SHELL
        SG=0.7839-0.CC0472*TEMP                                      SHELL
        VISC=0.7710-0.CC244C*TEMP                                    SHELL
        RETURN
    6   IF(FLUNC.NE.5.0) GC TC  7                                    CLARK
        SG=0.7480-0.CC040*TEMP                                       CLARK
        VISC=0.6740-C.001933*TEMP                                    CLARK
        RETURN
    7   IF(FLUNC.NE.6.C) CC TC  8                                    MAR'ON
        SG=2328.56812/(TEMP*1.8+32.0-2074.7644)+2.03898              MAR'ON
        VISC=118.12441/(TEMP*1.8+32.0+77.16928)-0.07321              MAR'ON
        RETURN
    8   IF(FLUNC.NE.7.0) GC TC  9                                    MIN SPIR
        SG=0.64C9+41.88/(TEMP+215.0)                                 MIN SPIR
        VISC=-0.1250+201.0/(TEMP+65.3)                               MIN SPIR
        RETURN
    9   IF(FLUNC.NE.8.0) GC TC  10                                   AIR
        SG=0.6360/(TEMP+459.6)                                       AIR
        VISC=12.0774+4.6452*TEMP/100.0                               AIR
        RETURN
   10   WRITE(6,11)
   11    FORMAT( 'NO FLUID PRCPERTIES LISTED IN FUNCTION FOR GIVEN CODE NU
     1MBER')
        RETURN
        END

MEMORY REQUIREMENTS 00055C BYTES
```

```
      FUNCTION CI(XX,Y,DX,XMAX,IMAX)
      DIMENSION Y(10)
      XSPAN=IMAX*DX-DX
      XZERO=XMAX-XSPAN
      X=(XX-XZERO)/DX+1.
      I=X
      IF(XX-XMAX+DX)1,1,2
    2 I=IMAX-1
    1 IF(XX-XZERO-DX)3,4,4
    3 I=2
    4 XH=(XX-XZERO-(I-1)*DX)/DX
      CI=Y(I)+.5*XH*(Y(I+1)-Y(I-1)+XH*(Y(I+1)+Y(I-1)-2.*Y(I)))
      RETURN
      END
```

BIBLIOGRAPHY

Metering of Oscillating Flow with Orifices

1. Bailey, N. P., "Pulsating Air Velocity Measurement", ASME Trans., Vol. 61, 1939, pp. 301-308.

2. Beitler, S. R., "The Effect of Pulsations on Orifice Flow Meters", ASME Trans., Vol. 61, 1969, pp. 309-313.

3. Beitler, S. R., E. J. Lindahl and H. B. McNichols, "Development in the Measuring of Pulsating Flows with Inferential Head Meters", ASME Trans. Vol. 65, 1943, pp. 353-356.

4. Benson, R. S. and H. M. F. Shafie, "Non-Steady Flow Through a Square Edged Orifice in a Pipe", Journal of Mech. Eng. Science, Vol. 7, No. 4, 1965.

5. Daneshyar, H., "Development of Unsteady Laminar Flow of an Incompressible Fluid in a Long Circular Pipe", International Journal of Mechanical Science, Pergamon Press, 1970, Vol. 12, pp 435-445.

6. De Mestre, N. J. and Guiney, D. C., "Low Reynolds Number Oscillation Flow Through a Hole in a Wall", Journal of Fluid Mechanics (1971), Vol. 47, Part 4, pp. 657-666.

7. Earles, S. W. E. and Zarek, J. M., "Use of Sharp-Edged Orifices for Metering Pulsative Flow", Proc. of Inst. of Mech. Engr., Vol. 177, No. 37, 1963, pp 997-1012.

8. Hodgson, J. L., "Commercial Metering of Air, Gas, and Steam", Proc. I.C.E., Vol. 104, 1916, 1917, Part 2, pp. 108-193.

9. Jeffery, B. J., "Pulsating Flow Through Orifices", Ph.D. thesis in the Faculty of Engineering, Kings College, University of London, 1965.

10. Moseley, D. S., "Measurement Error in the Orifice Meter on Pulsating Water Flow", Flow Measurement Symposium, ASME, Sept. 26-28, 1966, pp. 103-123.

11. Oppenheim, A.K. and E. G. Chilton, "Pulsating Flow Measurement - A Literature Survey", Trans. ASME, Feb. 1955, pp. 231-248.

12. Sparks, C. R., "A Study of Pulsation Effects on Orifice Metering of Compressible Flow", ASME Flow Measurement Symposium, ASME, N. Y., Sept. 26-28, 1966, pp. 124-138.

13. Williams, T. J., "Pulsation Errors in Manometer Gages", ASME paper, 55-A-92, No. 1955.

14. Zarek, J. M., "The Neglected Parameters in Pulsating Flow Measurement", Flow Measurement Symposium, ASME, N. Y., 1966.

Fuel Metering and Induction Systems

15. Blair, G. P., and Goulburn, J. R., "The Pressure-Time History in the Exhaust System of a High-Speed Reciprocating Internal Combustion Engine", SAE paper 670477, 1967.

16. Bolt, J. A., Derezinski, S. J. and Harrington, D. L., "The Influence of Fuel Properties on Metering in Carburetors", SAE paper 710207, 1971.

17. Brandstetter, Walter, "Der Gemischbild ungsvorgang im Ansaugsystem der Verbrennungskraftmaschine bei periodisch-instationaven Stromungen", (The Mixture Formation in the Induction System of the Internal Combustion Engine with Periodic Fluid Flow), Sonderdruck aus AI, Ausgabe 4 vom 25. November 1966, 11 Janhrgang, Vogel-Verlag Wurzburg.

18. Brandstetter, W. R., "Theoretical Analysis of Unsteady Flow Phenomena in Single-Cyclinder Four-Stroke Engines with Intake and Exhaust Pipes", General Motors Research Publication GMR-884, June 17, 1969.

19. Goyal, M., G. Scharpf, and G. Borman, "The Simulation of Single Cylinder Intake and Exhaust Systems", SAE paper No. 670478, May 15-19, 1967.

20. Harrington, D. L., "Analysis and Digital Simulation of Carburetor Metering", Ph.D. Thesis, University of Michigan, 1968. Also see SAE paper 700082.

21. Hosho, Yukio, "The Mixture Ratio Regulating Effect of the Air Bleed in Simplified Carburetors", Hitachi Review, Feb. 1963, pp. 36-42.

22. Hosho, Yukio, "Flow Quantities of Air Introduced Through Air Bleeds into Carburetors and Pulsating Fuel Jet Phenomena", Hitachi Review, Vol. 16, No. 4, 1967, pp. 173-178.

23. Huber, P. and Brown, J., "Computation of Instantaneous Air Flow and Volumetric Efficiency", SAE paper 812B, 1964.

24. Kastner, L. J., "An Investigation of the Air Box Method of Measurin the Air Consumption of Internal Combustion Engines", Inst. of Mech. Engr. Proceedings, Vol. 157, 1947, pp. 387-404.

25. Kastner, L. J., and T. J. Williams, "Pulsating Flow Measurement by Viscous Meters, with Particular Reference to the Air Supply of Internal Combustion Engines", Inst. of Mech. Eng. Proceedings, Vol. 169, 1955, pp. 419-432.

26. Klecka, M. E. and Oubre, C. L., "Mathematical Simulation of Automotive Fuel Systems", SAE paper 680436, 1968.

27. Oyama, Y., Tejima, T., and Hosho, Y., "Transient Flow of Carburetor Fuel Systems", Hitachi Review, Vol. 18 (1969), No. 4, pp. 162-167.

28. Prien, Walter F., "A Study of the Effect of Air Pulsations on the Operation of a Simple Carburetor", Thesis for Bachelor of Science Degree, M.I.T., May 1954.

29. Shinoda, K., Koide, H., and Yii, A., "Analysis and Experiments on Carburetor Metering at the Transition Region to the Main System", SAE paper 710206, 1971.

30. Taylor, C. F., Livengood, J. C. and D. H. Tsai, "Dynamics of the Inlet System of a Four-Stroke Single-Cylinder Engine", Trans. ASME, Oct. 1955, pp. 1133-1145.

Transient Flow Analysis and Simulation

31. Benson, R. S., "Some Recent Research on Non-Steady Flow Problems", Flow Measurement Symposium, ASME, Sept. 26-28, 1966, pp. 80-102.

32. Benson, R. S., R. D. Garg, and D. Woollatt, "A Numerical Solution to Unsteady Flow Problems", Int'l Journal of Mech. Science, Pergamon Press. Ltd., 1964, Vol. 6, pp. 177-144.

33. Carnahan, B., H. A. Luther, and J. O. Wilkes, Applied Numerical Methods, John Wiley and Sons, 1969.

34. Chaudhry, M. H., "Resonance in Pressurized Piping Systems", Journal of the Hydraulics Division, ASCE, Sept. 1970, pp. 1819-1839.

35. Streeter, V. L., "Computer Solution of Surge Problems", Symposium on Surges in Pipe Lines, Part I. Inst. of Mech. Eng., London, Nov. 1965.

36. Streeter, V. L., Fluid Mechanics, McGraw-Hill Book Company, 1958.

37. Streeter, V. L., "Water-Hammer Analysis of Distribution Systems", Journal of the Hydraulics Division, ASCE, Sept, 1967, pp. 185-201.

38. Streeter, V. L., Hydraulic Transients, McGraw-Hill Book Co., 1967.

39. Streeter, V. L., and Wylie, E. B., "Natural Gas Pipeline Transients", AIME paper SPE 2555, 1969.

40. Stoner, M. A., "Steady-State Analysis of Gas Production, Transmission, and Distribution Systems", AIME paper SPE 2554, 1969.

41. Stoner, M. A., "Sensitivity Analysis Applied to Steady State Model of Natural Gas Transportation Systems", AIME paper SPE 3056, 1970.

42. Wylie, E. B., Stoner, M. A., and Streeter, V. L., "Network System Transient Calculations by Implicit Method", AIME paper SPE 2963, 1970.

43. Yow, W., "Analysis and Control of Transient Flow in Natural Gas Piping Systems", Ph.D. thesis, University of Michigan, 1971.